Degradation of organic pollutants employing various photocatalytic systems

Michal Kolář

N° d'ordre : D. U. 1855

UNIVERSITE BLAISE PASCAL

(U. F. R. De Recherche Scientifique et Technique)
ECOLE DOCTORALE DES SCIENCES FONDAMENTALES
N° : 592

THESE EN COTUTELLE

Présentée pour obtenir le titre de

DOCTEUR D'UNIVERSITE DE L'UNIVERSITE BLAISE PASCAL A CLERMONT-FERRAND
et DE L'ECOLE NATIONALE SUPERIEURE DES TECHNOLOGIES CHIMIQUES A PRAGUE
Spécialité: chimie physique

Par

KOLÁŘ Michal

Magister de l'Université Charles

DEGRADATION OF ORGANIC POLLUTANTS EMPLOYING VARIOUS PHOTOCATALYTIC SYSTEMS

Soutenue publiquement le jeudi 27 novembre 2008 devant la commission d'examen.

Referee :	Pr. Tat'jana NEVĚČNÁ
	Dr.hab. Didier ROBERT
	Pr. Bohumil BERNAUER
Examiner :	Pr. Claude FORANO
Supervisor :	Dr. Michèle BOLTE
	Dr. Jaromír JIRKOVSKÝ
	Pr. Josef KRÝSA
	Dr. Gilles MAILHOT

ACKNOWLEDGEMENT

First of all, I would like to sincerely thank Dr. Gilles MAILHOT, Dr. Michèle BOLTE, Dr. Jaromír JIRKOVSKÝ and Assoc. Prof. Josef KRÝSA for being patient supervisors and for supporting this work with their ideas, experience and criticism.

I would like to thank Assoc. Prof. Taťjana NEVĚČNÁ, Dr. Didier ROBERT, Assoc. Prof. Bohumil BERNAUER and Prof. Claude FORANO for accepting participation in the jury.

I also highly appreciate the financial support of French government (BGF).

I would like to thank Dr. Jean-Pierre AGUER for his early support in photochemistry, Dr. Hana MĚŠŤÁNKOVÁ for many helpful advices concerning iron chemistry and for reading the manuscript, Dr. Otman ABIDA for his numerous suggestions on ferric citrate and Mr. Pierre BOULE for answering me questions about photochemistry. Many thanks belong to all members of the laboratory, particularly Guillaume VOYARD and Bernardette LAVEDRINE. I would like to thank my friends from both laboratories for their help and encouragement.

Last but not the least I would like to thank my family and Martina for the enormous support and patience they gave me.

INDEX

I. INTRODUCTION

The arrival of industrial revolution had a huge impact on the quality as well as on the order of magnitude of entire spectrum of human activities. The discovery of artificial fertilizers and pesticides enabled higher crop yields per area in agriculture, which helped to satisfy the nutrition demands of the increasing population and liberated significant part of the labour force. The fertilizers came to common use during the second half of 19^{th} century, as the pesticides became popular in the 50's. The overall consumption of pesticides increased since more than fifty times. Nowadays, 2.5 millions tons of various pesticides (herbicides, insecticides, fungicides, rodenticides, bactericides etc.) are used per year all over the world.

On the other hand, as the intensive agriculture increased, together with massive industrial production, the pressure on the environment, as the pollution of continental waters, atmosphere and surface soils became a serious issue. Vast range of pollutants is found recently in continental waters: various pesticides and its residues, heavy metals and wide sort of organic compounds, often halogenated, contained in industrial sewage, dissolved inorganic (especially sulphuric) oxides known as acid rains and many others.

The impact of the pesticides application on the human health and on the environment ensued in a short time. First health problems caused by the use of pesticides were reported some twenty years after its introduction. Besides, the organochloric compounds, like chlorophenols, which are often used as a precursor in the pesticides production and which are often found as intermediates in the degradation pathways of various compounds, are often classified as hazardous for the human health and for the environment as well.

Several attempts were already made in order to improve the situation. At the end of the nineties, the European Union issued a directive (98/83/EEC), which determined maximal concentration of various pollutants in drinking water. The limiting value for a single pesticide and its intermediates is $0.1 \mu g.L^{-1}$; the sum of different pesticides concentration within intermediates must not exceed $0.5\ \mu g.L^{-1}$.

Among all the used pesticides, the triazines (e.g. Atrazine) are the most abundant in continental surface waters and groundwaters. The pesticides derived from phenylurea

(Diuron, Monuron, Linuron, Isoproturon …) were the following most abundant group in continental surface waters and groundwaters.

Several processes of natural decontamination take place in aquatic and soil environment. The biodegradation by the microorganisms is the most important one, however, some compounds are resistant to this way, e.g. some pesticides and its residues. Other important process is the hydrolysis, which can induce fragmentation of some pollutants, and the redox reactions, which occur either in the soils (clays, various oxides etc.) or in the aquatic media. The humic acids, which are present in the organic soil, have an ability to accumulate the pollutants, as well as to photoinduce their degradation under irradiation. Furthermore, some pollutant molecules could be photochemically transformed after absorption of a photon with sufficient energy, and undergo so called direct phototransformation. The pollutant could be also photochemically transformed in the presence of other absorbing compound, and undergo so called photoinducted transformation. However, all these natural processes are often not sufficient enough to remove the contamination from the environment.

Intensive research work was carried out during the last three decades with the intent to respond the demand to withstand the problem of pollution of continental waters. Several water treatment methods were developed, known as Advanced Oxidation Processes (AOP). Most of these processes (O_3, O_3/H_2O_2, O_3/UV, Fenton reaction, photo-Fenton, H_2O_2/M^{n+}, H_2O_2/UV, H_2O_2/NaClO, TiO_2/UV etc.) were investigated thoroughly, and its efficiency of various pollutant degradation was published. The importance of water treatment by the AOP is evidenced by a constant increase of the publications dedicated to this problem since 1975, with a steep increase in last 10 years.

The photo-oxidation of carboxylic acids has long been known to be sensitized by Fe(III), but only till the 1960s attention has been paid to the coordinate species involved. The carboxylate group [$RC(O)O^-$] is one of the most common functional groups of the dissolved organic compounds present in natural waters. Low molecular weight organic acids have been identified and measured in a wide variety of environments, such as marine and continental air, rural and remote atmospheres and tropical and temperate zones. Various organic acids viz. EDTA, acetic, formic, citric, ascorbic, succinic, tartaric and oxalic acids are effective coordination reagents, which play an important role on the metal ions (especially copper and iron) removal. References report the formation of iron-carboxylate complexes, which can

undergo rapid photochemical reactions under solar irradiation. The photolysis of Fe(III)-polycarboxylates could represent an important source of hydroxyl radicals and H_2O_2 to some atmospheric and surface waters.

The aim of this thesis is to contribute to the development of new methods of water treatment. The main contribution is in combination of two photocatalytic systems a ferric citrate complex and TiO_2. The study was performed with Monuron, a herbicide of phenylurea group, which had been chosen due to previous experience with other herbicides from phenylurea group, and also due to known degradation mechanism, which permitted to focus on the other aspects of this complex system. Other goal of this work was to examine the conditions of pollutant removal in a semi-operational photoreactor, based on a fixed TiO_2 layer. The pollutant was to be repeatedly added in an organic solvent.

II. BIBLIOGRAPHY

II.A Iron and its forms

Iron is the most abundant transition metal and fourth most abundant element in the Earth crust. In the environment, it is present primarily in the rocks as well as in soils, and also in lower amounts in water systems (dissolved or suspended) and in atmosphere in a form of aerosols. It is one of the most important essential elements for almost all living organisms. Iron is also the metal most used by the modern human society.

In the solid phase, the iron is generally found in the form of oxides or oxyhydroxides. The most frequent ones are *hematite* (α-Fe_2O_3), *magnetite* ($FeO.Fe_2O_3$), *limonite* ($FeO(OH).nH_2O$), *goethite* (α-FeOOH) and *lepidocrocite* (γ-FeOOH). Other common iron minerals are *ilmenite* ($FeTiO_3$), *siderite* ($FeCO_3$) and *pyrite* (FeS_2). These forms of iron oxides and oxyhydroxides are scarcely soluble in water in the presence of siderophores, but as they absorb the visible light, they could undergo a process of photodissolution (***Sulzberger et al., 1994***). These minerals could be also oxidized and solubilized by chemolitothrophic bacteria (*Ferrobacillus*, *Siderocapsa*).

In the aquatic environment, the iron is present at different concentrations: in ocean sea water, the concentration varies between 0.2 and 4 $nmol.L^{-1}$ (***Martin et al., 1990; Johnson et al., 1997***). On the opposite, in atmosphere (clouds and fogs), the amount of iron can vary in order of 0.1 and 100 $\mu mol.L^{-1}$ up to 400 $\mu mol.L^{-1}$ in heavily industrialized zones (***Conklin and Hoffmann, 1988***). In the continental aquatic compartment, the concentration of iron in running water is inferior to 9 $\mu mol.L^{-1}$ in Czech Republic. The EU Council Directive 98/83/EC for drinking water limit the concentration of iron to 0.2 $mg.L^{-1}$, which corresponds to 3.6×10^{-6} $mol.L^{-1}$.

II.A.1 Iron in natural waters

The iron in natural waters is dissolved in ferric (Fe(III)) or ferrous (Fe(II)) oxidation state, which depends on the pH, on oxidative and reductive processes and also on the presence of organic or inorganic complexing agents. The ability of the ferric/ferrous couple to be reduced or oxidized is an important feature for the chemical and biological processes of iron in aquatic environment. Fe(II) is naturally present in anaerobic environment. In aerobic water, Fe(III) is the most stable form, and these soluble complexes species are found: $[Fe(H_2O)_6]^{3+}$, $[Fe(H_2O)_5(OH)]^{2+}$, $[Fe(H_2O)_4(OH)_2]^{+}$, $[Fe(H_2O)_3(OH)_3]$, $[Fe(H_2O)_2(OH)_4]^{-1}$, and possibly

$[Fe_2(H_2O)_8(OH)_2]^{4+}$, according to the conditions. However, these iron aquacomplexes comprise minor part of the total iron present in the natural waters. ***Eberle and Palmer (1986)*** have measured the concentrations of iron and have identified the different soluble species in the river of Rhine: of the 407 µg.L^{-1} total Fe(III), only 1.6 µg.L^{-1} of Fe(III) was really dissolved (after filtering solution by 0.4 µm filter). In the filtrate, 39% of the Fe(III) was in the form of $[Fe(H_2O)_4(OH)_2]^+$, 28% of $[Fe(H_2O)_3(OH)_3]$ and 13% of $[Fe(H_2O)_2(OH)_4]^{-1}$, the rest was not identified, but it was probably in a form of soluble Fe(III) colloids. The large difference between really dissolved Fe(III) species and total concentration of iron can be attributed to oxides and complexes with organic matter or polycarboxylic acids.

As above mentioned, the iron plays an important role in biological and chemical pathways. Thus, insufficiency of iron could lead to serious consequences. For example, in human body, *anemia*, lack of erythrocytes in blood, could be developed. Other example could be seen in oceans: low concentration of iron can limit the growth of phytoplancton (***Martin and Fitzwater, 1988***). The iron has an important role also in atmosphere, as presented at **Fig. II.A.1** by ***Behra and Sigg (1990)***. It interacts with all the other important cycles of the elements present in atmospheric compartment.

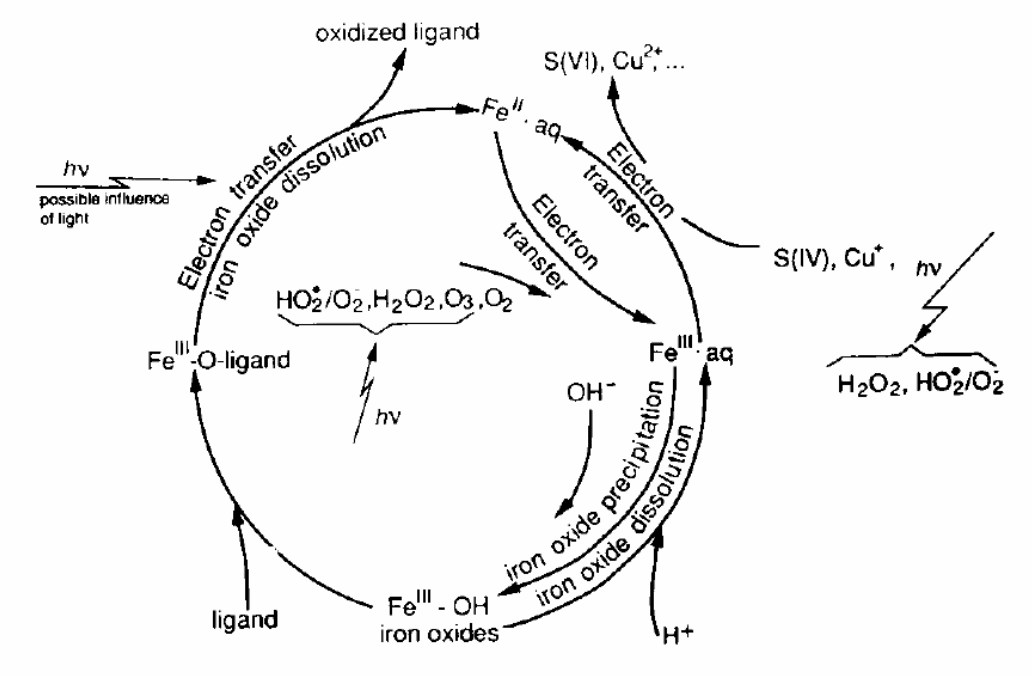

Fig. II.A.1: The cycle of iron in atmospheric water by ***Behra and Sigg (1990)***.

Sulzberger et al. (1994) have proposed a cycle of redox reactions of iron in natural waters. This scheme shows the presence of different species able to degrade the organic

compounds, either employing irradiation or not (**Fig. II.A.2**). Thus, the chemistry of iron in aquatic environment is quite complex, whether in experimental or real conditions.

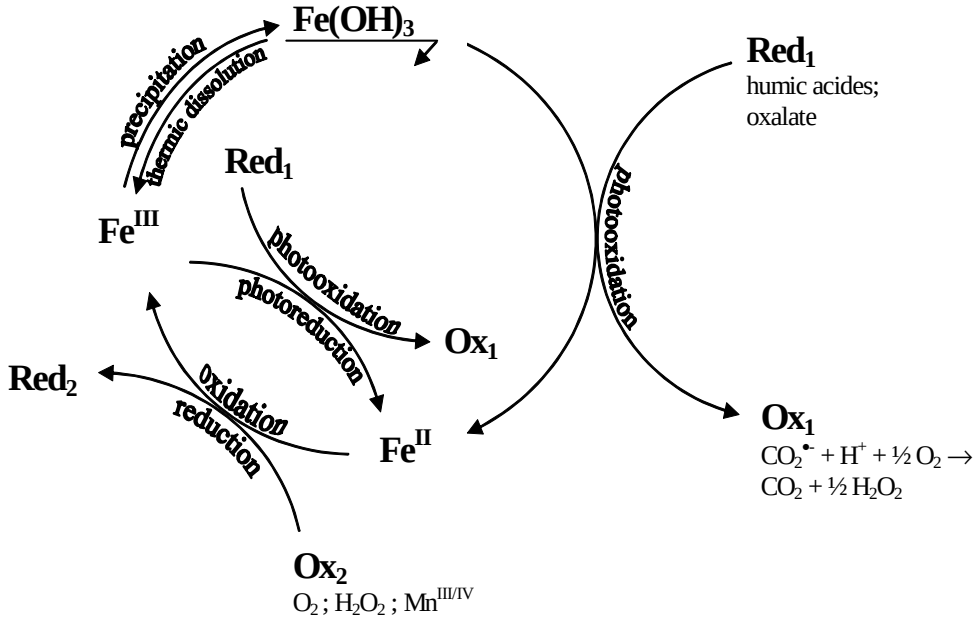

Fig. II.A.2: The cycle of iron in natural waters by ***Sulzberger et al. (1994)***.

II.A.2 Species of Fe(III) in aquatic environment

Hydrolysis of an iron salt in water can lead to different ferric (ev. ferrous) species, depending on several parameters like pH, initial concentration of the iron salt, temperature, composition of the solution (ionic force of the solution, type of the counter-anion, presence of complexing agents etc.). In purpose of explaining this phenomenon, ***Flynn (1984)*** has divided the process of hydrolysis of ferric salts into four stages:

• Formation of *low molecular weight* species (monomers and dimers)

• Formation of red cationic polymer

• Ageing and oxidation of the red polymer

• Formation of ferric oxides and hydroxides by precipitation of low molecular weight precursors

<u>Fe(III) complexes of low molecular weight complexes:</u>

◦ Monomer $[Fe(H_2O)_6]^{3+}$, corresponding to Fe^{3+} cation surrounded by six molecules of water which are placed in the corners of an octahedron, will be also noted as Fe^{3+} in our work.

◦ Monomer $[Fe(H_2O)_5(OH)]^{2+}$ or $Fe(OH)^{2+}$ where one molecule of water is replaced by a hydroxyl group.

◦ Monomer $[Fe(H_2O)_4(OH)_2]^+$ or $Fe(OH)_2^+$ where two molecules of water are replaced by two hydroxyl groups.

◦ Dimer $[Fe_2(H_2O)_8(OH)_2]^{4+}$ or $Fe_2(OH)_2^{4+}$ is a dimer complex with two coordination metal centres. Its structure had been discussed for a long time. Nowadays, the structure is supposed to be of the *dihydroxy*-form, corresponding to formula $[(H_2O)_4Fe(OH)_2Fe(H_2O)_4]^{4+}$, where the atoms of iron are connected by two hydroxyl bridges. In the less likely *oxo*-form $[(H_2O)_4FeOFe(H_2O)_4]^{4+}$ the atoms of iron are connected by a single oxygen bridge.

Fe(III) soluble species of higher molecular weight

◦ Trimer form had been denoted and two its forms were proposed: $[Fe_3(OH)_3(H_2O)_{12}]^{6+}$ or $Fe_3(OH)_3^{6+}$ and $[Fe_3(OH)_4(H_2O)_{14}]^{5+}$ or $Fe_3(OH)_4^{5+}$.

◦ The oligomers, polymers or aggregates of Fe(III) are equally present in the solution. However, their structure was not precisely identified yet.

The list of Fe(III) species, which are found in natural waters, is completed by ferric oxides or oxohydroxides in a form of colloidal or suspended particles, for example *goethite* α-FeO(OH), *lepidocrocite* γ-FeO(OH), *hematite* α-Fe_2O_3, *maghemite* γ-Fe_2O_3 or *ferrihydrate* $Fe(OH)_3$. These particles are scarcely soluble in water (***Langmuir and Whittemore, 1971***). As mentioned above, these particles could undergo a process of photodissolution (***Sulzberger et al., 1994***) or be solubilized by chemolitothrophic bacteria, both resulting in a formation of soluble Fe(II) or Fe(III) species.

All along the thesis, the chemical formulas of the iron aquacomplexes will be written in the form without indication on the complexed water molecules, in order to simplify the text. Attention should be paid to the difference between Fe(III) as a sum of entire present trivalent iron and Fe^{3+}, which corresponds to the complex of $[Fe(H_2O)_6]^{3+}$.

II.A.3 Influence of pH

The pH has a direct impact on the dissociation equilibriums of the species of Fe(III) and thus at their distribution in the aquatic environment. In the area of neutral and basic pH, the iron is present in oxidized form and tends to agglomerate or precipitate. In the area of $pH \leq 5.0$, various species of ferric ion exist: Fe^{3+}, $Fe(OH)^{2+}$, $Fe(OH)_2^+$ and dimer $Fe_2(OH)_2^{4+}$ at higher concentration of iron:

(1) $Fe^{3+} + H_2O \rightleftarrows Fe(OH)^{2+} + H^+$ $\quad K_1 = 2.7\times10^{-3}$ mol.L^{-1}

(2) $Fe^{3+} + 2\ H_2O \rightleftarrows Fe(OH)_2^{+} + 2\ H^+$ $\quad K_2 = 1.3\times10^{-8}$ (mol.L^{-1})^2

(3) $2\ Fe^{3+} + 2\ H_2O \rightleftarrows Fe_2(OH)_2^{4+} + 2\ H^+$ $\quad K_3 = 6.0\times10^{-4}$ mol.L^{-1}

The values of these constants of equilibrium were determined by ***Faust and Hoigné (1990)*** at 298 K and by ***Flynn (1984)*** at the ionic strength of 0.03 mol.L^{-1}. A distribution of monomer complex species of Fe(III) in the region of pH had been calculated using these constants, see **Fig. II.A.3**.

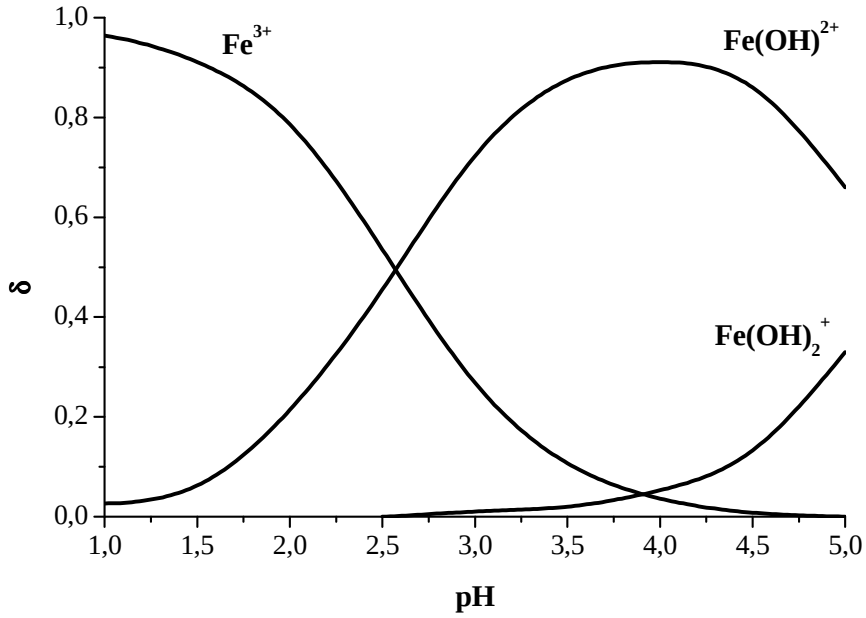

Fig. II.A.3: Diagram of distribution of monomer complexes of Fe(III) as a function of pH; 298 K, IS: 0,03 mol.L^{-1} ***(Měšťánková, 2004)***.

Formation of the species of monomer $Fe(OH)_2^{+}$ and dimer $Fe_2(OH)_2^{4+}$ arising from $Fe(OH)^{2+}$ was equally described by ***Murray (1974)***:

(4) $Fe(H_2O)_5(OH)^{2+} \overset{K_4}{\rightleftarrows} Fe(H_2O)_4(OH)_2^{+} + H^+$

(5) $2\ Fe(H_2O)_5(OH)^{2+} \overset{K_5}{\rightleftarrows} Fe_2(H_2O)_8(OH)_2^{4+} + 2\ H_2O$

Concerning the rates of equilibriums (1) and (4), ***Hemmes et al. (1971)*** had shown that the equilibrium (1) is much faster than (4). They propose the values $K1 > 3\times10^7$ s^{-1} and $K_4 = 6.1\times10^4$ s^{-1} respectively. This behaviour is different from the behaviour of the

aquacomplexes of $Al(H_2O)_6^{3+}$, $Cr(H_2O)_6^{3+}$, $Ir(H_2O)_6^{3+}$, for which K_1 is of the order of 10^5 s^{-1} (***Hemmes et al., 1971***). For these authors, this difference is linked to fact that the pK of Fe^{3+} is of the order of 2, while it is 5 for the other cited complexes. Concluding, after dissolving the crystals of Fe(III) in a weakly acid environment, the complex of Fe^{3+} will be present at low concentration and the complex of $Fe(OH)^{2+}$ will be formed rapidly.

II.A.4 Influence of concentration

The distribution of species of Fe(III) in the solution depends also on the initial concentration of Fe(III). ***Flynn (1984)*** has established a diagram of predomination of ferric species of low molecular mass as a function of both concentration and pH. The **Fig. II.A.4** shows that the dimer complexes exist only in the solution with high concentration of Fe(III) ([Fe(III)] > 5×10^{-2} $mol.L^{-1}$).

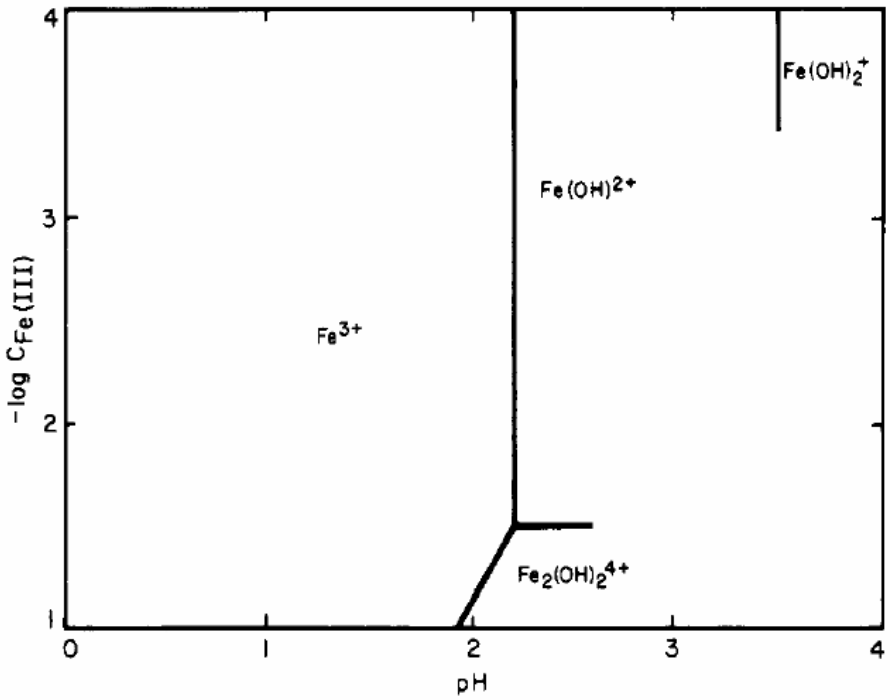

Fig. II.A.4: Predominance zones of Fe(III) complexes as a function of Fe(III) concentration together with pH (***Flynn, 1984***).

II.A.5 Spectral properties of iron aquacomplexes

Difference of the various Fe(III) species in their electronic configuration in aquatic environment results in difference of their absorption spectra (**Fig. II.A.5**). Thus, the absorption spectrum of dissolved iron will be dependent on the proportion of each species in the solution.

• The absorption spectrum of the Fe^{3+} complex ($[Fe(H_2O)_6^{3+}]$) is characterised by a maximum at 240 nm with molar absorption coefficient between 3850 and 4500 $L.mol^{-1}.cm^{-1}$ (***Langford and Carey, 1975; Knight and Sylva, 1975; Milburn, 1956***)

• The absorption spectrum of the $FeOH^{2+}$ complex ($[Fe(H_2O)_5(OH)^{2+}]$) is characterised by a maximum at 297 nm while the molar absorption coefficient is about 2000 $L.mol^{-1}.cm^{-1}$ (***Faust and Hoigné, 1990***)

• The complex of the $Fe(OH)_2^{+}$ complex ($[Fe(H_2O)_4(OH)_2^{2+}]$) has also a maximum at 297 nm, but the molar absorption coefficient is not well defined, it varies between 1100 (**Escot, 1973**) and 1800 $L.mol^{-1}.cm^{-1}$ for (***Knight and Sylva, 1975***). This ferric complex is quite unstable and tends to precipitate.

• The dimer $Fe_2(OH)_2^{4+}$ ($[Fe_2(H_2O)_8(OH)_2^{4+}]$) has a maximum at 335 nm with the molar absorption coefficient between 3500 (***Milburn, 1956***) and 8300 $L.mol^{-1}.cm^{-1}$ (***Knight and Sylva, 1975***).

• The soluble aggregates of Fe(III) give continuous increasing absorption from 500 to 200 nm without notable maximum.

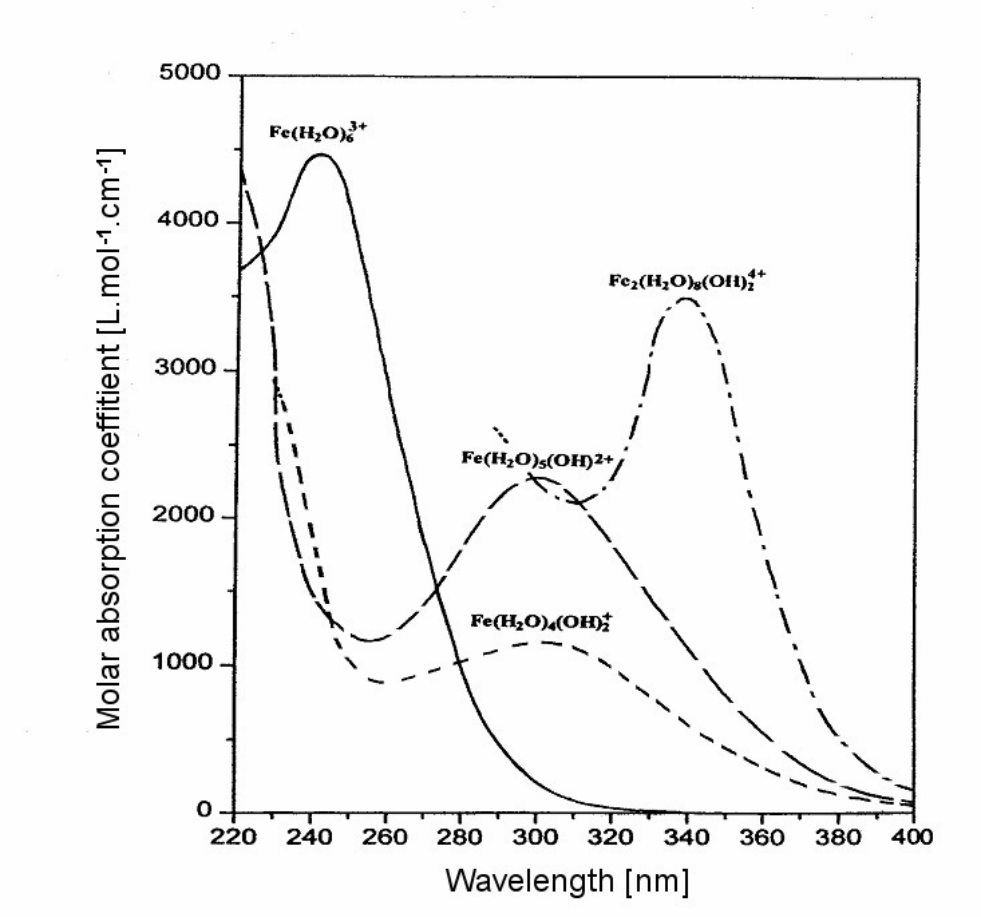

Fig. II.A.5: UV-visible absorption spectra of Fe(III) complexes (***Měšťánková, 2004)***.

II.A.6 Other complexes of iron

In presence of higher concentrations of sulphates in acid environment, these complexes are formed: $[FeSO_4]^+$, $[Fe(SO_4)_2]^-$, $[FeHSO_4]^{2+}$. Higher concentration of chlorides induces creation of $[FeCl]^{2+}$ and $[FeCl_2]^+$. The presence of phosphates leads to iron hydrogen- and dihydrogenphosphates; depending on the concentration of oxygen, soluble ferrous or insoluble ferric forms are created. Dissolved iron often makes complexes with organic polycarboxylic acids like (citrate, oxalate, malonate etc.); this phenomenon will be described in the next chapter.

II.B Photochemistry of iron

First observation of photochemical activity of iron salts had been given by ***Evans and Uri*** in 1947. They had demonstrated photopolymerisation of acrylonitrile and methyl-methacrylate in solution of $FeCl_3$.

In 1953, ***Bates and Uri*** had shown the activity of ferric ions in the presence of UV light source. Oxidation of organic compounds present in the system was observed under UV irradiation. As an agent responsible for this reaction, hydroxyl radical formed via photodissociation of $Fe(OH)^{2+}$ was supposed:

$$Fe(OH)^{2+} \xrightarrow{h\upsilon} Fe(II) + {}^{\bullet}OH$$

The photochemical behaviour of various aquatic complexes of Fe(III) was objective of many studies, especially in the later decades. Two major types of the processes, where the iron plays a role of photoinductor of pollutants degradation, can be separated:

• The first mechanism is based on the Fe(III) complexed solely by *hydroxyl/water groups* where the molecules of pollutant are principally attacked by hydroxyl radicals formed by photodissotiation of aquatic complexes of Fe(III).

• The second mechanism employs the complexation of Fe(III) by *organic complexing agents*, which could be molecules of pollutant, solvent etc. Absorption of light induces intramolecular photoredox process, reducing Fe(III) to Fe(II) and oxidizing the complexing agent.

II.B.1 Photochemical properties of aquacomplexes of Fe(III)

Formation of hydroxyl radicals from Fe(III) aquacomplexes under irradiation is explained through energetic diagram of transition metal complexes (**Fig. II.B.1**). Among the transitions indicated at the diagram, the “B” are those to be pursued. Irradiation at a sufficient wavelength of such metallic complexes let the intramolecular redox processes take place. Under irradiation, energy of the photons is absorbed and the complex gets excited. In the excited state, the metal and ligand are likely to undergo redox reactions. Deactivation of the excited state leads to either transfer of charge from ligand to metal (LMCT), liberating reduced metal and oxidized ligand, or to regeneration of the initial complex by non-redox radiation.

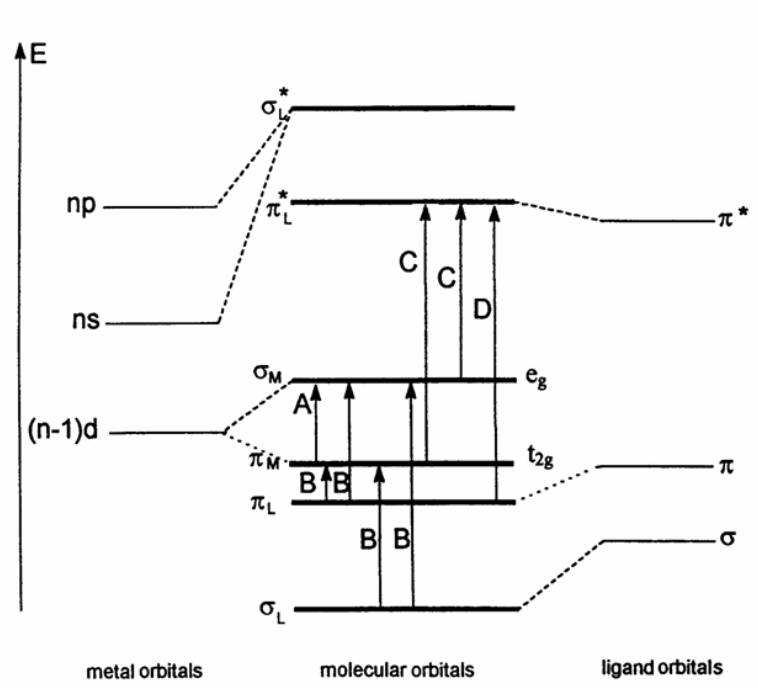

Fig. II.B.1: Energetic diagram of a transition metal complex. A – d-d ligand field transitions, B and C – ligand to metal charge transfer transitions, D – intra-ligand transitions.

The efficiency of the hydroxyl radical formation depends on the speciation of Fe(III) and on the wavelength of irradiation. This efficiency is often represented by a *quantum yield*, which is defined as a ratio of transformed molecules to all absorbed photons. In the following table, the efficiencies of hydroxyl radical's formation are expressed by such quantum yields values.

Fe(III) aquacomplex	λ_{irr} [nm]	$\Phi_{\bullet OH}$	Reference
Fe^{3+}	254	0.065	Langford and Carrey, 1975
	< 300	~ 0.05	Benkelberg and Warneck, 1995
$Fe(OH)^{2+}$	280	0.31	Benkelberg and Warneck, 1995
	300	0.19	Benkelberg and Warneck, 1995
	313	0.14	Baxendale and Magee, 1955
	373	0.065	Benkelberg and Warneck, 1995
$Fe(OH)_2^{+}$	280	0.30	Benkelberg et al., 1991
	360	0.071	
$Fe_2(OH)_2^{4+}$	350	0.007	Langford and Carrey, 1975

Table II.B.1: Quantum yields of hydroxyl radical formation for different Fe(III) species.

The **Table II.B.1** shows that the monomer complexes $Fe(OH)^{2+}$ and $Fe(OH)_2^{+}$ are the most photoactive species in forming the hydroxyl radicals, the other species of Fe(III) also form the hydroxyl radicals but with lower quantum yields. It should be noticed that at pH = 5, where the concentration of the species $Fe(OH)_2^{+}$ begins to be important, relatively fast precipitation of ferric hydroxide occurs and the source of hydroxyl radicals dries out rapidly. The differences in photoactivity implies the importance of good knowledge of Fe(III) speciation in aquatic solution; for hydrolysis of iron(III) see previous chapter.

The **Table II.B.1** also shows that the efficiency of hydroxyl radical formation depends on the irradiation wavelength. The quantum yield of hydroxyl radical formation increases with diminution of the irradiation wavelength. For a shorter wavelength of the light, the energy of a photon is higher. This is in accordance with the fact that the release of hydroxyl radical from the cage needs an amount of energy additional to the energy needed for the electronic transfer. This excess of energy increases with the decrease of wavelength, so the photodissociation of Fe(III) complex creating the hydroxyl radicals is more efficient at lower wavelengths.

During the irradiation of solutions of aquacomplexes of Fe(III), the redox process leads to formation of iron in ferrous oxidation state. In **Table II.B.2** the quantum yields of Fe(II) formation are gathered at different wavelengths of irradiation and different chemical composition of the solutions. The percentage of the monomer complexes is another parameter that should be taken into consideration. It is defined as a ratio of concentration of monomer complexes to total concentration of Fe(III).

	λ_{irr} [nm]	$\Phi_{Fe(II)}$	Reference
$Fe_2(OH)_2^{4+}$	350	0.010	Langford and Carey, 1975
$Fe(OH)^{2+}$	313	0.140	Faust and Hoigné, 1990
Presence of $^{\bullet}OH$ scavenger	360	0.017	
$[Fe^{III}]_0 = 1\times10^{-4}$ mol.L^{-1}	313	0.080	Mazellier et al., 1997/21
92 % $Fe(OH)^{2+}$	360	0.055	
$[Fe^{III}]_0 = 1\times10^{-4}$ mol.L^{-1}	313	0.020	Mazellier et al., 1997/21
10 % $Fe(OH)^{2+}$	365	0.008	

Table II.B.2: Quantum yields of Fe(II) formation for different solutions of Fe(III).

This table confirms that the efficiency of the process of Fe(II) formation is strongly dependent on both speciation of Fe(III) and the wavelength of irradiation as well.

The degradation of pollutants in aqueous phase photoinducted by Fe(III) aquacomplexes have been widely studied in the last 15 years. Various pollutants have been used, especially herbicides of triazine (***Krýsová et al., 2003***) and phenylurea group (***Poulain et al, 2003; Mazellier et al. 1997/49***), tenzides (***Brand et al., 1998***), derivates of benzene (***Mailhot et al. 2003***) and phenolic derivates (***Kawaguchi et al., 1994***). These studied molecules are generally not photochemically degraded directly by solar light ($\lambda > 300$ nm).

For these different molecules, the primary step of their degradation is common: formation of hydroxyl radicals which attack the pollutants at different sites according to their chemical structure.

II.B.2 Role of Fe(II) in the processes of degradation

The principal role Fe(II) in the photoinduced processes in aquatic media is based on the Fenton reaction. The reaction of Fe(II) with hydrogen peroxide, in oxygenated solution, could provide an additional source of hydroxyl radicals.

$$Fe^{II} + H_2O_2 \longrightarrow {}^{\bullet}OH + OH^- + Fe^{III} \qquad k = 53\ L.mol.s^{-1}$$ (***Barb et al., 1957***)

Hayon and Weiss (1960) also reported reaction of Fe^{II} in an aquatic oxygenated solution upon irradiation at 254 nm, leading via electron transfer to formation of superoxide anion.

$$Fe^{II} + O_2 \xrightarrow{h\nu} Fe^{III} + O_2^{\bullet -}$$

Despite low absorbance below 300 nm, it was described that this process could occur under our experimental conditions (***Catastini et al., 2002***). The superoxide radical can recombine with its protonated form, hydroperoxide radical (pKa = 4.8), to give molecular oxygen and hydrogen peroxide:

$$HO_2^{\bullet} + O_2^{\bullet -} + H_2O \longrightarrow H_2O_2 + O_2 + OH^-$$

$k = 9.7 \times 10^7\ L.mol^{-1}.s^{-1}$ (***Christensen and Sehested, 1988***)

Hydrogen peroxide can be also formed by recombination of hydroperoxide radicals:

$$HO_2^{\bullet} + HO_2^{\bullet} \longrightarrow H_2O_2 + O_2 \qquad k = 8.3 \times 10^5\ L.mol^{-1}.s^{-1}$$

Oxidation of ferrous ions on ferric ions by the intermediates of hydroxyl and hydroperoxide radicals is supposed. In both cases, the Fe^{III} is generated.

$$Fe^{II} + {}^{\bullet}OH \longrightarrow Fe^{III} + OH^{-}$$

$k = 3 \times 10^{8}$ L.mol^{-1}.s^{-1} (***Stuglik and Zagorski, 1981***)
$k = 4.6 \times 10^{8}$ L.mol^{-1}.s^{-1} (***Christensen and Sehested, 1988***)

$$Fe^{II} + HO_2^{\bullet} + H^{+} \longrightarrow Fe^{III} + H_2O_2$$

$k = 1.2 \times 10^{6}$ L.mol^{-1}.s^{-1} (***Jayson et al., 1973***)

These reactions comprise together a complex providing, under appropriate conditions, a continuous source of hydroxyl radicals, which attack the molecules of pollutant and its degradation intermediate until complete mineralization of the pollutant.

II.B.3 Photochemistry of iron oxides

As we mentioned above, the iron is the most abundant transition metal; it is also one of the most abundant element overall. However, practically all iron in the earth crust is found in the form of oxides, either hydrated or dehydrated.

The oxides and oxohydroxides of Fe(III) also undergo photochemical reactions. Formation of hydroxyl radicals during irradiation of goethite suspension (α-FeOOH) was observed by ***Cunningham et al. (1988)***. Photochemical activity of Fe(III) oxides was also reported by ***Goldberg et al (1993)*** and by ***Pehkonen et al (1995)***. ***Faust and Hoffmann (1986)*** explained the mechanism of photochemical activity of the oxides by the LCMT mechanism between the pollutant, which is adsorbed on the surface of Fe_2O_3, and the Fe(III) atom which the pollutant is attached to.

Degradation of dimethylphenol in the presence of goethite upon irradiation at 365 nm was observed by ***Mazellier and Bolte (2000)***. Surprisingly, no dissolved iron (Fe(II) or Fe(III)) was found in the solution, the degradation process was supposed to take place on the surface of goethite via the adsorption of dimethylphenol.

II.C Iron organic complexes: properties and photochemistry

The iron easily forms complexes with various ligands. The carboxylate group is one of the most common functional groups of the dissolved organic compounds present in natural waters (***Perdue and Gjessing, 1990***). The polycarboxylates are known to form strong complexes with Fe(III). The complexes of iron with organic polycarboxylic acids such as oxalate, malonate or citrate are usually very stable below the neutral pH. These acids could be found in biological systems, often participating in the transport of iron; they are also common constituents of precipitation, fog, urban and remote tropospheric aerosols, surface waters and soil solutions.

The iron equally forms complexes with synthetic polycarboxylic acids such as nitriloacetic acid (FeNTA) or ethylendiamintetracarboxylic acid (FeEDTA). Humic substances (fulvic and humic acids), natural organic polymers, are proposed to be involved for complexing Fe(III) as well.

II.C.1 Complexes of iron with organic acids

The ferric oxohydroxides and oxides are generally barely soluble under the conditions, which are typical for natural aquatic media. The concentration of Fe(III) in equilibrium with the oxohydroxides/oxides is very low. The amount of dissolved iron will increase with lower pH, and also with the presence of complexing agents such as (poly-) carboxylic acids.

The complexes of iron formed with organic ligands absorb in the visible region. ***Timberlake (1964)*** compared the complexes of Fe(III) in an excess of a carboxylic acid, the spectra are shown on **Fig. II.C.1**.

The existence of a ferric complex with a polycarboxylic acid was indicated by a spectral change, as a peak or a shoulder near 350 nm appeared in the presence of tartaric, citric, malic or lactic acid. Such complexes could undergo under irradiation (e.g. under exposure to solar light) a redox process, involving charge transfer from ligand to metal, as in the case of ferric aquacomplexes. As the complexes absorb in the visible range, they could be photoexcited by a solar light.

Spectra corresponding to other acids (tricarballylic and succinic) indicate very weak or almost none complexation of the acids to Fe(III).

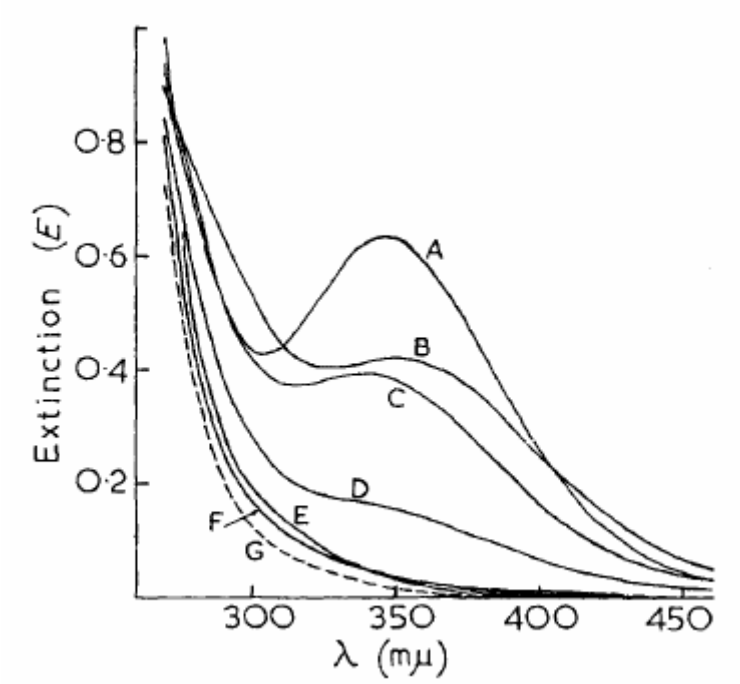

Fig. II.C.1: ***Timberlake (1964)***: spectra of mixture of ferric perchlorate and (poly-)carboxylic acids at pH = 1.51; A-tartaric acid, B-citric acid, C-malic acid, D-lactic acid, E-tricarballylic acid, F-succinic acid, G-without organic acid; [carb. acid] = 0.01 mol.L^{-1}, [Fe(III)] = 4.24×10^{-4} mol.L^{-1}]; mμ is equal to nm, extinction (*E*) refers to absorbance.

Ferric citrate complex

Citric acid is a natural compound present in plants and soils. It is a transporting agent of Fe(III) in biological systems (***Milewska, 1988***); it also helps to prevent the hydrolysis and precipitation of Fe(III) in the aquatic environment. The citrate is, together with isocitrate, an important intermediate in carbohydrate metabolism (***Glusker, 1980***). It is used in the food industry as a conserving agent or in soft drinks production; it is also employed as a reducing agent in photolytic and photocatalytic systems. Besides, its ability to complexate the various transient metals is used in detergents in order to separate the metals from cleaned surface (***Field et al., 1974***), in actinides separation, and further in extraction of toxic metals and radionuclides from various solid wastes, such as sediments, sludge and contaminated soils (***Dodge and Francis, 1997***).

The Fe(III) is easily complexed by citric acid; on the contrary, the complex of Fe(II) and citrate is much less stable (***Hamm et al., 1954; Martell and Smith, 1974***). Despite numerous studies, the structure and stoichiometry of ferric citrate complex in aqueous media was not completely revealed yet. Among the first attempts, ***Bobtelsky and Jordan (1947)*** proposed a structure corresponding to an iron to citrate ratio 2 : 3 for the solutions with an

excess of trisodium citrate. For the solutions with an excess of ferric sulphate, the iron to citrate ratio was supposed to be reverse 3 : 2. However, the validity of the conclusion is questioned as the ferric ion and the sulphate ion form a complex.

Lanford and Quinan (1948) employed the method of continuous variations (***Job, 1928***) to find out the iron to citrate ratio 1 : 1 for the solutions with identical concentrations of ferric nitrate and citrate. A formula of the ferric citrate complex ($FeHCit^{+}$) was proposed for pH around 1. The 1 : 1 iron to citrate ratio in the ferric citrate complex at pH 3 was confirmed by ***Warner and Weber (1953)***.

Hamm et al. (1954) performed a pH titration of a 1 : 1 mixture of ferric perchlorate and citric acid and suggested existence of four differently protonated complexes, formulated as $FeHCit^{+}$, FeCit, $Fe(OH)Cit^{-}$ and $Fe(OH)_2Cit^{-2}$. The form $FeHCit^{+}$ was considered as the major form at pH < 2.0. FeCit was believed as the major form in the pH range between 2.0 and 3.0. The form of $Fe(OH)Cit^{-}$ was consider to predominate in the pH range between 4.0 and 6.0, and the form $Fe(OH)_2Cit^{-2}$ was supposed to be found at basic pH. Constants of complexation (K) of the proposed forms are given in **Tab.C.1**.

Form of complex	Constant of complexation
$FeHCit^{+}$	2.0×10^{6}
FeCit	7.0×10^{11}
$FeOHCit^{-}$	2.5×10^{9}
$Fe(OH)_2Cit^{2-}$	8.0×10^{1}

Tab. II.C.1: Constants of complexation for the different forms of ferric citrate complex (***Hamm et al, 1954***).

Timberlake (1964) calculated the constant of complexation for the ferric citrate complex in pH region between 2 and 3 ($K = 2.5 \times 10^{11}$). A questionable binuclear “dimer” complex Fe_2Cit_2 is also proposed at pH below 3 ($\log \beta_{222} = 22.17$).

Abrahamson et al. (1994) discussed the disagreement, and suggests the existence of binuclear complexes rather than mononuclear. On the contrary, ***Quici et al. (2007)*** suggested the existence of mononuclear complexes, with the support of the work of ***Field et al. (1974)***.

Nansheng (1998) observed precipitation of the ferric citrate complex above pH 10.

In solid state, six anionic polynuclear species of ferric citrate complex were identified and characterised (***Gautier-Luneau et al., 2005***). Similarly as in aqueous media, the solid ferric citrate contains several complex species, depending essentially on the iron to citrate ratio and pH.

Briefly, a disagreement exists in the structure of ferric citrate complexes in aquatic media; the question of mono- or binuclearity of the citrate complexes is to be responded.

II.C.2 Photochemistry of Fe(III)-polycarboxylate complexes

The complexes of polycarboxylic acids with Fe(III) undergo rapid photochemical transformation. ***Balzani and Carassiti (1970)*** shown that the nature of ligand has an important impact at the complex photoactivity. The α-hydroxycarboxylic acids (e.g. malic or citric acid) are particularly susceptible to these redox decarboxylation reactions (***Benett et al., 1982***):

$$Fe(III)(RCH(OH)COO^{-})^{2+} \longrightarrow Fe(II) + RCHO + CO_2$$

The oxalate, the simplest polycarboxylic acid, has de facto two α-hydroxycarboxylic groups; this explains the enormous photoactivity of ferric oxalate complex. The quantum yields are very high: upon irradiation at 365 nm, the quantum yield of Fe(II) formation was 1.21 in acid pH (***Hatchard and Parker, 1956***) and 1.14 in neutral solutions (***Livingston, 1940***). The reason of such outstanding values of quantum yields ($\phi_{Fe(II)} > 1$) is in a series of consecutive reactions forming Fe(II). The impact of irradiation wavelength was observed as well; the quantum yield increases with decreasing of wavelength, as in the case of iron aquacomplexes.

After irradiation, the ferrioxalate complex undergoes intramolecular photoredox process by the LMCT mechanism, leading to formation of Fe(II) and radical species $C_2O_4^{\bullet -}$ and $CO_2^{\bullet -}$ (***Parker and Hatchard, 1959; Cooper and DeGraff 1971, 1972***). In fact, the $C_2O_4^{\bullet -}$ is quickly decomposed to $CO_2^{\bullet -}$ and CO_2 (***Mulazzani et al., 1986***):

$$C_2O_4^{\bullet -} \longrightarrow CO_2^{\bullet -} + CO_2$$

The formed radicals $C_2O_4^{\bullet -}$ and $CO_2^{\bullet -}$ reduce other molecule of ferrioxalate complex or react with dissolved oxygen:

$$C_2O_4^{\bullet -} + O_2 \longrightarrow 2CO_2 + O_2^{\bullet -}$$

$$CO_2^{\bullet -} + O_2 \longrightarrow CO_2 + O_2^{\bullet -}$$

The superoxide radical can recombinate with its protonated form, following the reactions mentioned in chapter II.B.2, forming hydrogen peroxide.

The global reaction mechanism of ferrioxalate photodegradation was resumed by ***Balzani and Carassiti (1970)***. More generalised scheme is to be found in **Fig. II.C.2**. This process is the principle of the actinometric method (***Calvert and Pitts, 1966***).

Faust and Zepp (1993) studied the photochemical properties of Fe(III) complexes with oxalate, malonate and citrate. The proposed general scheme of the photodegradation mechanism of ferric polycarboxylate complex is displayed in **Fig. II.C.2**.

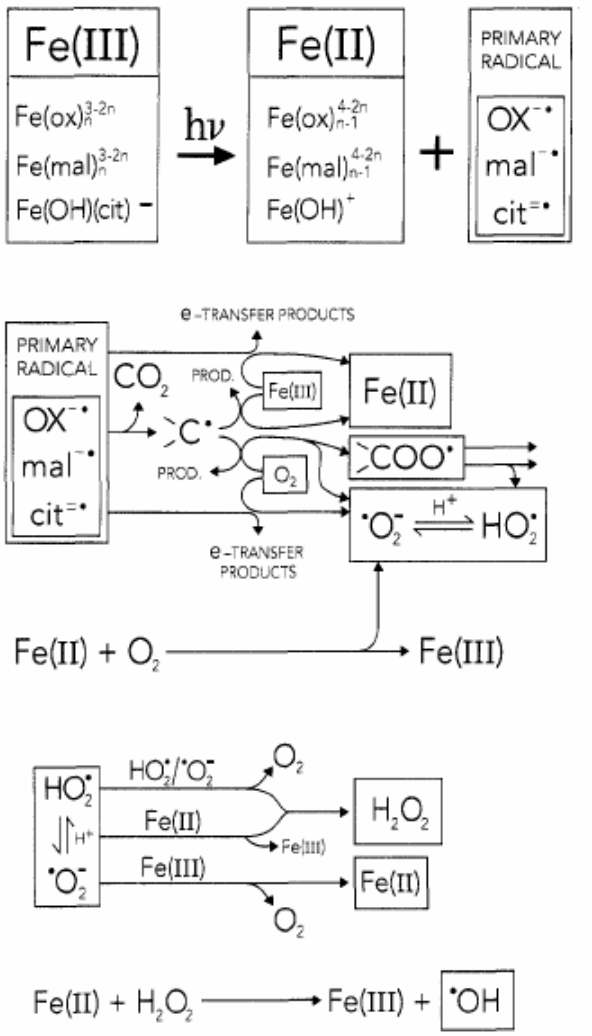

Fig. II.C.2: Photolysis of Fe(III) polycarboxylic complexes (***Faust and Zepp, 1993***).

Under irradiation, these complexes release primary radicals. The evolution of the primary radicals depends on several parameters like oxygen or Fe(II) concentration; however, the primary radical is often susceptible to undergo the decarboxylation process. The product of decarboxylation consequently reacts with molecular oxygen and gives a superoxide radical $O_2^{\bullet -}$. In compliance with the scheme we can assume, that the photodegradation process of the

ferric polycarboxylate processes together with the Fe(III)/Fe(II) cycle plays an important role in the environment.

Abrahamson et al. (1994) determined quantum yields of Fe(II) formation for different types of ferric polycarboxylate complexes at different pH's and in the absence of oxygen; irradiation wavelength was 366 nm.

Carboxylic acid (CA)	$\phi_{Fe(II)}$, CA/Fe = 5 [a]		$\phi_{Fe(II)}$, CA/Fe = 167 [b]
	pH = 2.7	pH = 4.0	pH = 2.9
Oxalic acid	0.65	0.30	0.32
L(+)-tartaric acid	0.40	0.58	
DL-tartaric acid	0.35	0.50	0.29
meso-tartaric acid	0.31	0.37	
Citric acid	0.28	0.45	0.40
DL-Isocitric acid	0.14	0.37	
L(–)-malic acid	0.21	0.29	
D(+)-malic acid	0.20	0.28	
DL-malic acid	0.20	0.29	0.26
Succinic acid			0.13
Formic acid			0.12

Tab. II.C.2: Quantum yields of Fe(II) formation for different types of carboxylate complexes of Fe(III); [Fe(III)] = 3×10^{-4} mol.L^{-1}; [a][CA] = 1.5×10^{-3} mol.L^{-1}; [b][CA] = 0.05 mol.L^{-1}; ***Abrahamson et al. (1994)***.

At pH = 2.7, the quantum yields of Fe(II) formation increased in the following order: malate > isocitrate > citrate > tartarate > oxalate. At pH = 4.0, the quantum yields increased by 50% except oxalate, where the quantum yield dropped to less than one half.

In same paper, lack of photoactivity of ferric-polycarboxylate was reported in water-free acetonitrile. Acetonitrile is a polar solvent, but it does not contain oxygen in the structure as a coordination site. This result indicates that the water presence is necessary during the photoreduction process, as it is likely to have a crucial role in the redox reaction.

II.C.3 Photochemistry of Fe(III)-amino(poly)carboxylate complexes (FeEDTA, FeNTA)

The amino(poly)carboxylic acids are synthetic products, which are widely used in the detergent production, and also in pharmaceutic, photographic and textile industry. Several works reported presence of amino(poly)carboxylic acids in industrial or home sewage, such as ethylenediaminotetraacetic acid (EDTA), cyclohexanediaminotetraacetic acid (CDTA), iminodiacetic acid (IDA) or nitrilotriacetic acid (NTA). The amino(poly)carboxylic acids do not absorb in visible region, and do not undergo the degradation by solar light in the environment. Therefore, these acids present a source of pollution for the aquatic environment (***Andrianirinaharivelo, 1992***).

Possible way of removal of the amino(poly)carboxylic acids is based on its ability of metal complexation. Formation of such a complex, e.g. with iron, will shift the absorbance to visible region; the complexes will absorb the solar light and undergo then the photoredox process (***Ogino et al., 1989; Gustavson and Martell, 1963***).

The structures and the photochemical processes observed during photoinduced degradation of Fe(III)-amino(poly)carboxylic complexes are described in the literature. The NTA is used as a substitute for the phosphates in the detergents. The NTA principally forms a complex of 1 : 1 stoichiometry with Fe(III), as described by ***Andrianirinaharivelo et al. (1993)***. The Fe(III)-NTA complex exists in two different forms, depending on the pH. A protolytic equilibrium is established between the two forms with a $pK_a = 5.5$, see **Fig.II.C.3**.

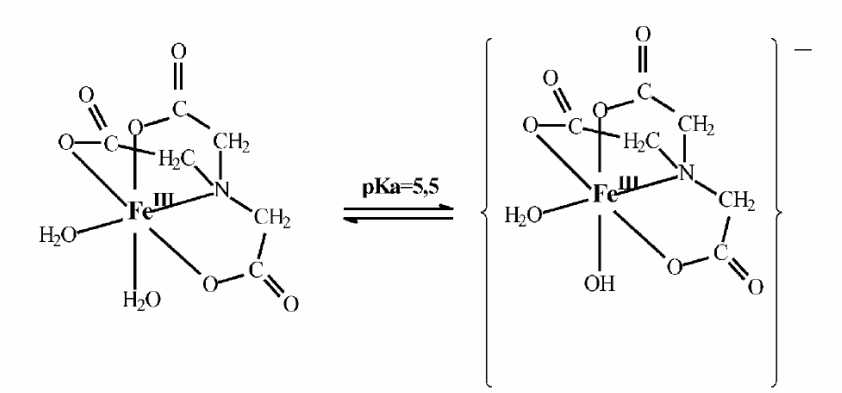

Fig. II.C.3: Protolytic equilibrium of Fe(III)-NTA complex (***Abida et al., 2006***).

In neutral media, the monohydroxylated form predominates. The irradiation of the Fe(III)-NTA complex at 365 nm results in decomplexation process. On the contrary, at shorter wavelengths (313 nm), an intramolecular photoredox process takes place, leading to Fe(II) formation and to decarboxylation of nitrilotriacetate (***Andrianirinaharivelo et al., 1993***).

In acidic media, ***Andrianirinaharivelo et al. (1993)*** observed that the photoredox process depends on the irradiation wavelength. Upon irradiation at 365 nm, the neutral form of complex leads to intramolecular photoredox process between Fe(III) and NTA. At shorter wavelengths, the photoredox reaction involves a process of charge transfer between Fe(III) and the oxygen atom of the complexed water molecules. However, the both processes lead to identical photoproducts: Fe(II), iminoacetic acid (IDA), formaldehyde, and CO_2. IDA is a hazardous compound as several of its forms are cancerogenous; for this reason, the studies of complete NTA mineralization are carried out with the IDA (***Mailhot et al., 1995***).

Besides, ***Andrianirinaharivelo et al. (1993)*** showed the dependence of the Fe(III)-NTA disappearance quantum yields on irradiation wavelength, as well as on pH (**Tab.II.C.3**).

λ_{exc} [nm]	ϕ_{dis} (pH = 4.0)	ϕ_{dis} (pH = 7.0)
254	0.50	0.19
296	0.40	0.18
313	0.30	0.08
334	0.22	
365	0.18	0.09

Tab. II.C.3: Quantum yields of FeNTA disappearance in function of wavelength and pH.

The quantum yields increased with shorter wavelength; lower quantum yields were observed at higher pH.

Abida et al. (2006) studied the mechanism of 4-chlorophenol degradation in presence of FeNTA complex. Short lived transients formed during the process of Fe(III)-NTA complex photodissociation were detected and identified; the two mechanisms leading to 4-CP degradation were elucidated. At longer wavelength (365 nm), a $RCO^{\bullet}$ radical is formed, resulting from intramolecular electron transfer from carboxylate group to Fe(III). 4-CP is attacked by the $^{\bullet}OH$ induced by the Fenton reaction. At shorter wavelength, the main detected radical species was $CO_3^{\bullet -}$, together with $^{\bullet}OH$. In this case, an electron is transferred from OH^- (or H_2O) to Fe(III).

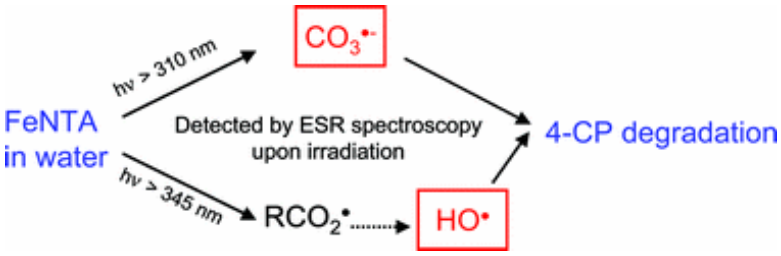

Fig. II.C.4: Scheme of FeNTA photoinduced 4-chlorophenol degradation (***Abida et al, 2006***).

II.C.4 Photochemistry of iron citrate complex

First studies of ferric citrate photoactivity were reported almost a hundred years ago (***Benrath, 1910***). The photodissolution process involved reduction of Fe(III) to Fe(II) together with oxidation of the citrate, giving acetone and carbon dioxide as final products (***Frahn, 1958; Buchanan, 1970; Krizek et al, 1982***).

Abrahamson et al. (1994), determined quantum yields of photodissociation of complex of Fe(III) with various carboxylic acids, with more detailed pH range for the complex with citrate. The quantum yields of Fe(II) formation for Fe(III)Cit complex at different citrate concentration are shown in **Fig II.C.5**.

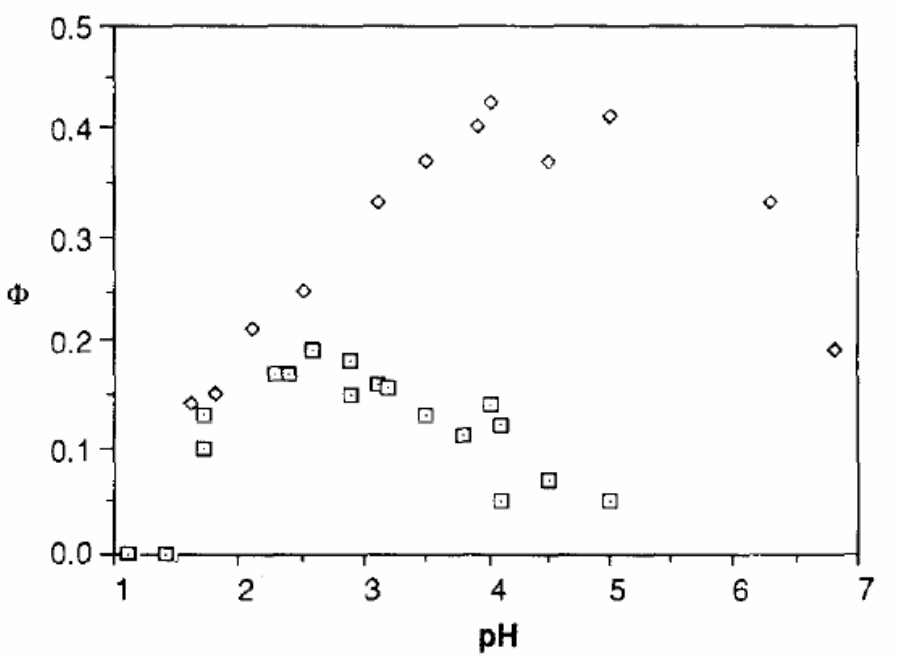

Fig. II.C.5: Comparison of the quantum yields of Fe(II) formation as a function of pH in the presence of citric acid (CA); [Fe(III)] = 3×10^{-4} mol.L^{-1}, [CA] = 1.5×10^{-3} mol.L^{-1} (◇) or 0.05 mol.L^{-1} (⊡); ***Abrahamson et al. (1994)***.

With the Fe(III) to citrate ratio 1 : 5, the highest quantum yields were observed between pH = 4.0 and 5.0. In the high excess of citrate (1 : 167), the highest quantum yields are less than halved, an they are found at lower pH between 2.5 and 3.0. The quantum yield is dependent on the speciation of the complex. The speciation depends, besides pH, on the ligand concentration; in the excess of ligand, more complicated complexes are formed. ***Abrahamson et al. (1994)*** proposed existence of photoactive ferric citrate dimer, which is formed above pH 2.0, and a photo-inactive monomer, present between pH 0.5 and 3.0.

Nansheng et al (1998) studied the degradation of five colorants (C.I. reactive red 2, C.I. reactive blue 4, C.I. reactive black 8, C.I. basic red 13, C.I. basic yellow 2) photoinduced by ferric citrate in aquatic solution at pH = 2.0, λ_{irr} = 313 nm. During the irradiation, the photolysis led to formation of very reactive radical species, which induced the colorant degradation.

A study of various ratios of Fe(III) and citrate concentrations in the initial solution were carried out. The mixtures with Fe(III) to citrate ratios higher than 1 : 1 presented lower rate of colorant disappearance; on the contrary, the highest rate was achieved at 1 : 4 Fe(III) to citrate ratio; [Fe(III)] = 1×10^{-4} mol.L^{-1}. Impact of pH on degradation of colorant (C.I. reactive red) was equally followed (**Fig II.C.6**).

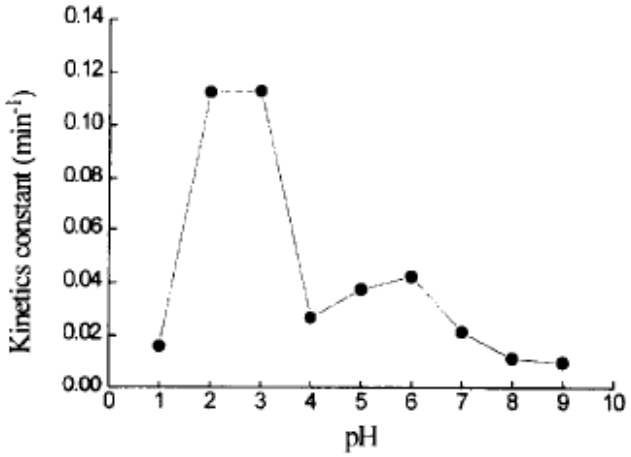

Fig. II.C.6: Impact of pH on the rate of colorant degradation, photoinduced by ferric citrate; [Fe(III)] = 1×10^{-4} mol.L^{-1}, [CA] = 2×10^{-4} mol.L^{-1}; ***Nansheng et al. (1998)***.

The degradation was highest at pH 2.0 and 3.0; the impact of ferric citrate complex speciation was indicated.

Abrahamson et al. (1994) also observed that photoirradiation of ferric citrate produced Fe(II) and a stable intermediate acetonedicarboxylic acid (ADCA; also known as β-oxoglutaric acid). However, more detailed study was not published yet:

$$Fe(III)Cit + h\nu \longrightarrow \longrightarrow Fe(II) + ADCA$$

The ultimate decarboxylation product of ferric citrate photodissociation was acetone.

II.D TiO_2 as a photocatalyst

In 1972, when ***Fujishima and Honda (1972)*** reported water dissociation at titanium dioxide (TiO_2) electrodes, a new field of research concerning TiO_2 application emerged. In 1976, ***Carey et al. (1976)*** observed degradation of polychlorined biphenyls (PCB) in a TiO_2 upon irradiation by UV light. Since then, lots of research works on degradation of different pollutants employing TiO_2/UV system were published, as well as the elementary studies of the mechanism of degradation.

II.D.1 Physico-chemical properties

Titanium dioxide exists primarily in three natural crystalline forms: anatase, rutile and brookite. Besides, other forms of TiO_2 could be synthesized under high pressure.

In presence of water, the surface of TiO_2 is covered by hydroxyl groups (***Augustynski, 1988; Parfitt 1976***). Water is bound at the TiO_2 surface, either in molecular or dissociated form, where following interactions take place:

$$Ti^{IV} + H_2O \rightleftharpoons Ti^{IV} - H_2O$$

$$Ti^{IV} - H_2O + >O_L^{2-} \rightleftharpoons Ti^{IV} - OH^- + O_LH^-$$

Ti^{IV} corresponds to surface titanium atom, O_L represents the oxygen from original external layer. Two different types of hydroxyl groups formed at the TiO_2 surface were described by ***Turchi and Ollis (1990)***. ***Boehm and Herrmann (1967)*** determined the density of OH/nm^2 equal from 5 to 15 (OH^- and OH from H_2O), corresponding to total coverage of TiO_2 particles by hydroxyl group or water molecules.

The oxides of titanium present amphoteric behaviour in water media.

$$>TiOH + H^+ \overset{pK_{a1}}{\rightleftharpoons} >TiOH_2^+$$

$$>Ti - OH \overset{pK_{a2}}{\rightleftharpoons} >TiO^- + H^+$$

The equilibrium constants for TiO_2 P25 were determined by ***Korman et al. (1991)***: $pK_{a1} = 4.5$ and $pK_{a2} = 8.0$. These results lead to value of pH zero charge at pH = 6.25; at this pH, the total charge of the TiO_2 surface is neutral.

II.D.2 Photochemical properties

In the semiconducting materials, the valence and conduction bands are separated by an energy band gap, which is in the order of electron volts. An electron could be, after absorption of certain amount of energy, excited from the valence to conduction band.

The initial process of heterogeneous photocatalysis at TiO_2 is induced by absorption of a photon by a particle of TiO_2; if the energy of the photon is sufficient, an electron-hole pair is generated for a short period of time. Part of the electron-hole pairs gets recombined and the energy is dissipated in a non-radiating form (e.g. heat). Other part of these pairs can be trapped at the surface in metastable states on the surface. Finally, remaining part of the electron-hole pairs undergoes reactions with electrons donors or electrons acceptors, which are adsorbed on the surface or present in the double layer of the charged TiO_2 particles. The scheme is shown in **Fig. II.D.1**.

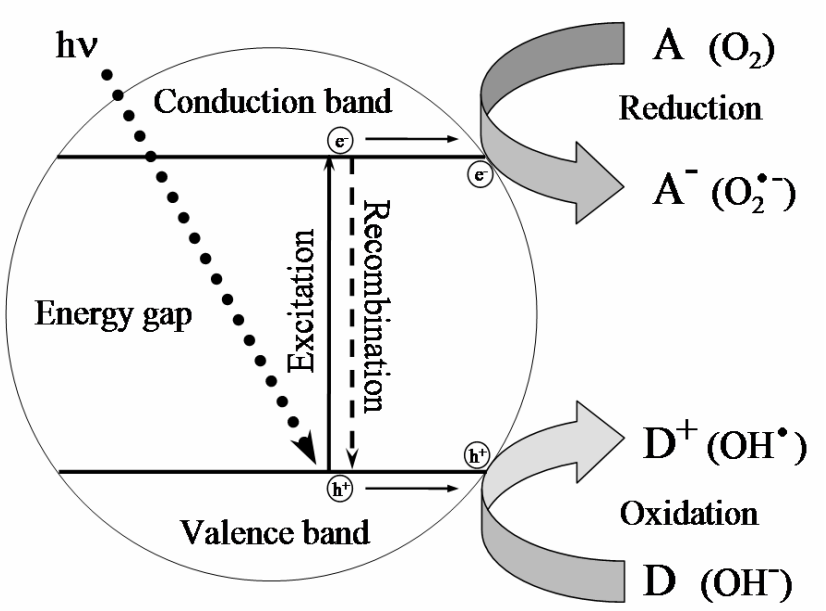

Fig. II.D.1: Elementary processes taking place after irradiation of a semiconductor.

The hole on the surface can oxidize surface OH groups, generating $^{\bullet}OH$ radicals. The electron on the surface is consumed by reduction of dissolved molecular oxygen. As already mentioned in the chapter II.B.2, the $^{\bullet}OH$ radicals are able to oxidize practically all organic molecules present in the system, e.g. the organic pollutants.

The reactivity of a semiconductor is defined by the energy of transition at certain wavelength. The transition energy for the anatase is 3.23 eV (corresponding to 384 nm); for the rutile it equal to 3.02 eV (corresponding 411 nm) (***Rajeshwar, 1995***).

II.D.3 Mechanism of TiO_2 photocatalysis

A general mechanism for heterogeneous photocatalysis at TiO_2 was described basing on the results of laser photolysis (***Hoffmann et al., 1995***). Following processes taking place are shown with the required times:

Generation of charge carriers

$TiO_2 + h\nu \longrightarrow h_{vb}^{+} + e_{cb}^{-}$ very fast [several fs]

Trapping of charge carriers

$h_{vb}^{+} + >Ti^{IV}OH \longrightarrow \{ >Ti^{IV}OH^{\bullet} \}^{+}$ fast [10 ns]

$e_{cb}^{-} + >Ti^{IV}OH \longleftrightarrow \{ >Ti^{III}OH \}$ surface trapping [10 ps]

$e_{cb}^{-} + >Ti^{IV} \longrightarrow >Ti^{III}$ (irreversible) internal layers trapping [10 ns]

Recombination of charge carriers

$e_{cb}- + \{ >Ti^{IV}OH^{\bullet} \}^{+} \longrightarrow \{ >Ti^{IV}OH \}$ slow [100 ns]

$h_{vb}+ + \{ >Ti^{III}OH \} \longrightarrow Ti^{IV}OH$ fast [10 ns]

Transfer of charge to the interface

$\{ >Ti^{IV}OH^{\bullet} \}^{+} + Red \longrightarrow >Ti^{IV}OH + Red^{\bullet +}$ slow [100 ns]

$e_{tr}^{-} + Ox \longrightarrow >Ti^{IV}OH + Ox^{\bullet -}$ very slow [ms]

(e_{tr}^{-} corrensponds to electron trapped at the TiO_2 surface)

The holes in the valence band possess high oxidation power. The potential is from 1 to 3.5 V (vs. NHE), depending on the semiconductor and pH; the electrons excited in the conduction band have strong reductive ability with a potential from 0.5 to –1.5 V (vs. NHE) (***Grätzel, 1989***). The oxidation potential of numerous molecules is lower than the potential of valence band, thus the molecules could be oxidised directly by the reaction with the holes on the surface of the semiconductor; this ability is used for the degradation of the pollutants.

Trapping of charge carriers

After its generation, the electron and the hole migrate to the surface. The migration is very fast, even in relatively large particles like Degussa P25, where the migration time is of the order of 10 picoseconds (***Hufschmidt et al, 2004***). The electrons are trapped by two different sites: at the surface with a dynamic equilibrium $Ti^{IV/III}$ or irreversibly in the volume

of the particle, giving Ti^{III}. The mechanism of hole trapping is has not well explained yet. Earlier works proposed forming of weakly adsorbed hydroxyl radicals by reaction of hydroxyl groups on the surface. Recently, several theories oppose with making difference between the holes trapped at the subsurface by oxygen anion or by the oxygen radical on the surface of TiO_2 particles. The trapping by the hole is analogous to electron trapping process, undergoing reversible or irreversible way.

The principal oxidant formed at the surface is the hydroxyl radical. The hydroxyl radicals can be formed at the surface by oxidation of water molecules or surface hydroxyl anions by holes trapped at the surface. The oxidation can proceed, when the redox potential of the reaction is lower to the potential of the semiconductor valence band. The potential of anatase valence band is equal to +2.6 V (vs. NHE) for neutral pH, and varies by – 0.059 by pH unit. The potentials of hydroxyl radical formation are thus lower than the valence band potential of anatase for all pH. The reaction of $Ti^{IV}OH$ with holes will be favoured in basic pH, as the hydroxyl radical formation by water oxidation will be predominant in acidic solutions.

The existence of hydroxyl radicals was confirmed by ESR spectroscopy. It was equally shown, that the majority of primary products in the system are hydroxylated molecules.

The superoxide radical is the other important radical, formed by the reaction of oxygen with electron:

$$O_2 + e^- \longrightarrow O_2^{\bullet -}$$

The superoxide radical is less reactive, but it could attack some of the other molecules adsorbed at the surface. It could also be a source of hydroxyl radicals via the formation of hydrogen peroxide (***Bielski and Allen, 1977; Izumi et al., 1981; Sawyer and Gibial, 1979; Munuera et al., 1979***).

$$O_2^{\bullet -} + H^+ \rightleftharpoons HO_2^{\bullet} \qquad pK_a = 4.74$$

$$2\ HO_2^{\bullet} \longrightarrow H_2O_2 + O_2 \qquad k = 7.6 \times 10^5\ L.mol^{-1}.s^{-1}$$

$$HO_2^{\bullet} + O_2^{\bullet -} \longrightarrow HO_2^- + O_2 \qquad k = 8.5 \times 10^7\ L.mol^{-1}.s^{-1}$$

$$HO_2^- + H^+ \longrightarrow H_2O_2 \qquad pK_a = 1.5 \times 10^{-12}$$

The hydrogen peroxide is a source of hydroxyl radical, indeed, either by direct photolysis or reductive attack:

$$H_2O_2 + h\nu \longrightarrow 2\ {}^{\bullet}OH$$

$$H_2O_2 + O_2^{\bullet -} \longrightarrow {}^{\bullet}OH + O_2 + OH^- \quad k = 0.3\ L.mol^{-1}.s^{-1}$$ (***Bielski et al., 1985***)

$$H_2O_2 + e^- \longrightarrow {}^{\bullet}OH + OH^-$$

It should be noticed that the principal species taking place, the holes and the electrons, possess a slightly different regioselective properties, as reported by ***Richard (1993)***.

II.D.4 Impact factors of photocatalysic efficiency of TiO_2

In the following list, several important parameters, which can influence the efficiency of TiO2 photocatalysis, are mentioned.

Adsorption on photocatalyst surface

Numerous works showed that the degradation of various compounds by heterogeneous photocatalysis follows the Langmuir-Hinshelwood law. This model counts with the preadsorption of molecules on the surface of the photocatalyst (***Turchi et Ollis, 1990; Cunningham and Srijaranai, 1991***).

Oxygen

The absence of oxygen often leads to total inhibition of the reaction. The necessity of molecular oxygen presence is caused by its ability to participate on trapping electrons in the conduction band and prevent the electron-hole recombination as well. The reduced photocatalytical efficiency of rutile, comparing to anatase, could be also explained by lower adsorption of O_2 at rutile surface (***Lewis and Rosenbluth, 1989***).

Concentration of photocatalyst

The efficiency of the reaction also depends on the amount of the photocatalyst in the system, especially at its lower concentration. When increasing the concentration of the photocatalyst, since certain value where no additional positive effect on the reaction efficiency will be achieved. At very high concentrations of the photocatalyst, a shielding effect is observed, as the photocatalyst in a space further from the irradiation source will be prevented by the layer of zero transmittance from creating reactive species at their surface.

The optimal concentration of catalyst differs for each reactor as well as for other experimental conditions.

Impact of pH

The size of TiO_2 aggregates, its surface charge and the position of valence/conduction band of TiO_2 are influenced by the pH. Due to the surface charge of TiO_2, the degradation of ionised compounds is highly affected by the pH. In the system with pH higher than pH_{PZC}, the interactions with the cationic electron donors/acceptors are preferred and vice versa for lower $pH < pH_{PZC}$. A decrease of photocatalytic activity could be observed close to pH_{PZC}; as the electrostatic repulsion between the TiO_2 particles is minimal, the TiO_2 particles tend to agglomerate. The agglomerates prevent the diffusion of light in the solution and decrease the photocatalytic activity. The position of valence/conduction bands, and consequently reaction progress, are also influenced by the pH, as mentioned in the preceding chapter.

However, the differences in speed are often minimal, and the majority of studied non-ionic molecules present degradation rates of same order.

Effect of temperature

The photocatalytical reactions are not influenced by the temperature changes. On the contrary, the adsorption/desorption equilibriums and the migration to surface are temperature-dependent. In the photodegradation mechanisms, these processes are not the limiting steps for the reaction rate, and its impact is very low. However, the temperature can influence the following degradation rates and thus global efficiency of the degradation.

Presence of inorganic ions

Inorganic ions are always present in waters; they could be formed during the degradation process as well. Adsorption of the anions on the TiO_2 surface prevents adsorption of other molecules. Moreover, the presence of ions on the photocatalyst surface can lead to forming of polar environment around the particles, which can prevent the diffusion of other molecules to the surface of the photocatalyst.

The inorganic ions could also consume the hydroxyle radicals, forming less reactive radicals, like the carbonate (***Legrini et al., 1993***), or more reactive radicals. For example, by the reaction with hydroxyl radicals, the sulphate ions can form sulphate radicals, which are also capable to attack other molecules or creating hydroxyl radicals. The anions like I^- or Br^-

could react with the surface holes, thus preventing the recombination and favours the reduction reactions on the photocatalyst surface (***Herrmann and Pichat, 1980***).

Intensity of irradiation

Impact of irradiation intensity on the rate of pollutant degradation was studied by several research teams. At low intensity, the degradation rate is directly proportional to irradiation intensity; for moderate flux, the reaction rate is proportional to no more than square root of light intensity; $k = f(I)^{0.5}$. At high intensities of irradiation, constant value of reaction rates are observed, as other parameters became to be the limiting factors.

Crystalline structure of TiO_2

The anatase is generally considered as more efficient crystalline TiO_2 form than the rutile for the photocatalytic degradation for majority of the pollutants (***Ohtani and Nishimoto, 1993; Karakitsou and Verykios, 1993***); moreover, the rutile is not able to degrade certain pollutants (***Mills et al., 1993***). However, ***Doménech et al. (1993)*** observed noticeably higher efficiency of cyanate degradation by rutile than by anatase.

Tanaka et al. (1993) examined the impact of methods of TiO_2 preparation on the photocatalytical activity, e.g. temperature of calcination or specific surface. However, higher specific surface has not always positive effect on the photocatalytic activity. ***Kolář et al. (2006)*** observed decreased rates of 4-chlorophenol degradation in a solution containing colloidal Q-TiO_2 (quantum-sized) particles of lower size. Small size of the Q-TiO_2 particles (< 10 nm) led to increased electron-hole recombination, and lower photocatalytic activity. ***Ohno et al. (2001)*** reported synergic effect of anatase-rutile mixture (Degussa P25) on naphthalene degradation, comparing to the separate use of anatase or rutile.

II.E Combined system: TiO_2 + iron

One of the ways to ameliorate the photodegradation efficiency in the suspensions of semiconductors is the addition of electron acceptors in the system. The electron acceptors increase the efficiency of a photocatalyst by hindering the electron-hole recombination. The electrons consumed by the acceptor can not recombinate with the holes, which are then the source of hydroxyl radicals. The possible electron acceptors must fulfil the condition of having lower potential of redox reaction to the Fermi band of TiO_2. Among the possible acceptors, oxygen, hydrogen peroxide and transition metals could be found.

Several works reported positive effect of transition metals; more attention was given to copper and iron (***Fujihira et al., 1982; Okamoto et al., 1985; Wei et al., 1990***). Influence of different dissolved transition metals (Mg^{2+}, Ni^{2+}, Zn^{2+}, Mn^{2+}, Co^{2+}, Cu^{2+}, Cr^{3+} and Fe^{3+}) on the degradation of phenols in the suspension of TiO_2 (Degussa P25) was studied by ***Brezová et al. (1995)***. No effect was observed in presence of Ca^{2+}, Mg^{2+}, Zn^{2+} and Ni^{2+}. For the other cations, more or less positive effect was observed.

Numerous studies showed an increase of pollutant degradation rate in TiO_2 suspension and in presence of ferric/ferrous ions. The impact of ferric ions as electron acceptor was also studied for water oxidation in TiO_2 suspension (***Ohno et al., 1997; Bamwenda et al., 2001***). In the absence of electron acceptors, no oxygen production in irradiated TiO_2 suspension was observed. When Fe(III) was added in the suspension, an evolution of oxygen and Fe(II) was observed. The concentration of formed Fe(II) was in stoichiometric ratio with formed oxygen: 1 mol O_2 for 4 mol of Fe(II), which corresponded to four changed electrons.

Unusual phenomenon was observed in the system: almost no reoxidation of Fe(II). This unique effect was explained by the adsorption properties of Fe(III) and Fe(II) on the TiO_2 surface. The adsorption of Fe(II) is much weaker in comparison to Fe(III). The adsorption isotherms showed that even in the mixture containing an excess of Fe(II), the amount of adsorbed Fe(II) is negligible compared to the adsorbed Fe(III). This result indicates that the ferrous cations formed at the TiO_2 surface are quickly replaced by the ferric cations. Due to its weak adsorption, the reoxidation of ferrous ions on the TiO_2 surface is negligible. The oxidation capacity remained available for the water to produce the oxygen; however this reaction was less favourable thermodynamically.

Sclafani et al. (1991) also studied the system of TiO_2 combined with ferric and ferrous cations, using phenol as pollutant. No significative increase of phenol degradation efficiency in presence of Fe(III)/Fe(II) was observed in the rutile suspension comparing to the anatase suspension. A notable difference between two crystalline phases was in the adsorption of oxygen, which was very weak on the surface of rutile, on the contrary to anatase. The amount of peroxide species ($HO_2^{\bullet}$, H_2O_2) was thus found negligible in the rutile suspension. The difference between the two phases of TiO_2 will be on the level of following decomposing reactions of peroxide type compounds. The production of hydrogen peroxide is increased by following reaction:

$$Fe^{2+} + HO_2^{\bullet} + H^+ \longrightarrow Fe^{3+} + H_2O_2 \qquad k = 1.2 \times 10^6\ L.mol^{-1}.s^{-1}$$ (***Bielski et al., 1985***)

Fe^{2+} plays also an important role in hydroxyl radicals formation (Fenton reaction):

$$Fe^{2+} + H_2O_2 + H^+ \longrightarrow Fe^{3+} + {}^{\bullet}OH + H_2O \qquad k = 53\ L.mol^{-1}.s^{-1}$$ (***Dunford, 2002***)

In absence of Fe(III)/Fe(II), the hydrogen peroxide is consumed by the reaction with electron in the valence band producing hydroxyl radical:

$$H_2O_2(ads) + e_{cb}^- \longrightarrow {}^{\bullet}OH + OH^-$$

However, the reaction is slower than the Fenton reaction (above). Hence, in the case of anatase, where the adsorption of oxygen is higher, the presence of iron in the solution will play an important role, not only to hinder the electron-hole recombination, but will also help to decompose the hydrogen peroxide, which is an additional source of hydroxyl radicals.

II.E.1 Impact of pH

Butler and Davis (1993) studied the impact of pH on toluene degradation in TiO_2 (anatase) suspension in presence of Fe(III) upon irradiation at 365 nm. The concentration of TiO_2 was $2\ g.L^{-1}$, the concentration of Fe(III) was $1 \times 10^{-5}\ mol.L^{-1}$, pH was adjusted by sulphuric acid. Maximal rate was achieved at pH = 3.0. The effect of pH was not clearly explained by the authors. However, with regard to the experience achieved in the Laboratory of Photochemistry, we assumed that the effect of pH was caused by iron speciation. At pH = 3.0 and under the described experimental conditions, the form of $Fe(OH)^{2+}$ is predominating in the solution. This form is the most photoactive in the redox or photoredox processes, its presence at high concentration can explain the results of ***Butler and Davis (1993)***.

II.E.2 Impact of Fe(III) concentration

All over the works found in the literature, a negative effect was found for higher concentrations of iron. Too high quantity will hinder the formation of peroxide species as the Fe(III) will consume high proportion of electrons and the formed ferrous cations will consume all the holes or formed hydroxyl radicals. This is so called shortcut presented by ferric/ferrous couple on the TiO_2 particle. Moreover, too high concentration of iron will cause notable increase of the absorbance mixture. The increase of absorption caused by iron will have a shielding effect on the TiO_2 particles. This will result in lower amount of photons, which reach the surface of TiO_2, and less reactive species will be released. The optimal concentration varies between 1×10^{-5} and 5×10^{-3} $mol.L^{-1}$ of Fe(III), depending on the geometry of reactor.

Moreover, it should be also noted that the pH (and thus the speciation of present ferric salt), type of used TiO_2 and the nature of the pollutant will influence in the kinetics of pollutant disappearance. With the contemporary results, it is still impossible to predict the optimal concentration of iron to obtain the highest degradation efficiency in the combined system with TiO_2.

Klauston and Preis (2005) observed a dramatic increase of 2-ethoxyethanol degradation efficiency after addition of low amount of ferrous ions in TiO_2 suspension (Degussa P25). On the contrary, at high concentration of Fe(II), the degradation efficiency sharply decreased.

Měšťánková et al. (2005/57) compared the degradation of Monuron in presence of iron or TiO_2 suspension, and in the combined system. At lower concentrations of iron, the efficiency of combined system of TiO_2 and Fe(III) was higher than the addition of separate systems efficiencies. On the other hand, at higher concentrations of iron, the situation is reversed. Speciation and concentration of iron were among the most important factors influencing the Monuron degradation efficiency, as well as the number of absorbed photons by each photocatalyst.

Similar comparison was also performed with TiO_2 fixed on a layer (***Měšťánková et al., 2005/58***).

The scheme of important interactions in the combined system iron-TiO_2 is shown in **Fig II.E.1**.

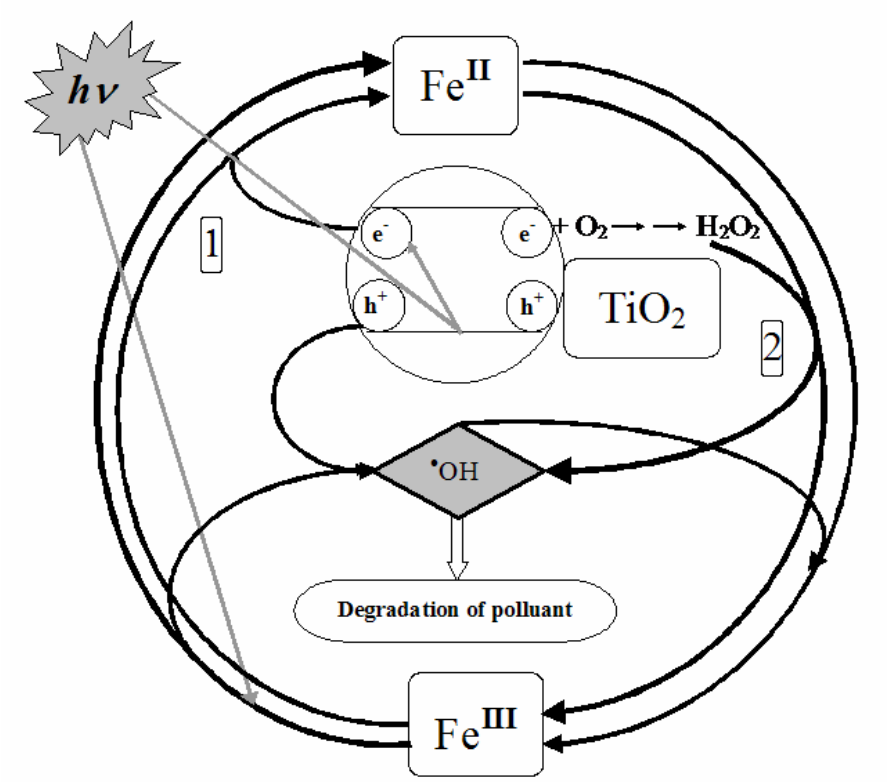

Fig. II.E.1: Scheme of the most important interactions between TiO_2 and iron: [1] Interaction of Fe(III) with electrons photogenerated at TiO_2 surface, [2] Reactions of Fe(II) to Fe(III) reoxidation intermediated by the oxidative species ($HO^{\bullet}$, $O_2^{\bullet -}$, $HO_2^{\bullet}$, H_2O_2) formed at TiO_2 surface.

The process reaction of ferric cations with electrons at TiO_2 surface followed by creation of h^+ and $^{\bullet}OH$ was concluded to be less efficient than the direct formation by photodissociation of $Fe(OH)^{2+}$. Moreover, the reaction of Fe(III) with the electrons on the surface of TiO_2 is detrimental for the photochemical activity of monomer complexes $Fe(OH)^{2+}$. However, a positive impact of reaction 1 on the Monuron degradation was observed in the presence of Fe(III) aggregates. These species could be slowly reduced to Fe(II), which can be then oxided to more photoactive Fe(III) species.

As it was mentioned in the chapter II.B.2, the hydroxyl radicals can be also formed from hydrogen peroxide in the TiO_2 suspension. In presence of Fe(II), the formation of hydroxyl radicals from H_2O_2 is increased by the Fenton reaction:

$$Fe^{II} + H_2O_2 \longrightarrow {}^{\bullet}OH + OH^- + Fe^{III} \qquad k = 53\ L.mol^{-1}.s^{-1}$$

Furthermore, the reoxidated Fe(III) is formed, which is also a source of hydroxyl radicals. In the systems without TiO_2 and with low concentration of Fe(III), the disappearance

of pollutant could be slowed down in some time, due to relatively slow reoxidation of Fe(II) to Fe(III) by oxygen. If the TiO_2 is added, the Fenton reaction will accelerate the reoxidation of Fe(II), which is the limiting process of pollutant photodegradation by iron complexes, as well as the process of $^{\bullet}OH$ creation. Thus, the Fenton reaction is the key reaction of the combined system.

Quici et al. (2007) studied the impact of Fe(III) addition on degradation of citric acid by TiO_2 under irradiation at 366 nm. Concentration of TiO_2 suspension was 1 $g.L^{-1}$, and concentration of citric acid was 0.024 $mol.L^{-1}$; pH was adjusted to 3.7 and was maintained constant through all the irradiation by periodical addition of $HClO_4$. In the combined system of Citrate, Fe(III) and TiO_2, the optimal ratio of Cit : Fe(III) was 1 : 1. With higher amounts of Fe(III), although the degradation of citric acid was faster in the earlier part of the degradation, it almost stopped in the later stage.

In the same work, impact of H_2O_2 addition was studied. The addition of hydrogen peroxide in the combined system of citrate and TiO_2 accelerates the citrate degradation efficiency, with most notable increase of the H_2O_2 : Cit ratio of 0.1 : 1; further increase of H_2O_2 concentration does not have higher impact. In the system of citrate, TiO_2 and of Fe(III), the impact of H_2O_2 presence is even more emphasized; the optimal H_2O_2 : Cit : Fe(III) ratio was found as 1 : 1 : 1.

II.F Competitive photocatalytic degradation

The linking of selective sorption on non ionogenic polymeric sorbent with photocatalytic decomposition seems to be a promising way of the removal and subsequent destruction of hazardous chemicals. In regular intervals (after the saturation) sorbent has to be regenerated by an organic solvent (methanol, acetonitrile) and this concentrated solution is then repeatedly added to an aqueous photocatalyst (TiO_2) suspension where the destruction of pollutant takes place.

As it was mentioned above, the photocatalysis on TiO_2 (***Fujishima et al., 2000; Mills and Wang, 1998; Bahnemann, 1999; Carp et al., 2004***) is intended to be both supplementary and complementary (***Christensen and Walker, 1996***) to some of the more conventional approaches to the destruction or transformation of hazardous chemical wastes. It utilizes the high oxidizing potential of $^{\bullet}OH$ radical (+2.85 V vs. NHE (***Bard et al., 1985***)). However, there exists an important disadvantage. Inorganic ions present in the treated water can act as radical scavengers (***Christensen and Walker, 1996***) that may cause inhibiting of the photocatalyst activity. Another important feature is the necessity to deal with large amounts of water contaminated by very low concentrations of pollutants.

In this respect, the linking of semiconductor photocatalysis with selective sorption on non ionogenic polymeric sorbent seems to be a promising way. It offers the advantages of treating small volumes of concentrated pollutant solutions that originate from the sorbent regeneration in a batch mode. Moreover, the possible negative effect of various inorganic ions present in the waste water is thus eliminated.

The whole process proceeds in two steps. The first is the removal of pollutant from aqueous media using non-ionic sorption. In regular intervals (after the saturation) sorbent has to be regenerated by an organic solvent (methanol, acetonitrile).

The second step is then TiO_2 photocatalysis in an aqueous system where this concentrated solution of pollutant in organic solvent is repeatedly added to the mixture. The organic solvent, which is present in the aqueous solution of pollutant, will kinetically compete with the pollutant for $^{\bullet}OH$ radicals. As a result, reaction rate of the pollutant photodegradation is reduced. Rate constant of $^{\bullet}OH$ radical with 4-chlorophenol (***Stafford et al., 1994***) is 9.3×10^9 $dm^3\,mol^{-1}\,s^{-1}$. The analogous value for methanol is about 10 times lower (***Buxton et al., 1988***) (9.7×10^8 $dm^3\,mol^{-1}\,s^{-1}$) while for acetonitrile it is 400 times lower (***Neta and Schuler, 1975***) (2.2×10^7 $dm^3\,mol^{-1}\,s^{-1}$). It would mean that for molar ratio of solvent to

4-chlorophenol 1000:1 the degradation rate of 4-chlorophenol would decrease by about 2 orders of magnitude in the case of methanol while only by less than one order of magnitude for acetonitrile.

Two main types of reactors can be used for photodegradation of pollutant with TiO_2. First type is based on a use of aqueous suspensions (slurries); the second employs immobilized TiO_2 on a suitable support. The advantage of suspensions is in their high interfacial surface area resulting in high degradation efficiency; however, it demands complicated separation of photocatalyst (most currently sedimentation or filtration) from the treated system. Immobilization of photocatalyst eliminates the separation process but may have a negative impact on the degradation efficiency.

II.G The pollutants

II.G.1. The Monuron

The Monuron is an herbicide from phenylurea family, which has been synthesized in the 50's (**Fig.II.G.1)**. Wide range of other urea or phenylurea derivates was prepared. The character of the substituents brings about change in properties like herbicide selectivity, involving thus its application.

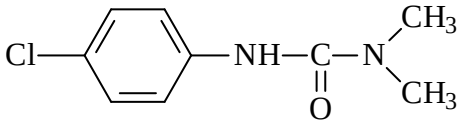

Fig.II.G.1: structure of Monuron, or N-(4-chlorophenyl)-N',N' dimethylurea.

The phenylurea herbicides penetrate the plants by roots, and are transported to leafs, where they inhibit the photosynthesis. The inhibition is caused by blocking the electron transfer in the photosystem II at the level of chlorophyll. This action of herbicides causes two effects: blocking of NADPH synthesis and formation of toxic singlet oxygen.

The Monuron can be used as total weed killer on not cultivated sites (maintenance of road, paths and railways) or in agricultural zones. However, its use was minimized in last years, so it's found only sporadically in the natural waters.

<u>Direct or induced phototransformation of Monuron</u>

The absorption spectrum of Monuron has a maximum at 245 nm with a molar absorption coefficient of 1.78×10^4 $L.mol^{-1}.cm^{-1}$ (**Fig. II.G.2**). Monuron does not absorb above 300 nm, so its direct photodegradation at solar light is very low.

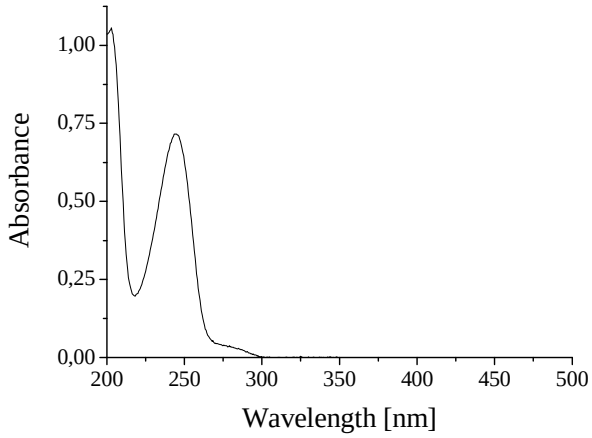

Fig. II.G.2: Absorption spectra of 4×10^{-5} $mol.L^{-1}$ solution of Monuron.

The phototransformation of Monuron by sunlight was studied by ***Hill et al. (1955)***. After 48 days exposure to solar light, 83% of Monuron disappeared.

Crosby and Tang (1969) identified different photoproducts and proposed a mechanism of Monuron phototransformation. The photocatalytic degradation of Monuron using TiO_2 was also investigated in detail (***Augugliaro et al., 1993; Pramauro et al., 1993***).

The photodegradation of Monuron in the systems producing hydroxyl radicals was described by ***Měšťánková et al. (2004)***. The degradation of Monuron by hydroxyl radical starts by the attack of $^{\bullet}OH$ at one of two sites: methyl group or aromatic nucleus. The attack of aromatic ring leads to addition of hydroxyl radical on the position ortho and continues by ring opening. Further intermediates do not absorb in UV/vis and can not be detected by HPLC. Attack on methyl group leads to detachment of hydrogen atom and formation of $RCH_2^{\bullet}$ radical (**Fig.II.G.3**).

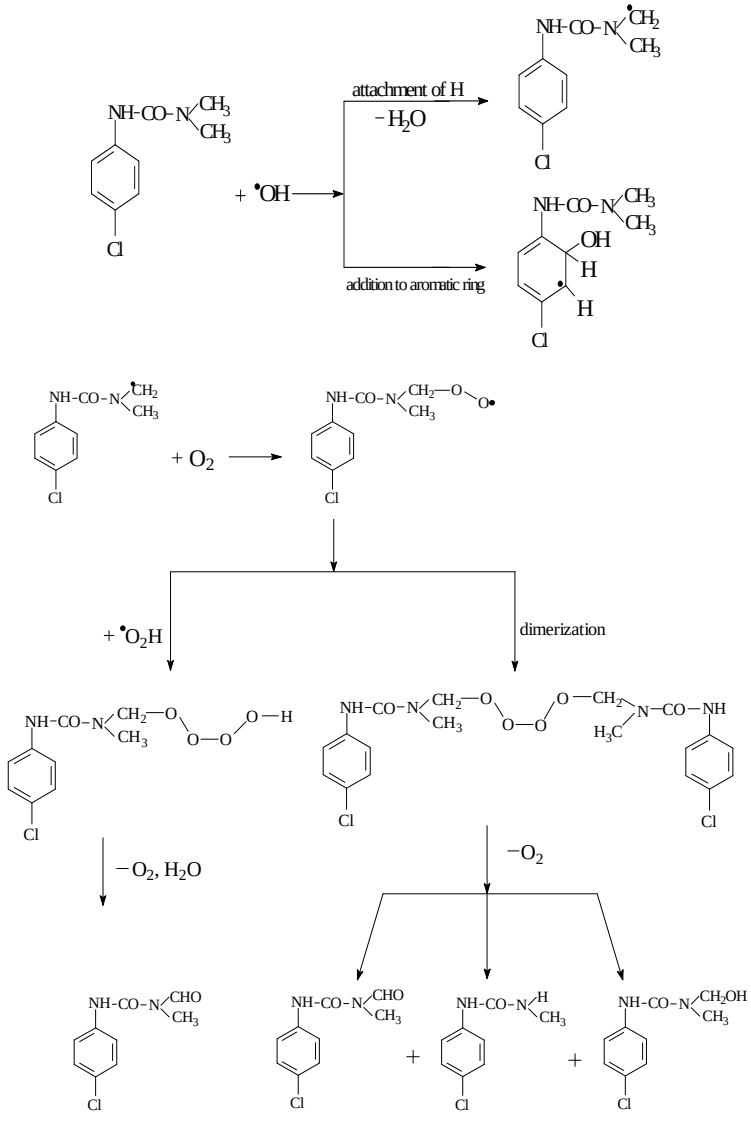

Fig.II.G.3: Monuron reaction with $^{\bullet}OH$; further reactions of $RCH_2^{\bullet}$ radical.

The radical $RCH_2^{\bullet}$ formed after hydrogen detachment quickly reacts with molecular oxygen giving peroxyl radical $RCH_2OO^{\bullet}$. In aquatic media, the peroxyl radical undergo preferentially bimolecular reaction of condensation. In fact, the termination reaction of two secondary peroxyl radicals leads to formation of tetroxide RCH_2OOOOH_2CR. Its decomposition by different routes leads to the primary products; some of them are identical for different degradation ways.

The peroxyl radical $RCH_2OO^{\bullet}$ can also react with the radical $HO_2^{\bullet}$ to form the tetroxide RCH_2OOOOH. Degradation of this unstable tetroxide leads to carbonylate intermediate, releasing molecular oxygen and water. The path of degradation via methyl group attack represents 20% of Monuron degradation by TiO_2 and only 10% in the presence of Fe(III).

II.G.2. The 4-chlorophenol

For the purpose of the competitive photocatalytic degradation study, 4-chlorophenol (4-CP, **Fig. II.G.4**) was chosen as a model pollutant due to previous experience in its photodegradation with TiO_2 layers performed at the Institute of Chemical Technology in Prague. Moreover, its mechanism of degradation is already well known, as well as its intermediates.

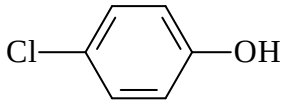

Fig. II.G.4: Structure of 4-chlorophenol (4-CP).

The 4-chlorophenol is a white crystalline substance, well soluble in water (27 $g.L^{-1}$). It is used for synthesis of more chlorinated phenols or other phenol derivates, as the herbicides of chlorophenoxyacetic family. 4-chlorophenol also participates in synthesis quinizarin (a dye), chlofibrate (a drug), chlorophenesin and dichlorophen (fungicides) (***Oudjehani and Boule, 1992***). Besides, it is a frequent degradation intermediate of these (and other) products.

The 4-chlorophenol has, (likes other chlorophenols), toxic effects on human health. It is accumulated particularly in the liver, less favourably in brain, muscles and fat tissue. High doses can lead to death (estimated lethal dose of pentachlorophenol for male is 29 $mg.kg^{-1}$).

Photodegradation of 4-chlorophenol

Photocatalytic degradation of 4-chlorophenol (4-CP) in TiO_2 suspensions (Degussa P25) was studied by ***Theurich et al. (1996)***; the proposed scheme is shown in **Fig II.G.5**.

Besides the formation of 4-chlorocatechol (4-CC), the major degradation pathway is the dechlorination of 4-CP resulting in hydroquinone (HQ) and benzoquinone (BQ) as primary intermediates. These compounds can be further oxidized to hydroxyhydroquinone (HHQ) and hydroxybenzoquinone (HBQ), the secondary intermediates. Further reactions of the hydroxyphenyl radical (HPR) at pH values above 5.0, formed bicyclic compounds and phenol. The formation of bicyclic products could be explained through intermediate free radical pathways.

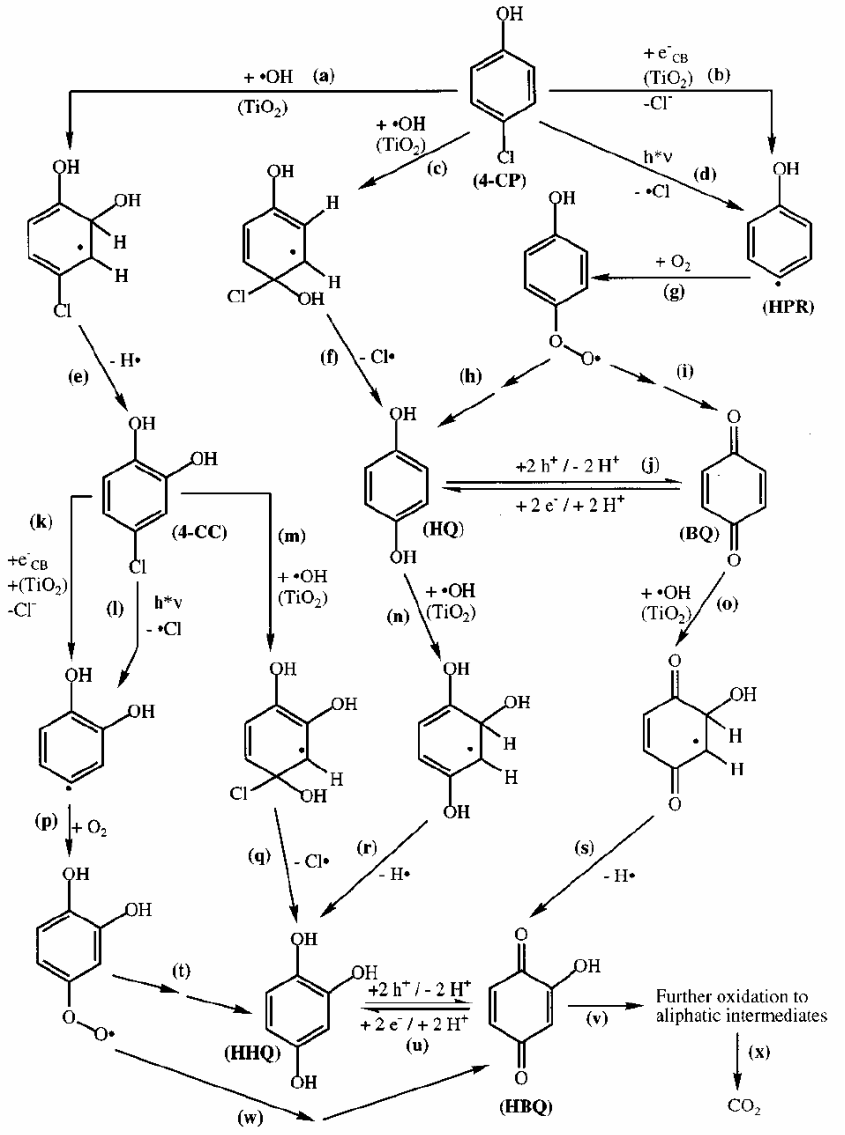

Fig. II.G.5: Scheme of the photocatalytic degradation of 4-chlorophenol in TiO_2 suspension (***Theurich et al., 1996***).

The authors also suggested that the HQ/BQ photosystem could be detrimental substances (leading to a short circuit) for photocatalytic processes and therefore seems to have a key function for the photocatalytic oxidation of aromatic pollutants.

References:

Abida O., Mailhot G., Litter M. and Bolte M., *Photochem. Photobiol. Sci.*, **2006**, 5, 395.

Abrahamson H. B., Rezvani A. B., Brushmiller J. G., *Inorg. Chim. Acta*, **1994**, 226, 117.

Andrianirinaharivelo S. L., *Thèse de doctorat à l'Université Blaise Pascal*, Clermont-Ferrand (France), **1992**.

Andrianirinaharivelo S. L., Jirkovský, P., Bolte, M., *Trans. Met. Chem.*, **1993**, 18, 37.

Augugliaro V., Marcí G., Palmisano L., Pramauro E., Bianco-Prevot A., *Res. Chem. Intermed.*, **1993**, 19 ,839.

Augustynski J., *Structure and Bonding*, **1988**, 69, 1.

Bahnemann D.W. In *Enviromental Photochemistry*; ed.: Boule, P., **1999**, Springer-Verlag: Berlin, pp 285-351.

Balzani V., Carassiti V., Photochemistry of Coordination Compounds, Academic Press, New York, 1970, pp. 172-174.

Bamwenda G.R., Uesigi T., Abe Y., Sayama K., Arakawa H., *Appl. Catal. A: General*, **2001**, 205, 117.

Barb W.G., Baxendale J.H., George P., Hargrave K.R., *Trans. Faraday Soc.* **1951**, 47, 462.

Bard A.J., Parsons R. and Jordan J., 'Standard Potentials in Aqueous Solution', **1985**, Marcel Dekker, New York.

Bates H.G.C., Uri N., *Nature*, **1953**, 75, 2754.

Baxendale J.H., Magee J., *Trans. Faraday Soc.*, **1955**, 51, 205.

Behra P., Sigg L., *Nature*, **1990**, 334, 419.

Benkelberg H.J., Warneck P.J., *J. Phys. Chem.*, **1995**, 99, 5214.

Benkelberg H.J., Schäfer A., Warneck P., In: Air Pollution research Report 33: Atmospheric Oxidation Processes, ed. Becker K.-H., **1991**, CEC, Brussel, 130.

Bennett J.H., Lee E.H., Krizek D.T., Olsen R.A., Brown J.C., *J. Plant Nutr.*, **1982**, 5, 335.

Benrath A., *Z. Phys. Chem.*, **1910**, 74, 115.

Bielski B.H.J., Allen A.O., *J. Phys. Chem.*, **1977**, 81, 1048.

Bielski B.H.J., Cabelli D.E., Arudi R.L., Ross A.B., *J. Phys. Chem. Ref. Data*, **1985**, 14, 1041.

Bobtelsky M., Jordan. J., *J. Am. Chem. Soc.*, **1947**, 69, 2286.

Boehm H.P., Herrmann M., *Z. Anorg. Chem.*, **1967**, 352, 156.

Brand N., Mailhot G., Bolte M., *Environ. Sci. Technol.*, **1998**, 32, 2715.

Brezová V., Blažková A., Borošová E., Čeppan M., Fiala R., *J. Mol. Catal. A: Chem*, **1995**, 98, 109.

Buchanan D.N.E., *J. Inorg. Nucl. Chem.*, **1970**, 32, 3531.

Butler C.B., Davis A.P., *J. Photochem. Photobiol. A: Chem.*,**1993**, 70, 273.

Buxton G.V., Greenstock C.L., Helman W.P., Ross A.B., *J. Phys. Chem. Ref. Data*, **1988**, 17,513-886.

Calvert J.G., Pitts J.M., *Photochemistry*, **1966**, 783.

Carey J.H., Lawrence J., Tosine H.M., *Bull. Eviron. Toxicol.*, **1976**, 16, 697.

Carp O., Huisman C.L., Reller A., *Prog. Solid State Chem*. **2004**, 32 (1-2), 33-177.

Catastini C., Sarakha M., Mailhot G., Bolte M., *Sci. Total Environ.*, **2002**, 298, 219.

Christensen H., Sehested K., *J. Phys. Chem.*, **1988**, 92, 3007.

Christensen P.A. and Walker G.M., 'Opportunities for the UK in solar detoxification', ETSU S/P4/00249/REP, **1996**.

Conklin M.H., Hoffman M.R., *Environ. Sci. Technol.*, **1988**, 22, 899.

Cooper, G. D., DeGraff, B. A., *J. Phys. Chem.*, **1971**, 75, 2897.

Cooper, G. D., DeGraff, B. A., *J. Phys. Chem.*, **1972**, 76, 2618.

Crosby D.G., Tang C.S., *J. Agric. Food Chem.*, **1969**, 17, 1041.

Cunningham K. M., Goldberg M.C., Weiner E.R., *Environ. Sci. Technol.*, **1988**, 22, 1090.

Cunningham J., Srijaranai S., J. *Photochem. Photobiol. A*: Chem., **1991**, 58, 361.

Dodge C.J., Francis A.J., *Environ. Sci. Technol.*, **1997**, 31, 3062.

Doménech X., *In :Photocatalytic Purification and Treatment of Water and Air*, Al-Ekabi H., Ollis D. F. eds., Elsevier, **1993**, 337.

Dunford H.B., *Coord. Chem. Rev.*, **2002**, 233/234, 311.

Eberle S.H., Palmer W., *Z. Wasser Abwasser Forsch.*, **1986**, 19, 233.

Escot M.T., *Thèse de doctorat en Pharmacie*, Université d'Auvergne, Clermont-Ferrand (France) **1973**.

Evans M.G., Uri N., *Nature*, **1949**, 164, 404.

Faust B.C., Hoffmann M.R., *Environ. Sci. Technol.*, **1986**, 20, 943.

Faust B.C., Hoigné J., *Atmosp. Envir.*, **1990**, 24A, 79.

Faust B.C., Zepp R.G., *Environ. Sci. Technol.*, **1993**, 27, 2517.

Feng W., Nansheng D., *Chemosphere*, **2000**, 41, 1137.

Field T.B., McCourt J.L., McBryde W.A.E., *Can. J. Chem.*, **1974**, 52, 3119.

Flynn C.M., *Chem. Rev.*, **1984**, 54, 31.

Frahn J.L., *Aust. J. Chem.*, **1958**, 11, 399.

Fujihira M., Satoh Y., Osa T., *Bull. Chem. Soc. Jpn.*, **1982**, 55, 666.

Fujishima A., Honda K., *Nature*, **1972**, 37, 238.

Fujishima A., Rao T.N., Tryk D.A., *J. Photochem. Photobiol. C: Photochem. Rev.* **2000**, 1, 1.

Gautier-Luneau I., Merle C., Phanon D., Lebrun C., Biaso F., Serratrice G., Pierre J.-L., *Chem. Eur. J.* **2005**, 11, 2207.

Glusker J.P., *Act. Chem. Res.*, **1980**, 13, 345.

Goldberg M.C., Cunningham K.M., Weiner E.R., *J. Photochem. Photobiol. A: Chem.*,**1993**, 73, 105.

Grätzel M., Heterogeneous Photochemical Electron Transfer, CRC Pres, Boca Raton, FL, **1989**.

Gustavson, R. L., Martell, A. E., *J. Phys. Chem.*, **1963**, 67, 576.

Hamm R.E., Schull C.M. Jr., Grant D.M., *J. Amer. Chem. Soc.*, **1954**, 76, 2111.

Hatchard C.G., Parker C.A., *Proc. R. Soc. Lond.*, **1956**, 235A, 518.

Hayon E, Weiss J., *J. Chem. Soc.*, **1960**, 3866.

Hemmes P., Rich L.D., Cole D.L., Eyring E.M., *J. Phys. Chem.*, **1971**, 75, 929.

Herrmann J.M. et Pichat P., *J. Chem. Soc., Faraday Trans. I*, **1980**, 76, 1138.

Hill G.D., MacGahen J.W., Baker H.M., Finnerty D.W., Bingeman C.W., *Agronom. J.*, **1955**, 47, 93.

Hoffmann M.R., Martin S.T., Choi W., Bahnemann D.W., *Chem. Rev.*,**1995**, 95, 69.

Hufschmidt D., Liu L., Selzer V., Bahnemann D. *In:* Oxidation Technologies for water and wastewater treatment, **2004**, CUTEC-serial publication No 57, 270.

Izumi I., Fan F.F., Bird A.J., *J. Phys. Chem.*, **1981**, 85, 218

Jayson G.G., Parson B.J., Swallow A.J., *J. Chem. Soc. Faraday Trans. 1*, **1973**, 69, 236.

Job P., *Ann. chem.*, **1928**, 9, 113.

Johnson K.S., Gordon R.M., Coale K.H., *Mar. Chem.*, **1997**, 57, 137.

Karakitsou K.E, Verykios K.E., *J. Phys. Chem.*, **1993**, 97, 1184.

Kawaguchi H., Inagaki A., *Chemosphere*, **1994**, 28, 57.

Klauson D., Preis S., *International Journal of Photoenergy*, **2005**, 7(4), 175.

Knight R. J., Sylva R.N., *J. Inorg. Nucl. Chem.*, **1975**, 37, 779.

Kolář M., Měšťánková H., Jirkovský J., Heyrovský M., Šubrt J., *Langmuir* **2006**, 22, 598.

Kormann C., Bahnemann D., Hoffmann M.R., *Environ. Sci. Technol.*, **1991**, 25, 494.

Krizek D.T., Bennett J.H., Brown J.C., Zaharieva T., Norris K.H, *J. Plant. Nutr.*, 1982, 5, 323.

Krýsová H., Jirkovský J., Krýsa J., Mailhot G., Bolte M., *Appl. Catal. B: Environ.*, **2003**, 40, 1.

Lanford O. E., Quinan J. R., *J. Am. Chem. Soc.*, **1948**, 70, 2900

Langford C.H., Carey J.H., *Can. J. Chem.*, **1975**, 53, 2430.

Langmuir, D., Whittemore, D.O., *Adv. Chem. Ser.*, **1971**, 106, 209.

Legrini O., Oliveros E., Braun A.M., *Chem. Rev.*, **1993**, 93, 671.

Lewis N.S., Rosenbluth M.L., *In:. Photocatalysis-Fondamentals and Applications*, Serpone N., Pelizzetti E., eds, Wiley Interscience: New York, **1989**.

Litter M.I., Navio J.A., *J. Photochem. Photobiol. A: Chem.*,**1996**, 98, 171.

Livingston R., *J. Phys. Chem* , **1940**, 44, 601.

Mailhot G., Bordes A. L., Bolte M., *Chemosphere*, **1995**, 30, 1729.

Mailhot G., Hykrdová L., Jirkovský J., Lemr K., Grabner G., Bolte M., *Appl. Catal. B: Environ.*, **2004**, 50, 25.

Martell A.E., Smith R.M., Critical Stability Constants, Vol. 3, Plenum Press, New York and London, **1974**, 163.

Martin J.H., Fitzwater S.E., *Nature*, **1988**, 331, 341.

Martin J.H., Gordon R.M., Fitzwater S.E., *Nature*, **1990**, *345*, 156.

Mazellier P., Jirkovský J., Bolte M., *Pestic. Sci.*, **1997**, 49, 259.

Mazellier P., Mailhot G., Bolte M., *New J. Chem.*, **1997**, 21, 389.

Mazzelier P., Bolte M., *J. Photochem. Photobiol. A: Chem.*,**2000**, 132, 129.

Měšťánková H., Mailhot G., Pilichowski J.-F., Jirkovský J., Krýsa J., Bolte M., *Chemosphere*, **2004**, 57, 1307.

Měšťánková H., Mailhot G., Jirkovský J., Krýsa J., Bolte M., *Appl. Catal. B: Environ.*, **2005**, 57, 257.

Měšťánková H., Krýsa J., Jirkovský J., Mailhot G., Bolte M., *Appl. Catal. B: Environ.*, **2005**, 58, 185.

Milburn R. M., *J. Am. Chem. Soc.*, **1956**, 79, 537.

Milewska M.J., *Z. Chem.*, **1988**, 28, 204.

Mills A., Morris S., Davies R., *J. Photochem. Photobiol. A: Chem*, ***1993***, 70, 183.

Mills A., Wang J., *J. Photochem. Photobiol. A: Chem.* **1998**, 118, 53-63.

Mulazzani Q.G., D'Angelantonio M., Venturi M., Hoffman M.Z., Rodgez M.A.J., *J. Phys. Chem.*, **1986**, 90, 5347.

Munuera G., Rives-Arnau V., Saucedo A., *J. Chem. Soc., Faraday Trans. I.*, **1979**, 75, 736.

Murray, K.S., *Coord. Chem. Rev.* **1974**, 12, 1.

Nansheng D., Feng W., Fan L., Mei X., Chemosphere, **1998**, 36, 3101.

Neta P., Schuler R.H., *J. Phys. Chem*. **1975**, 79, 1-6.

Ogino, H., Nagata, T., Ogino, K., *Inorg. Chem.*, **1989**, 28, 3656.

Ohno T., Haga D., Fujihara K., Kaizaki K., Matsumura M., *J. Phys. Chem. B*, **1997**, 101, 6415.

Ohno T., Sarukawa K., Tokieda K., Matsumara M., *J. Catal.*, **2001**, 203, 82.

Ohtani B., Nishimoto S. J., *J. Phys. Chem.*, **1993**, 97, 920.

Okamoto K., Yamamoto Y., Tanaka H., Tanaka M., Itaya A., *Bull. Chem. Soc. Jpn.*, **1985**, 58, 2015.

Oudjehani K., Boule P.J. , *Photochem. Photobiol. A: Chem.*, **1992**, 68, 363.

Parfitt G.D., *Prog. Surf. Membr. Sci.*, **1976**, 11, 181.

Parker, C. A., Hatchard, C., G., *J. Phys. Chem.*, **1959**, 63, 22.

Pehkonen S.O., Siefert R.L., Hoffmann M.R., *Environ. Sci. Technol.*, **1995**, 29, 1215.

Perdue E.M. and Gjessing E.T., Organic Acids in Aquatic Ecosystems, Wiley, New York, **1990**.

Poulain L., Mailhot G., Wong-Wah-Chung P., Bolte M., *J. Photochem. Photobiol. A: Chem.*, **2003**, 159, 81.

Pramauro E., Vincenti M., Augugliaro V., Palmisano L., *Environ. Sci. Technol.*, **1993**, 27, 1790.

Quici N., Morgada M.E., Gettar R.T., Bolte M., Litter M.I., *Appl. Catal. B: Environ.*, **2007**, 71, 117.

Rajeshwar K., *J. Appl. Electrochem.*, **1995**, 25, 1067.

Richard C., *J. Photochem. Photobiol. A*: Chem., **1993**, 72, 179.

Sawyer D.T., Gibian M.J., *Tetrahedron*, **1979**, 35, 1471.

Sclafani A., Palmisano L., Davì E., *J. Photochem. Photobiol. A: Chem.*, **1991**, 56, 113.

Stafford U., Gray K.A., Kamat P.V., *J. Phys. Chem*., **1994**, 98, 6343-6351.

Stuglik Z., Zagorski Z.P., *Radiat. Phys. Chem.* **1981**, 17, 229.

Sulzberger B., Laubscher H., Karametaxas G., In: Aquatic and Surface Photochemistry ed.: Helz G.R., Zepp R.G., Crosby D.G., **1994**, Lewis Publisher, 53.

Theurich J., Lindner M., and Bahnemann D.W, *Langmuir*, **1996**, 12, 6375.

Timberlake C.F., *J. Chem. Soc.*, **1964**, 5078.

Turchi C.S., Ollis D.F., *J. Catal.*, **1990**, 122, 178.

Wei T.-Y., Wang Y.-Y., Wan Ch.-Ch., *J. Photochem. Photobiol. A*: Chem., **1990**, 55, 115.

Warner R.C., Weber I., *J. Am. Chem. Soc.*, **1953**, 75, 5086.

III. EXPERIMENTAL

III.A Chemicals

• Monuron or N-(4-chlorophenyl)-N',N'-dimethylurea, supplied by Riedel-de-Haën, analytical standard.

• Ferric citrate (Fe(III)Cit), Aldrich, technical grade (batch #083 KO 656)

• Ferric perchlorate, hydrated $(FeClO_4)_3.nH_2O$, Sigma-Aldrich, 98%

• Citric acid (CA), J. T. Baker, > 99%.

• Nitrilotriacetic acid (NTA), Aldrich, 99%

• 4-chlorophenol (4-CP), Aldrich, > 99%; Merck p.a.

• Hydroquinone (HQ), Merck, p.a.

• Titanium dioxide TiO_2, Degussa P25 (anatase: rutile = 70 : 30), particle size 0.1 µm; BET surface area 55 ± 12 $m^2.g^{-1}$

• Acetonedicarboxylic acid (ADCA), Fluka, purum (≥ 95%)

• Perchloric acid $HClO_4$, Fluka, 60% p.a.; Merck 70-72%

• Sodium hydroxide NaOH, Aldrich, 99,99% (semiconductor grade)

Chemicals for Fe(II) and total iron titration:

• 2,2'-bypiridine, Merck, p.a.

• Sodium acetate CH_3COONa, Prolabo, > 99%

• Sulphuric acid H_2SO_4, 96%

• Ferrocine, Aldrich, 97%

• Hydroxylamine chlorhydrate, Aldrich, > 99%

• Ammonia 25%, Merck, p.a.

• 1,10-phenanthroline, Fluka, 99%

Solvents for HPLC:

• Acetonitrile, Riedel-De Haën, gradient HPLC grade or Merck, HPLC grade

• Methanol, Merck, HPLC grade

III.B Preparation of solutions

All aqueous solutions were prepared with ultra-pure water (Millipore MilliQ), whose resistivity was 18.2 MΩ.cm.

The pH of the solutions was measured with a pH meter Orion equipped with a combined electrode. The precision of the measurements was 0.1 units. For pH adjustments, diluted solutions of $HClO_4$ and NaOH were used. All along the thesis, the ionic strength was not controlled.

In several experiments, the pH was controlled by a pH stat apparatus *TitraLab 856* from *Radiometer Analytical SAS*. The apparatus was equipped with a combined glass electrode, and maintaining the pH throughout the experiment by addition of either 1 $mol.L^{-1}$ $HClO_4$ or 1 $mol.L^{-1}$ NaOH. Unless otherwise noted, the pH was not stabilised.

The oxygen concentration was adjusted in the following ways:

• *Deoxygenated solutions* – nitrogen bubbling was used for 20 minutes before starting the irradiation and during the course of the reaction.

• *Oxygenated solutions* – oxygen bubbling was used for 10 minutes before starting the irradiation and during the course of the reaction.

• Batch mode reactors with flowing liquid phase – air bubbling was used during the course of the reaction. Oxygen concentration was about 8 $mg.L^{-1}$ in solution without bubbling.

The concentrations of both, Monuron and 4-chlorophenol, were not affected by these manipulations. If it is not indicated, the oxygen concentration was not controlled.

The samples containing TiO_2 suspension were centrifuged before HPLC analysis or the determination of iron(II).

III.B.1 Solutions for the titrations

Solution of 2,2'-bipyridine

A 0.05 $mol.L^{-1}$ solution of bipyridine was prepared by dissolving 0.390 g of this product in 50 ml of water. The solution was heated up in a water bath at approximately 50°C in order to accelerate the dissolution process.

Buffer of sodium acetate

The buffer of sodium acetate was prepared by mixing 600 ml of a 1N solution of sodium acetate and 360 ml of 1N sulphuric acid solution and completed to 1 litre with water.

Solution of 1,10-phenanthroline

The 0.1% (percentage in weight) solution of 1,10-phenanthroline was prepared by dissolving 0.0100 g of phenanthroline in 100 ml of water.

Solution of ferrocine

The solution of ferrocine was prepared by dissolving 0.985 g of the sodium salt of 3-(2-pyridyl)-5,6-diphenyl-1,2,4-triazine-4,4'-disulphonic acid in 100 ml of water. The solution was kept at 6°C and remained stable for one month.

Buffer of ammonium acetate

The buffer of ammonium acetate was prepared by dissolving of 192.7 g of ammonium acetate in 150 ml followed by the addition of 170 ml of ammonia (25%). The solution was then completed to 500 ml with water.

Solution of hydroxylamine chlorhydrate

A 3 $mol.L^{-1}$ solution of hydroxylamine chlorhydrate was prepared by dissolving 104.25 g of hydroxylamine chlorhydrate in 200 ml of 32% hydrochloric acid. The solution was then completed to 500 ml with water.

III.B.2 Solution of ferric citrate

Two ways of preparation of iron citrate stock solution (usually 2.55×10^{-3} $mol.L^{-1}$) were used. The first one was based on an equimolar mixture of ferric perchlorate and citric acid. The stoichiometry 1 to 1 was chosen due to the results from the literature and from the lab. However, this way of preparation leaded to low reproducibility. For this reason, only few results will be presented using the complex prepared by this method. Only results obtained with the same stock solution are presented and no comparison with two different preparations of the stock solution is presented in this work. Unless otherwise noted, the commercial ferric citrate was used.

The second one involved a commercial product of technical grade (see list of chemicals) by dissolution in water accelerated by warm bath. However, several problems with stoichiometry occurred during use of the commercial product. The percentage of iron of ferric citrate provided by the producer was 17.4% (***Sigma Certificate of Analysis, see link in references***). This value was confirmed by the supplier on a direct demand, and other ratio for

iron and citrate than 1 : 1 was also suggested. In order to determine the exact composition of the product, elementary analyses of elements present in citrate and in other common inorganic acids ions were performed (see **Tab. III.B.1**).

Element ratio	Theoretical [a]	Elementary analysis	Corrected [b]
Carbon	29.39%	25.75 ± 0.3%	25.70%
Hydrogen	2.04%	3.20 ± 0.3%	3.34%
Iron	22.86%	18.46 ± 0.4%	18.51%
Nitrogen	–	<0.10%	–
Phosphorus	–	<0.01%	–
Sulphure	–	<0.20%	–
Chlorine	–	<0.2%	–
Molecular weight	244.9 $g.mol^{-1}$	–	287.7 $g.mol^{-1}$

Tab. III.B.1: Elementary analysis of commercial ferric citrate compared to theoretical and corrected element weight ratios;
[a] Values corresponding to formula Fe(III)(Citrate), non-hydrated.
[b] Values corresponding to calculated formula $(Fe^{3+})(Citrate)_{1.08} \cdot 2.37\ H_2O$.

The theoretical mass ratios and results of elementary analysis were in a severe disagreement. Negligible presence of elements such as nitrogen, phosphorus, sulphur and chlorine indicated that the derived inorganic ions were not present, and that the difference should be caused by additional water and citrate molecules. Finally, the best agreement of elementary data was found with an addition of 2.37 water molecules per one central Fe^{3+} ion together with an excess of citrate of 8% (see **Tab. III.B.1**). Thus, the new ferric citrate formula corresponds to $\mathbf{(Fe^{3+})(Citrate)_{1.08} \cdot 2.37\ H_2O}$ and the value of molar mass given by the supplier (249.9 $g.mol^{-1}$) had to be corrected to **287.7 $g.mol^{-1}$**. With the new value, the expected concentration of 3×10^{-3} $mol.L^{-1}$ was revised to 2.55×10^{-3} $mol.L^{-1}$.

The photochemistry itself was not affected by the excess of citrate, as it absorb below 210 nm (see **Fig. III.B.2)**; at this wavelength no photons were emitted by the irradiation source. The stoichiometry of ferric citrate complex 1 : 1 was unaffected by the 8% citrate excess.

The stock solutions of ferric citrate were always kept at 6°C.

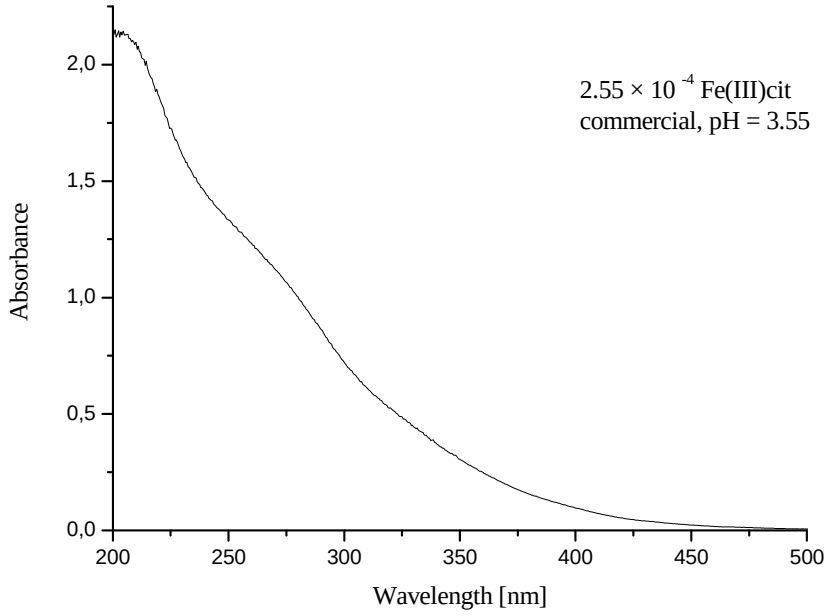

Fig. III.B.1: Spectrum of 2.55×10^{-4} mol.L^{-1} commercial ferric citrate at natural pH.

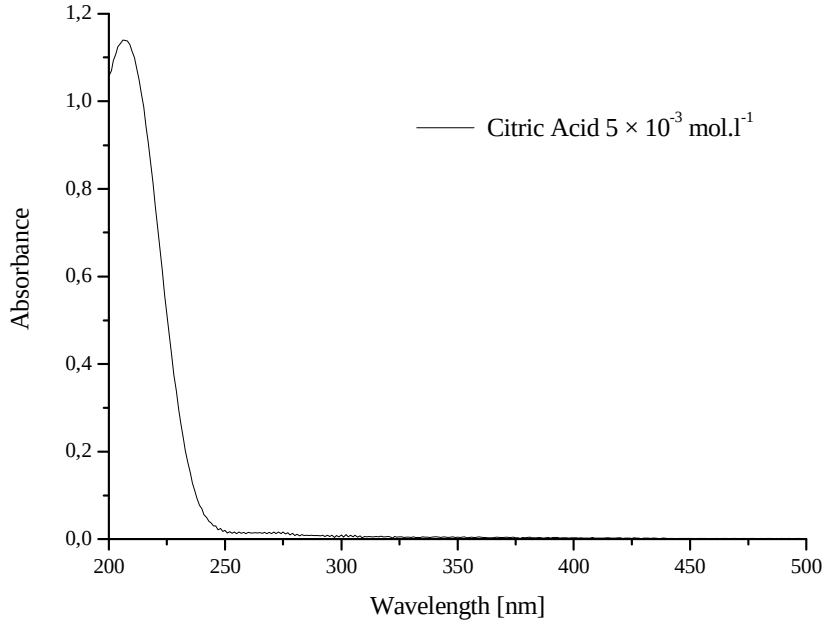

Fig. III.B.2: Spectrum of 5×10^{-3} mol.L^{-1} citric acid.

If not mentioned otherwise, the general experimental conditions in our system were:

- $[Fe(III)Cit]_{initial} = 2.55 \times 10^{-4}$ mol.L^{-1} (commercial product)
- [Monuron] = 1.0×10^{-4} mol.L^{-1}
- $[TiO_2] = 24$ mg.L^{-1}
- pH = 3.0 (not stabilised)

III.C Methods of analysis

III.C.1 Spectroscopic methods

Spectrophotometry

The absorption spectra were recorded in 1 cm quartz cells by two spectrophotometers:

- UV/VIS Spectrometer *Cary 3* with double beam, operated by included software absorption precision ± 0.002
- UV/VIS/NIR spectrophotometer *Lambda 19* (Perkin-Elmer) with double beam, operated by included software, absorption precision ± 0.001

Scanning electron microscopy

For the study of TiO_2 layers morphology, SEM images were recorded by *Hitachi S4700*. The accelerating voltage was 10 kV.

III.C.2 Chromatographic methods

Two HPLC systems were used through this work to carry out the analysis:

- HPLC *Waters* with diode array UV/VIS detector type *996*, autosampler type *717* and two pumps type *5210*. The set is controlled by *Millennium* software.
- *Shimadzu* chromatographic set with *LC-10ADvp* pump and *SPD-M10Avp* diode array UV/VIS detector. The set is operated by included software *Class-VP*.

The inversed phase column was a LiChrospher 100 RP-18 (type LiChroCART 125-4, Merck, Germany). For Monuron analysis, a mobile phase acetonitrile/water (30:70; vol.) was used with a flow rate of 1 $mL.min^{-1}$. Monuron and its degradation products were detected at 245 nm. For 4-chlorophenol analysis, a mobile phase acetonitrile/water (40:60; vol.) was used with a flow rate of 1 $mL.min^{-1}$. Both 4-chlorophenol and hydroquinone were detected at 226 nm.

The experimental error was estimated to be ± 5%.

III.C.3 Elementary analysis

The elementary analysis of the commercial ferric citrate (iron, carbon, hydrogen, sulphur, chlorine and phosphorus) was performed by Service Central d'Analyse, CNRS, Vernaison (69), France. Two sets of analysis were performed.

III.C.4 Methods of titration

Titration of Fe(II)

Three different methods were used to determine the concentration in ferrous ions.

• By 2,2'-bypiridine

In a 5 ml flask, 1 ml of bypiridine solution and 1 ml of sodium acetate buffer were put in. Then, 2 ml of the studied solution were added. After 20 minutes, the absorbance at 520 nm was measured. The concentration of Fe(II) is obtained from the following formula:

$$Fe(II) = \frac{\left(A_{520} - A_{520,b}\right) \times V_{total}}{V_s \times l \times \varepsilon_{520}},$$

where A_{520} is absorbance of the sample, $A_{520,b}$ absorbance of blank solution of bipyridine and buffer, V_{total} volume of the solution, V_s volume of the analysed sample, l is the length of optical path and ε_{520} is the molar absorption coefficient of Fe(II) complexed with bypiridine (**Fig. 3.C.1**) at 520 nm, which is equal to 8600 $l.mol^{-1}.cm^{-1}$.

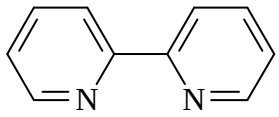

Fig. 3.C.1: Structure of 2,2'-bypiridine.

• By ferrocine

This method of determination of ferrous ions by ferrocine is the final step of the method of ***titration of total iron***, which is described later in this chapter, but could be used also for the determination of the Fe(II).

• By 1,10-phenanthroline

The method of dosage of Fe(II) by phenanthroline is described in the next chapter as a part of the method of ***actinometry*** (determination of photon flux), but it is also useful for Fe(II) determination. This method provided the most reproducible results among the mentioned methods of Fe(II) titration used during the work on the thesis.

Titration of total iron

The concentration of total iron present in the solution was determined by a complexometric method employing ferrocine, as described by ***Stookey (1970)***. The ferrocine is a monosodium salt of 3-(2-pyridyl)-5,6-diphenyl-1,2,4-triazine-4,4'-disulphonic acid (see **Fig. 3.C.2**), which is capable of efficient complexation of Fe(II): $k = 3.10^{11}$ l.mol^{-1}.s^{-1} (***Thompsen and Mottola, 1984***). This method correctly works only in a pH range between 4 and 8, where the complex is stable (***Kundra et al., 1974; Stookey, 1970***).

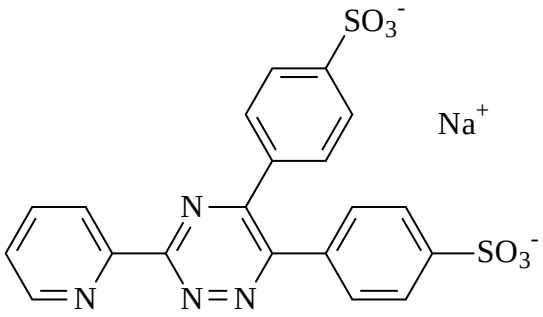

Fig. 3.C.2: Structure of ferrocine.

Before the complexation with ferrocine, the ferric ions have to be reduced into Fe(II) by hydroxylamine chlorhydrate.

The following sequence of operations was implemented:

In a 10 ml flask, 500 µl of hydroxylamine chlorhydrate (3 mol.L^{-1}) and 250 µl of sample were added. After mixing, mild warming of the solution and 10 minutes of waiting, 500 µl of ferrocine (2×10^{-2} mol.L^{-1}) and 1 ml of ammonium acetate buffer were added. The volume was then completed to 10 ml by water.

The absorbance of so prepared solution was measured immediately at 562 nm and the concentration of total iron was calculated from the following formula:

$$[Fe_{total}] = \frac{(A_{562} - A_{562,b}) \times V_{total}}{V_s \times l \times \varepsilon_{562}}$$

where A_{562} is absorbance of the sample, $A_{562,b}$ absorbance of the blank solution without any addition of iron, V_{total} volume of the solution, V_s volume of the analysed sample, l length of optical path and ε_{562} is the molar absorption coefficient of the $Fe^{II}(ferrocine)_3$ complex at 562 nm, which is equal to 27600 l.mol^{-1}.cm^{-1}.

The absorbance should be measured as soon as possible, as the complex is not stable more than 20 minutes. The determination of total iron could be skewed by the presence of other metallic ions such as of copper or cobalt. The amounts of such metals in our solutions were negligible.

Determination of Total Organic Carbon (TOC)

The measurements of total organic carbon (TOC) were performed by *Shimadzu TOC-V WS* system employing "wet" method. The method is based on oxidation of all organic carbon in aquatic media acidified by phosphoric acid. However, the instrumental setup needs 5 ml sample volume for one determination, which limited the amount of samples taken during one experiment.

Determination of Fe(III)Cit adsorption on TiO_2

The pH of ferric citrate solution 3×10^{-4} mol.L^{-1} (total volume of 50 mL) was adjusted to desired value. Then, 10 mL of the solution was put into a plastic vial and 10 mg of TiO_2 were added. After 24 hours of agitation, the suspension was centrifuged. The separated solution was analysed by the method of total iron determination.

III.D Photochemical methods

III.D.1 Actinometry

The photon flux was measured by actinometry with potassium ferrioxalate (***Calvert and Pitts, 1966***) in order to determine the quantum yield of the photoreaction. The method is based on the photochemical reactivity of the ferrioxalate. Under irradiation in acidic medium the reduction of iron(III) into iron(II) and the oxidation of oxalate to CO_2 proceeded according to the reactions:

$$[Fe^{III}(C_2O_4)_3]^{3-} \xrightarrow{h\upsilon} [Fe^{II}(C_2O_4)_2]^{2-} + C_2O_4^{\bullet -}$$

$$[Fe^{III}(C_2O_4)_3]^{3-} + C_2O_4^{\bullet -} \longrightarrow [Fe^{III}(C_2O_4)_3]^{2-} + (C_2O_4)^{2-}$$

$$[Fe^{III}(C_2O_4)_3]^{2-} \longrightarrow [Fe^{II}(C_2O_4)_2]^{2-} + 2\ CO_2$$

Concentration of ferrous ions was determined by a method based on the formation of a complex with 1,10-phenanthroline. The molar absorption coefficient at 510 nm (ε_{510}) is equal to 11180 $L.mol^{-1}.cm^{-1}$.

The procedure was the following: after irradiation of volume V_1 of a potassium ferrioxalate solution (6×10^{-3} $mol.L^{-1}$) during a period of time *t*, a sample of 2 ml (V_2) of this volume was transferred to a 5 ml flask (V_3) with 1 ml of sodium acetate buffer and 0.5 ml of 1,10-phenanthroline (0.1% wt.). The solution was then completed with pure water to 5 ml (V_3). After mixing, the solution was left in dark for one hour before measuring the absorbance at 510 nm.

The number of Fe(II) ions liberated during the photolysis was calculated as follows:

$$n_{Fe^{2+}} = \frac{6.023 \times 10^{20} \cdot V_1 \cdot V_3 \cdot A_{510}}{\varepsilon_{510} \cdot V_2 \cdot l},$$

where A_{510} = $A(sample)_{510} - A(blanc)_{510}$, the value of the blank absorbance corresponded to non irradiated solution of potassium ferrioxalate.

The number of the ferrous ions is proportional to the fraction of light absorbed by the solution during time *t*; the intensity emitted by the system, in photons per second for the volume V_1, is therefore equal to:

$$I_0 = \frac{n_{Fe^{2+}}}{\phi_{Fe^{2+}} \cdot t \cdot (1-10^{-A_0})} \quad [\text{photons.s}^{-1}]$$

A_0 represents the absorbance of the solution at the irradiation wavelength at $t = 0$, therefore $(1 - 10^{-A_0})$ corresponds to the ratio of photons absorbed by the solution to the number of incident photons I_0, $\phi_{Fe^{2+}}$ is the quantum yield of ferrous ion formation at irradiation wavelength (see chapter ***Calculation of quantum yield***).

Accordingly,

$$n_{Fe^{2+}} = \frac{6.023\times10^{20} \cdot V_1 \cdot V_3 \cdot A_{510}}{\phi_{Fe^{2+}} \cdot t \cdot (1-10^{-A_0}) \cdot \varepsilon_{510} \cdot V_2 \cdot l} \quad [\text{photons.s}^{-1}] \text{ for } V_1 \text{ ml}$$

Finally, when the length of optical path of the irradiated cell l_{irr} was taken into account:

$$n_{Fe^{2+}} = \frac{6.023\times10^{20} \cdot V_3 \cdot l_{irr} \cdot A_{510}}{\phi_{Fe^{2+}} \cdot t \cdot (1-10^{-A}) \cdot \varepsilon_{510} \cdot V_2 \cdot l} \quad [\text{photons.s}^{-1}.\text{cm}^{-2}]$$

III.D.2 Determination of the photon flux by photodiode

For the experiments at Prague, the determination of the light intensity was performed with a photodiode *Hamatsu S1337-BQ*. This apparatus is based on the photovoltaic effect, i.e. on the generation of an electric current under irradiation. The generated current is determined by measuring the potential decrease as a function of known resistance. For the purpose of this measurement, resistance of 101.4 Ω was used. The current was calculated from the Ohm's law.

$$I = \frac{U}{R}$$

Intensity of flux of energy P_f (in W.m^{-2}) was calculated with the constant of sensibility S, which was given for each wavelength of the light.

$$P_f = \frac{I}{S}$$

The photonic flux (in $\text{photons.s}^{-1}.\text{m}^{-2}$) was calculated from the following formula:

$$J_{h\nu} = \frac{P_f \cdot \lambda}{h \cdot c},$$

where h was the Planck constant and c was the speed of light in vacuum. For the calculation, the wavelength of irradiation λ was used. The obtained intensity of photon flux

was an integral value for all the wavelengths that are in the range of sensibility of the photodiode (200 – 600 nm).

With help of filters selective in a certain range of wavelengths, it was possible to determine the photon flux for this range only. The use of the filters demanded a correction of intensity of the flux of energy due to transmittance T_f of the filter.

$$P_f = \frac{P_{f,\exp}}{T_f}$$

III.D.3 Calculation of quantum yield

The set up providing monochromatic irradiation allows to determine the quantum yields. The quantum yield ϕ characterises the efficiency of photochemical reactions. The quantum yield is defined as the ratio of a number of transformed molecules (Δn) to the number of absorbed photons (I_a) during same period of time t.

$$\phi = \frac{\Delta n}{I_a}$$

Similarly in our case:

$$\phi = l \cdot \frac{\frac{\Delta c}{\Delta t} \cdot 6.023 \times 10^{20}}{I_0 \cdot (1 - 10^{-A_{\lambda irr}})},$$

where l is the length of optical path of the irradiation cell (in centimetres), I_0 photon flux (in photons.s^{-1}.cm^{-2}) determined by actinometry at the irradiation wavelength, $\left(1 - 10^{-A_{\lambda irr}}\right) = \frac{I_a}{I_0}$ is the fraction of light absorbed by the initial solution.

In any case, for the calculations of quantum yields, the irradiation times have to be chosen in order to not exceed a limit of 10% disappearance or transformation of the initial product. If this condition is not fulfilled, the degradation intermediates of initial product could interfere with the measures of the primary conversion.

The accuracy of measurement of quantum yields was principally dependent on the precision of the actinometry. The standard error was around 10%.

III.E Irradiation systems

III.E.1 Monochromatic irradiation

The monochromatic irradiations at 365 nm were performed by a monochromator *Bausch et Lomb* equipped with a high-pressure polychromatic mercury-vapour lamp *Osram HBO 200 W*. This device enabled us to determine the quantum yields. The beam of light is homogenous and collinear which allows measuring the light intensity. A cylindrical quartz cell with 2 cm length of optical path and 1.85 cm of internal diameter was used as a reactor. The photonic flux was determined by the ferrioxalate method as described earlier. The value of photon flux at 365 nm was 2.6×10^{15} photons.s^{-1}.cm^{-2}.

III.E.2 Batch mode photoreactors

Cylindrical reactor

For the kinetics studies concerning the iron complexes, an experimental set-up with larger volume and more powerful source ($I_0 \approx 1.5 \times 10^{16}$ photons.s^{-1}.cm^{-3}) was used. Three lamps are placed in the corners of a hypothetical equilateral triangle, while the water-jacketed *Pyrex* cylindrical reactor (d = 2.8 cm) is situated in the centre. The irradiation system is enclosed by a cylindrical aluminium reflexive jacket, whose vertical axis passes through the vertical axis of the reactor, see **Fig. III.E.1**.

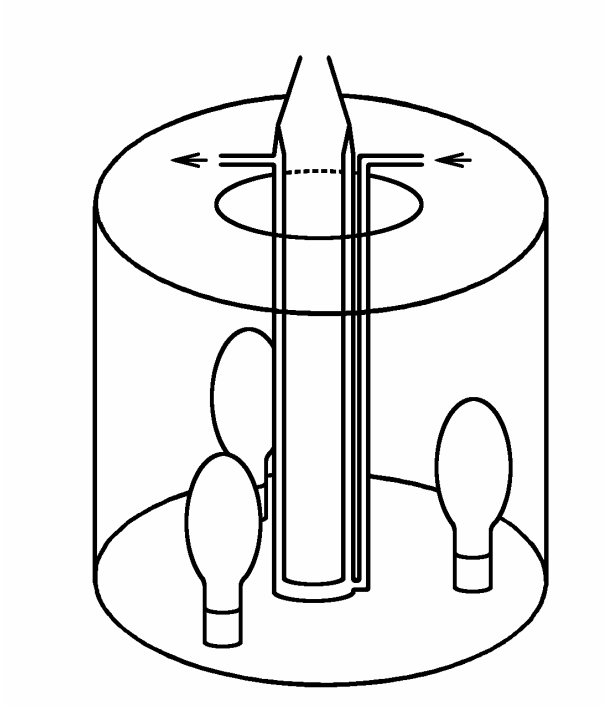

Fig. III.E.1: Scheme of cylindrical batch mode reactor

The solutions were well stirred all along the irradiation. Three middle-pressure mercury vapour lamps *Mazda MAW 125 W* were used as a source of irradiation. Their emission spectrum is shown in **Fig. III.E.2**. The light is practically monochromatic at 365 nm, which represents about 93% of the emitted light. The infrared component of spectra is filtered by the water shield surrounding the reactor.

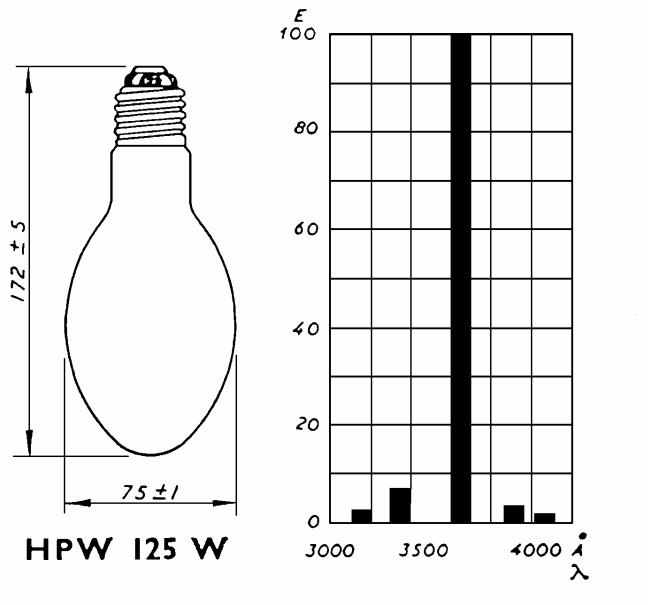

Fig. III.E.2: The emission spectrum of the *Mazda MAW 125 W* lamp.

Plate and tube reactors

For the purpose of this thesis, essentially for the studies concerning TiO_2, two types of batch-mode reactors with circulating solution were used. The first one was designed for the flow of suspension of the photocatalyst, with an effective irradiation area consisting of several parallel Pyrex tubes, and will be called ***tube*** reactor. The second reactor was arranged for the use of a thin layer of photocatalyst fixed on a glass plate, and will be called ***plate*** reactor.

The ***tube*** reactor was placed under the UV source, as displayed in **Fig. III.E.3**. The contaminated aqueous (with or without acetonitrile) suspension was pumped from the holding tank employing a centrifugal pump (*Nova*, Sicce Italy) to the inlet of the reactor. The inlet and outlet of the reactor were placed on a pair of thick parallel Pyrex tubes (diameter = 20 mm), which were orthogonally connected by an array of seven parallel thin Pyrex tubes (diameter = 9 mm, length = 190 mm). Total volume of suspension circulating in the system was 0.75 L. A reflective aluminium foil was placed under the array of tubes. The irradiated area corresponded to 0.0192 m^2. Three tubes *Sylvania Lynx (S 11W/350 BL)* were used as a UV source (broad maximum at 350 ± 20 nm, see **Fig. III.E.4**). The average incident photon

flux on the photoreactor plate at wavelengths below 400 nm was determined as 1.0 ± 10^{-4} einstein.m^{-2}.s^{-1}, using a silicon photodiode *Hamamatsu S1337-BQ*.

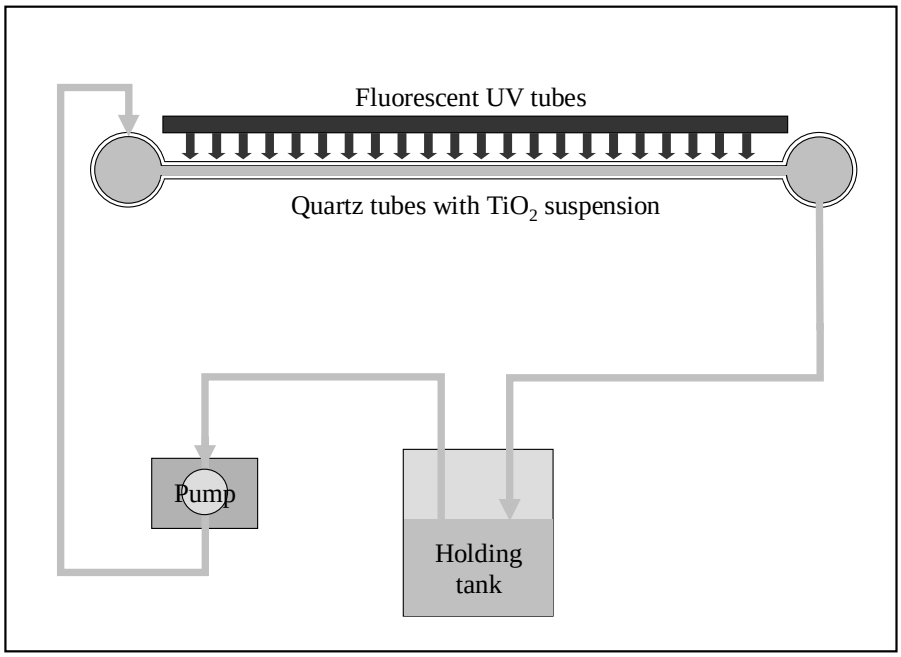

Fig. III.E.3: Scheme of a batch-mode tube photoreactor, lateral view.

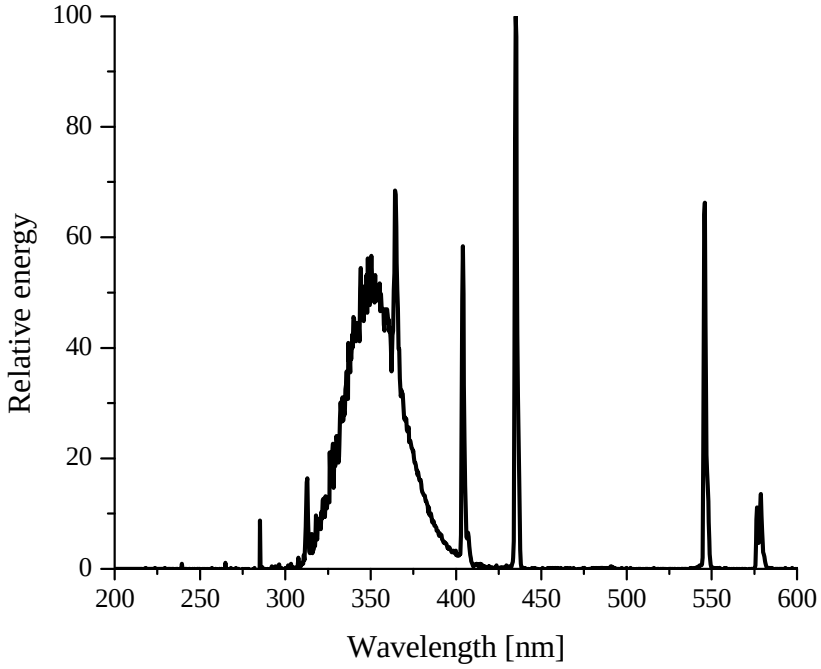

Fig. III.E.4: Emission spectrum of the fluorescent tubes *Sylvania Lynx S*.

The batch mode ***plate*** photoreactor was constructed from rectangular polymethyl-methacrylate trays with troughs at both ends; the pump was of same type to that used for the suspension reactor and transported the polluted aqueous solution to upper trough of the reactor, see **Fig. III.E.5**. The trays between upper and lower troughs were dimensioned to accommodate a glass plate 15 cm long and 10 cm wide. Thus, the irradiated area of layer in batch mode plate reactor was 0.015 m^2. The polluted solution of total volume of 0.8 L was circulating in a thin liquid film at the angle of 10° over an immobilized particulate layer of TiO_2 photocatalyst. The distance of UV tubes from TiO_2 layers was 12.5 cm. UV source was the same as in the glass tube reactor.

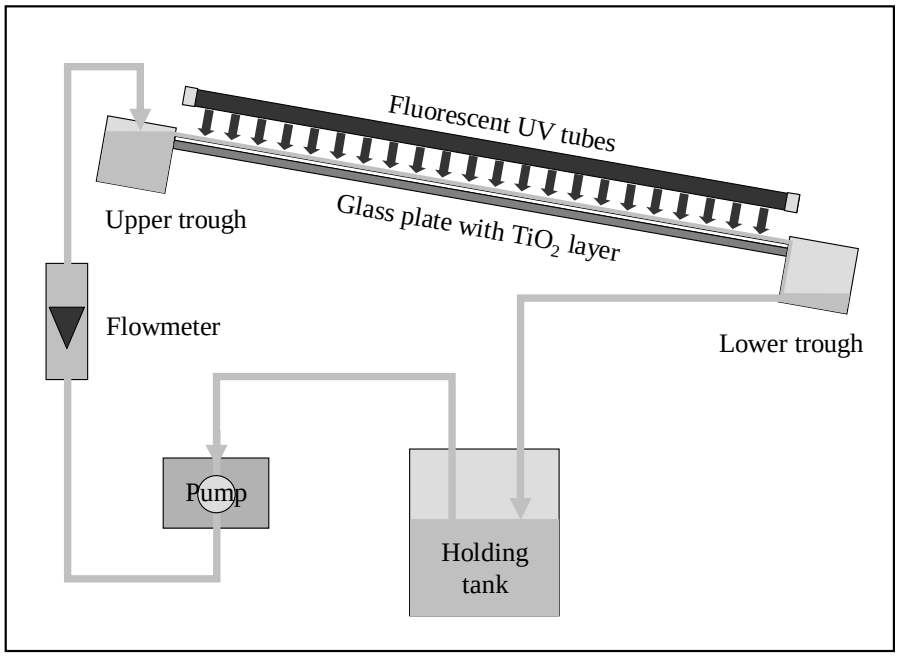

Fig. III.E.5: Scheme of a batch-mode plate photoreactor with a thin liquid film.

Both systems were air-bubbled and thermostated at 20°C, using the thermostats *Haake DC10*. The flow rate of the irradiated solution was at 100 $L.h^{-1}$.

Preparation of the TiO_2 layers by electrophoresis:

The immobilized particulate P25 TiO_2 layers were prepared on surface-conducting glass (Specific resistance 10 Ohms/square) sheets (length 15 cm, width 10 cm). The glass conducting plates had been placed in a methanolic suspension of P25 (10 $g.L^{-1}$) and exposed to potential of 10 V for 30 seconds. The layers were annealed at 300°C. The stability of

prepared layers was tested by 100 hours of water washing; the mass of photocatalyst remained practically unchanged. The weight gain mass of deposited photocatalyst on a glass sheet was 0.31 $mg.cm^{-2}$ and its hypothetic thickness was calculated as 0.80 µm, using the bulk TiO_2 density 3.8 $g.mL^{-1}$ (***Krýsa et al., 2005***). The surface morphology of the layers was determined by SEM (**Fig. III.E.6**).

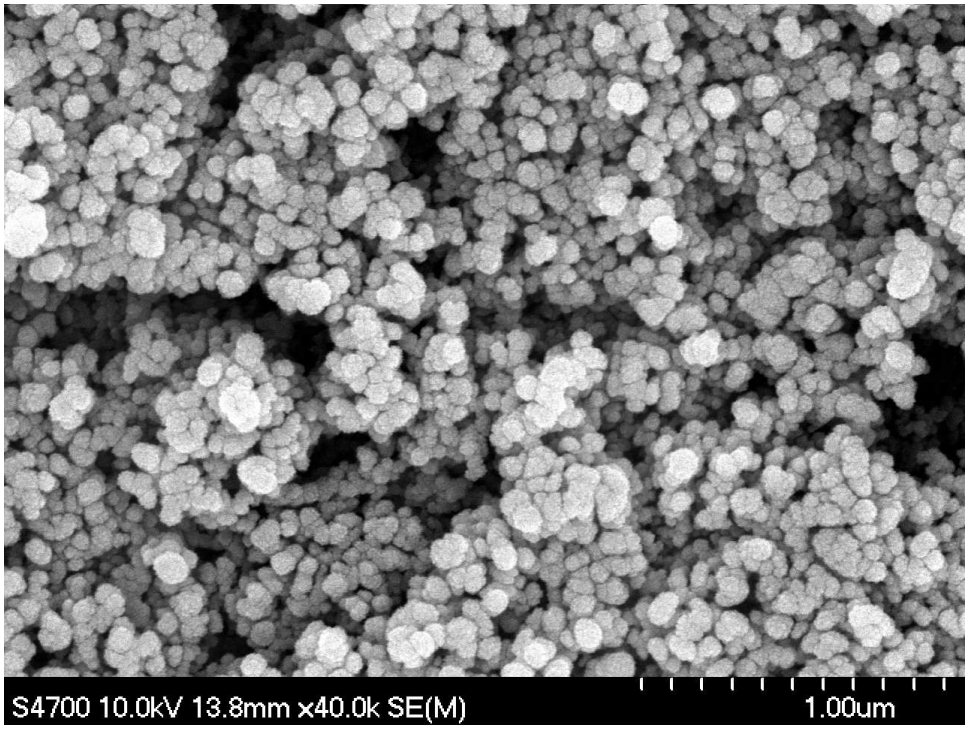

Fig. III.E.6: SEM image of the electrophoretically attached P25 layers

References:

Calvert J.G., Pitts J.M., *Photochemistry*, **1966**, 783.

Krýsa J., Keppert M., Waldner G., Jirkovský J., *Electroch. Act.*, **2005**, 50, 5255.

Kundra S.K., Katyal M., Singh R.P., *Anal. Chem.*, **1974**, 46, 1605.

Stookey L., *Anal. Chem.*, **1970**, 42, 779.

Thompsen J.E., Mottola H.Z., *Anal. Chem.*, **1984**, 56, 755.

Sigma Certificate of Analysis URL:
http://www.sigmaaldrich.com/catalog/search/CertOfAnalysisPage/F6129?LotNo=083K0656

IV. RESULTS

IV.A Characterization of ferric citrate complex

IV.A.1 Physico-chemical properties

The first step of the work was to characterize the acid-base behaviour of the ferric citrate complex in order to bring new insights into the current knowledge. The complex was investigated by UV-Vis absorption spectrophotometry. Two sets of spectroscopic measurements of ferric citrate 2.55×10^{-4} mol.L^{-1} in aqueous solution at different pH's were performed. The first set of measurements was carried out at pH between 0.75 and 3.65, which was obtained by additions of perchloric acid, pH 3.65 being the natural pH of a 2.55×10^{-4} mol.L^{-1} ferric citrate solution. In the second case, a solution of NaOH was used for setting pH between 3.65 and 8.1. Selected recorded spectra are shown in **Fig. IV.A.1**.

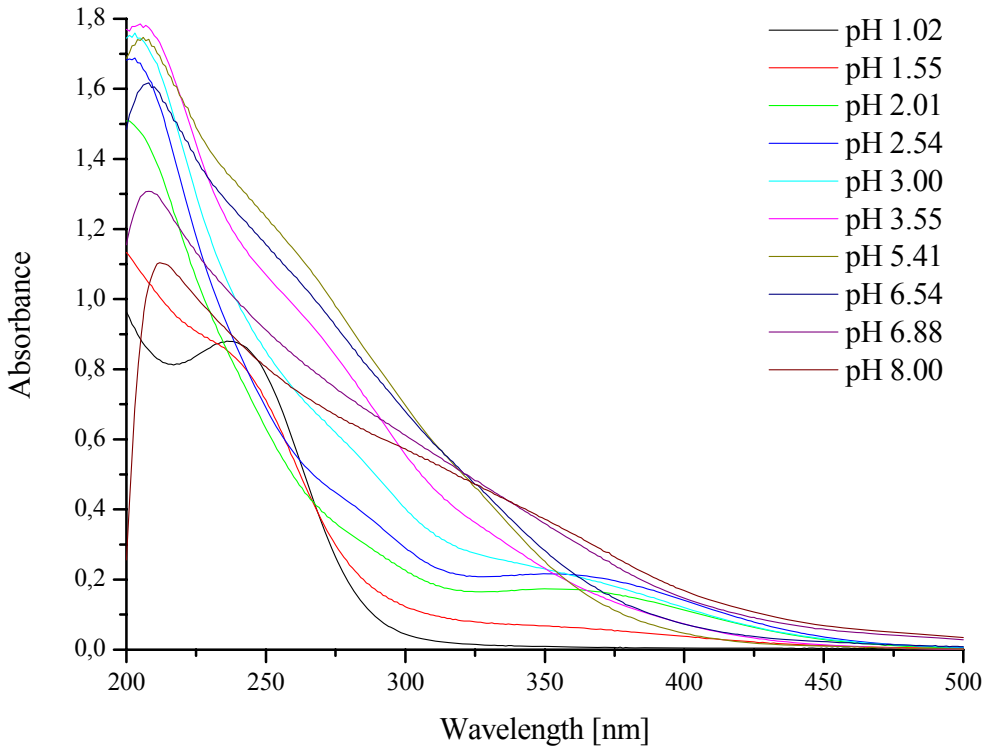

Fig. IV.A.1: Selected ferric citrate spectra recorded in a pH range between 1.02 and 8.00, [Fe(III)Cit] = 2.55×10^{-4} mol.L^{-1}.

For easier comparison and comprehension, an additional isometric view is presented in **Fig. IV.A.2**.

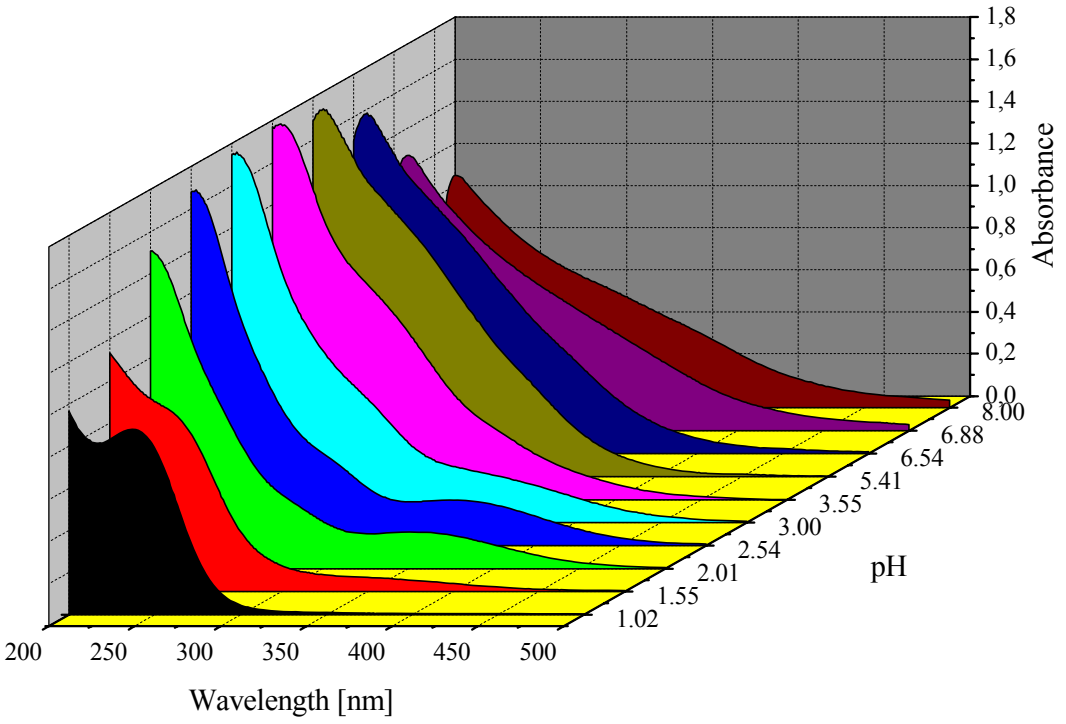

Fig. IV.A.2: Isometric view of selected ferric citrate spectra recorded in a pH range between 1.02 and 8.00, [Fe(III)Cit] = 2.55×10^{-4} mol.L^{-1}.

The spectrum at **Fig. IV.A.1** and **Fig. IV.A.2** at pH 1.55 well corresponds to the spectrum reported by ***Timberlake (1964)*** (see curve B at **Fig. II.C.1**). The shoulder around 350 nm could be seen in both spectra. Spectra observed at other pH's are similar to those observed by ***Abida (2005)***.

Differences in rates of pH stabilisation were also observed: at pH < 3.5, the pH was stabilised in a few seconds. On the contrary, the stabilisation of pH was getting slower at pH > 4, and taking longer time with further increase of pH. This fact was due to low concentration of H_3O^+ or OH^- ions than was comparable with the concentration of ferric citrate. Any buffer was used not to influence the complex equilibrium between Fe(III) and citric acid.

Another observation was made related to the reversibility of the complexes – in the pH range from 1 to around 9, the spectra were reversible when titrated by NaOH and back with $HClO_4$ or oppositely. Above pH 9, an irreversible polymerisation of Fe(III) species and possible consecutive aggregation of iron oligo- and polymers occured.

The spectra of ferric citrate are obviously pH dependent. This fact was already described in the literature. Several interpretations with various stoichiometries were proposed, some of which are described in the Bibliographic part. However there is a general agreement that several species exist in the acidic pH range, none of those described the system with equimolar low concentrations of Fe(III) and the citrate, which permits to explain our results sufficiently.

However, it is a difficult task to estimate structures of different acid-base forms of ferric citrate basing on measurements of UV-Vis absorption spectra as a function of pH. To start, let us summarize the acid-base properties of the ligand. Citric acid, abbreviated for this reason as H_3CitOH, has in its molecule three carboxylic groups and one hydroxyl group:

$$H_3CitOH \underset{}{\overset{K_{a1} = 2.7}{\rightleftharpoons}} H_2CitOH^- \overset{pK_{a2} = 4.2}{\rightleftharpoons} HCitOH^{2-} \overset{pK_{a3} = 5.3}{\rightleftharpoons} CitOH^{3-} \overset{pK_{a4} = 11}{\rightleftharpoons} CitO^{4-}$$

Eq. IV.A.1

The corresponding distribution diagram of particular acid-base forms of citric acid is plotted in **Fig. IV.A.3**. In the pH range of possible existence of the ferric citrate complex, e.g. below pH = 9, four acid-base forms of citric acid occur. The fifth form, which corresponds to deprotonation of the hydroxyl group of citric acid, takes place only in a basic solution at pH > 9.

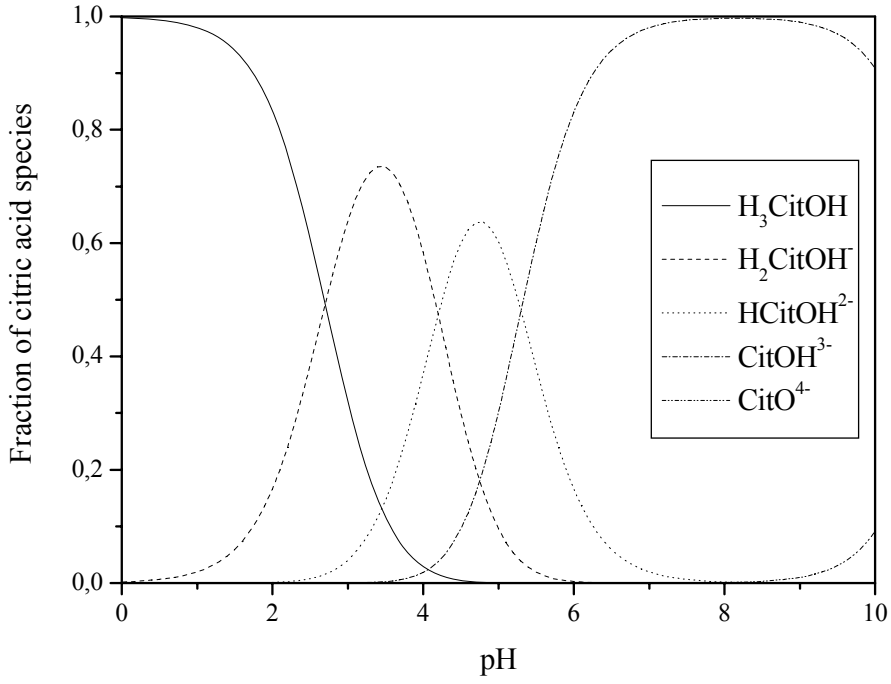

Fig. IV.A.3: Distribution diagram of acid-base forms of citric acid in aqueous solution.

Isosbestic points in absorption spectra are generally helpful for estimation the number of particular forms in thermodynamic equilibrium. The pH evolution of the spectra of ferric citrate (**Fig. IV.A.1**) gradually reveals two isosbestic points at about 235 and 270 nm between pH 1 and 2, next one at 350 nm between pH 2.5 and 3.5 and another one at 315 nm between pH 5.4 and 6.9. Existence of the isosbestic points at three different pH values indicates an existence of three thermodynamic equlibria between four acid-base forms.

Estimation of pK values from of isosbestic points

The classical method of pK estimation is based on plotting absorbance at wavelengths, where the particular acid-base forms absorb differently. At such curves, the pH of the inflection point (outlined from the inflection point to pH axis) corresponds to pK value of the equilibrium between these two forms. We selected four various wavelengths (230, 265, 320 and 350 nm) in two different pH regions to estimate pK values of the acid-base equilibria of ferric citrate. In **Fig. IV.A.4 and Fig. IV.A.5**, the plots of absorbances vs. pH at the selected wavelengths, corresponding to pH ranges from 0.75 to 2.50, and between pH 1 and 8 respectively, are presented.

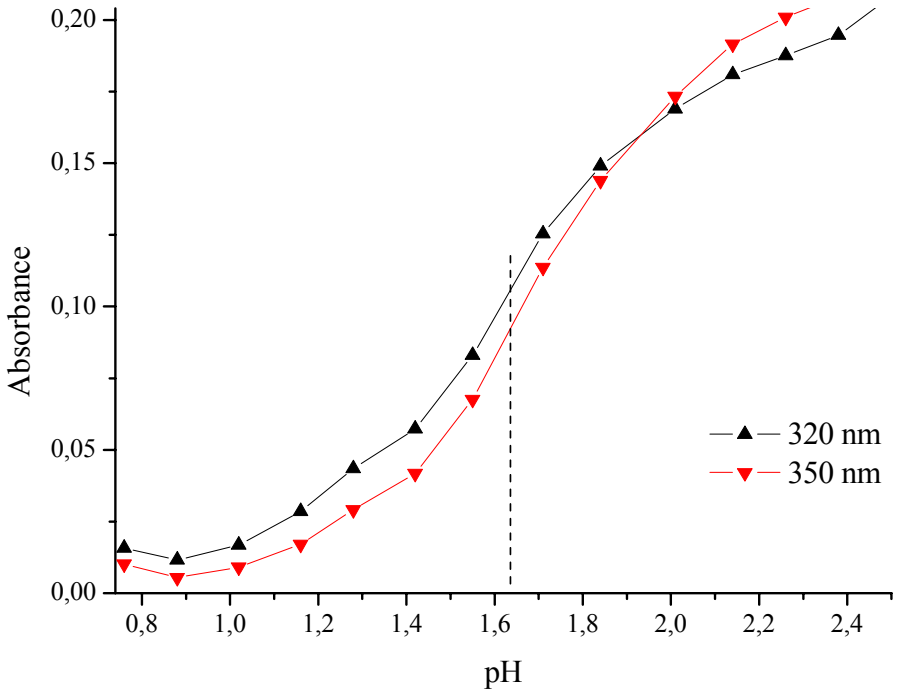

Fig. IV.A.4: Plot of absorbance vs pH at 320 and 350 nm of 2.55×10^{-4} mol.L^{-1} ferric citrate solution.

If we outline the inflection points in **Fig. IV.A.4**, we get the pK value around 1.6 of the corresponding acid-base equilibrium.

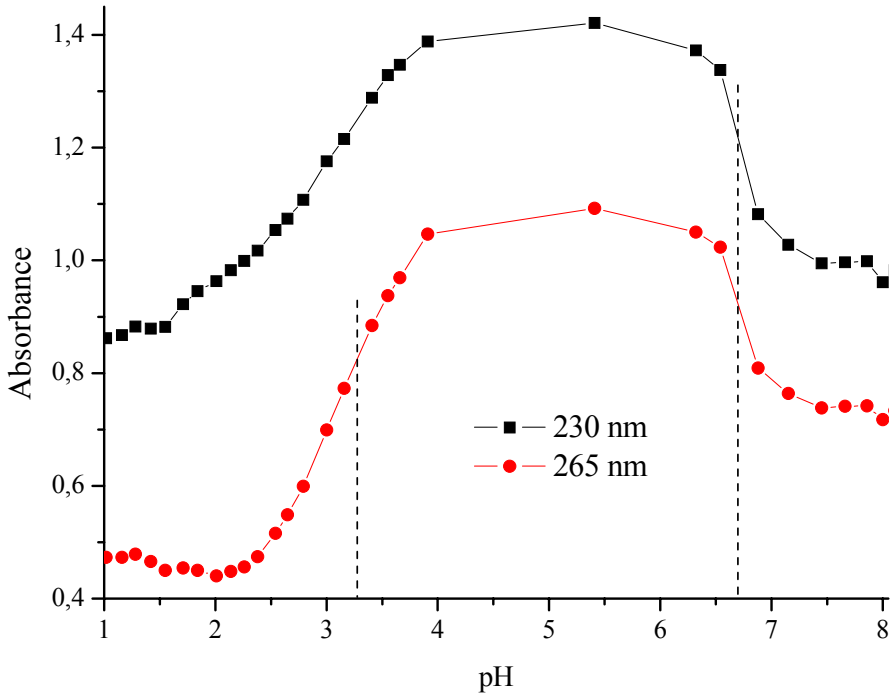

Fig. IV.A.5: Plot of absorbance vs. pH at 230 and 265 nm of 2.55×10^{-4} mol.L^{-1} ferric citrate solution.

By outlining the inflection points in **Fig. IV.A.5**, we can estimate two additional pK values. In the case of pH between 2.5 and 3.8, the pK value around 3.3, and for pH between 6 and 7, the pK close to 6.7.

Thus, three pK values of 1.6, 3.3, and 6.7 were estimated for the ferric citrate complex from the positions of isosbestic points in its absorption spectra measured as a function of pH. Base on it, existence of four acid-base forms of ferric citrate complex can be supposed.

Determination of equilibrium constants by non-linear regression

In order to improve the precision of the pK values estimated employing inflection points, a mathematical treatment of the spectra was performed. First of all, absorbances at selected wavelengths were plotted against pH, as shown in **Fig. IV.A.7**.

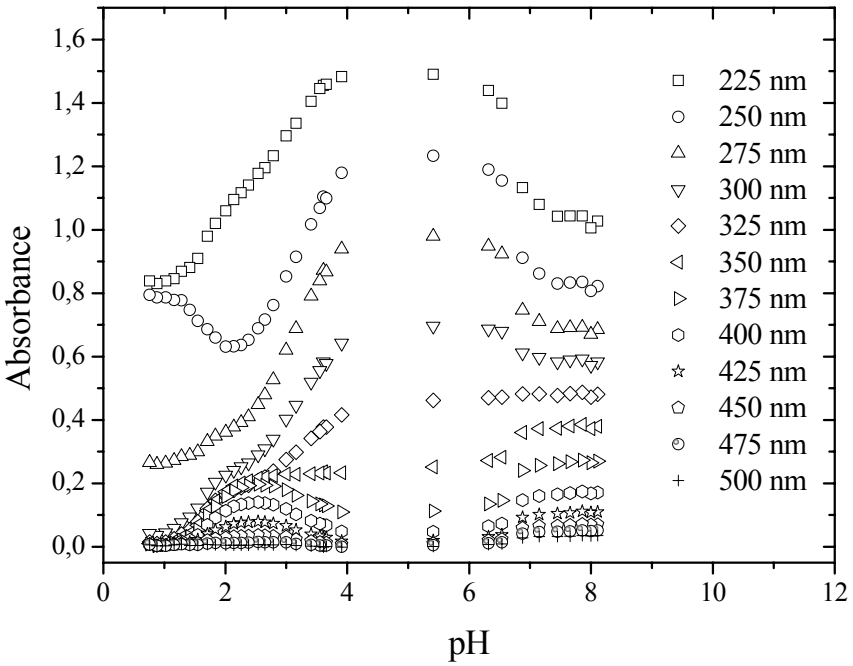

Fig. IV.A.7: Plots of absorbance vs. pH of ferric citrate complex at selected wavelengths.

There is a wide "empty" space between pH 4 and 6. In this range, the stabilisation of pH without buffering took a long time and was very sensitive to the addition of hydroxide. However, the spectra did not change during the stabilisation in the dark. The values of pH were measured only after stabilisation was completed.

The dependences of absorbance vs. pH were fitted all together as a multiple dataset by non-linear regression procedure. It was based on a model of thermodynamic equilibrium among four acid-base forms, which are supposed for the ferric citrate complex:

$$BH_3 \overset{K_{a1}}{\rightleftharpoons} BH_2 \overset{K_{a2}}{\rightleftharpoons} BH \overset{K_{a3}}{\rightleftharpoons} B \qquad \textbf{Eq. IV.A.2}$$

In classical acid-base equilibria, the participating forms are supposed to differ only in the number of protons and corresponding charges. However, the same mathematical model can be approximately applied also in more general cases, e.g., when some of the participating forms reversibly transform to other compounds with changed molecular skeleton. For example, we suppose that the most acidic form of the ferric citrate complex (**BH_3**) is not stable enough and reversibly dissociates to equimolar mixture of ferric aqua complex and citric acid, which formally represent the new product (**C**) with changed molecular skeleton.

However, both ferric aqua complex and citric acid appear in their acid-base forms corresponding to the particular pH. Their occurrence should influence the primary acid-base equlibria (**Eq. IV.A.2**) only negligibly otherwise the model will not fit the experimental data well or we will not interpret the results correctly. This is the approximation limit mentioned above. Taking into account this discussion, the classical acid-base equilibria (**Eq. IV.A.2**) can be changed to more general:

$$\mathbf{C} \overset{K_{a1}}{\rightleftharpoons} \mathbf{D} \overset{K_{a2}}{\rightleftharpoons} \mathbf{E} \overset{K_{a3}}{\rightleftharpoons} \mathbf{F} \qquad \textbf{Eq. IV.A.3}$$

Mathematical solution of both models leads the following equations for equilibrium concentrations of particular components as a function of proton concentration:

$$[C] = [BH_3] = \frac{C_{BH_3} \cdot [H^+]^3}{[H^+]^3 + ([H^+]^2 + ([H^+] + K_{BH})K_{BH_2})K_{BH_3}} \qquad \textbf{Eq. IV.A.4}$$

$$[D] = [BH_2] = \frac{C_{BH_3} \cdot [H^+]^2 \cdot K_{BH_3}}{[H^+]^3 + ([H^+]^2 + ([H^+] + K_{BH})K_{BH_2})K_{BH_3}} \qquad \textbf{Eq. IV.A.5}$$

$$[E] = [BH] = \frac{C_{BH_3} \cdot [H^+] \cdot K_{BH_2} \cdot K_{BH_3}}{[H^+]^3 + ([H^+]^2 + ([H^+] + K_{BH})K_{BH_2})K_{BH_3}} \qquad \textbf{Eq. IV.A.6}$$

$$[F] = [B] = \frac{C_{BH_3} \cdot K_{BH} \cdot K_{BH_2} \cdot K_{BH_3}}{[H^+]^3 + ([H^+]^2 + ([H^+] + K_{BH})K_{BH_2})K_{BH_3}} \qquad \textbf{Eq. IV.A.7}$$

The theoretical value of absorbance can be calculated, applying a Lambert-Beer law and introducing corresponding molar absorption coefficients ε_{BH3}, ε_{BH2}, ε_{BH}, and ε_B, as a sum of absorbances of the particular components BH_3, BH_2, BH, and B (for optical path of 1 cm):

$$A = A_0 + \varepsilon_{BH_3}[BH_3] + \varepsilon_{BH_2}[BH_2] + \varepsilon_{BH}[BH] + \varepsilon_B[B] \qquad \textbf{Eq. IV.A.8}$$

A_0 corresponds to formal absorbance of the background. The fitted theoretical dependences of absorbance on pH and pK values corresponding to the optimized equilibrium constants K_{a1}, K_{a2}, K_{a3} are shown in **Fig. IV.A.8**.

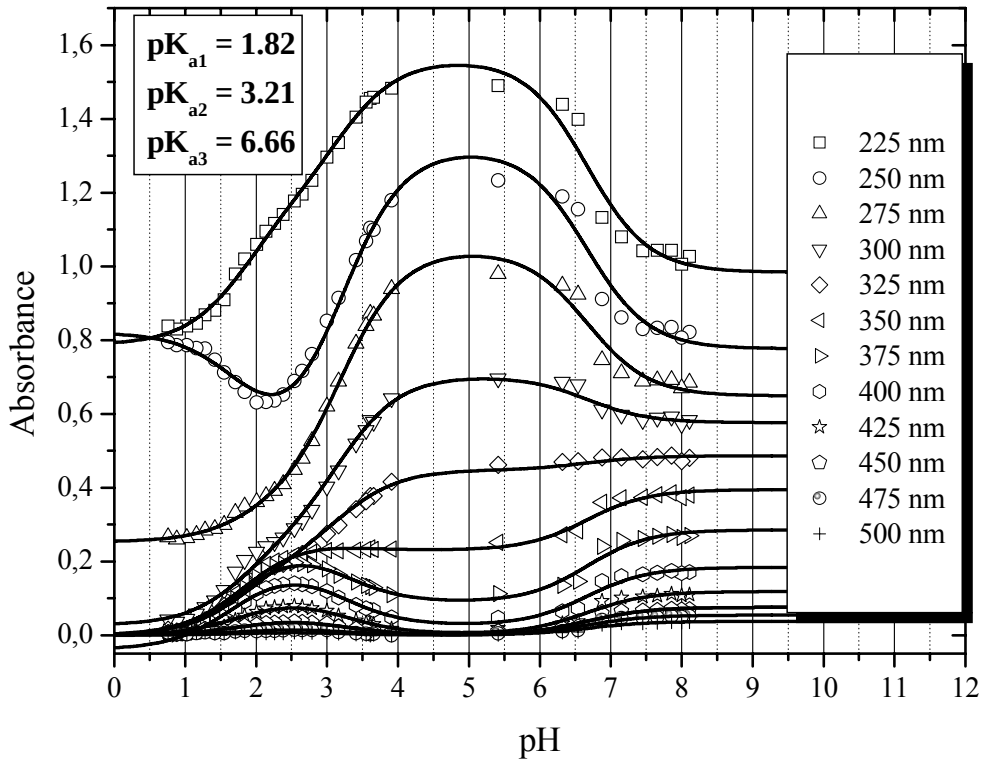

Fig. IV.A.8: Fits of dependences of absorbance on pH and optimized pK values of acid-base equilibria of ferric citrate complex.

The inflection points on calculated curves corresponding to the optimized pK values shown in **Fig. IV.A.8** agree well with their manual estimates given above.

Employing the optimized molar absorption coefficients of the particular acid-base forms of ferric citrate complex, their optimized absorption spectra can be plotted (**Fig. IV.A.9**).

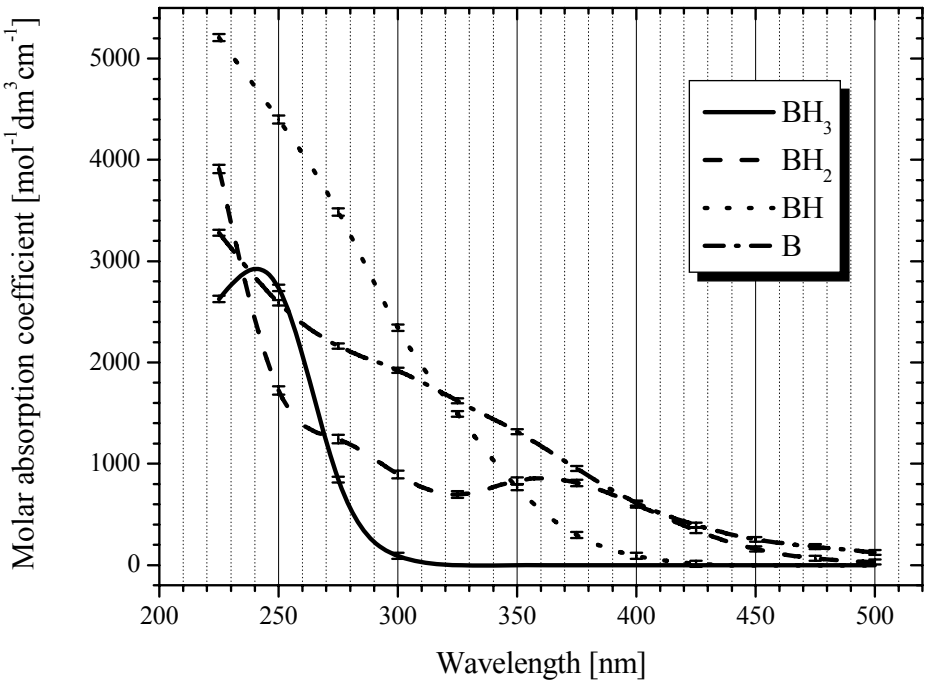

Fig. IV.A.9: Calculated absorption spectra of particular acid-base forms of ferric citrate complex.

In basic pH higher than 9, polymerisation and precipitation processes take place, as mentioned above. The spectrum of the most basic form (**F** or **B**) is gradually decreasing from UV to visible region over 480 nm and has a weak shoulder near 325 nm. It looks similar to the spectrum obtained during the ageing of aqueous solution of ferric perchlorate, which was attributed to the transformation of monomer ferric species into soluble ferric aggregates (***Měšťánková, 2004***), see **Fig. IV.A.10**. According this assignment, the most basic form of the ferric citrate complex should reversibly transform into soluble ferric aggregates.

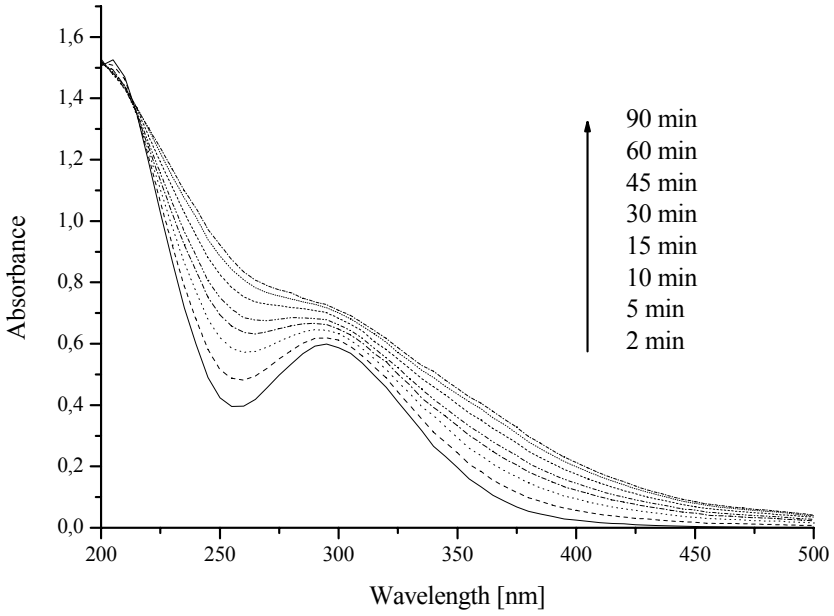

Fig. IV.A.10: Evolution of absorption spectra of 3×10^{-4} mol.L^{-1} aqueous solution of ferric perchlorate at room temperature, initial pH = 3.2, (***Měšťánková, 2004***).

Spectrum of the next acid-base form (**E** or **BH**) of ferric citrate complex starts at 440 nm and has a shoulder at 275 nm. It is close to the spectrum ferric citrate complex at its natural pH of 3.55 for the concentration 2.55×10^{-4} mol.L^{-1}, see **Fig. IV.A.11**.

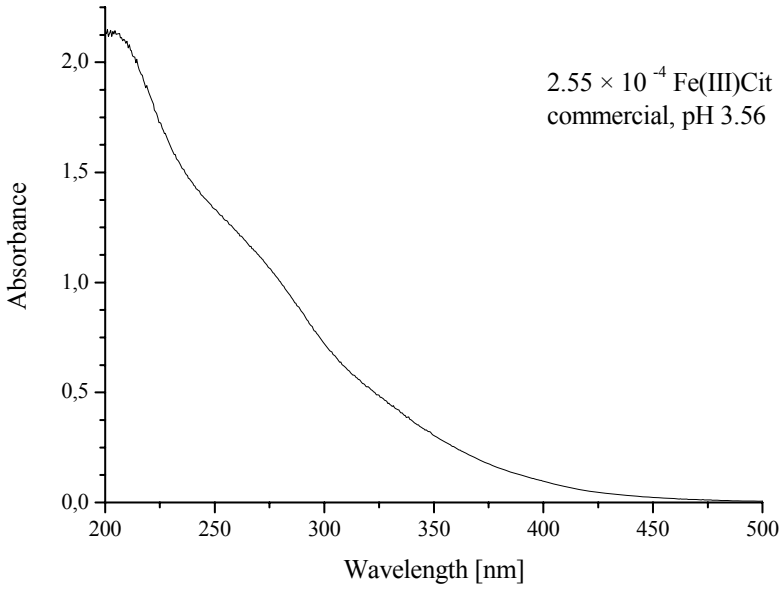

Fig. IV.A.11: Absorption spectrum of 2.55×10^{-4} mol.L^{-1} ferric citrate complex at natural pH.

Spectrum of the following acid-base form of ferric citrate complex (**D** or $\mathbf{BH_2}$) starts at 500 nm and has a well developed maximum at around 365 nm and a shoulder at about 275 nm. No similar spectrum was found in the literature.

Spectrum of the most acidic form of ferric citrate complex (**C** or $\mathbf{BH_3}$) looks very similar to the spectrum of hexaaqua ferric complex $[Fe(H_2O)_6]^{3+}$, as shown in **Fig. II.A.5**. The absorption starts at 300 nm and has a maximum at 240 nm. This assignment was confirmed by additional measurements performed at pH = 1 (see in **Fig. IV.A.12**). The observed differences between the spectrum of ferric citrate complex and the sum spectrum of citric acid plus ferric perchlorate can be attributed to the fact that at pH = 1.0 approximately ten percent of the second acidic form of ferric citrate complex (**D** or $\mathbf{BH_2}$) still occurs.

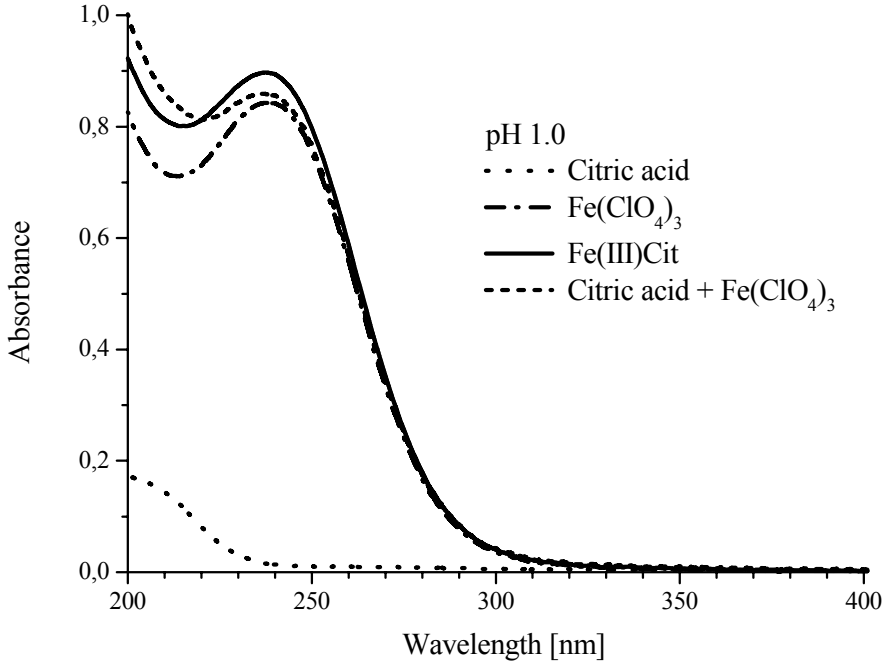

Fig. IV.A.12: Absorption spectra of citric acid, ferric perchlorate and ferric citrate complex, sum spectrum of citric acid plus ferric perchlorate, pH = 1, concentrations of all components were 2.55×10^{-4} mol.L^{-1}.

The optimized values of equilibrium constants were applied with the equations **Eq. IV.A.1 – 4** to calculate a distribution diagram of the particular components occurring in the acid-base equilibria of ferric citrate complex, see plots **Fig. IV.A.13**. We can see that practically all the ferric ions are complexed at around natural pH of 3.5. With decreasing pH, the concentration of ferric hexaaqua complex (**C** or $\mathbf{BH_3}$) is gradually increasing.

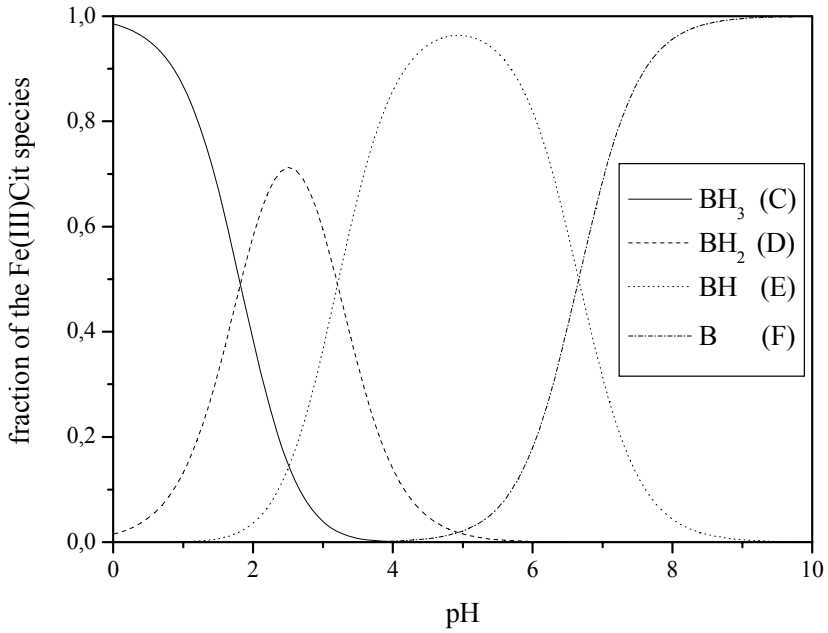

Fig. IV.A.13: Distribution diagram of particular components in acid-base equilibria of ferric citrate complex.

The optimized values of equilibrium constants of the ferric citrate complex could be also compared to the dissociation constants of citric acid, the distribution diagram of which is shown in **Fig. IV.A.3**. However, it does not have any direct relevance, as the acidic groups in both systems are different.

That is why DFT/B3LYP/6-31G(d) quantum chemical computations were performed to investigate and compare possible structures of ferric citrate triaqua and ferric hydroxyaqua complexes in their various acid-base forms. The main results can be shortly summarized:

- Systems containing one ferric ion have open-shell electronic structure with degenerated molecular orbitals.
- The most stable multiplicity is sextet, which corresponds to five degenerated HOMO orbitals.
- Coordination sphere of ferric ion is octahedral.
- In ferric citrate triaqua complexes, citrate is bound to ferric ion through hydroxy, carboxyl and methylencarboxyl group while the other methylencarboxyl group is not coordinated.
- Systems containing two ferric ions, such as dimer $[(FeO)_2(H_2O)_8]^{2+}$, have close-shell singlet electronic structure.

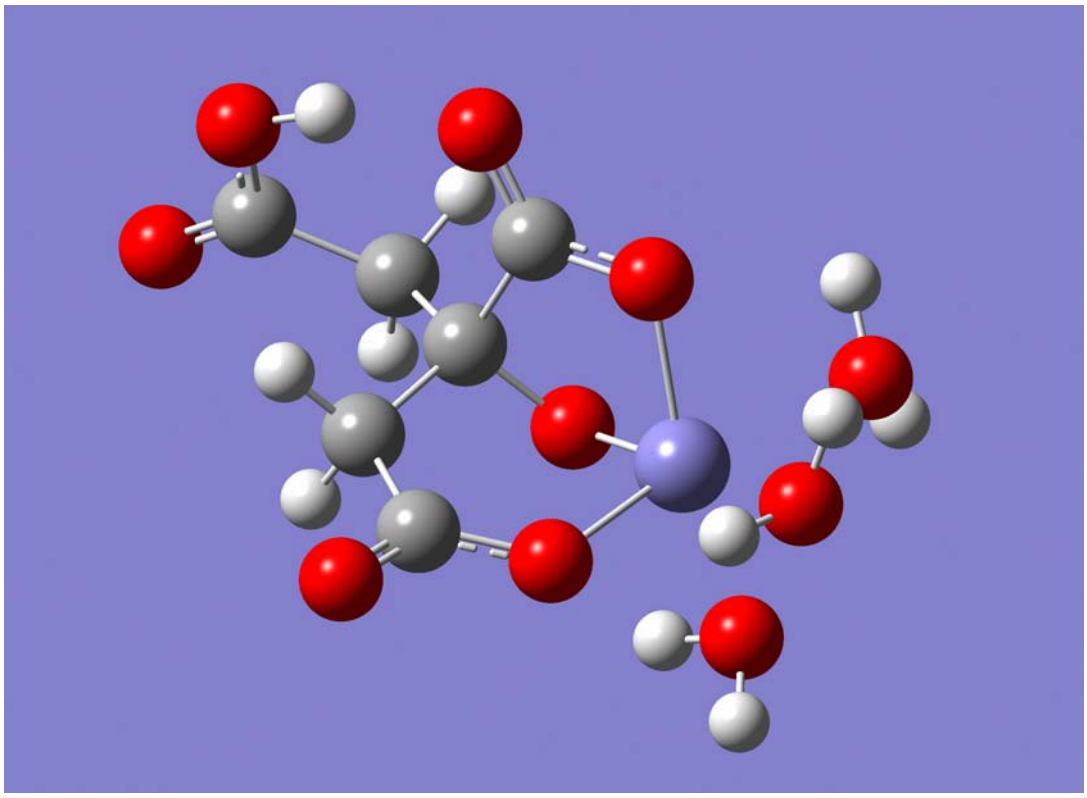

Fig. IV.A.14: Optimized structure of a tridentate ferric triaqua citrate complex [FeCit$(H_2O)_3$] in the most stable sextet electronic configuration.

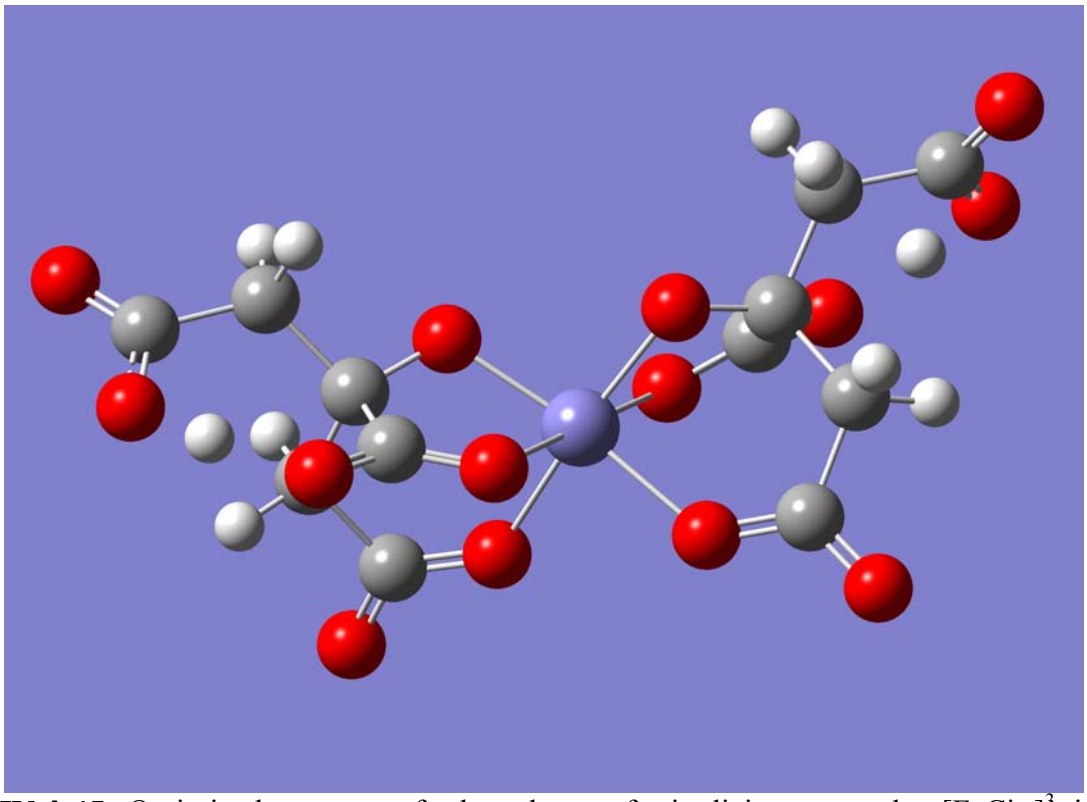

Fig. IV.A.15: Optimized structure of a hexadentate ferric dicitrate complex $[FeCit_2]^{3-}$ in the most stable sextet electronic configuration.

The theoretical DFT/B3LYP/6-31G(d) computations indicated a possible existence of ferric dicitrate complexes (**Fig. IV.A.15**). To search for them, two sets of additional experiments were performed.

In the first case, UV-Vis absorption spectra of aqueous solutions containing perchloric acid to give an exact pH = 1.9, 10^{-4} mol.L^{-1} ferric perchlorate and variable concentration of citric acid (from 10^{-4} to 10^{-3} mol.L^{-1}) were measured (**Fig. IV.A.16**).

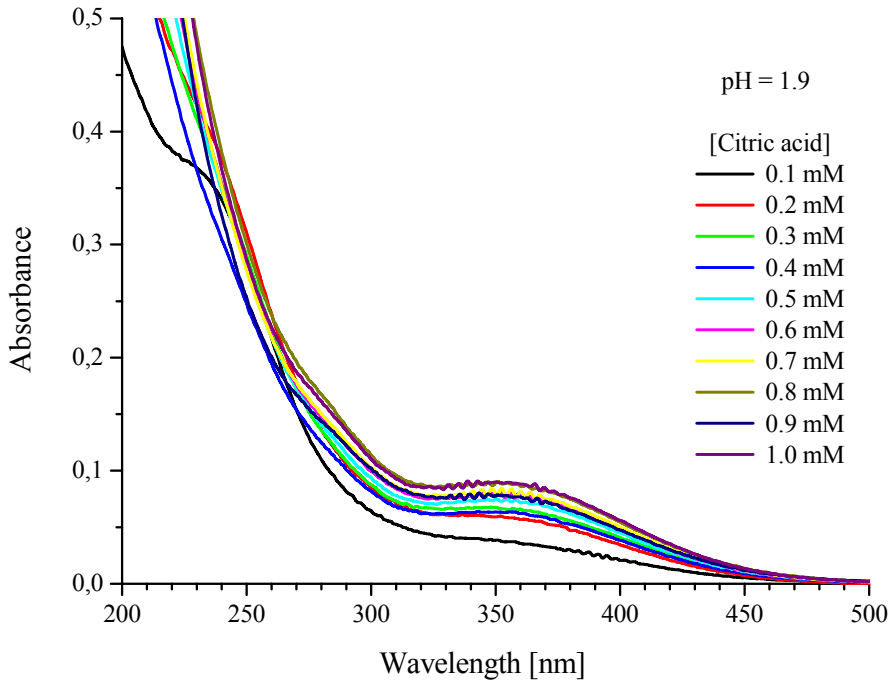

Fig. IV.A.16: Absorption spectra of ferric citrate complexes in acidified aqueous solution (pH = 1.9) of ferric perchlorate (10^{-4} mol.L^{-1}) with various concentrations of citric acid.

The second additional experiment consisted of measurements of UV-Vis absorption spectra of acidified aqueous solutions (pH = 1.9) containing 10^{-4} mol.L^{-1} citric acid and various concentrations of ferric perchlorate from 10^{-4} to 7×10^{-4} mol.L^{-1} (**Fig. IV.A.17**).

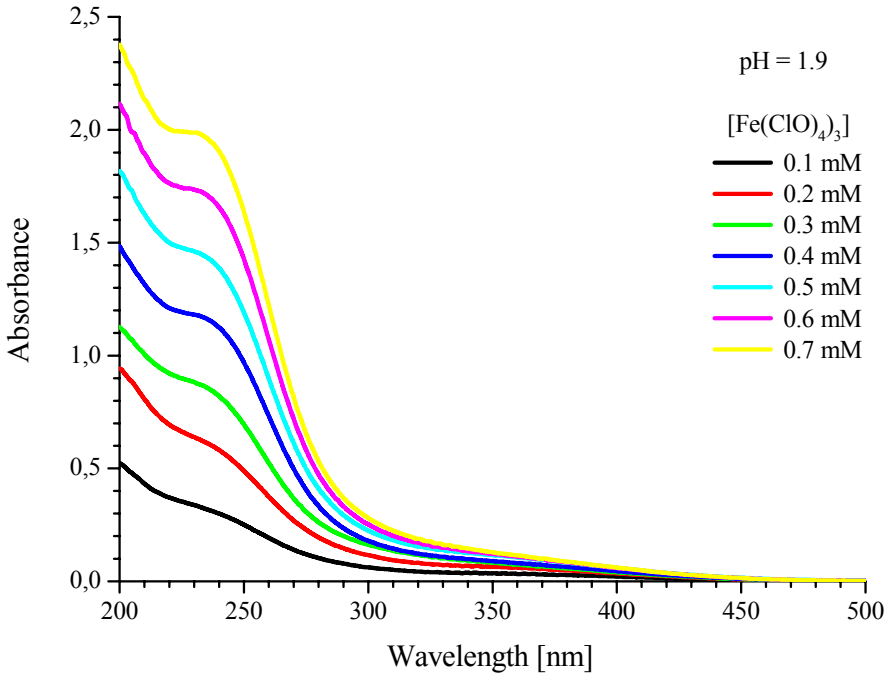

Fig. IV.A.17: Absorption spectra of ferric citrate complexes in acidified aqueous solution (pH = 1.9) of citric acid (10^{-4} mol.L^{-1}) with various concentrations of ferric perchlorate.

For wavelengths from 250 to 450 nm each 10 nm, twenty one dependences of absorbance on the varied concentration of either citric acid or ferric perchlorate were selected from the measured spectra. Then, all these dependences were fitted together as a multiple dataset employing a non-linear regression procedure based on a model of thermodynamic equilibrium between a metal ion (**M**) and a ligand (**L**) forming a 1 : 1 complex (**ML**):

$$\mathbf{M} + \mathbf{L} \overset{K_1}{\rightleftharpoons} \mathbf{ML} \qquad \textbf{Eq. IV.A.9}$$

Mathematical solution of this model leads the following equations for equilibrium concentrations of particular components as a function of the analytical concentrations of both metal (c_M) and ligand (c_L):

$$[M] = \frac{c_M K_1 - c_L K_1 - 1 + \sqrt{4c_L K_1 + (1 - c_L K_1 + c_M K_1)^2}}{2K_1} \qquad \textbf{Eq.IV.A.10}$$

$$[L] = \frac{c_L K_1 - c_M K_1 - 1 + \sqrt{4c_L K_1 + (1 - c_L K_1 + c_M K_1)^2}}{2K_1} \qquad \textbf{Eq.IV.A.11}$$

$$[ML] = \frac{c_L K_1 + c_M K_1 + 1 - \sqrt{4c_L K_1 + (1 - c_L K_1 + c_M K_1)^2}}{2K_1} \qquad \textbf{Eq.IV.A.12}$$

The theoretical value of absorbance (A) can be calculated, applying a Lambert-Beer law and introducing corresponding molar absorption coefficients ε_M, ε_L, and ε_{ML}, as a sum of absorbances of the particular components ***M***, ***L***, and ***ML*** (for optical path of 1 cm):

$$A = \varepsilon_M [M] + \varepsilon_L [L] + \varepsilon_{ML} [ML] \qquad \textbf{Eq.IV.A.13}$$

The fitted theoretical dependences of absorbance on c_M and c_L are shown in **Fig. IV.A.18** (full view) and **Fig. IV.A.19** (detail for lower absorbances).

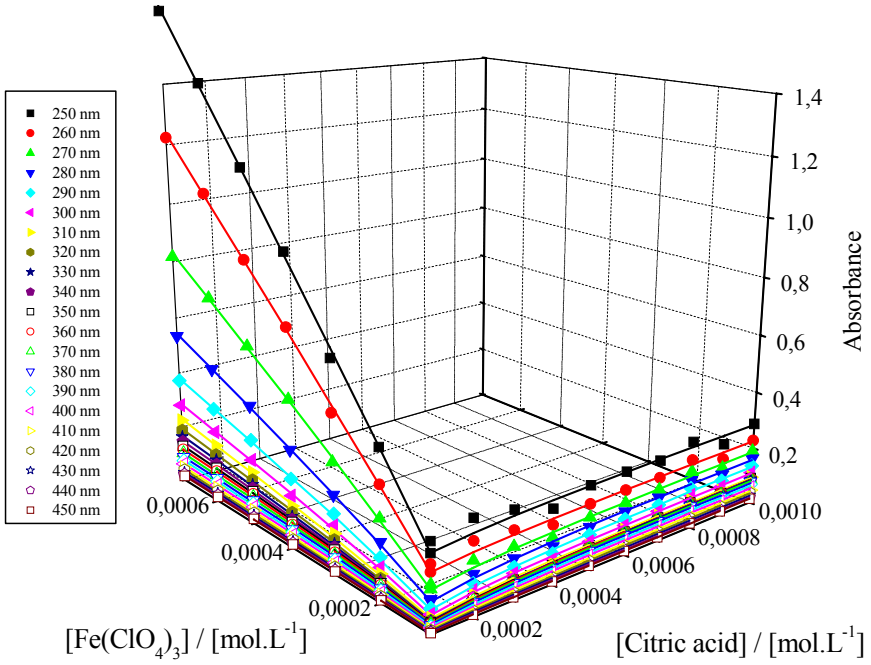

Fig. IV.A.18: Three-dimensional fits of dependences of absorbance on analytical concentrations of both ferric perchlorate and citric acid for 1 : 1 complex formation.

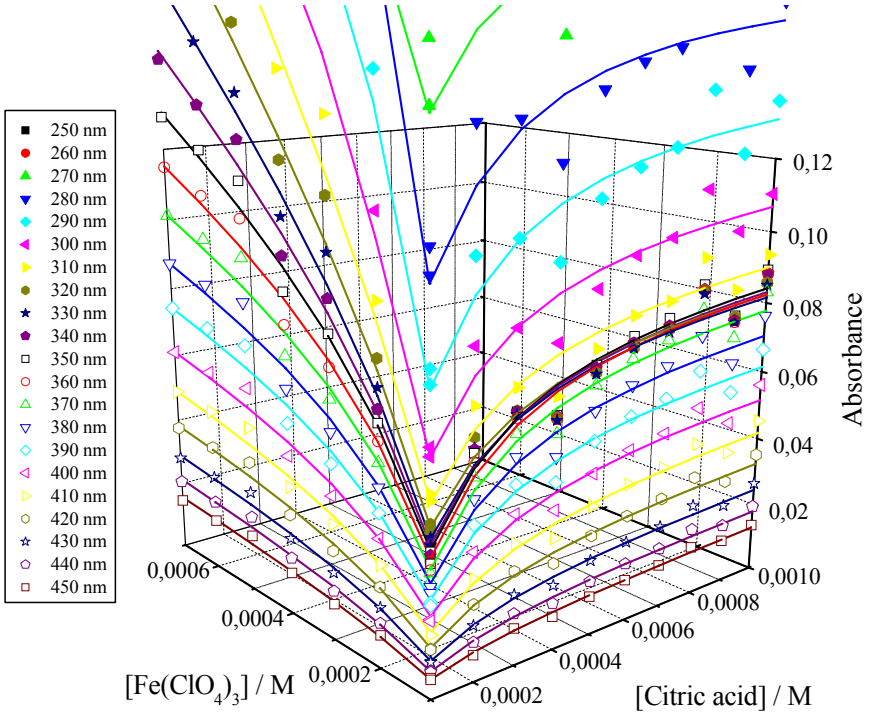

Fig. IV.A.19: Three-dimensional fits of dependences of absorbance on analytical concentrations of both ferric perchlorate and citric acid for 1 : 1 complex formation (detail view for lower absorbances).

As one can see in **Fig. IV.A.18** and **Fig. IV.A.19**, the calculated curves fit the experimental points over all wavelengths well, without any systematic deviation for particular regions of concentrations of both ferric perchlorate and citric acid. It means that the applied model of a 1 : 1 complex formation describes the real thermodynamic equilibrium. If consecutively a 1 : 2 complex will be created, systematic deviations in the branch of higher concentrations of citric acid might be expected. If directly a 1 : 2 complex will be formed, the initial slope of dependences of absorbance on concentration of ligand would be higher and of metal ion would be lower than for the 1 : 1 complex. However, a direct 2 : 2 complex creation can not be distinguished from 1 : 1 complexation. Then the calculated molar absorption coefficients would differ by a factor 2.

Employing the optimized molar absorption coefficients of the particular components of ferric citrate complex equilibrium, their absorption spectra can be plotted (**Fig. IV.A.20**).

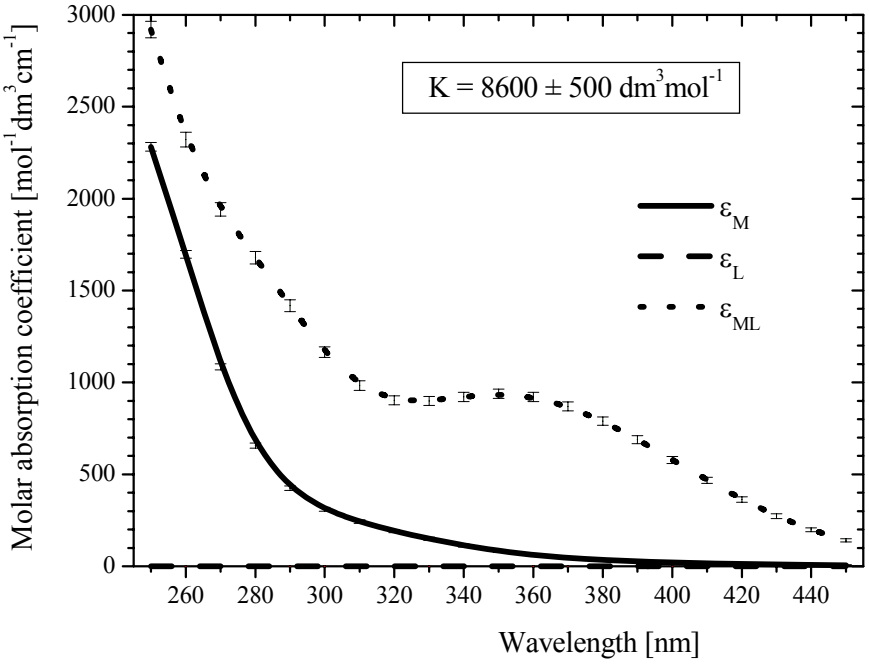

Fig. IV.A.20: Calculated absorption spectra of particular components of ferric citrate complexation and corresponding equilibrium constant.

At pH = 1.9, the ferric citrate complex exists partly (approximately 44 %) in the most acidic form (**C** or $\mathbf{BH_3}$), partly (about 53 %) in the next one (**D** or $\mathbf{BH_2}$) and partly (about 3%) in the following one (**E** or **BH**). This due to an acid-base equilibrium between them with pK_{a1} = 1.82 (see **Fig. IV.A.13**). The comparison of the calculated spectra of these two forms (in proportion 44 : 53 : 3) on one hand (**Fig. IV.A.9**) with the calculated spectrum of ferric citrate complex at pH = 1.9 on the other hand (**Fig. IV.A.20**) shows a good agreement.

It is worth to note that they resulted from experiments of different kind (i.e., varied pH at constant concentration of ferric citrate on one hand, and varied concentrations of both ferric perchlorate and citric acid at constant pH on the other hand). The relatively high value of the formal equilibrium constant of $(8.5 \pm 0.5) \times 10^4$ $mol^{-1}.L$ of ferric citrate complexation at pH = 1.9 corresponds well with the strong binding, which can be expected for the tridentate complex structure computed theoretically by quantum chemical method. The formal equilibrium constant represents a linear combination of real equilibrium constants of the acid-base forms that occur at pH = 1.9, i.e., 44 % of the most acidic (**C** or $\mathbf{BH_3}$) and 53 % of the second acidic form (**D** or $\mathbf{BH_2}$). Provided that the most acidic form (**C** or $\mathbf{BH_3}$) is fully

dissociated giving ferric hexaaqua complex, as was proposed above (**Fig. IV.A.12**), the real equilibrium constant of the second acidic form (**D** or $\mathbf{BH_2}$) would be even by 44 % higher.

IV.A.2 Conclusion on physico-chemical properties

Based on the results of our experimental as well as theoretical studies, chemical structures of the components participating in the acid-base equilibrium of ferric citrate complex could be proposed. The most basic form (**F** or **B**) and most acidic form (**C** or $\mathbf{BH_3}$) were already assigned, according to spectral similarities, to ferric soluble agglomerates and ferric hexaaqua complex, respectively.

Our theoretical study showed that an octahedral coordination is the only stable conformation of the ferric citrate triaqua complexes, either deprotonated or variously protonated. Citrate is bound to ferric ion through hydroxyl, carboxyl and methylencarboxyl groups while the other methylencarboxyl group is not coordinated. Because of general acidity of carboxylic groups, one could expect a considerable deprotonation of the unbound methylencarboxyl group after dissolution of the solid ferric citrate in water. As referred above, spectrum of the second basic form (**E** or **BH**) of ferric citrate complex is very similar to the spectrum of ferric citrate complex at its natural pH (compare **Fig. IV.A.9** and **Fig. IV.A.11**). Thus, one could deduce that the second basic form (**E** or **BH**) of ferric citrate complex is an anion with deprotonated methylencarboxylic group.

As a consequence, the second acidic form (**D** or $\mathbf{BH_2}$) of ferric citrate complex should be uncharged with protonated methylencarboxylic group. However, one should take into account the open-shell character of monomeric ferric species. In the case of ferric hexaaqua complex, the triple positive charge represents, due to corresponding electrostatic repulsion, a sufficient energy barrier against dimerization. However, the electroneutral form of ferric citrate complex might tend to dimerize and thus to recombine its unpaired electrons to a close-shell structure. The resulting 2 : 2 ferric citrate complex was already proposed by some authors in the literature (***Timberlake, 1964***). As mentioned above, our spectroscopic experiments could not distinguish between 1 : 1 and 2 : 2 stoichiometries. Nevertheless, we can propose additional experiments, e.g., employing EPR technique, that could answer the question about stoichiometry of the uncharged ferric citrate complex. However, this overreached the topic of this thesis.

IV.A.3 Photochemical properties

A solution of ferric citrate complex (2.55×10^{-4} mol.L^{-1}) was irradiated at 365 nm. On the basis of our results (**Fig IV.A.13)**, ferric citrate complex exists in three acid-base forms at the initial pH = 3: **D** or **BH_2** (59 %), **E** or **BH** (37 %), and **C** or **BH_3** (4 %). The spectral evolution in the course of irradiation is shown in **Fig. IV.A.21**.

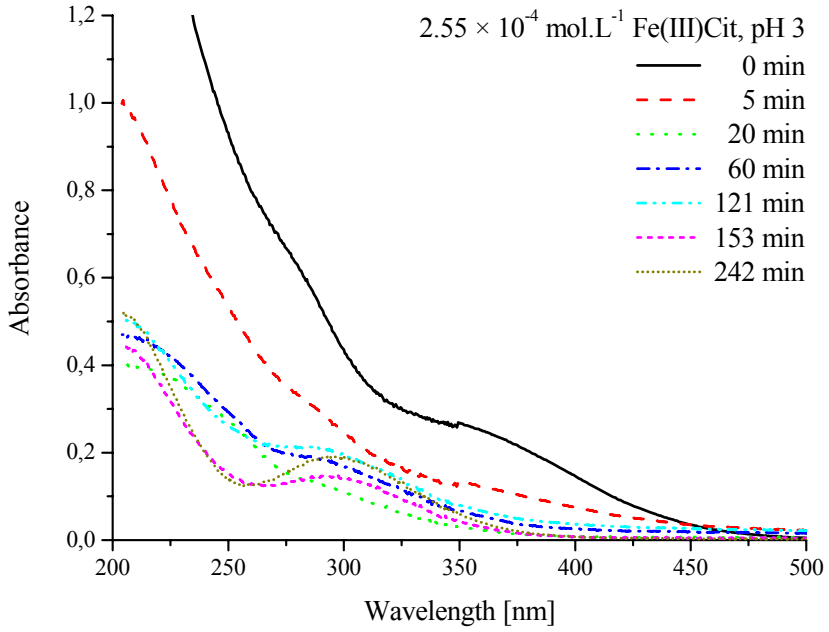

Fig. IV.A.21: Selected spectra of 2.55×10^{-4} mol.L^{-1} Fe(III)Cit complex irradiated at 365 nm (3 lamps), initial pH = 3.

Initial decrease of the absorbance was observed at all the wavelengths below 450 nm. The shoulder at 275 nm in the initial solution was no longer visible after 20 minutes. A shoulder at 300 nm cleared out at 60 minutes and was becoming more distinct with time; at 120 minutes it started reshaping to a clear peak with maximum at 300 nm. Since 60 minutes of irradiation, an increase of absorbance was observed between 200 and 220 nm.

Impact of Fe(III)Cit concentration:

Analogous experiments were carried out for three other concentrations of ferric citrate (**Fig. IV.A.22 – 24**).

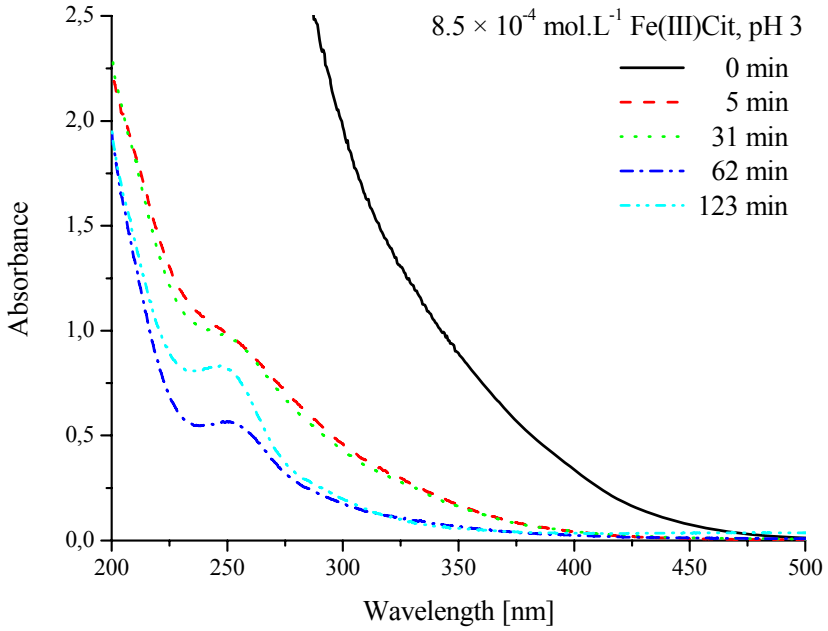

Fig. IV.A.22: Selected spectra of 8.5×10^{-4} mol.L^{-1} Fe(III)Cit complex irradiated at 365 nm (3 lamps), initial pH = 3.

A huge decrease of absorbance all over the spectra was observed in first 5 minutes of irradiation of the ferric citrate solution of initial concentration 8.5×10^{-4} mol.L^{-1}; a shoulder at 250 nm appeared. This shoulder transformed to a peak at same wavelength upon continuous irradiation until 60 minutes, while the absorbance was decreasing all over the spectrum. Further irradiation up to 120 minutes led to an increase of absorbance between 200 and 320 nm. The absorbance at the top of the peak at 250 nm increased from 0.57 to 0.82.

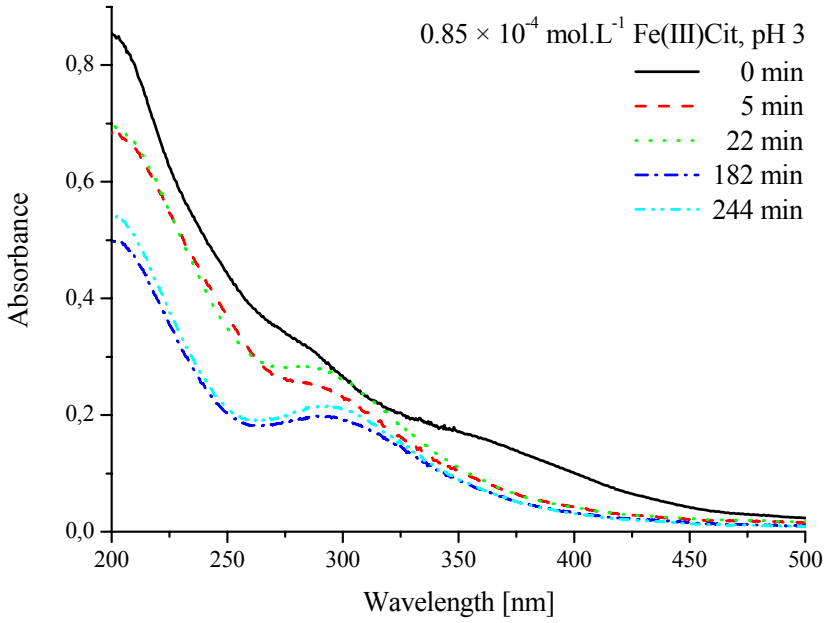

Fig. IV.A.23: Selected spectra of 0.85×10^{-4} mol.L^{-1} Fe(III)Cit complex irradiated at 365 nm (3 lamps), initial pH = 3.

The absorbance of the irradiated 0.85×10^{-4} mol.L^{-1} ferric citrate was decreasing all along the spectrum up to 5 minutes, while a shoulder moved from initially 275 nm to 300 nm. The absorbance between 260 and 360 nm was then increasing up to 20 minutes. With further irradiation, the absorbance was then decreasing all along the spectra up to 180 minutes, while the shoulder at 300 nm transformed to a peak at the same wavelength. Finally, the absorbance slightly increased all over the spectrum up to 240 minutes.

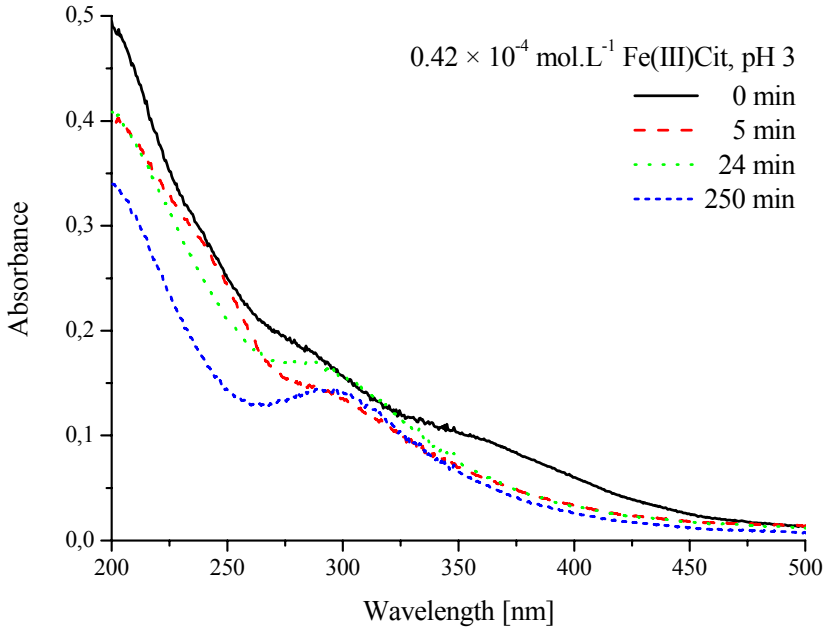

Fig. IV.A.24: Selected spectra of 0.42×10^{-4} mol.L^{-1} Fe(III)Cit complex irradiated at 365 nm (3 lamps), initial pH = 3.

The evolution of absorbance of irradiated 0.42×10^{-4} mol.L^{-1} ferric citrate looks like the previous one. The absorbance was decreasing all along the spectrum. The shoulder at 275 nm shifted to 300 nm. Then, the absorbance below 265 nm decreased and the absorbance between 265 and 355 nm increased up to 24 minutes. With further irradiation up to 250 minutes, the absorbance was decreasing all over the spectrum, while the shoulder at 300 nm transformed to a peak at identical wavelength.

Generally, the band with a maximum near 300 nm appeared for long irradiation time at lower ferric citrate concentrations ($< 2.55 \times 10^{-4}$ mol.L^{-1}). This band could correspond to the formation of a monomeric hydroxyaqua complex $Fe(OH)^{2+}$, which exists in the range of pH between 3.0 and 5.0. The observed spectral evolutions showed that the ferric citrate complex was photodecomposing fast under complementary formation of Fe(II). The hydroxyaqua complex $Fe(OH)^{2+}$ observed was appearing consecutively due to reoxidation of Fe(II). The band centred near 250 nm appeared at higher concentrations of ferric citrate.

Impact of pH:

The impact of pH on the speciation of ferric citrate complex was described above. Thus, an effect of pH on the photodecomposition of ferric citrate was also supposed. On the

basis of our previous results (**Fig IV.A.13**), the ratio of form **D** to **E** (or $\mathbf{BH_2}$ to **BH**) at pH = 4 will be about 14 : 86. The spectral evolution of 2.55×10^{-4} mol.L^{-1} ferric citrate at initial pH = 4 upon irradiation at 365 nm is presented at **Fig. IV.A.27**.

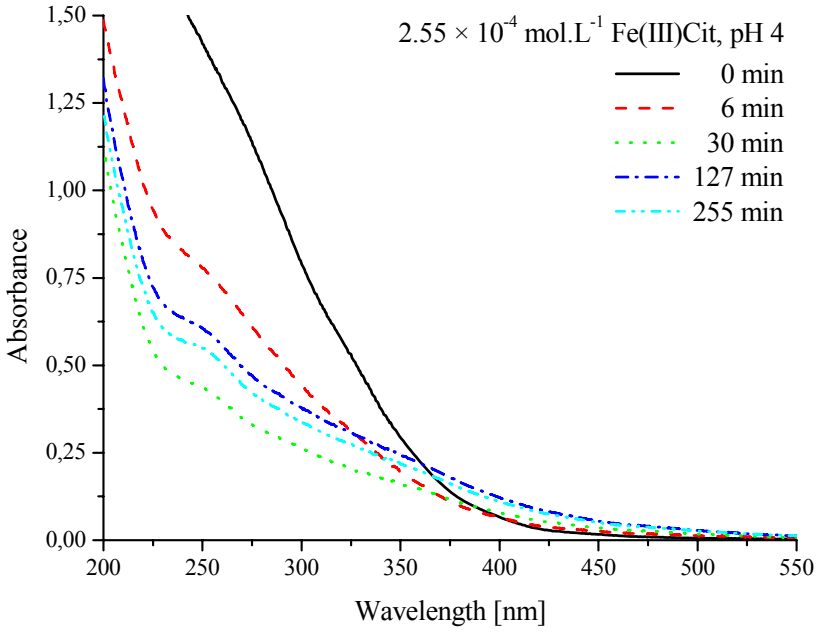

Fig. IV.A.27: Selected spectra of 2.55×10^{-4} mol.L^{-1} Fe(III)Cit complex irradiated at 365 nm (3 lamps), initial pH = 4.

The absorbance of the irradiated 2.55×10^{-4} mol.L^{-1} ferric citrate solution was decreasing up to 30 minutes for the wavelengths shorter than 380 nm. A shoulder at 250 nm appeared at 5 minutes and remained practically unchanged up to 255 minutes. Between 30 and 127 minutes of irradiation, the absorbance was increasing all along the spectrum. With further irradiation, the absorbance again decreased all along the spectrum.

The band centred near 250 nm, which appeared at higher concentrations of ferric citrate, also occurred at higher pH.

Evolution of pH and kinetics of [Fe(II)]:

The evolution of pH (**Fig. IV.A.25**) and kinetics of Fe(II) (**Fig. IV.A.26**) were followed in the course of all four preceding experiments of the photodecomposition of ferric citrate complex. For comparison, another irradiation experiment with starting pH = 4 was performed, too.

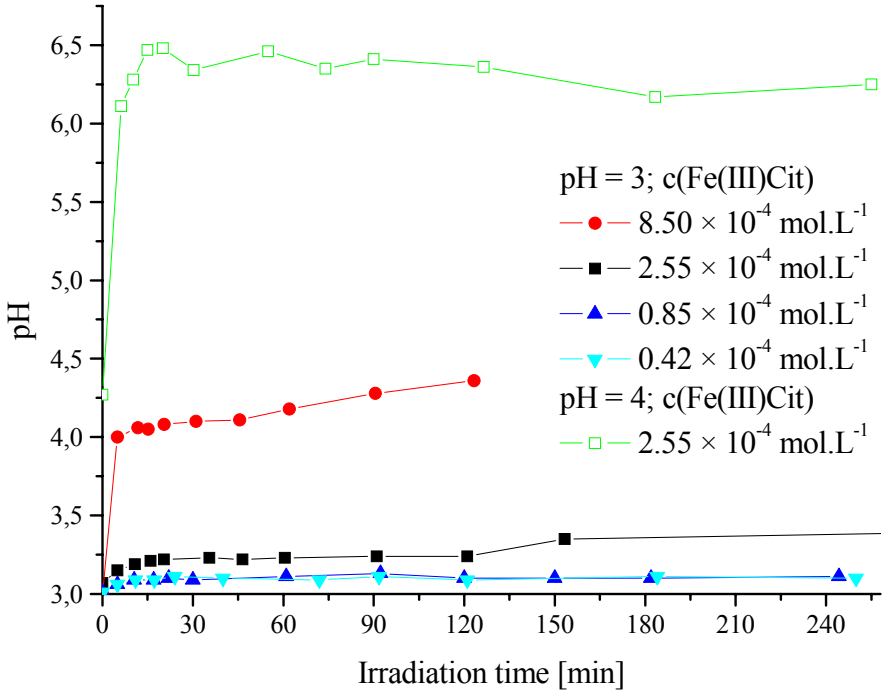

Fig. IV.A.25: Evolution of pH in solutions containing various initial concentrations of Fe(III)Cit complex under irradiation at 365 nm (3 lamps).

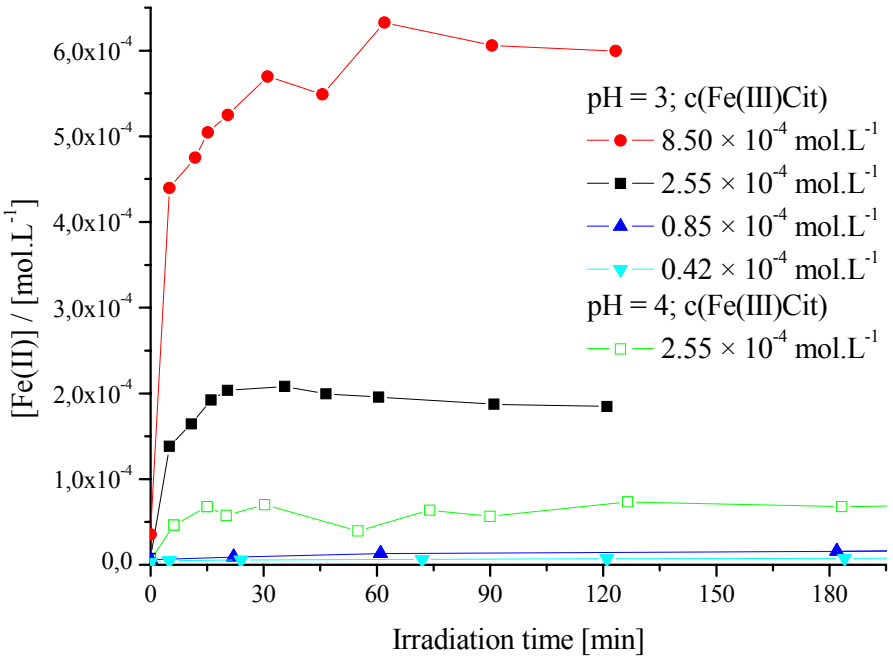

Fig. IV.A.26: Kinetics of [Fe(II)] in solutions containing various initial concentrations of Fe(III)Cit complex under irradiation at 365 nm (3 lamps).

In all cases, the pH was rapidly increasing during the first 15 minutes and then reached a plateau. For the same starting pH, the total change was proportional to the initial concentration of ferric citrate. For the same initial concentration of ferric citrate, the total pH change was proportional to its starting value. The increase of pH is a result of the consumption of H^+ ion during the photolysis of the ferric citrate complex. The values of pH at plateaus and the total change of concentration of H^+ ion are given in **Tab. IV.A.1**.

Initial conditions		Plateau values		[Fe(II)] / $[Fe(III)Cit]_{init}$	$\Delta[H^+]$ [mol.L^{-1}]
pH	[Fe(III)Cit] [mol.L^{-1}]	Final pH	[Fe(II)] [mol.L^{-1}]		
3	8.50×10^{-4}	4.05	6.0×10^{-4}	71%	-9.1×10^{-4}
	2.55×10^{-4}	3.21	2.0×10^{-4}	78%	-3.6×10^{-4}
	8.50×10^{-5}	3.10	1.1×10^{-5}	13%	-1.8×10^{-4}
	4.25×10^{-5}	3.09	6.1×10^{-6}	14%	-1.6×10^{-4}
4	2.55×10^{-4}	6.47	6.8×10^{-5}	27%	-9.7×10^{-5}

Tab. IV.A.1: Plateau values of pH and [Fe(II)] at irradiation of ferric citrate complex of various concentration or initial pH; ratio of [Fe(II)] to $[Fe(III)Cit]_{init}$ = $[Fe_{total}]$; ratio of consumed H^+ ions to initial concentration of ferric citrate complex; 3 lamps.

The formation of Fe(II) was also the fastest at the beginning of irradiation. The concentration of Fe(II) reached a plateau value after 30 minutes of irradiation. The concentrations of Fe(II) at plateau are given also in **Tab. IV.A.1**.

The highest Fe(II) ratios to total iron (71 – 78%) were observed at initial pH = 3 for the initial concentration of ferric citrate higher than 2.55×10^{-4} mol.L^{-1}. The ratio for the other concentration at pH = 3 was about 13 – 14%. At initial pH = 4, the ratio was 27% that is much lower than the corresponding value 78% at pH = 3.

The quantum yields:

The quantum yields of Fe(II) formation were determined using monochromatic irradiation at 365 nm. The values for various initial pH and their comparison with results from literature are given in **Tab. IV.A.2**.

pH	ϕ (Fe(II))	*Abida* [a]	*Abrahamson* [b]
2	0.16 ± 0.02	0.07	
2.5	0.14 ± 0.02		
2.7			0.28
2.75	0.19 ± 0.02		
3	0.28 ± 0.03	0.28	
4	0.22 ± 0.03	0.29	0.45
5	0.19 ± 0.02		
6	0.11 ± 0.01	0.08	

Tab. IV.A.2: Quantum yields of Fe(II), [Fe(III)Cit] = 2.55×10^{-4} mol.L^{-1} and comparison with results from literature.

[a] ***Abida (2005)***: quantum yield of Fe(II) appearance; [Fe(III)Cit] = 3×10^{-4} mol.L^{-1}.

[b] ***Abrahamson et al. (1994)***: quantum yield of Fe(II) appearance (± 15%), [Fe(III)] = 3×10^{-4} mol.L^{-1}, [Citric Acid] = 1.5×10^{-3} mol.L^{-1}, $I_0 = 7.66 \times 10^{-9}$ einstein.s^{-1}, irradiation source spectra not given.

The highest quantum yield was observed at initial pH = 3. It was in a good agreement with the result of ***Abida (2005)***. For both higher and lower values of the initial pH than pH = 3, the quantum yield of Fe(II) formation was decreasing.

Impact of pH stabilisation:

In order to simplify the interpretation of kinetics of the occurring processes, a new set of experiments under lower irradiation flux (one lamp instead of three) and at constant pH was carried out (**Fig. IV.A.28 – 30**). Employing the pH-stat titration, the previously observed increase of pH during the photodecomposition of ferric citrate could be eliminated. The spectral evolution upon irradiation of the 2.55×10^{-4} mol.L^{-1} ferric citrate complex by one lamp at stabilized pH = 2.9 is shown in **Fig. IV.A.28**.

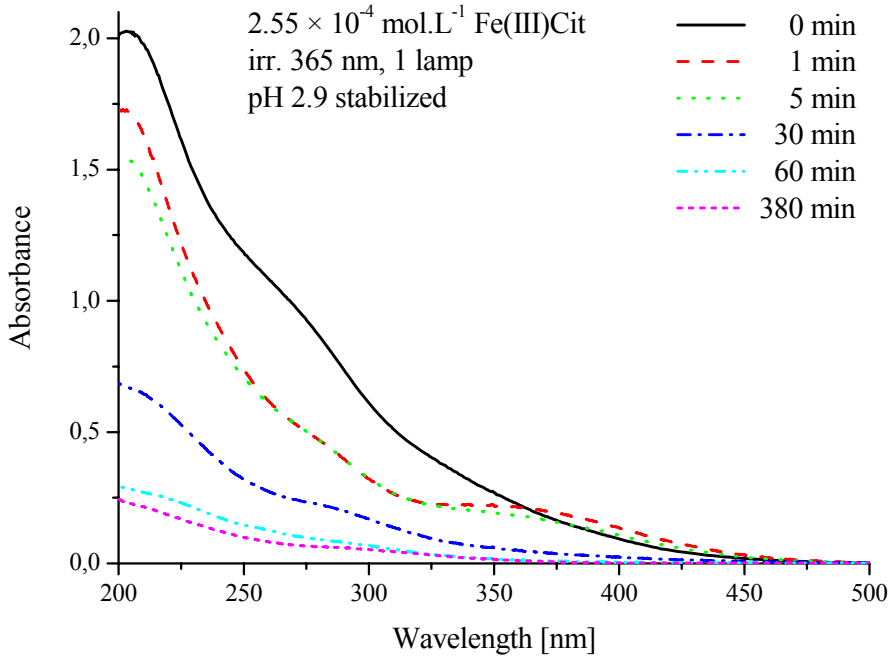

Fig. IV.A.28: Selected spectra of 2.55×10^{-4} mol.L^{-1} Fe(III)Cit complex irradiated upon irradiation at 365 nm (1 lamp) at stabilized pH = 2.9.

The absorbance was decreasing between the wavelengths 200 and 360 nm; between 360 and 460 nm a slight increase was observed after 1 minute of irradiation. The shoulder at 275 nm shifted to 280 nm and a new band with maximum at 370 nm appeared. After 5 minutes of irradiation, the band at 370 nm decreased, and the absorbance between 200 and 255 nm decreased. A decrease all along the spectrum continued upon further irradiation up to 380 minutes. The absorbance at 200 nm notably decreased, and the shoulder, which was initially at 275 nm, shifted to 300 nm.

The spectral evolution upon irradiation of the 2.55×10^{-4} mol.L^{-1} ferric citrate complex by one lamp at stabilized pH = 4 is shown in **Fig. IV.A.29**.

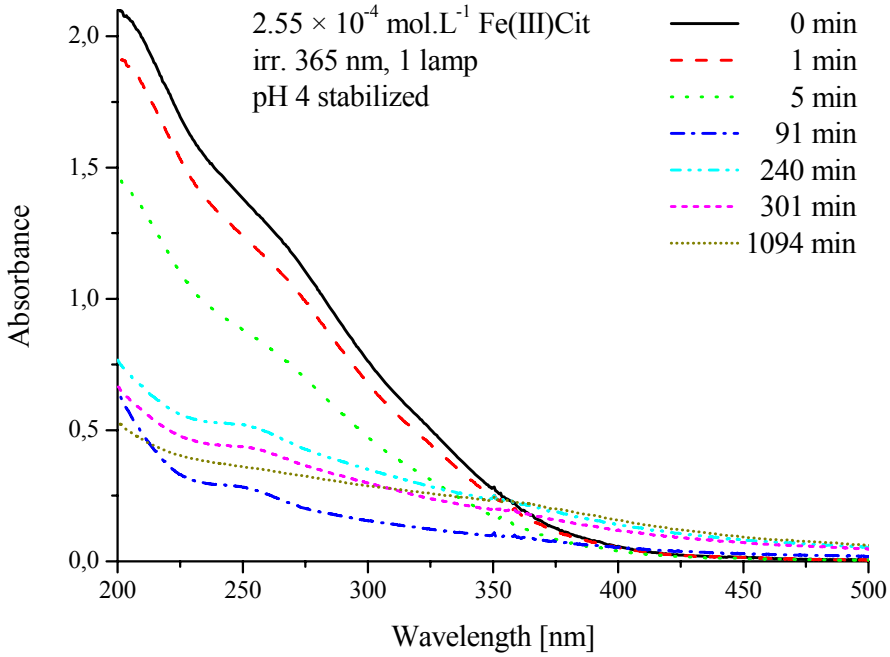

Fig. IV.A.29: Selected spectra of 2.55×10^{-4} mol.L^{-1} Fe(III)Cit complex irradiated upon irradiation at 365 nm (1 lamp) at stabilized pH = 4.0.

The absorbance was decreasing below 400 nm up to 90 minutes. A shoulder, which was initially present at 270 nm, shifted to 250 nm. With further irradiation, an increase of absorbance was observed up to 240 minutes; a slight shoulder at 360 nm started to come out. With continued irradiation, the absorbance decreased all over the spectrum up to 301 minutes. Subsequently, the absorbance above 310 nm increased again; at 1094 minutes the shoulder at 250 minutes dissapeared, and a slight shoulder was still observed at 360 nm.

The spectral evolution upon irradiation of the 2.55×10^{-4} mol.L^{-1} ferric citrate complex by one lamp at stabilized pH = 5 is shown in **Fig. IV.A.30**.

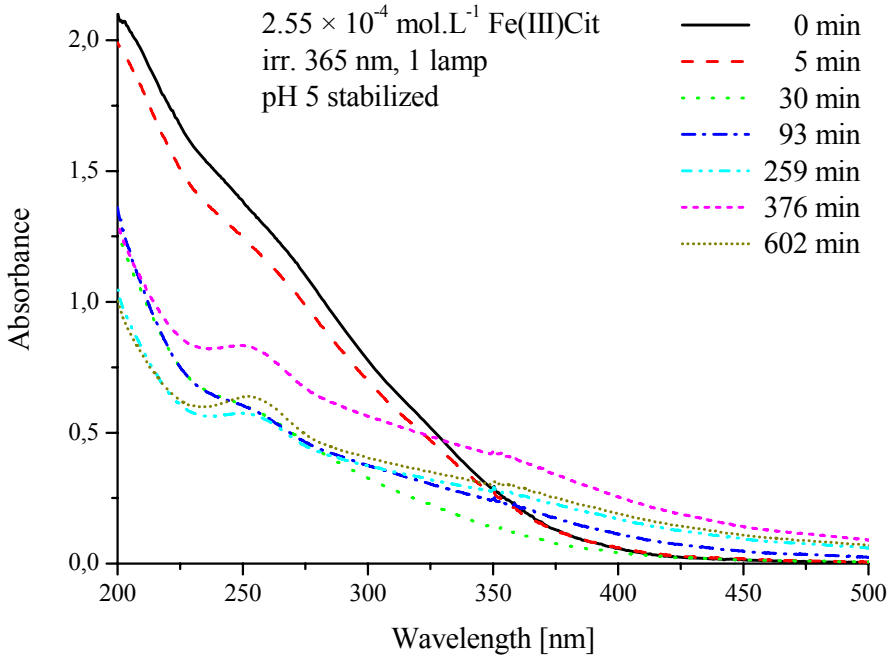

Fig. IV.A.30: Selected spectra of 2.55×10^{-4} mol.L^{-1} Fe(III)Cit complex irradiated upon irradiation at 365 nm (1 lamp) at stabilized pH = 5.0.

The absorbance was decreasing all over the spectrum up to 30 minutes of irradiation. The shoulder, which was initially present at 275 nm, decreased and shifted to 250 nm. With further irradiation, up to 93 minutes, the absorbance above 275 nm increased, and a shoulder at 250 nm appeared. With continued irradiation to 259 minutes, the absorbance above 220 nm was increasing, and the absorbance below 220 nm slightly decreased; the shoulder at 250 nm transformed to a clear peak. At 376 minutes, the absorbance increased all over the spectrum. The continued irradiation up to 602 minutes led to another decrease all along the spectrum.

The pH stabilisation lowers the number of parameters of the reaction system that simplifies its kinetic behaviour. Generally, the species that occurred in the non stabilised systems (λ_{max} = 250 or 300 nm) were not always present in the stabilised systems, even if the other parameters were identical. For example, the specie with the maximum at 250 nm was observed only at high pH after several hours of irradiation. On the contrary in the not stabilised systems, it was seen at high initial concentration of ferric citrate or at starting pH = 4. In the stabilised system, it was visible at the stabilised pH ≥ 4. As a contrary, the band at 300 nm was observed for lower concentrations ($\leq 2.55 \times 10^{-4}$ mol.L^{-1}) and starting pH = 3.

It was never observed when the pH was stabilised. This fact could be also due to the lower irradiation intensity used in the experiments with stabilised pH values.

Complexation by acetonedicarboxylic acid:

As mentioned in the bibliographic part, one of the primary intermediates of the photodecomposition of ferric citrate is acetondicarboxylic acid (ACDA), as reported by ***Abrahamson et al. (1994)***.

In order to find out a possible complexation of ferrous ions with ACDA, the spectra of ACDA and $Fe(ClO_4)_2$ mixtures as well as of their separate solutions at different concentrations were measured. The observed differences were very low, practically negligible. We can conclude that the Fe(II) does not form any complex with acetondicarboxylic acid.

Analogous experiments were performed also for ferric ions. However, no complexation between $Fe(ClO_4)_3$ and ACDA was seen. Thus, neither ferric nor ferrous ions form complexes with ADCA.

IV.A.4 Conclusion on photochemical properties

Mechanism of ferric citrate degradation:

Based on our results, a probable mechanism of the photochemical transformation of ferric citrate in its anionic acid-base form (**E** or **BH**), which is most abundant at natural pH, can be proposed as follows:

$$Fe(III)Cit^{-} + h\upsilon + H^{+} \longrightarrow Fe^{2+} + {}^{\bullet}OOCC(OH)(CH_2COO)_2^{2-}$$

A fast decarboxylation the citrate radical dianion will probably follow. The decarboxylated radical dianion will probably react with molecular oxygen to give the corresponding dianion of acetone dicarboxylic acid (ADCA) and hydroperoxyl radical:

$${}^{\bullet}OOCC(OH)(CH_2COO)_2^{2-} \longrightarrow {}^{\bullet}C(OH)(CH_2COO)_2^{2-} + CO_2$$

$${}^{\bullet}C(OH)(CH_2COOH)_2^{2-} + O_2 \longrightarrow OC(CH_2COO)_2^{2-} + HO_2^{\bullet}$$

Hydroperoxyl radical occurs in acid-base equilibrium with superoxide radical anion:

$$HO_2^{\bullet} \rightleftharpoons O_2^{\bullet -} + H^{+}$$

These radicals can disproportionate to hydrogen peroxide and oxygen (***Christensen and Sehested, 1988***). This reaction is faster at lower pH due to presence of the uncharged form, i.e., hydroperoxyl radical:

$$HO_2^{\bullet} + HO_2^{\bullet} \rightarrow H_2O_2 + O_2$$

Fe(II) will undergo a Fenton reaction with the formed hydrogen peroxide giving ferric monohydroxy complex and hydroxyl radical:

$$Fe^{2+} + H_2O_2 \longrightarrow Fe(OH)^{2+} + {}^{\bullet}OH$$

The formed ferric monohydroxy complex can be photodissociated to Fe(II) and hydroxyl radical. This photoreaction represents, beside the Fenton reaction mentioned above, another source of hydroxyl radical:

$$Fe(OH)^{2+} + h\nu \longrightarrow Fe^{2+} + {}^{\bullet}OH$$

Beside participation in Fenton reaction, Fe^{2+} can react also with hydroxyl radical, hydroperoxyl radical or superoxide radical anion to regenerate Fe(III):

$$Fe^{2+} + {}^{\bullet}OH \longrightarrow Fe(OH)^{2+} + OH^{-}$$

$$Fe^{2+} + HO_2^{\bullet} + H^{+} \longrightarrow Fe(III) + H_2O_2$$

$$Fe^{2+} + {}^{\bullet}O_2^{-} + 2H^{+} \longrightarrow Fe(III) + H_2O_2$$

The photodissociation of $Fe(OH)^{2+}$ giving Fe^{2+} and hydroxyl radical and oxidation of Fe^{2+} back to $Fe(OH)^{2+}$ represents an iron redox cycle. On its repeated turnover, photoinduced degradation of organic substances is based. The produced hydroxyl radical namely attacks any organic molecule to initiate its partial oxidation. Finally, all organic structures present in aqueous solutions of iron salts under irradiation will be fully mineralized to simple inorganic substances such as water, carbon dioxide and corresponding mineral acids.

Thus ADCA, which does not form either ferric or ferrous complexes, will be further oxidized and finally mineralised to water and carbon dioxide.

$$ADCA + {}^{\bullet}OH \longrightarrow \text{oxidized intermediates} \longrightarrow H_2O + CO_2$$

The scheme of reactions is shown on the **Fig IV.A.31**.

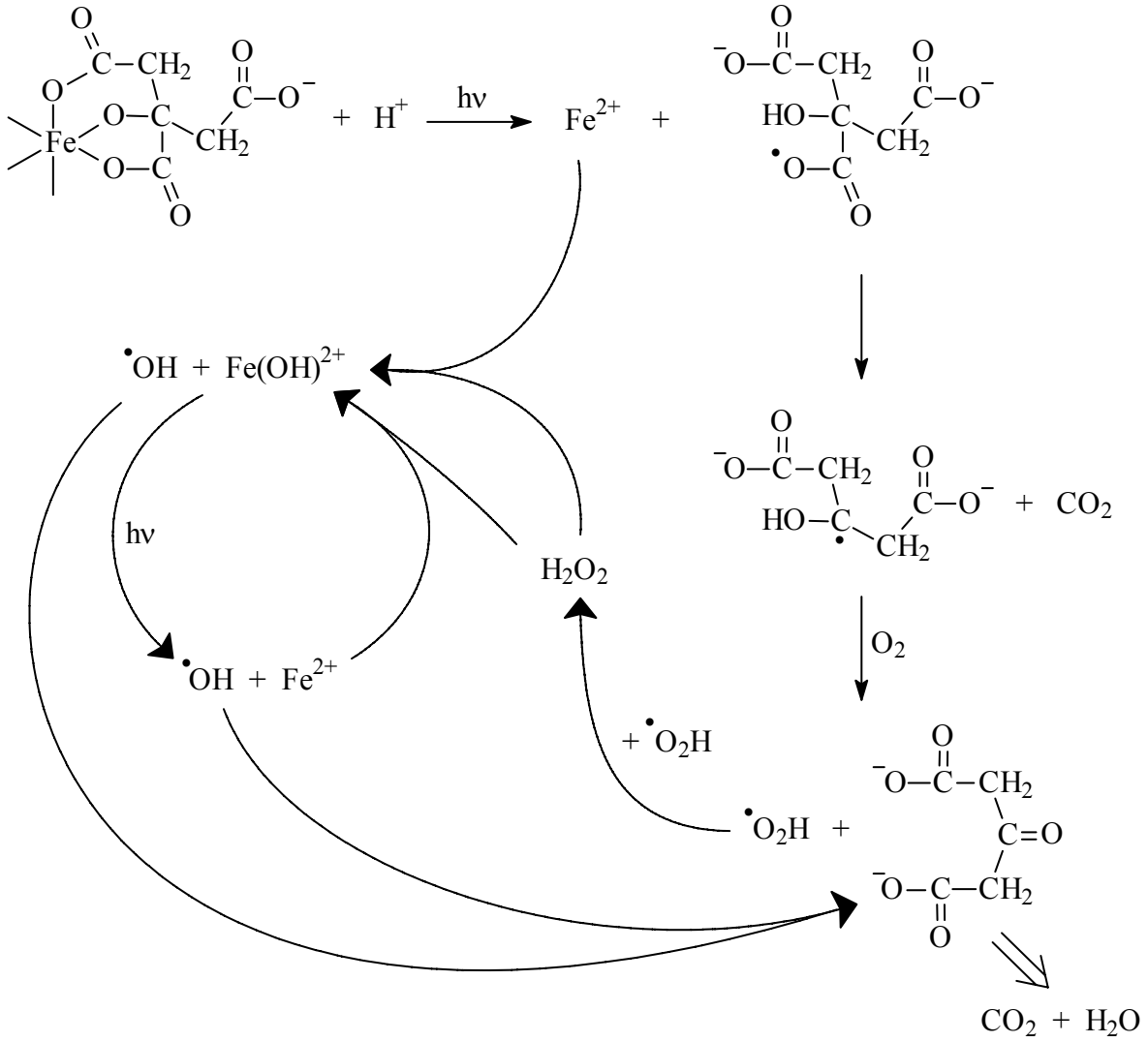

Fig IV.A.31: Scheme of ferric citrate photodecomposition.

The measured quantum yields of Fe^{2+} formation show that photoactive forms of ferric citrate exist in a wide range of pH between 2 and 6. However, the most photoactive forms occur around pH = 3.

IV.B Photodegradation of Monuron in the presence of ferric citrate

If nothing is mentioned, all the irradiations were carried out in a photoreactor with three lamps emitting at 365 nm.

IV.B.1 Photochemical properties of Monuron

The absorption spectrum of Monuron has a maximum at 245 nm with a molar absorption coefficient of 1.78×10^4 L.mol^{-1}.cm^{-1} and a low shoulder at 280 nm (**Fig. II.G.2**). As mentioned in the bibliography Monuron does not absorb above 300 nm, therefore its photolysis by sunlight is a negligible process in order of days, in 48 days 83% of Monuron disppearance (***Hill et al., 1955***).

A solution of 1×10^{-4} mol.L^{-1} Monuron at pH = 3.0 was irradiated at 365 nm (**Fig. IV.B.1**). No degradation of Monuron was observed after several hours of irradiation. Therefore, no direct photolysis takes place in the system.

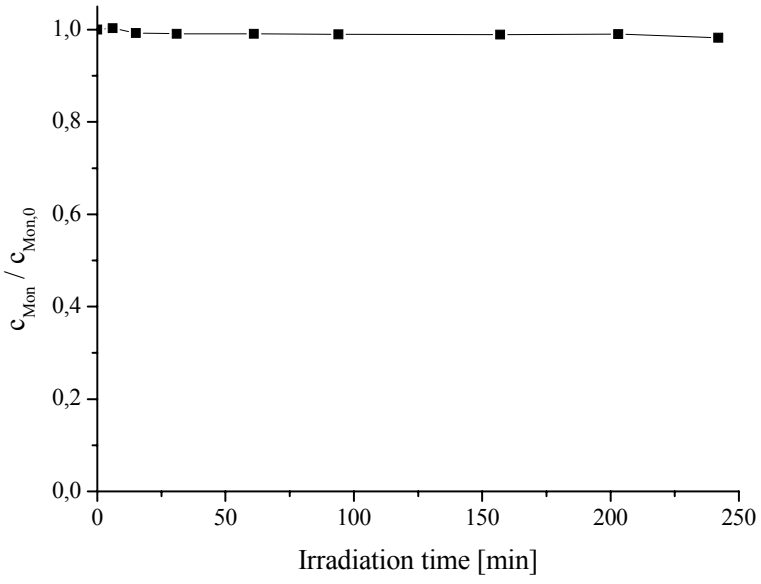

Fig. IV.B.1: Irradiation of 1×10^{-4} mol.L^{-1} solution of Monuron at 365 nm.

The mixture of 2.55×10^{-4} mol.L^{-1} iron-citrate and 1×10^{-4} mol.L^{-1} Monuron was kept in the dark at room temperature for several days. The UV-visible spectrum, corresponding to the sum of the spectra of the both components, was repeatedly measured, see **Fig. IV.B.2**.

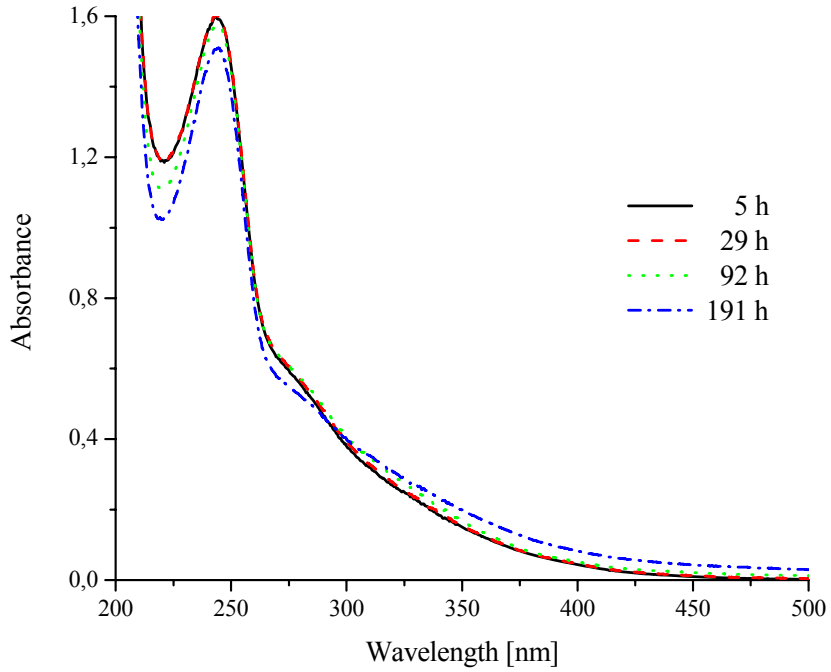

Fig. IV.B.2: Spectra of a mixture of 2.55×10^{-4} mol.L^{-1} ferric citrate and 1×10^{-4} mol.L^{-1} Monuron, as a function of time (natural pH = 4.8, length of the absorption cell = 0.5 cm).

During one day, the solution was stable and no significant transformation was observed. Thus, there was no interaction between ferric citrate complex and Monuron in the groundstate. After three other days and further, a decrease of absorption was observed at the wavelengths below 260 nm, and also an increase of absorption occurred above 300 nm. These spectral changes indicated a partial degradation of the ferric citrate complex. The decrease of absorbance below 260 nm was also affected by a slight disappearance of the Monuron. However, the thermal effect was negligible in all the performed experiments, as its duration was always shorter than one day.

IV.B.2 Kinetic behaviour

A mixture of ferric citrate complex (2.55×10^{-4} mol.L^{-1}) and Monuron (1.0×10^{-4} mol.L^{-1}) was irradiated at 365 nm at initial pH = 6. The UV-visible spectral evolution is presented in the following figure (**Fig. IV.B.3**). After irradiation, a decrease of absorption was observed at the wavelengths below 330 nm, and also an increase of absorption occured above 330 nm. These spectral changes indicated the degradation of the ferric citrate complex and the subsequent degradation of Monuron.

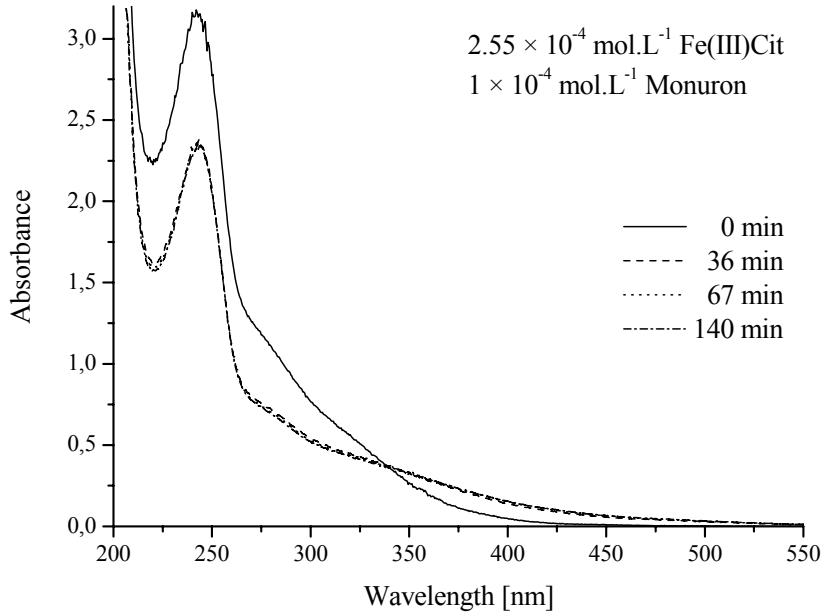

Fig. IV.B.3: Spectra of a ferric citrate and Monuron mixture at initial pH = 6, as a function of irradiation time at 365 nm.

The analysis by HPLC confirmed the disappearance of Monuron. The kinetics of its degradation in the presence of ferric citrate at initial pH = 3 is presented in **Fig. IV.B.4**.

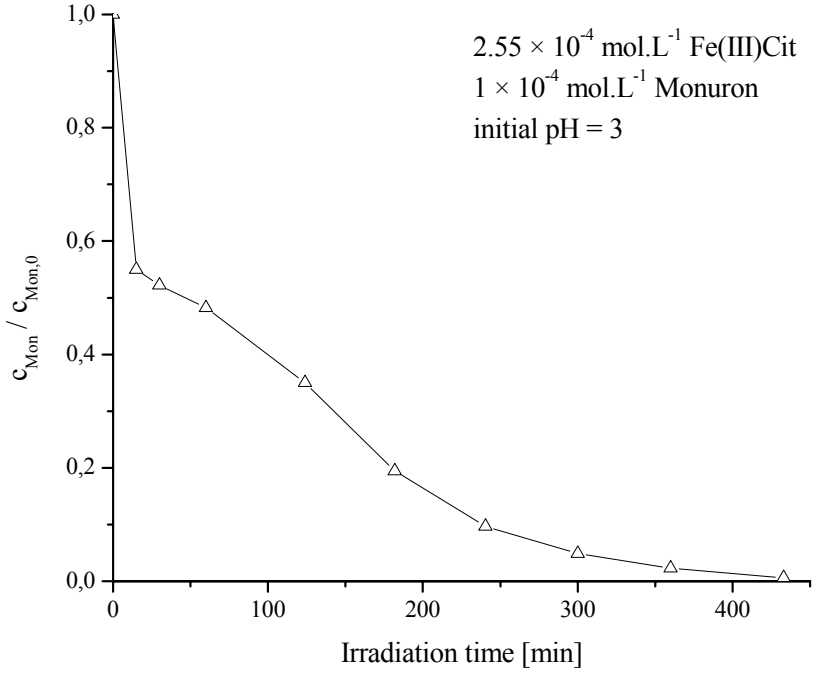

Fig. IV.B.4: Degradation kinetic of Monuron in the presence of ferric citrate upon irradiation.

At initial pH = 3, the Monuron was degraded up to 99% after 435 minutes of irradiation. A roughly two-step process was generally observed. The first step was fast and took place in the first 15-30 minutes of irradiation. The concentration of Monuron underwent a relatively substantial decrease (45% degraded in the first 15 minutes) due to the reaction with reactive radical species arising from the photodissociated ferric citrate complex. A significant increase of both pH and Fe(II) concentration occurred during the photolysis of ferric citrate complex (see **Fig. IV.B.5** and **Fig. IV.B.6**). These evolutions of pH and [Fe(II)] are practically identical to the ones observed during the degradation of ferric citrate alone, as described in the previous chapter.

The second step of Monuron degradation was slower than the first step. At that progress of the reaction the ferric citrate complex was practically degraded. The dissolved ferric and ferrous ions were thus involved in photocatalytic Fe(III)/Fe(II) cycle, which comprises several redox equilibria and photochemical reactions (***Poulain et al., 2003***). The Fe(III)/Fe(II) cycle produces other reactive radical species (like hydroxyl radicals) which continue the degradation of Monuron and its intermediates until its total mineralisation.

As it was mentioned before the pH is not stable and it generally increased during the photochemical process. The evolution of pH is shown in **Fig. IV.B.5**.

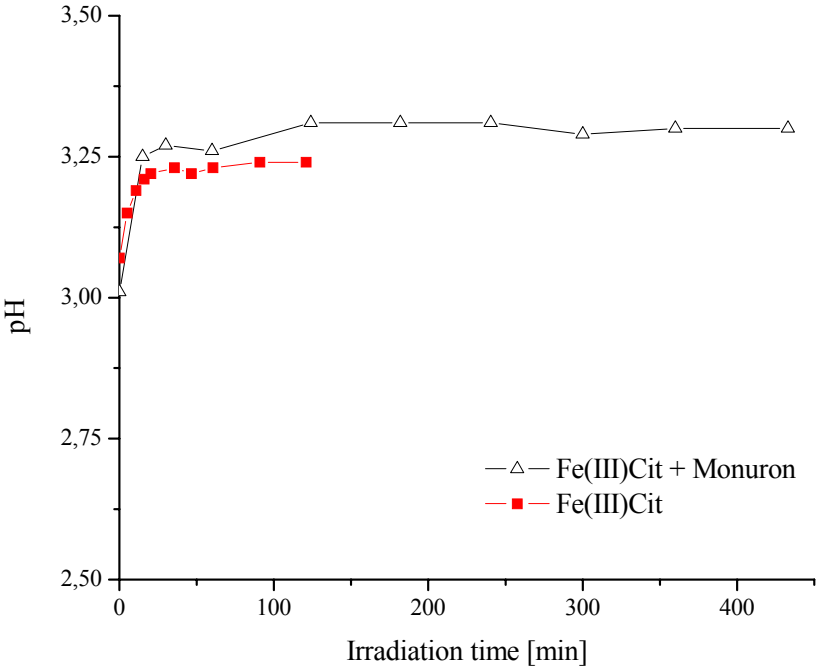

Fig. IV.B.5: Evolution of pH during Monuron degradation in the presence of ferric citrate upon irradiation; comparison with irradiation of ferric citrate alone; [Fe(III)Cit] = 2.55×10^{-4} mol.L^{-1}, [Monuron] = 1×10^{-4} mol.L^{-1}, initial pH = 3.

A substantial change of pH was observed within the first 30-60 minutes of irradiation, which corresponds to the first step of degradation kinetics. The curve of pH evolution then reaches a plateau and practically does not change any longer. The value of pH at the plateau was 3.30. As described in the previous chapter, the increase of pH was also observed during the photolysis of the ferric citrate complex. For the initial pH = 3, the plateau value of pH was 3.25. The difference of the pH evolution in the photoirradiated ferric citrate system with or without Monuron, was almost negligible.

Fe(II) concentration was followed during irradiation of the mixture of ferric citrate complex and Monuron, see **Fig. IV.B.6**.

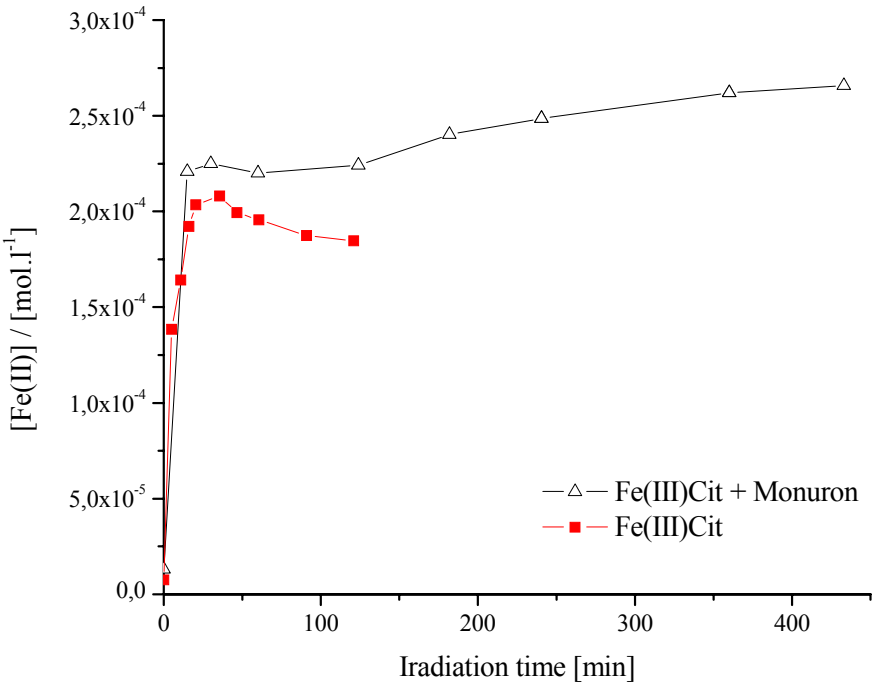

Fig. IV.B.6: Evolution of Fe(II) concentration during Monuron degradation in the presence of ferric citrate upon irradiation; comparison with irradiation of ferric citrate alone; [Fe(III)Cit] = 2.55×10^{-4} mol.L^{-1}, [Monuron] = 1×10^{-4} mol.L^{-1}, initial pH = 3.

For the initial pH of 3, Fe(II) concentration increased rapidly during the first 15-30 minutes of irradiation, which correspond to the first step of degradation kinetics again. In the second step, the concentration of Fe(II) increased very slowly. After 400 minutes the Fe(II) concentration reached its maximum, corresponding to the total concentration of iron (initial concentration of ferric citrate). In the presence of Monuron and more precisely of its

degradation products (stable or not) the concentration of Fe(II) is higher. Indeed, without organic compounds the oxidation of Fe(II) by hydroxyl radicals is more important and so the concentration of Fe(II) is less important.

IV.B.3 Impact of oxygen

The concentration of oxygen is one of the most important parameters in photocatalysis process. Irradiations of mixture of ferric citrate with Monuron at diffent concentrations of oxygen were performed. The kinetics of degradation in a system saturated by oxygen and in a desoxygenated system are shown in **Fig. IV.B.7**.

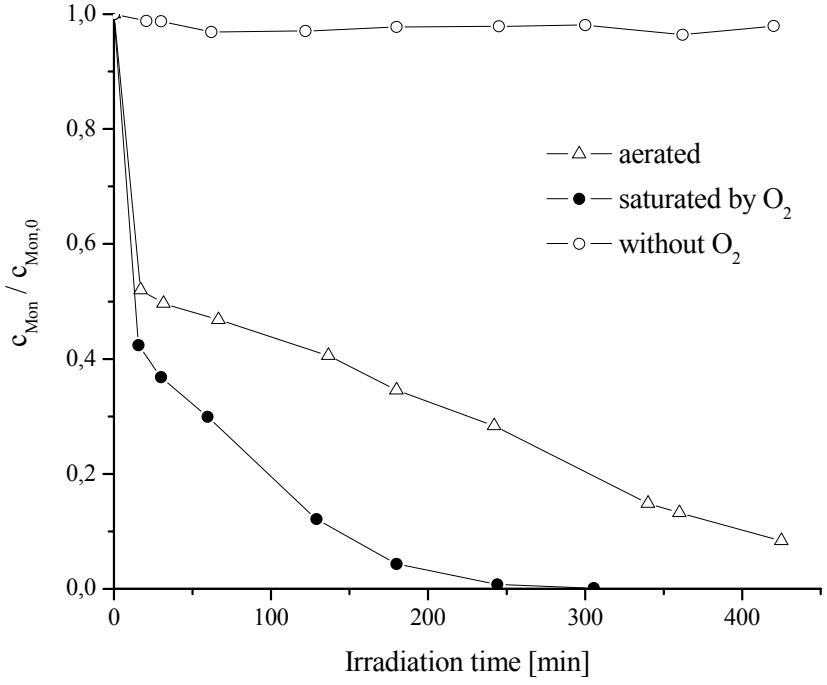

Fig. IV.B.7: Impact of oxygen on Monuron photodegradation in the presence of ferric citrate; irradiated at 365 nm, [Monuron] = 1×10^{-4} mol.L^{-1}, [Fe(III)Cit] = 3×10^{-4} mol.L^{-1}; initial pH = 3.0.

The saturation by oxygen has a positive effect on both steps of Monuron degradation. A relatively higher impact was observed on the second step. On the contrary, the absence of oxygen has an inhibiting effect on the kinetics of Monuron degradation. For the system of 3×10^{-4} mol.L^{-1} ferric citrate complex and 1×10^{-4} mol.L^{-1} Monuron at initial pH = 3.0, only 2% of Monuron were degraded during the first step. This slight decrease of Monuron

concentration can be due to insufficiently deoxygenated solution. No Monuron degradation was observed in the second step.

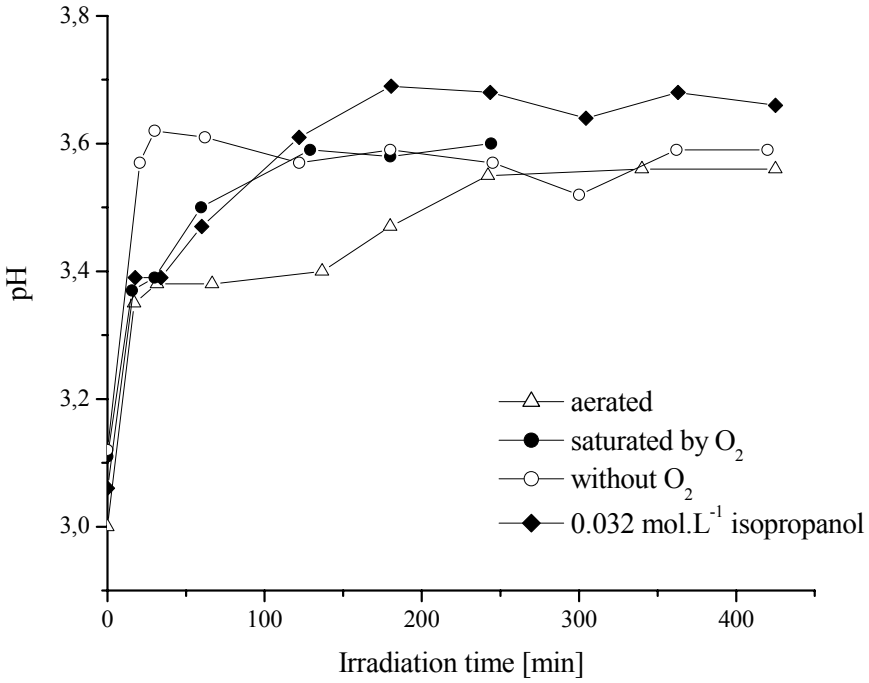

Fig. IV.B.8: Evolution of pH during Monuron photodegradation in a ferric citrate presence and different concentration of oxygen; irradiated at 365 nm, [Monuron] = 1×10^{-4} mol.L^{-1}, [Fe(III)Cit] = 3×10^{-4} mol.L^{-1}; initial pH = 3.0.

The evolution of pH observed in a system without oxygen has the usual two-steps shape. The value of pH at the plateau corresponded to 3.6. The evolution of pH in the system saturated by oxygen was also similar to the usual two-steps shape; however the pH plateau value of 3.6 was reached in 120 minutes. On the contrary, the pH plateau value was reached more quickly in the absence of oxygen.

The curve with the indication "0.032 mol.L^{-1} isopropanol" corresponds to the pH evolution in the presence of isopropanol, whose impact is described in the next paragraph. Oxygen and isopropanol had no real impact on the pH evolution during the photochemical process.

IV.B.4 Impact of isopropanol

Isopropanol is a radical scavenger, and it reacts efficiently with hydroxyl radicals. Thus it is used to indicate the appearance of the hydroxyl radicals in the studied degradation

mechanism. Irradiation of Monuron and ferric citrate mixture in the presence of 0.032 mol. l^{-1} isopropanol was performed, see **Fig. IV.B.9**.

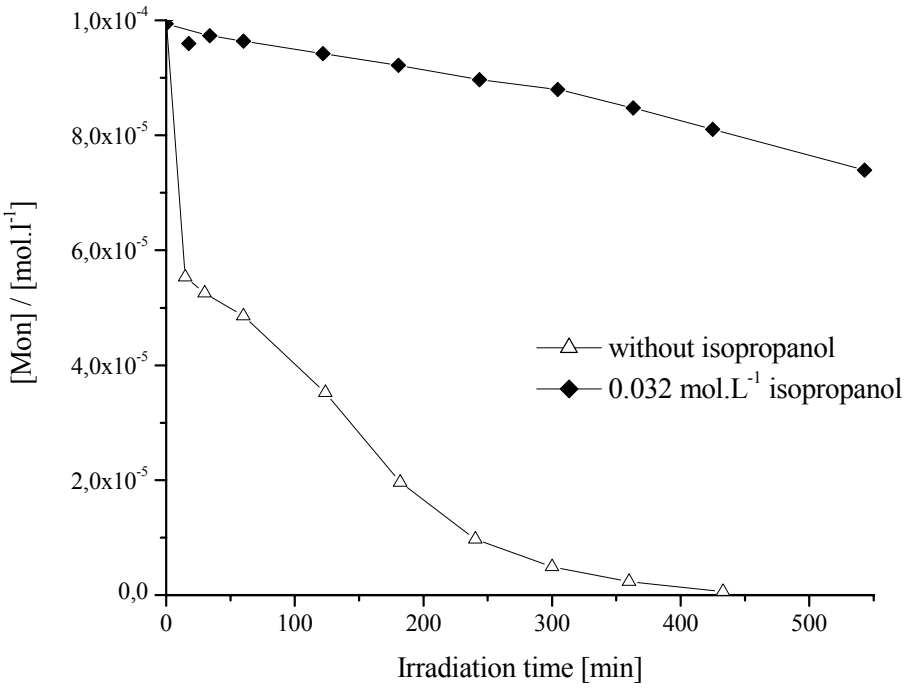

Fig. IV.B.9: Impact of isopropanol at Monuron photodegradation in a ferric citrate presence; irradiated at 365 nm; [Monuron] = 1×10^{-4} mol.L^{-1}, [Fe(III)Cit] = 3×10^{-4} mol.L^{-1}; initial pH = 3.0.

The presence of isopropanol has an inhibiting impact on Monuron degradation on both steps of degradation kinetics. Thus, the isopropanol competes with Monuron for the attack by hydroxyl and other radicals. We can conclude that Monuron degradation is mainly driven by hydroxyl radicals. However, the Monuron degradation process is not completely inhibited due to presence of other radicals not trapped, so efficiently, by isopropanol.

The evolution of pH during the process shown at **Fig. IV.B.8** was similar to the usual two-steps shape; however, the pH plateau value of 3.68 was reached not before than 180 minutes of irradiation.

IV.B.5 Impact of pH

The pH is another important parameter in homogenous photocatalysis as one of the determining factor for the speciation of iron complexes. Kinetics of 1×10^{-4} mol.L^{-1} Monuron

degradation in presence of ferric citrate was followed at different initial pH's; the curves of Monuron disappearance kinetics are given in **Fig. IV.B.10**.

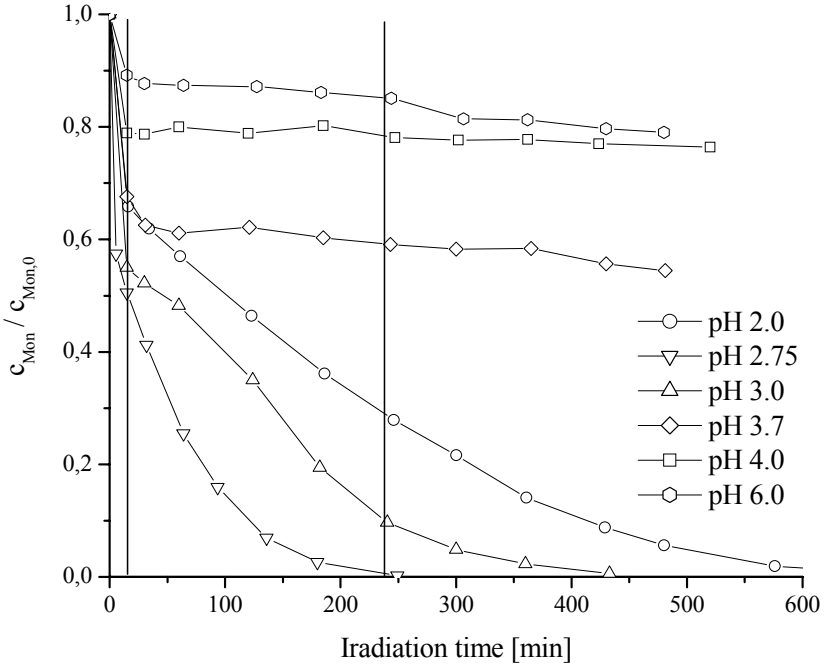

Fig. IV.B.10: Degradation kinetics of Monuron in ferric citrate presence at different initial pH's; λ_{irr} = 365 nm. [Monuron] = 1×10^{-4} mol.L^{-1}, [Fe(III)Cit] = 2.55×10^{-4} mol.L^{-1}.

The kinetics of Monuron degradation was obviously highly dependent on the initial pH. The kinetics of Monuron disappearance was faster in more acidic solution. The degradation efficiency is displayed in **Tab. IV.B.1**.

Initial pH	Degraded Monuron	
	15 min	240 min
2	33%	72%
2.75	**50**%	**99**%
3	42%	91%
3.7	32%	41%
4	21%	22%
6	11%	15%

Tab. IV.B.1. Degradation efficiency of 1×10^{-4} mol.L^{-1} Monuron in the presence of 2.55×10^{-4} mol.L^{-1} ferric citrate complex at various initial pH's, irradiated at 365 nm.

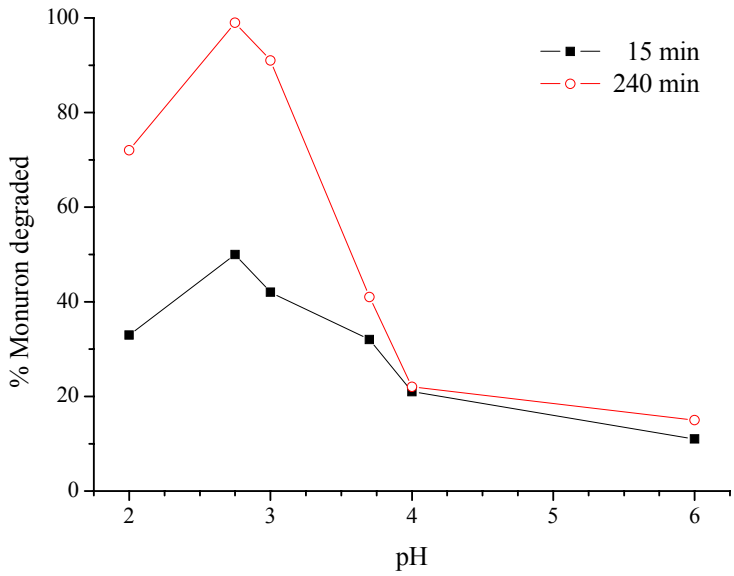

Fig. IV.B.11: % of Monuron degraded after 15 and 240 minutes of irradiation vs pH; [Monuron] = 1×10^{-4} mol.L^{-1}, [Fe(III)Cit] = 3×10^{-4} mol.L^{-1}.

The fastest overall degradation efficiency was observed at initial pH = 2.75 and pH = 3.0. At initial pH ≥ 3.7, the degradation kinetics in both steps was slower with the increase of pH. At initial pH = 4.0 and 6.0, the Monuron degradation almost stops in the second step.

In **Fig. IV.B.12**, the curves of pH change during Monuron degradation at different initial pH's are shown.

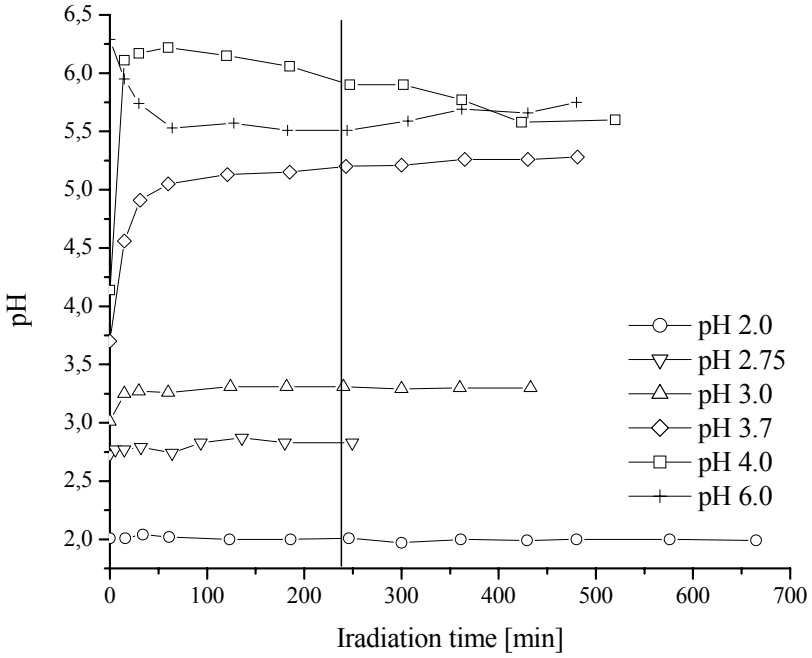

Fig. IV.B.12: Evolution of pH during Monuron photodegradation in a ferric citrate presence; λ_{irr} = 365 nm. [Monuron] = 1×10^{-4} mol.L^{-1}, [Fe(III)Cit] = 2.55×10^{-4} mol.L^{-1}.

The change of pH seemed to be most significant at the initial pH higher than 3.5. However, H^+ consumption was also calculated (**Tab.IV.B.2**), what confirms maximum at initial pH = 3.0. At the lowest initial pH = 2.0, the overall change of pH was below the experimental error of the pH measurement. In the first step of degradation kinetics, the pH generally increased. In second step, the pH remained practically unchanged at the value of the plateau reached at the end of first step. The only exception was observed at pH = 6.0, which reflects the carbonation of the solution.

Initial pH	Plateau pH (240 min)	ΔH^+ [mol.L^{-1}]
2	2.01	-2.3×10^{-4} *
2.75	2.83	-3.8×10^{-4}
3	3.31	**-5.1×10^{-4}**
3.7	5.20	-1.9×10^{-4}
4	5.90	-9.9×10^{-5}
6	5.51	2.1×10^{-6}

* within the experimental error

Tab. IV.B.2. Values of pH and consumed H^+ at the plateau (240 min) during the degradation of Monuron (1×10^{-4} mol.L^{-1}) in the presence of ferric citrate complex (2.55×10^{-4} mol.L^{-1}) at various initial pH's, upon irradiation.

It could be seen that the Monuron degradation process was almost stopped when the pH reaches the value of 5.0 and more. The increase of pH has a major impact on the speciation of the ferric citrate complex and of iron, and results in the formation of less photoactive species. At pH higher than 5.0, the solubility of Fe(III) species is very low and as a consequence the photocatalytic cycle observed at lower pH's is no more present. When Fe(II) is oxidized at pH > 5.0, Fe(III) species precipitate.

The concentration of Fe(II) was followed throughout the irradiations. Evolutions of [Fe(II)] during Monuron degradation at different initial pH are shown in **Fig. IV.B.13**.

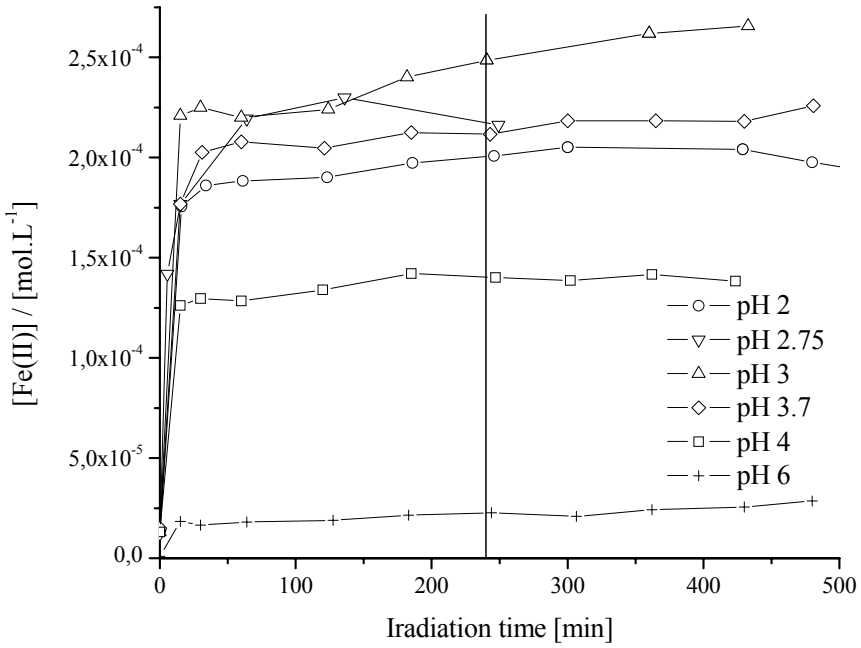

Fig. IV.B.13: Evolution of Fe(II) concentration during Monuron degradation in ferric citrate presence at different initial pH's; λ_{irr} = 365 nm. [Monuron] = 1×10^{-4} mol.L^{-1}, [Fe(III)Cit] = 2.55×10^{-4} mol.L^{-1}.

Initial pH	$[Fe^{2+}]/[Fe_{total}]$ 240 min
2	79%
2.75	85%
3	97%
3.7	83%
4	55%
6	9%

Tab. IV.B.3. Ratio of plateau values of [Fe(II)] to total iron during the degradation of 1×10^{-4} mol.L^{-1} Monuron in the presence of 2.55×10^{-4} mol.L^{-1} ferric citrate complex at various initial pH's upon irradiation.

The concentration of Fe(II) always rapidly increased to a plateau value in the first step. In the second step it was generally slightly increasing or remained constant. At initial pH = 3.0, the plateau value reached a maximum equal to the concentration of total iron. The highest concentrations of Fe(II) (from 80% to 100% of total iron) were found at low initial pH up to 3.7 (**Tab.IV.B.3**). At initial pH = 4.0, the concentration of Fe(II) corresponded 55% of total iron. At initial pH = 6.0, the Fe(II) concentration only reached 9% of total iron after 15 minutes of irradiation, which parallels the degradation of Monuron which almost stops; as already mentioned, the Fe(II) spontaneously reoxides to Fe(III) at this pH. But at this higher pH, Fe(III) species precipitated and the concentration of soluble iron decreased. The photocatalytic cycle is no more present.

Stabilized pH

The usage of pH stabilisation enabled us to both simplify the system and better approach to natural conditions, comparing to systems with non-controlled pH. The effect of pH stabilisation is presented in **Fig. IV.B.14**.

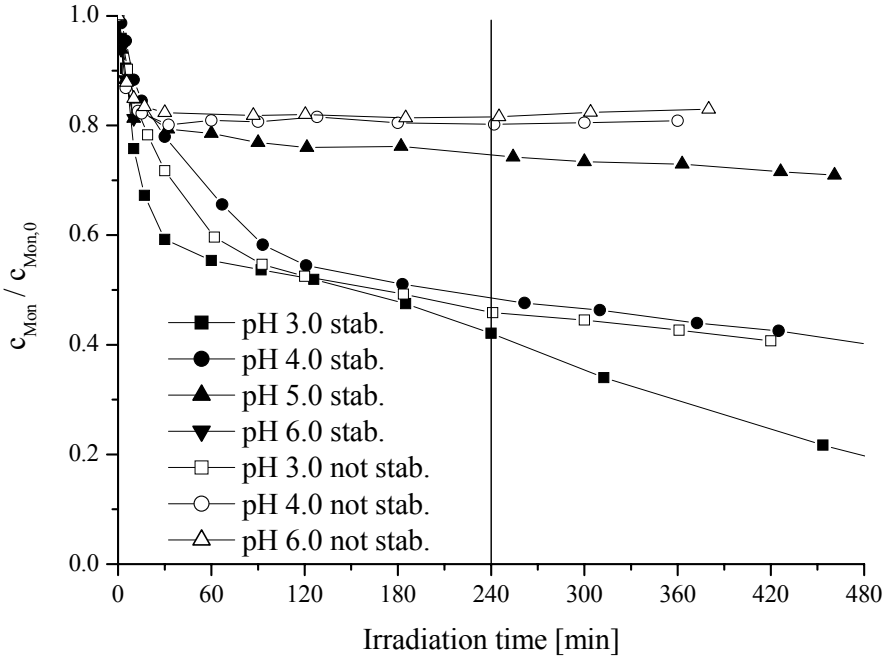

Fig. IV.B.14: Degradation kinetics of Monuron (1×10^{-4} mol.L^{-1}) in the presence of ferric citrate (2.55×10^{-4} mol.L^{-1}), comparison of stabilized and uncontrolled initial pH; λ_{irr} = 365 nm, 1 lamp.

The effect of pH stabilization was significant, see **Tab. IV.B.4**. The Monuron degradation efficency was always higher for all values of initial pH in systems with pH stabilization. Most notable impact was observed at pH 4.

Initial pH	Degraded Monuron			
	Non-stabilized pH		Stabilized pH	
	15 min	240 min	15 min	240 min
3.0	19%	54%	31%	58%
4.0	18%	20%	15%	51%
5.0	–	–	17%	29%
6.0	16%	19%	19%	–

Tab. IV.B.4. Degradation efficiency of 1×10^{-4} mol.L^{-1} Monuron in the presence of 2.55×10^{-4} mol.L^{-1} ferric citrate complex at various initial pH's, irradiated at 365 nm, 1 lamp.

The difference between stabilized and non-stabilized pH has to be directly connected with the increase of pH that occurs very fast and makes the condition less favorable for the degradation process.

The formation of Fe(II) concentration is presented in **Fig. IV.B.15**.

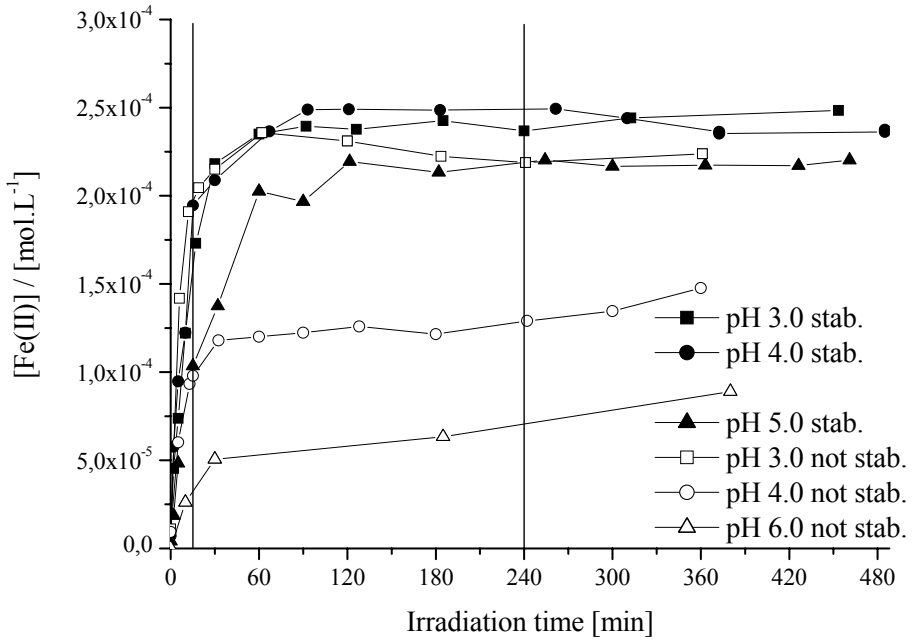

Fig. IV.B.15: Evolution of [Fe(II)] during the degradation of Monuron (1×10^{-4} mol.L^{-1}) in the presence of ferric citrate (2.55×10^{-4} mol.L^{-1}) at different initial pH's; comparison of stabilised and not stabilised pH, irradiated at 365 nm, 1 lamp.

The difference between stabilised and non stabilised system was evident: in stabilised systems, 80-100% of iron were present as Fe(II) at all pH's. With uncontrolled pH, this value was only reached at initial pH = 3. At pH = 4.0 and 6.0 the percentages of iron present as Fe(II) were 50 and 25% respectively.

IV.B.6 Quantum yields

Quantum yields of Monuron degradation in the presence of ferric citrate complex for various initial pH's are shown in **Tab. IV.B.5**.

pH	ϕ (Monuron)
2.0	0.013 ± 0.002
2.5	0.017 ± 0.002
2.75	0.020 ± 0.002
3.0	0.019 ± 0.002
4.0	0.020 ± 0.002
5.0	0.018 ± 0.002
6.0	0.017 ± 0.002

Tab. IV.B.5: Quantum yields of Monuron degradation for various pH's, [Fe(III)Cit] = 2.55×10^{-4} mol.L^{-1}, [Monuron] = 1×10^{-4} mol.L^{-1}.

The Monuron is degraded in entire studied pH range. The highest quantum yields were found in a wide range of pH between 2.5 and 6. This pH range corresponds to the presence of the most photoactive species generated from ferric citrate complex. However, the difference between the quantum yields is not high – lowest quantum yield at pH = 2 reaches 65% of the highest quantum yields. This indicates existence of photoactive species in the whole range of pH. This result proves that such complexes have a real impact in the natural environment whatever the pH.

IV.B.7 Impact of ferric citrate concentration

The initial concentration of ferric citrate complex is another important parameter that was studied. The kinetics of Monuron degradation was studied in the presence of ferric citrate at initial concentrations in the range from 5×10^{-5} to 1×10^{-2} mol.L^{-1}. The natural pH of ferric citrate solution depends on its concentration; the initial pH was therefore set to 3 by addition of perchloric acid. The results are shown at **Fig. IV.B.16**. The absorbance of the ferric citrate

in the concentration range between 5×10^{-5} to 1×10^{-3} mol.L^{-1} at 365 nm was lower than 1 and increased practically linearly according to Lambert-Beer's law. The absorbance of 1×10^{-2} mol.L^{-1} ferric citrate at 365 nm was deep below the value corresponding to Lambert-Beer's law; this could be explained by a partial precipitation of iron or by the formation of other ferric citrate complex with a lower absorption.

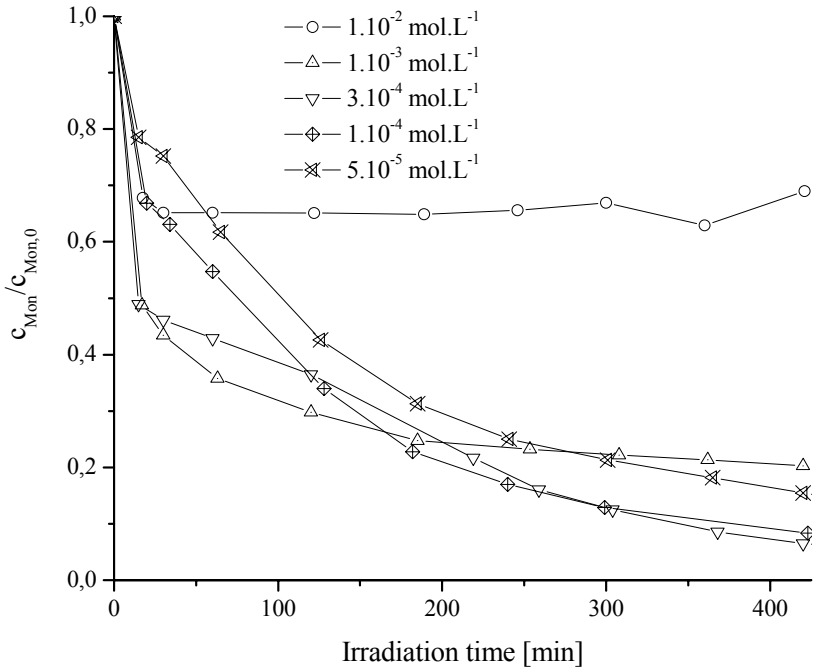

Fig. IV.B.16: Impact of ferric citrate concentration on the degradation of Monuron, initial pH = 3.0; λ_{irr} = 365 nm.

$[Fe(III)Cit]_{init}$ [mol.L^{-1}]	Degraded Monuron		
	15 min	240 min	420 min
1×10^{-2}	32%	35%	35%
1×10^{-3}	51%	77%	80%
3×10^{-4}	51%	81%	94%
1×10^{-4}	32%	83%	92%
5×10^{-5}	21%	75%	85%

Tab. IV.B.6. Degradation efficiency of 1×10^{-4} mol.L^{-1} Monuron in the presence of various ferric citrate concentrations at initial pH = 3 upon irradiation at 365 nm.

The impact of initial concentration of ferric citrate on the kinetics of Monuron degradation is not directly proportional. Surprisingly, the highest degradation efficiency was not observed at highest concentration, but at 3×10^{-4} mol.L^{-1}, where 94% of Monuron were

transformed in 7 hours. In contrary, the lowest Monuron degradation efficiency was found at the highest ferric citrate concentration (1×10^{-2} mol.L^{-1}), which corresponded to only 35% of degradation after the same irradiation time (7 hours). On the contrary, the degradation efficiency for the lowest concentration of ferric citrate (5×10^{-5} mol.L^{-1}) reached 85% of transformed Monuron. Monuron degradation efficiency increases with the ferric citrate concentration until a certain value (3×10^{-4} mol.L^{-1}). With further increase of the ferric citrate concentration the degradation efficiency decreases. The low degradation of Monuron at a concentration of ferric citrate equal to 1×10^{-2} mol.L^{-1} can be due to the presence of high concentration of citric acid, whom the photogenerated radical species can react with. There is a competition between Monuron and citrate for the reactivity of radical species. At lowest ferric citrate concentration (5×10^{-5} mol.L^{-1}) the degradation of Monuron is important (85%). This result shows the efficiency of such complex for the degradation of organic pollutants.

The evolutions of pH during Monuron photodegradation at different starting ferric citrate concentrations are presented in **Fig. IV.B.17**.

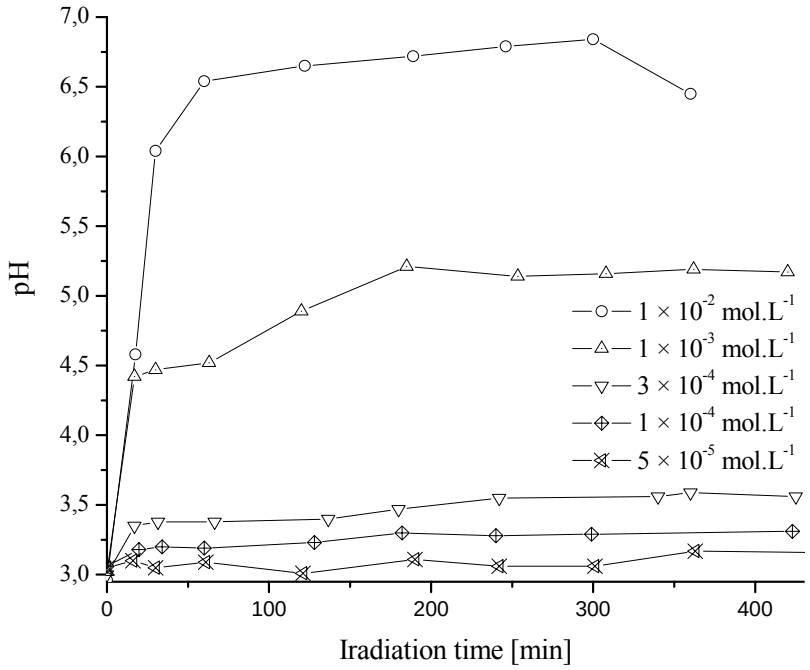

Fig. IV.B.17: Evolutions of pH during degradation of Monuron (1×10^{-4} mol.L^{-1}) at various Fe(III)Cit concentrations; initial pH = 3.0, λ_{irr} = 365 nm.

The pH evolution curves observed during the Monuron degradation in the presence of the ferric citrate shown that the pH increased with the initial ferric citrate concentration. With higher starting concentration, the pH increased to higher value. This is in an agreement with

the previous chapter, where we proposed that the increase of pH which occurred during irradiation of ferric citrate complex illustrates the consumption of H^+ during the photoredox process of the complex. The higher the initial ferric citrate concentration is, the higher H^+ consumption is.

In chapter "Impact of pH" we already showed that the Monuron degradation efficiency decreased when the pH of the system increased at the value of 5.0 or above. This is in a good agreement with observed lower degradation efficiency at ferric citrate concentrations 1×10^{-2} mol.L^{-1} and less significantly at 1×10^{-3} mol.L^{-1}. The increase of pH seems to be the main parameter for the efficiency of photochemical process, and consequently for Monuron degradation.

IV.B.8 Impact of irradiation intensity

The irradiation intensity provided by three mercure vapour lamps was too high for certain experiments; in this case, only one lamp was used. Comparison of the irradiation intensity (1 lamp and 3 lamps) on the Monuron degradation kinetics is shown in **Fig. IV.B.18**.

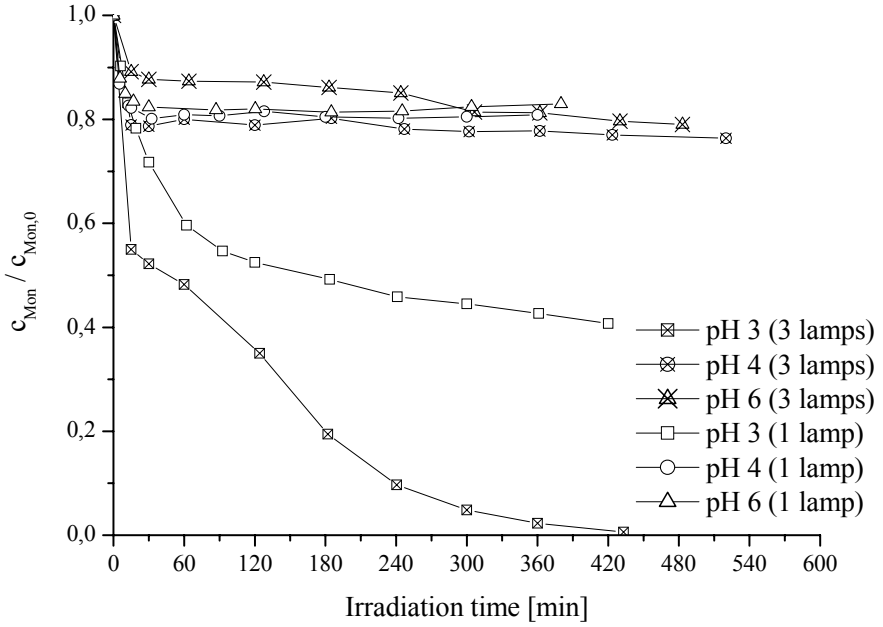

Fig. IV.B.18: Degradation kinetics of Monuron (1×10^{-4} mol.L^{-1}) in the presence of ferric citrate (2.55×10^{-4} mol.L^{-1}) at various initial pH's; comparison of irradiation source intensity.

At initial pH = 3.0, the Monuron degradation efficiency decreased with reduction of the source power. The slowdown of Monuron degradation observed between 15 and 60 minutes upon irradiation with three lamps, was not found with the use of one lamp, and the

kinetics appeared rather as of the pseudo-first order. At initial pH = 4.0 and 6.0, only a slight difference was observed between the use of one or three lamps. The degradation practically did not continued in the second step, as pH increased above 5.0 after 30 minutes of irradiation.

IV.B.9 Impact of Monuron concentration

Impact of Monuron concentration at kinetics of its degradation is presented in **Fig. IV.B.19**.

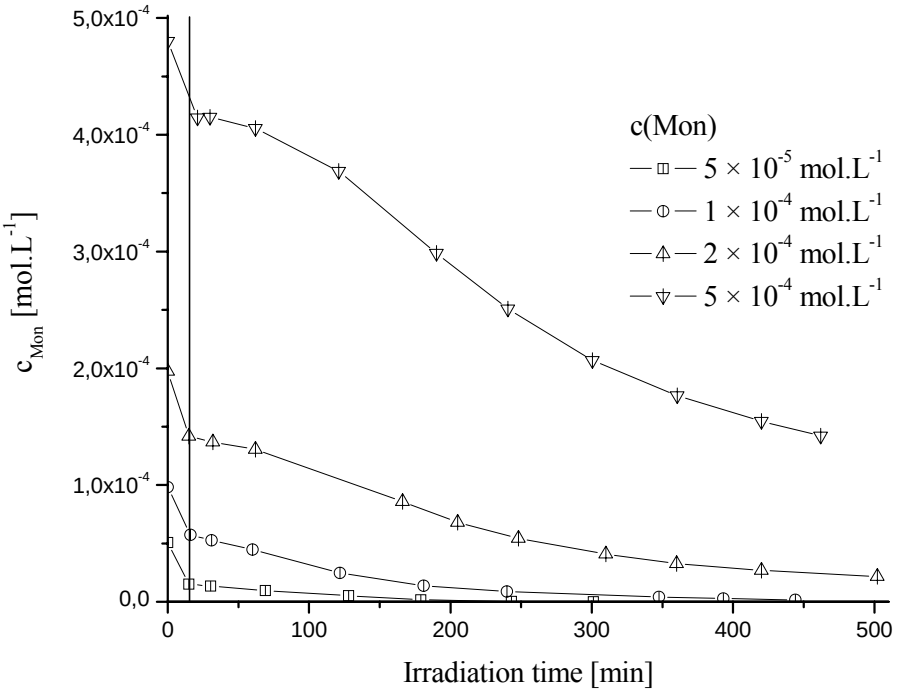

Fig. IV.B.19: Degradation kinetics of Monuron in presence of ferric citrate (2.55×10^{-4} mol.L^{-1}) at various initial concentrations of Monuron; initial pH = 3.0.

$c(Mon)_{init}$ [mol.L^{-1}]	Monuron degraded in 15 min / [mol.L^{-1}]
5×10^{-5}	3.54×10^{-5}
1×10^{-4}	4.09×10^{-5}
2×10^{-4}	5.58×10^{-5}
5×10^{-4}	6.55×10^{-5}

Tab. IV.B.7. Degraded Monuron in first 15 min in the presence of 2.55×10^{-4} mol.L^{-1} ferric citrate complex at various initial Monuron concentrations upon irradiation at 365 nm.

Change of Monuron initial concentration did not change the degradation kinetics. The kinetics of Monuron degradation could be still divided into two steps. The efficiency of Monuron degradation increased with concentration of the pollutant (**Tab. IV.B.7**). The higher concentration of Monuron increases its degradation efficiency, as the Monuron is competing for the photogenerated hydroxyl and other radicals with Fe(II) and to other extent with the organic compounds, which are released by photolysis of the ferric citrate complex.

IV.B.10 Comparison with other systems

The process of Monuron degradation in the presence of ferric citrate complex was compared to systems with different complexation agent (nitrilotriacetic acid) or pollutant (4-chlorophenol). The comparison of impact nitrilotriacetic and citric acid as Fe(III) complexing agents on the kinetics of Monuron degradation is presented in **Fig. IV.B.20**.

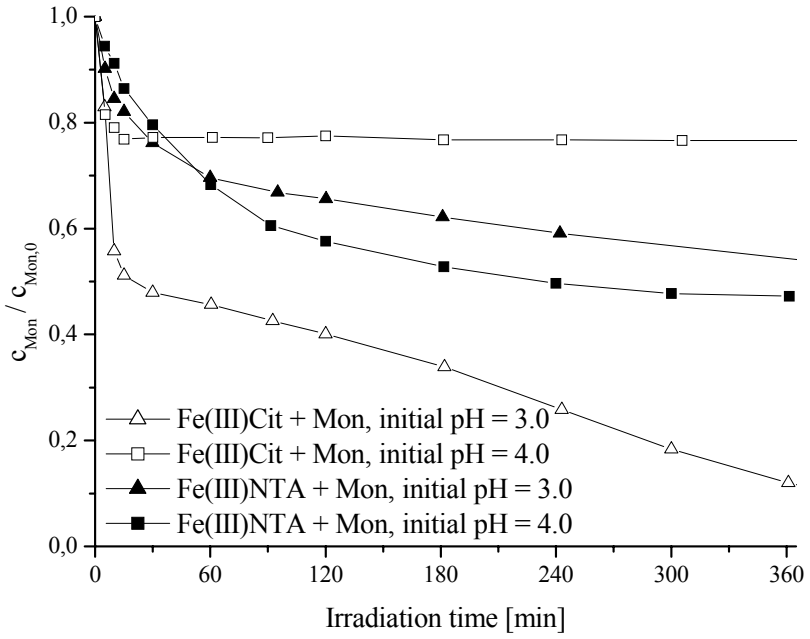

Fig. IV.B.20: Degradation kinetics of Monuron (1×10^{-4} mol.L^{-1}) in the presence of Fe(III)Cit or Fe(III)NTA (both 3×10^{-4} mol.L^{-1}) upon irradiation at 365 nm.

The Monuron degradation efficency in the presence of Fe(III)NTA was slower than in presence of Fe(III)Cit at initial pH = 3.0; on the contrary, at initial pH = 4.0, the degradation efficiency with Fe(III)NTA was higher when compared to the one with Fe(III)Cit. The impact of pH on kinetics of Monuron degradation in the presence of Fe(III)NTA was negligible

compared to kinetics in Fe(III)Cit system. Moreover, for Fe(III)NTA complex the overall degradation efficiency was higher at initial pH = 4.0.

The evolutions of pH during Monuron degradation in presence of Fe(III)Cit or Fe(III)NTA are presented at **Fig. IV.B.21**.

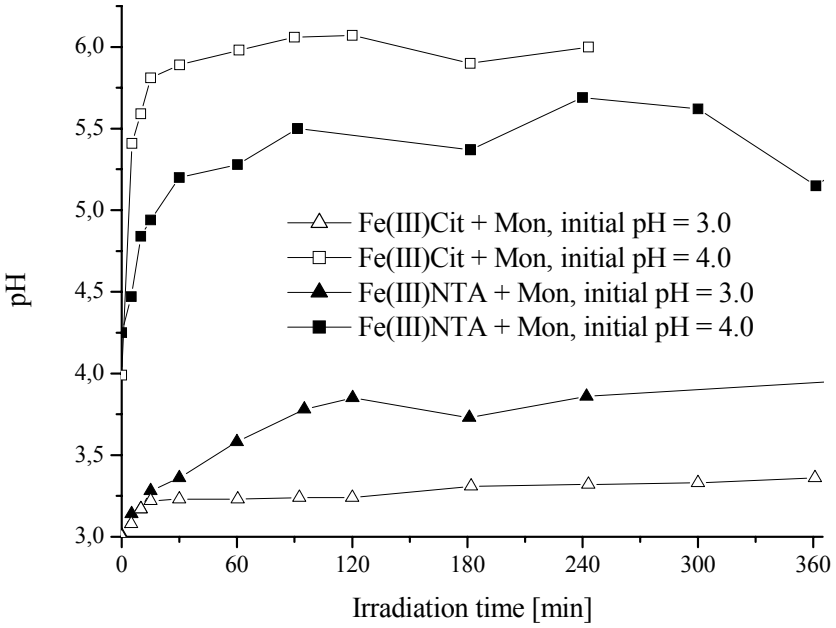

Fig. IV.B.21: Evolution of pH during the degradation of Monuron (1×10^{-4} mol.L^{-1}) in presence of Fe(III)Cit or Fe(III)NTA (both 3×10^{-4} mol.L^{-1}) upon irradiation.

Morever, although the pH increases during the irradiation from 3.0 to 4.0 and from 4.0 to 5.5 in the system with initial Fe(III)NTA presence, the impact of pH on the Monuron degradation efficiency remained negligible. This result showed that degradation by Fe(III)NTA complex is less sensitive to pH change.

The evolutions of Fe(II) concentration during Monuron degradation in presence of Fe(III)Cit or Fe(III)NTA are also presented in **Fig. IV.B.22**.

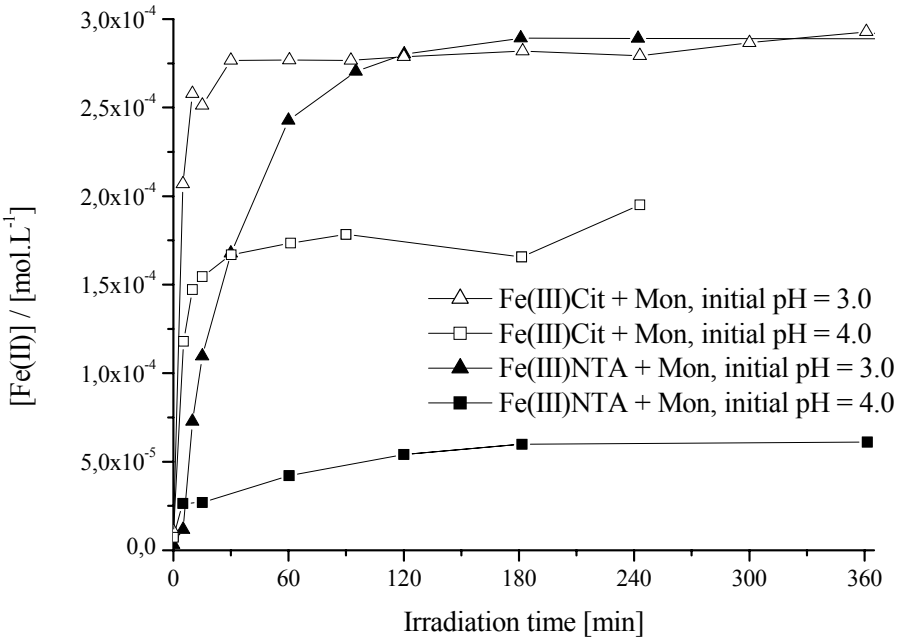

Fig. IV.B.22: Evolution of Fe(II) concentration during degradation of Monuron (1×10^{-4} mol.L^{-1}) in presence of Fe(III)Cit or Fe(III)NTA (both 3×10^{-4} mol.L^{-1}) upon irradiation.

The concentration of Fe(II) increases generally much slower in the system with Fe(III)NTA than with Fe(III)Cit.; the plateau value is reached in 180 min. At initial pH = 3.0, both system reached the same plateau concentration corresponding to the total concentration of iron. At initial pH = 4.0, 65% of the total iron concentration was present as Fe(II) in the presence of citrate, and only 20% in the presence of nitriloacetate. This result indicates that Fe(II) is stabilized by organic intermediates (probably from the degradation of citrate) present in the system with citrate which is not the case with nitriloacetate. Indeed near pH = 6.0, the oxidation of Fe(II) is very fast in water.

Comparison of the degradation of Monuron and 4-chlorophenol in a presence of ferric citrate are presented in **Fig. IV.B.23**.

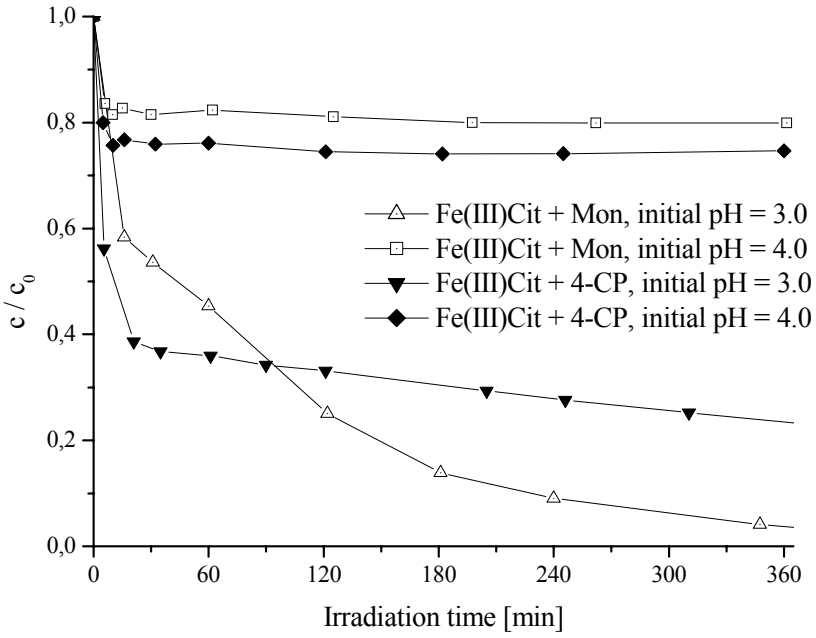

Fig. IV.B.23: Degradation kinetics of Monuron and 4-chlorophenol (both 1×10^{-4} mol.L^{-1}) in presence of Fe(III)Cit (2.55×10^{-4} mol.L^{-1}) at two pH's (3.0 and 4.0) upon irradiation.

The degradation kinetic curves of Monuron and 4-chlorophenol in the presence of ferric citrate were different. At the initial pH = 3.0, the degradation of 4-chlorophenol was faster in the first step. In the second step, a cross-over was observed as the degradation of 4-chlorophenol was strongly slowed down. Accordingly we can put forward to the following hypothesis: the degradation photoproducts of 4-chlorophenol are degraded faster than the 4-chlorophenol itself, which is not the case for Monuron. Other hypothesis could be also proposed: the hydroquinone/benzoquinone couple create a "shortcut" in the photocatalytic system; similar phenomenon was observed at the degradation of 4-chlorophenol in the suspension of TiO_2 (***Theurich et al., 1996***). At the initial pH = 4.0, not much difference was observed. The degradation of either Monuron or 4-chlorophenol was practically stopped after 30 minutes of irradiation. So, an impact of pH on degradation of 4-chlorophenol photoinduced by ferric citrate was observed as it was already described for Monuron.

The change of pH during the degradation of the different pollutants in presence of ferric citrate complex at various initial pH's is shown in **Fig. IV.B.24**.

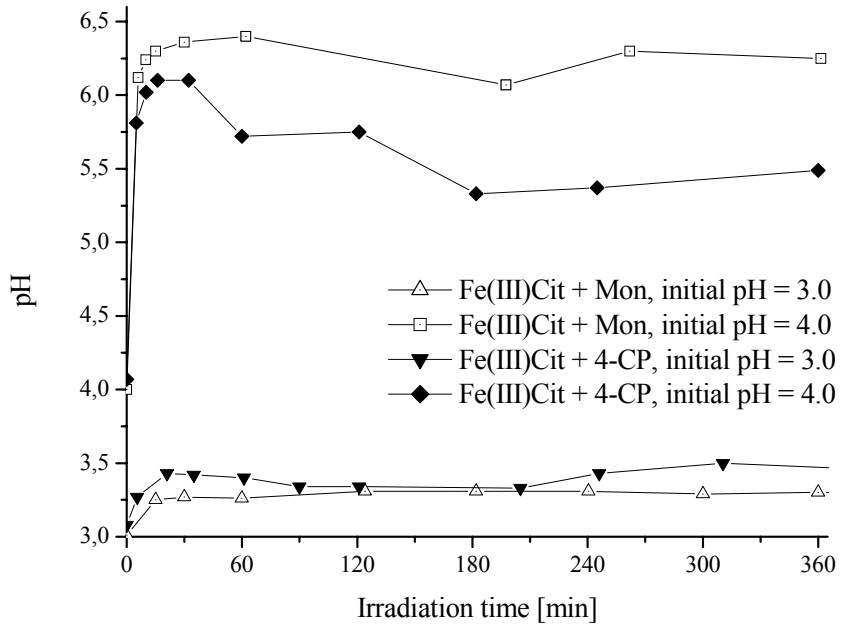

Fig. IV.B.24: Evolution of pH during degradation of a pollutant (Monuron or 4-chlorophenol) in presence of Fe(III)Cit (2.55×10^{-4} mol.L^{-1}) upon irradiation; [Monuron] = [4-CP] = 1×10^{-4} mol.L^{-1}.

Not significant difference between the pollutants was observed in the evolution of pH. A slightly higher pH increase was observed during degradation of 4-chlorophenol at initial pH = 3.0. At initial pH = 4.0 a slightly higher increase of pH was also observed during the degradation of Monuron. The degradation efficiency of both pollutants corresponded well to the change of pH; at higher pH lower pollutant degradation efficiency was observed.

The change of Fe(II) concentration during degradation of the different pollutants in presence of ferric citrate complex at various initial pH is shown at **Fig. IV.B.25**.

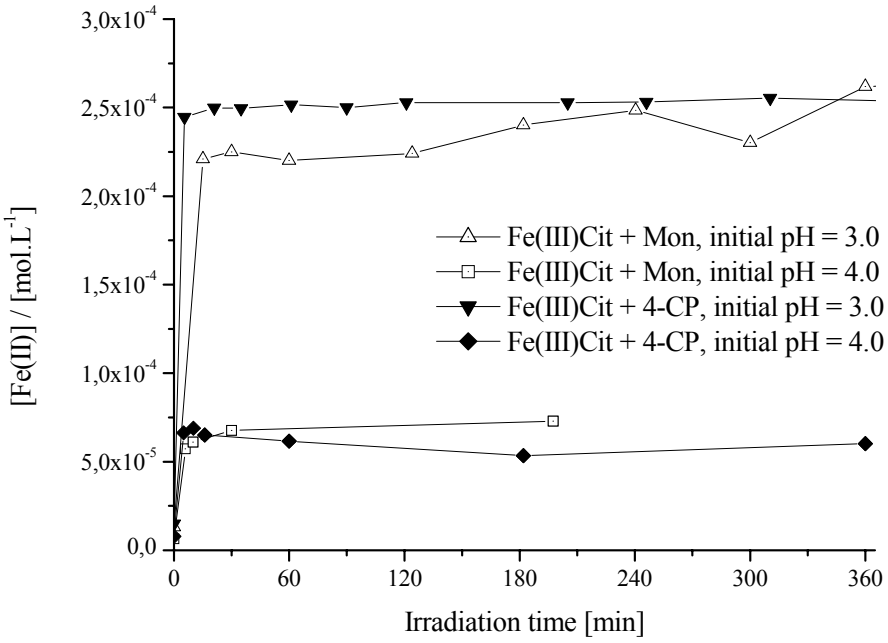

Fig. IV.B.25: Evolution of Fe(II) concentration during degradation of pollutants (Monuron or 4-chlorophenol) in presence of Fe(III)Cit (2.55×10^{-4} mol.L^{-1}) upon irradiation; [Monuron] = [4-CP] = 1×10^{-4} mol.L^{-1}.

The curve of Fe(II) concentration was observed in its usual time course. The curve of Fe(II) concentration during 4-chlorophenol has an interesting shape. At initial pH = 3.0, the plateau of Fe(II) is reached immediately in first five minutes of irradiation and corresponds approximately to the total concentration of iron in the system. Anyway, use of two pollutants with different structure did not have a major impact on the evolution of Fe(II) concentration.

IV.B.11 Conclusion

Photodegradation of Monuron was investigated in the presence of Fe(III)-Citrate complex. Irradiation experiments for the determination of the quantum yield and the kinetics of Monuron degradation were carried out at the wavelength of 365 nm. The results indicate that oxygen, Fe(III)-Cit concentration, Monuron concentration, oxygen concentration, all have an impact on the quantum yields of Monuron disappearance and also on the kinetics of Monuron degradation. However, the crucial parameter, controlling the efficiency of such system, is the pH.

Whatever the conditions of the degradation kinetics of Monuron, the kinetic presents two well defined steps. The first part of the kinetics, where the degradation of Monuron is very fast, is attributed to the radical species (mainly OH radicals) photogenerated during the photoredox process of the Fe(III)Cit. The second part, where the degradation of Monuron is slowed down, is attributed to the photocatalytic cycle based on the Fe(III)/Fe(II) species released after the photodegradation of the complex. This second part is strongly pH dependent.

The best efficiency for Monuron degradation is obtained at pH around 3.0 with a value of quantum yield equal to approximately 0.02. The effect of pH is less pronounced for the quantum yield, reflecting an initial reaction, but is very important for the kinetics of Monuron degradation. Indeed for a starting pH equal to 3.0, the degradation of Monuron is complete after 240 min of irradiation, and only 22% of Monuron is degraded for an initial pH = 4.0 during the same irradiation time. This effect is mainly attributed to the speciation of Fe(III)Cit complex which is very sensitive to the pH. Moreover, during the photoredox process a consumption of H^+ is observed and as a consequence an increase of pH. The Fe(III)Cit species present at higher pH than 4.0 are less photoactive. But as I mentioned before, the increase of pH is very detrimental for the photocatalytic cycle based on the Fe(III)/Fe(II) couple due to the formation of less photoactive Fe(III) species and to the process of Fe(III) precipitation, which occurs at higher pH.

The second important parameter for the efficiency of Monuron degradation is the oxygen. Indeed, the disappearance of Monuron is almost totally inhibited without oxygen dissolved in the solution. Oxygen is essential for the formation of oxidative species and, as a consequence, for the degradation of the pollutant. The impact of initial concentration of Fe(III)Cit complex is very interesting. In fact, the degradation of Monuron is optimum for a concentration equal to 3×10^{-4} mol.L^{-1}; 94% of degradation after 420 min of irradiation. At higher concentration 1×10^{-2} mol.L^{-1} only 35% of Monuron is degraded. This result can be explained by a competition of radical species reactivity on the different organic compounds present in solution. The reactivity of OH radicals on citric acid (rate constants = 5.0×10^7 L.mol^{-1}.s^{-1}) and on its degradation product is not negligible and at higher complex concentration they can interfere on the Monuron degradation efficiency. At lower concentration (5×10^{-5} mol.L^{-1}), 85% of Monuron is degraded after 420 min of irradiation. This result is very close to the optimum value of Monuron degradation (94%) and show a good efficiency of such complex for the degradation of pollutants from the aqueous solution.

The comparison with other complex (FeNTA) shows a better efficiency at pH 3.0 but a lower efficiency at pH 4.0. FeNTA complex is less sensitive to the pH than Fe(III)Cit complex.

This study demonstrates the real role that such complexes can play in the natural environment, surface and atmospheric waters, on the fate of organic matter present in these compartment.

IV.C Photodegradation of Monuron in the combined system: Ferric citrate / TiO_2

The so called "binary system" corresponds to either ferric citrate/Monuron or TiO_2/Monuron mixture. The so called "combined system" contained all the three components.

IV.C.1 Photodegradation of ferric citrate in the presence of TiO_2

The impact of TiO_2 presence on the ferric citrate behaviour was examined prior to the study of Monuron degradation in the combined system of ferric citrate complex and commercial TiO_2 (P25). The adsorption of ferric citrate at the surface of suspended TiO_2 was measured using the method of total iron determination. The results are shown in **Table IV.C.1**.

	Total iron [$mol.L^{-1}$]	
	pH 2.75	pH 4.85
Before absorption	2.45×10^{-4}	2.48×10^{-4}
After 24h absorption	1.41×10^{-4}	1.67×10^{-4}
Difference	1.04×10^{-4}	8.12×10^{-5}
Adsorbed iron [%]	42 ± 4%	33 ± 3%

Table IV.C.1: Adsorption of ferric citrate (2.55×10^{-4} $mol.L^{-1}$) on 1 $g.L^{-1}$ of TiO_2.

The adsorption did not depend on the pH very much, 33% of Fe(III)Cit were adsorbed at pH 4.85 and 42% at pH 2.75. The concentration of ferric citrate was 2.55×10^{-4} $mol.L^{-1}$, which was the typical value used in this work. The typical TiO_2 concentration found in the literature was 1 $g.L^{-1}$, was more then 50 times higher than the typical concentration of TiO_2 used throughout the experiments and equal to 24 $mg.L^{-1}$. This typical TiO_2 concentration, which corresponds to 3×10^{-4} $mol.L^{-1}$, was chosen due to compatibility with the results obtained by the Laboratory of Photochemistry (***Měšťánková et al., 2004***). Under the use of the typical TiO_2 concentration (24 $mg.L^{-1}$), the ferric citrate adsorption on TiO_2 was considered to be negligible.

The impact of TiO_2 presence on degradation of ferric citrate upon irradiation was also studied. The evolutions of Fe(II) concentration and of pH were followed. The evolution of Fe(II) concentration is shown in **Fig IV.C.1**.

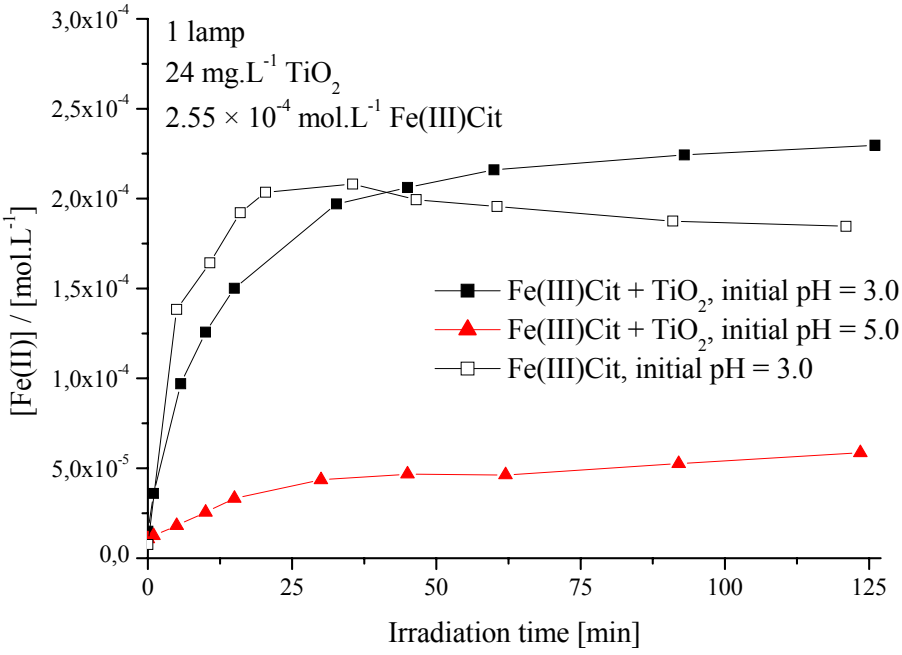

Fig. IV.C.1: Evolution of Fe(II) concentration during ferric citrate degradation in the presence of 24 $mg.L^{-1}$ TiO_2 upon irradiation by 1 lamp.

The evolutions of Fe(II) in the irradiated system of ferric citrate and TiO_2 was similar to those observed with ferric citrate alone. However, the increase of Fe(II) concentration was slower, the plateau was reached within 30 – 60 minutes of irradiation, comparing to 15 minutes without TiO_2. At initial pH = 3.0, the Fe(II) concentration corresponding to 77% of total iron was reached in 30 minutes. With further irradiation up to 125 minutes, the Fe(II) concentration was slightly increasing up to 90% of total iron. At initial pH = 5.0, the plateau concentration (17% of total iron) was reached in 30 minutes. The concentration increased to 23% of total iron with further irradiation up to 125 minutes.

The evolution of pH during ferric citrate degradation in presence of TiO_2 upon irradiation is shown in **Fig IV.C.2**.

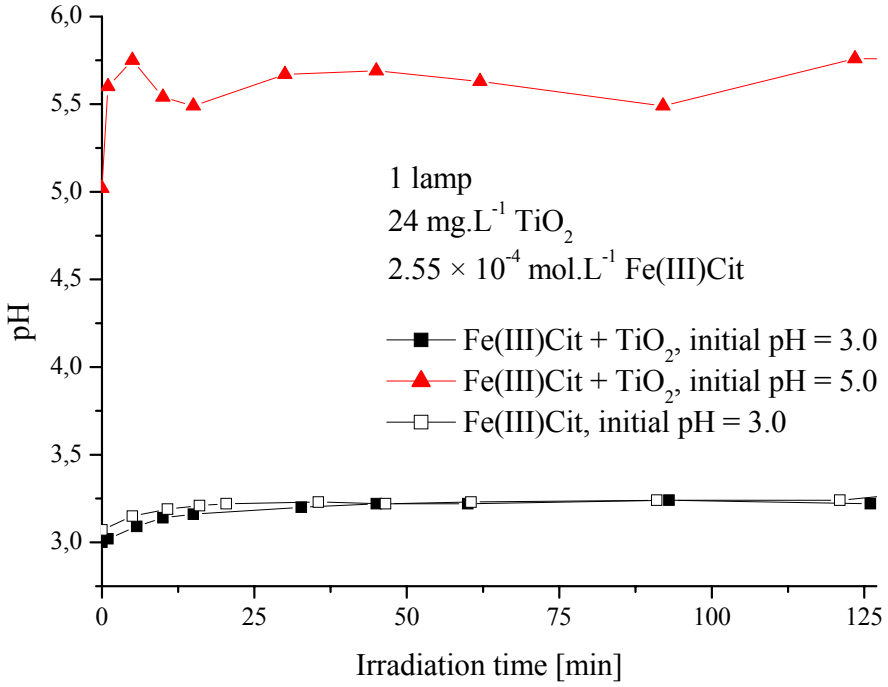

Fig. IV.C.2: Evolution of pH during ferric citrate degradation in the presence of 24 $mg.L^{-1}$ TiO_2 upon irradiation by 1 lamp (λ_{irr} = 365 nm).

The pH evolutions in the system of ferric citrate and TiO_2 were also similar from those observed upon irradiation of ferric citrate alone. A two-step process was observed again; at initial pH = 3.0, the pH arose to 3.20 in 30 minutes. At initial pH = 5.0, the pH increased to a plateau value of 5.7 in less than 5 minutes.

IV.C.2 Photodegradation of Monuron in the presence of TiO_2

Adsorption of Monuron on TiO_2 was studied by ***Měšťánková (2004)***. The equilibrium of Monuron adsorption on the TiO_2 surface was reached within a 30 minutes stirring of the suspension in the dark before the exposure to irradiation. This experiment shows that the adsorption of Monuron on TiO_2 is negligible. The impact of TiO_2 concentration on Monuron degradation kinetics upon irradiation is shown in **Fig. IV.C.3**.

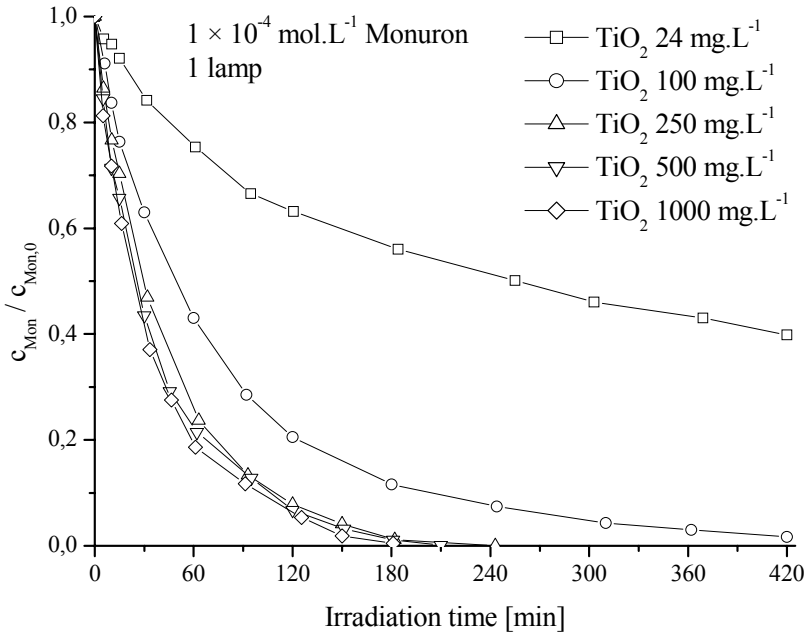

Fig. IV.C.3: Impact of TiO_2 concentration on kinetics of Monuron degradation upon irradiation by 1 lamp; natural pH = 6.2.

The Monuron degradation is roughly similar for TiO_2 concentrations of 250 $mg.L^{-1}$ and above; at these concentrations, the degradation follows a first order kinetics. Rate constants of Monuron degradation at different concentrations of TiO_2 were calculated by first order exponential decay fitting. The results together with initial rates are diplayed in **Table IV.C.2**.

TiO_2 concentration [$mg.L^{-1}$]	Rate constant [s^{-1}]	Initial rate [$mol.L^{-1}.s^{-1}$]
24	–	7.2×10^{-5}
100	2.4×10^{-4}	2.6×10^{-4}
250	3.8×10^{-4}	3.9×10^{-4}
500	4.5×10^{-4}	4.9×10^{-4}
1000	4.8×10^{-4}	4.9×10^{-4}

Table IV.C.2: Initial rates and rate constants of 1×10^{-4} $mol.L^{-1}$ Monuron degradation at different TiO_2 concentration upon irradiation by 1 lamp, natural pH.

Increase of TiO_2 concentration had a positive impact on the Monuron degradation rate up to 500 $mg.L^{-1}$. While the TiO_2 concentration grown more than twenty times from 24 $mg.L^{-1}$, the initial rate increased only seven times. Thus, the Monuron degradation efficiency per $g.L^{-1}$ of TiO_2 decreased. Further increase of TiO_2 concentration to 1000 $mg.L^{-1}$ did not have any major effect to the rate constant values.

The same experiments with a concentration of TiO_2 equal to 24 $mg.L^{-1}$ were carried out at four pH's (3.0, 4.0, 5.0 and 6.0). The fitting by first order exponential decay did not provide satisfactory values. The initial rates are shown in **Table IV.C.3**.

Initial pH	Initial rates $[mol.L^{-1}.s^{-1}]$
3	6.0×10^{-5}
4	6.6×10^{-5}
5	6.8×10^{-5}
6	6.7×10^{-5}

Table IV.C.3: Initial rate of 1×10^{-4} $mol.L^{-1}$ Monuron degradation with 24 $mg.L^{-1}$ of TiO_2 at different initial pH's upon irradiation by 1 lamp.

A slight difference of Monuron degradation efficiency was noticed. The observed impact of pH on initial rate of Monuron degradation was negligible.

IV.C.3 Photodegradation of Monuron in the combined system (Ferric citrate and TiO_2)

In the combined system we always worked with TiO_2 concentration of 24 $mg.L^{-1}$. The TiO_2 suspension (24 $mg.L^{-1}$) is slightly opaque, but still transparent. When ferric citrate and Monuron were added, the suspension changed of colour and turned pale red. Hence, a possibility of shielding effect among the components of such a suspension had to be considered. The absorption of the ferric citrate and Monuron mixture at 365 nm was compared to the absorption of TiO_2; the spectra are shown in **Fig. IV.C.4**.

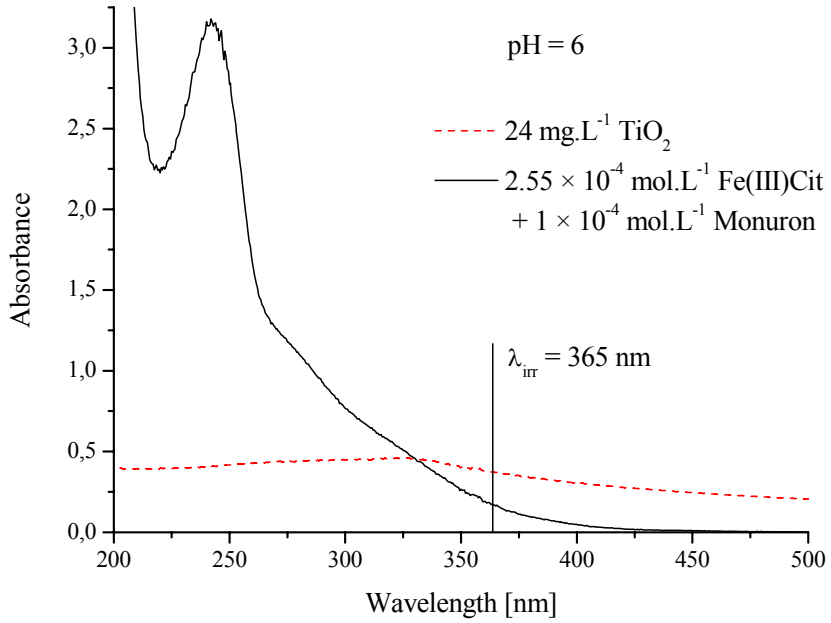

Fig. IV.C.4: Comparison of absorption spectra of TiO_2 and of a Monuron and ferric citrate mixture.

The Monuron does not absorb at 365 nm. The absorption of TiO_2 at 365 nm is double than the absorption of the ferric citrate. However, the sum of absorption at 365 nm is lower than 0.7, which permits to suppose sufficient flux of photons in the entire irradiated volume in the reactor (internal diameter 2.8 cm).

The kinetics of Monuron degradation in the combined photocatalytic system of ferric citrate and TiO_2 at initial pH = 3.0 is shown in **Fig. IV.C.5**.

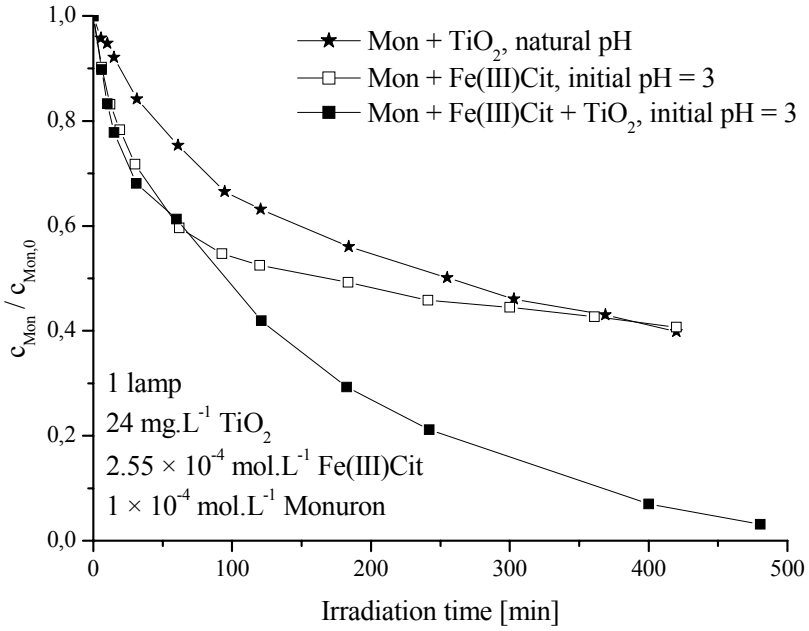

Fig. IV.C.5: Kinetics of Monuron degradation in the combined ferric citrate/TiO_2 system upon irradiation by 1 lamp; comparison with binary systems with ferric citrate or TiO_2.

The kinetics of the binary systems was different, the Monuron degradation efficiency of ferric citrate system was higher in the first step of the kinetics; subsequently, the degradation slowed down. In the TiO_2 system, the curve of Monuron degradation corresponded to first order kinetics. However, practically same amount of Monuron (about 40%) was degraded after 420 minutes of irradiation in both systems.

The combined system showed upon irradiation promising 93% degradation efficiency after 400 minutes. In the first step, the kinetics curve of the combined system was similar to the one of ferric citrate alone. After 60 minutes of irradiation, about 40% of Monuron were degraded. With further irradiation of the combined system, the degradation continued: after 480 minutes, 97% of Monuron disappeared.

The comparison of the pH evolution during the Monuron degradation in both combined and binary ferric citrate systems is shown in **Fig. IV.C.6**.

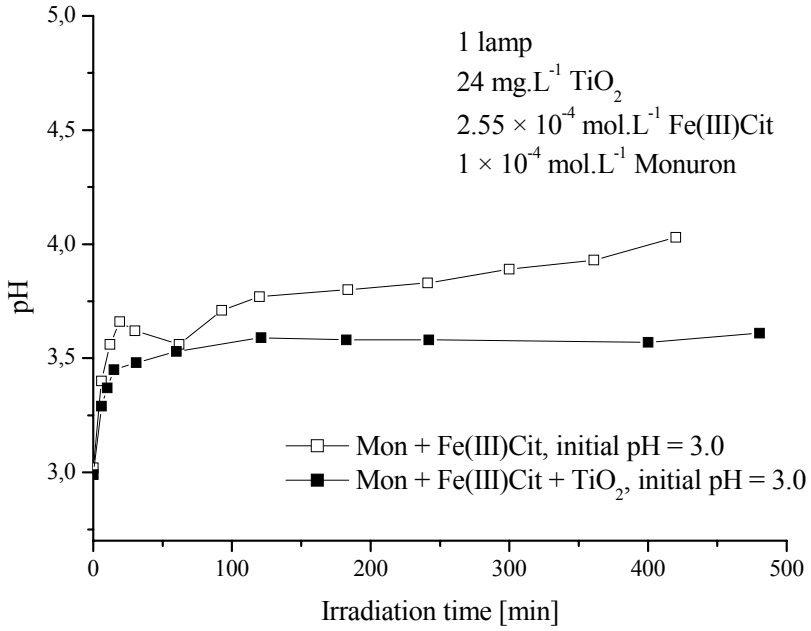

Fig. IV.C.6: Evolution of pH during Monuron degradation in combined ferric citrate/TiO_2 system and in binary system with ferric citrate irradiated by 1 lamp.

In the combined system at initial pH = 3, the pH evolution in the first step during Monuron degradation shown similar characteristics to the system with ferric citrate alone. A steep increase of pH to 3.45 after 15 minutes of irradiation in the combined system was followed by a plateau at pH 3.55. In the system without TiO_2, the pH quickly increased to 3.65 in 15 minutes and in the second step; on the contrary, the pH kept increasing with further irradiation: pH = 3.8 at 240 minutes of irradiation and pH = 4.0 at 420 minutes of irradiation.

The comparison of Fe(II) concentration during the Monuron degradation in both combined and binary ferric citrate system is displayed in **Fig. IV.C.7**.

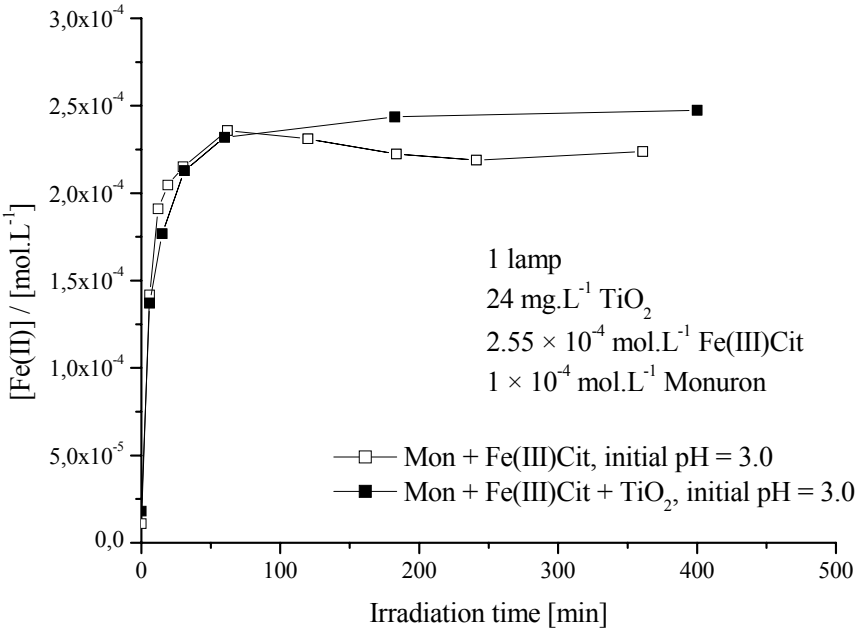

Fig. IV.C.7: Evolution of Fe(II) concentration during Monuron degradation in combined ferric citrate/TiO_2 system and in binary system with ferric citrate irradiated by 1 lamp.

The evolution of Fe(II) concentration observed during Monuron degradation in the combined system was almost identical to the separate ferric citrate system within first 60 minutes. In first 30 minutes of irradiation, fast increase of Fe(II) concentration to 84% of total iron was observed in both systems. After 60 minutes, where the Fe(II) comprised more than 90% of total iron in both systems; with further irradiation, the Fe(II) concentration in combined system was continuously increasing to 97% of total iron after 420 minutes of irradiation. On the contrary, the Fe(II) slowly decreased to 88% in 360 minutes, which goes together with the simultaneous slight increase of pH.

IV.C.4 Impact of pH on the combined system

The pH had an enormous impact on the efficiency of Monuron degradation photoinduced by ferric citrate, as we have shown in the previous chapter. An impact of pH was observed in the combined systems as well. The kinetics of Monuron degradation in the combined systems at various initial pH's with comparison to binary systems are shown in **Figs. IV.C.8** and **IV.C.9**.

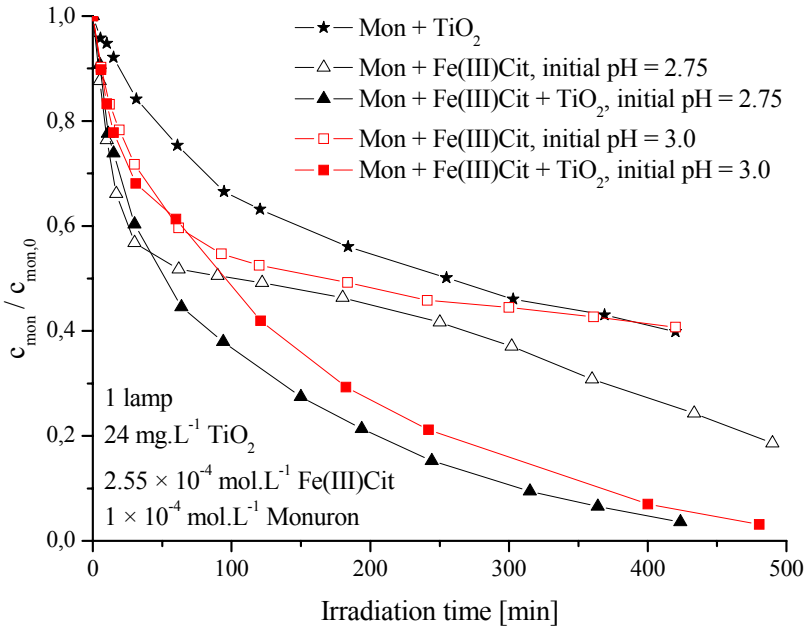

Fig. IV.C.8: Kinetics of Monuron degradation in combined system of ferric citrate/TiO_2 upon irradiation by 1 lamp; initial pH = 2.75 or 3.0; comparison with binary systems with ferric citrate or TiO_2.

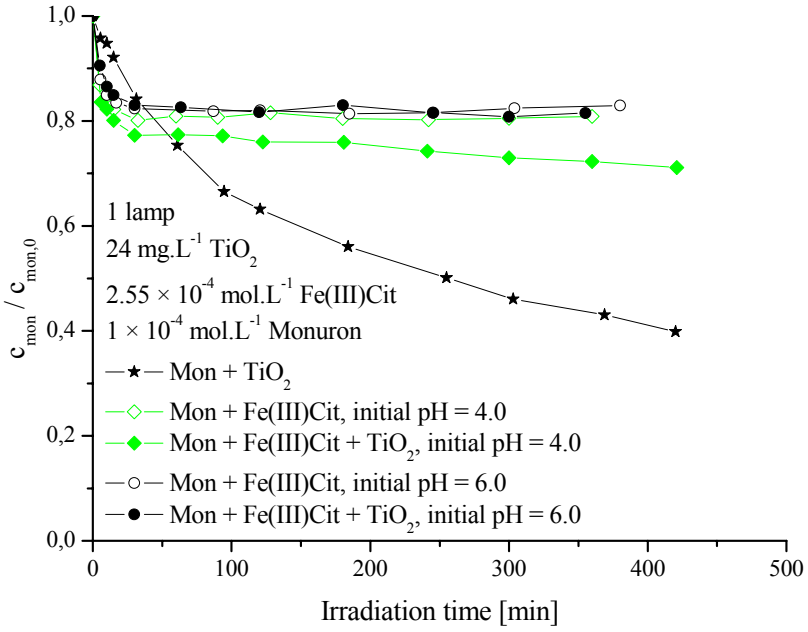

Fig. IV.C.9: Kinetics of Monuron degradation in combined system of ferric citrate/TiO_2 upon irradiation by 1 lamp; initial pH = 4.0 or 6.0; comparison with binary systems with ferric citrate or TiO_2.

The kinetics of Monuron degradation by the combined system at initial pH = 3.0 and pH = 2.75 were faster than the degradation in any particular binary systems. The highest Monuron degradation efficiency of the combined system was achieved at initial pH = 2.75, as 93% of Monuron were degraded in 360 minutes; with the use of ferric citrate or TiO_2 alone, for the same irradiation time the Monuron degradation efficiency was only 69%, or 57% respectively. The impact of combined system at initial pH = 3.0 was already described in detail in previous subhead of this chapter. After 360 min of irradiation, 90% of Monuron was degraded.

On the contrary, not much difference between Fe(III)Cit and Fe(III)Cit/TiO_2 systems was observed at initial pH = 4.0 and pH = 6.0. At initial pH = 4.0 in the system with ferric citrate alone, the Monuron degradation efficiency in the second step was practically negligible. The presence of TiO_2 slightly accelerated the degradation in the second step; however, only 28% of Monuron were degraded after 360 minutes of irradiation. At initial pH = 6.0, the degradation in the second is no more present even in the presence of TiO_2.

The addition of TiO_2 into the ferric citrate system generally accelerated the degradation. Nevertheless, if no degradation was observed with ferric citrate alone, the impact of TiO_2 on the degradation efficiency was negligible. By other words, the impact of TiO_2 was notable when active species of iron were present. The impact of pH on the degradation efficiency is critical also in the combined system of ferric citrate/TiO_2.

The degradation efficiencies are shown in **Tab. IV.C.4**.

Initial pH	Fe(III)Cit		Fe(III)Cit + TiO_2		TiO_2	
	15 min	360 min	15 min	360 min	15 min	360 min
2.75	31%	69%	26%	93%	–	–
3	19%	57%	22%	90%	–	–
4	18%	20%	20%	28%	–	–
6	16%	18%	15%	19%	–	–
Natural (6.2)	–	–	–	–	8%	57%

Tab. IV.C.4. Degradation efficiency of 1×10^{-4} mol.L^{-1} Monuron in binary and combined systems (2.55×10^{-4} mol.L^{-1} ferric citrate and 24 mg.L^{-1} TiO_2) at various initial pH's; irradiated by 1 lamp; natural pH correspond to about 6.2.

The impact of TiO_2 presence on the evolution of pH during Monuron degradation photoinduced by ferric citrate at various initial pH's is shown in **Figs. IV.C.10** and **IV.C.11**.

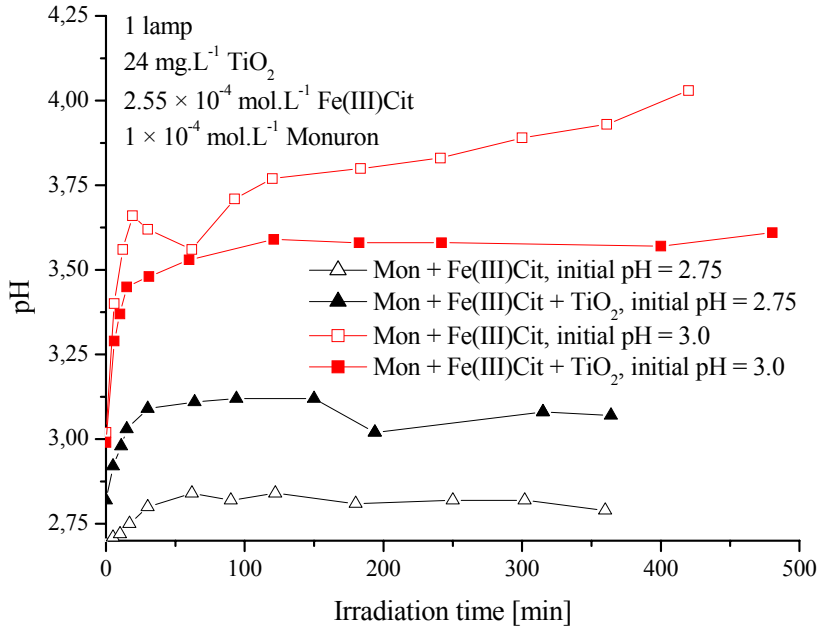

Fig. IV.C.10: Evolution of pH during Monuron degradation in combined ferric citrate/TiO_2 system irradiated by 1 lamp; initial pH = 2.75 or 3.0; comparison to Monuron degradation induced by ferric citrate.

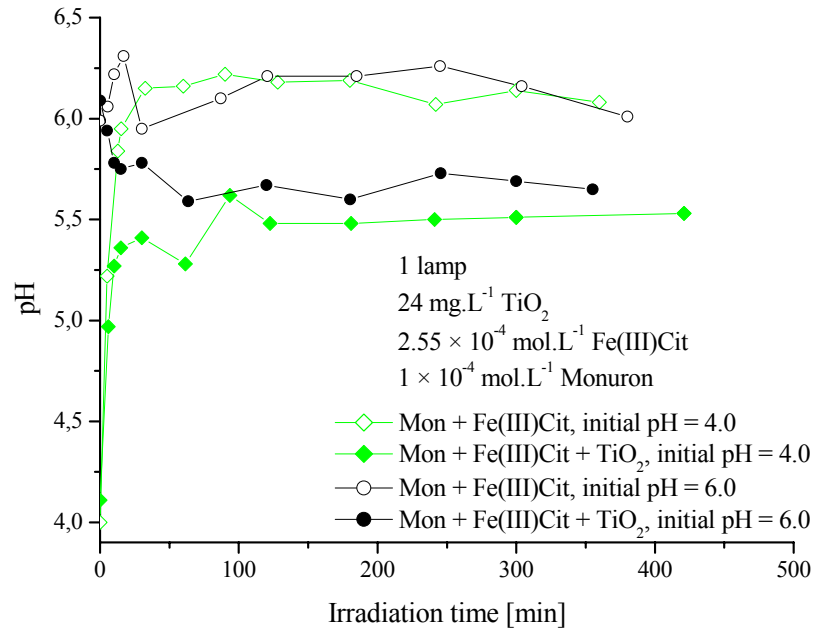

Fig. IV.C.11: Evolution of pH during Monuron degradation in combined ferric citrate/TiO_2 system irradiated by 1 lamp; initial pH = 4.0 or 6.0; comparison to Monuron degradation induced by ferric citrate.

The evolution of pH shows that the pH values are lower during the entire Monuron degradation process in the combined system than in the system without TiO_2. An exception was observed at the initial pH = 2.75, where the effect was inverse, see **Tab. IV.C.5**. A steep increase of pH close to plateau values was generally observed after 15 – 30 minutes of irradiation, which was usually followed by a plateau. An exception was observed at initial pH = 6.0, where the pH did not practically change in the binary system with Fe(III)Cit.

Initial pH	Fe(III)Cit		Fe(III)Cit + TiO_2	
	30 min	360 min	30 min	360 min
2.75	2.80	2.79	3.03	3.07
3	3.61	3.93	3.45	3.57
4	6.15	6.14	5.41	5.52
6	5.95	6.01	5.78	5.65

Tab. IV.C.5. pH values during degradation of 1×10^{-4} mol.L^{-1} Monuron in binary and combined systems (2.55×10^{-4} mol.L^{-1} ferric citrate and 24 mg.L^{-1} TiO_2) at various initial pH's; irradiated by 1 lamp.

In the combined system at initial pH = 2.75, the pH evolution during Monuron degradation shown similarity to the system of ferric citrate alone. The trend was identical for all system, however the plateau values were different: pH 3.05 in the combined system and pH 2.8 in the ferric citrate system; thus, the pH in combined system was higher than in a binary system, which is in contrast to the effect observed for other initial pH's. The combined system at initial pH = 3.0 was already commented in previous subhead of this chapter. At initial pH = 4.0, a steep increase of pH to 5.4 was observed in the combined system after 30 minutes; with further irradiation, the pH practically did not change. In the system without TiO_2, the pH value rose to 6.15 and remains practically unchanged with further irradiation. The evolutions of pH in both the Fe(III)Cit and Fe(III)Cit/TiO_2 systems at initial pH = 6 were affected by the carbonation process. In the ferric citrate system the pH remained in the range between 6.0 and 6.3 all along the irradiation; in the combined system, the pH remained, after initial decrease, constant at about 5.7.

The impact of TiO_2 presence on the evolution of Fe(II) concentration during Monuron degradation photoinduced by ferric citrate at various initial pH's is displayed in **Figs. IV.C.12** and **IV.C.13**.

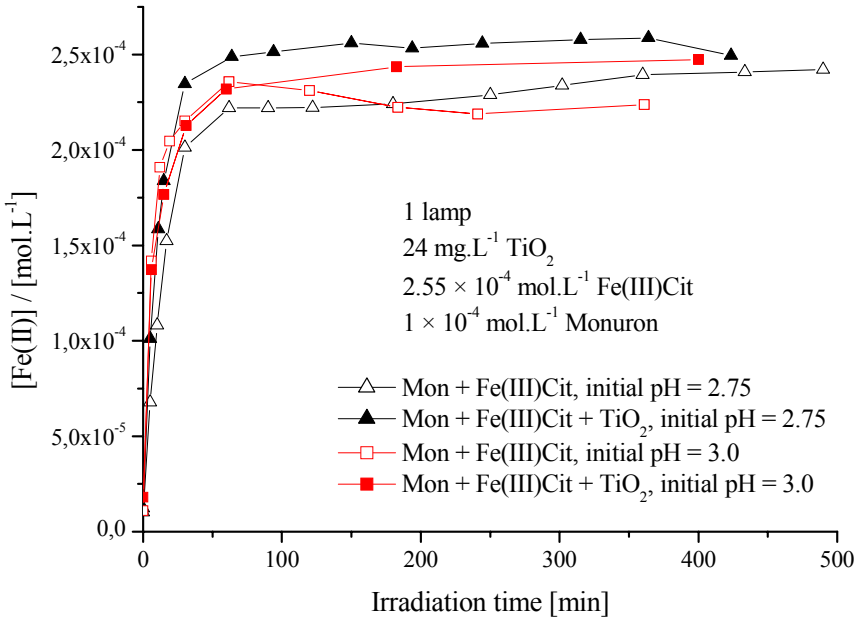

Fig. IV.C.12: Evolution of Fe(II) concentration during Monuron degradation in combined ferric citrate/TiO_2 system or in binary system with ferric citrate irradiated by 1 lamp; initial pH = 2.75 or 3.0.

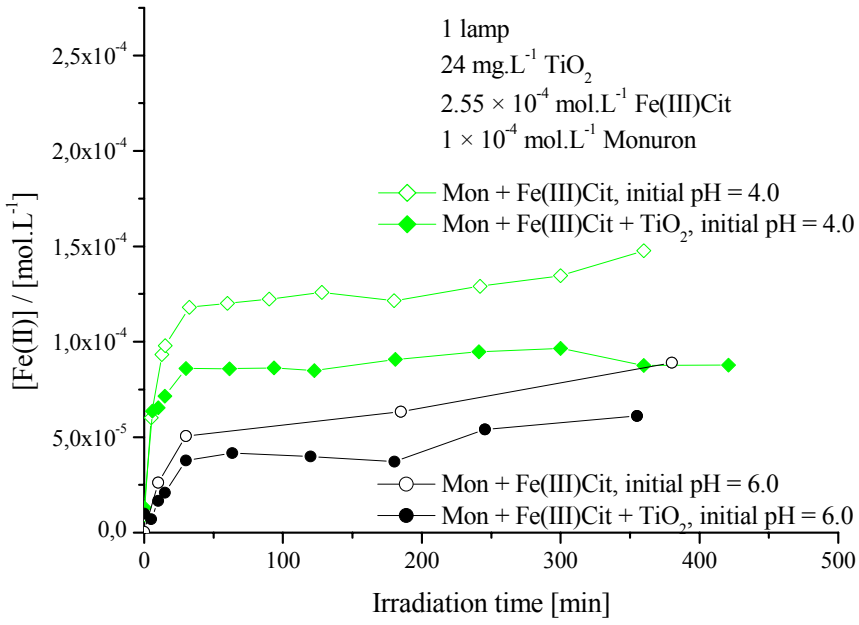

Fig. IV.C.13: Evolution of Fe(II) concentration during Monuron degradation in combined ferric citrate/TiO_2 system or in binary system with ferric citrate irradiated by 1 lamp; initial pH = 4.0 or 6.0.

The evolutions of Fe(II) concentration observed during Monuron degradation in the combined system were generally similar to those of ferric citrate without TiO_2. In the first 30 minutes of irradiation, the concentration of Fe(II) quickly increased; with further irradiation, a plateau was observed. The percentage of Fe(II) as a function of total iron for both systems are shown in **Tab. IV.C.6**.

Initial pH	Fe(III)Cit		Fe(III)Cit + TiO_2	
	30 min	360 min	30 min	360 min
2.75	79%	94%	92%	100%
3.0	84%	88%	83%	97%
4.0	38%	58%	28%	34%
6.0	20%	34%	15%	24%

Tab. IV.C.6. Percentage of Fe(II) observed during degradation of 1×10^{-4} mol.L^{-1} Monuron in binary and combined systems (2.55×10^{-4} mol.L^{-1} ferric citrate and 24 mg.L^{-1} TiO_2) at various initial pH's; irradiated by 1 lamp.

At initial pH = 2.75 and pH = 3.0, the presence of TiO_2 during the Monuron degradation photoinduced by ferric citrate had a weak positive effect on the Fe(II) concentration. At initial pH = 2.75, the Fe(II) concentration reached around 100% of total iron after irradiation of the combined system for 150 minutes. At the same irradiation time, the Fe(II) concentration in ferric citrate system represented 87% of total iron. The [Fe(II)] was higher in combined system despite higher pH observed. The ferric citrate system with/without TiO_2 at initial pH = 3.0 was already described in the previous subhead of this chapter. The increase of Fe(II) concentration could be caused by the reduction of Fe(III) by the electrons present at TiO_2 surface.

On the contrary, at initial pH = 4.0 and pH = 6.0, the presence of TiO_2 during the degradation of Monuron photoinduced by ferric citrate had a negative effect on the Fe(II) concentration. At the initial pH = 4.0, the concentration of Fe(II) reached 28% of total iron after 30 minutes of irradiation; with further irradiation, the Fe(II) concentration remained at the plateau value corresponding to 34% of total iron. In the system without TiO_2, the Fe(II) concentration was higher all over the irradiation (58% of total iron at 360 minutes), despite observed lower Monuron degradation efficiency.

Both at initial pH = 4.0 and 6.0, lower concentrations of Fe(II) were found in the combined systems than in the binary ones, despite lower pH in the combined systems, where

the pH plateau value was about 5.5. Normally, the Fe(II) concentration in water increase when the pH decreases. This could be explained by a reoxidation of Fe(II) by the holes on the TiO_2 surface. The surface of TiO_2 is positively charged at acid pH; with an increase of pH, the positive charge is being neutralized. When the pH increases to 6.25, the point of zero charge of TiO_2 is reached and the TiO_2 particle becomes electroneutral. Thus, at higher pH (e.g. pH = 5.5 was still high enough), the electrostatic repulsion between the ferric/ferrous ions and the surface of TiO_2 decreased enough to permit a closer approach of ferric and ferrous ions to the partially discharged TiO_2 particles. However, the enhanced Monuron degradation efficiency was caused by the photocalysis on TiO_2, generating the hydroxyl radicals. At initial pH = 6.0, the degradation of Monuron in combined system was practically inhibited in the second step. We can assume that notable part of Fe(II) was reoxidized on the surface of the TiO_2 particles, and that the photocatalysis on TiO_2 was inhibited by this short-cut.

IV.C.5 Impact of Fe(III)Cit concentration on the combined system

The impact of ferric citrate concentration on the Monuron degradation efficiency in the ferric citrate system with/without TiO_2 was examined, see **Fig. IV.C.14**.

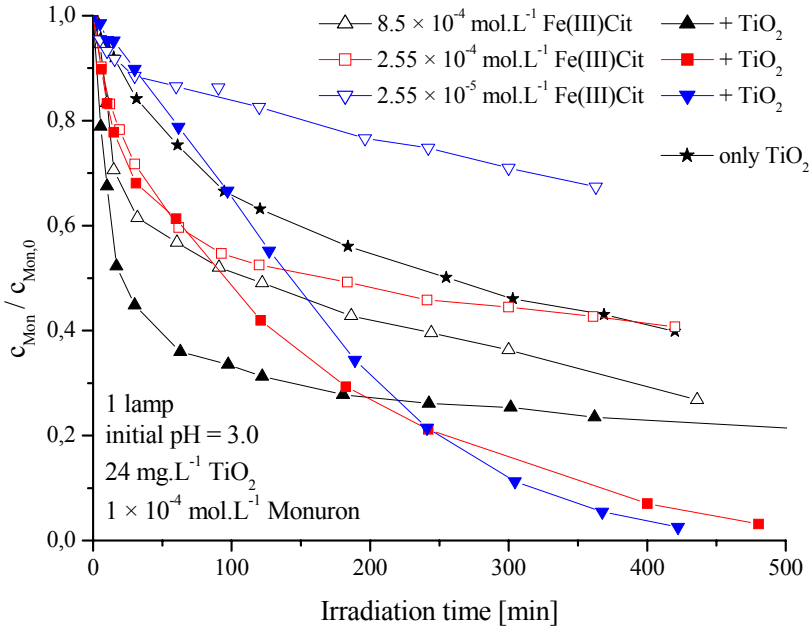

Fig. IV.C.14: Impact of ferric citrate concentrations on the kinetics of Monuron degradation in the system of ferric citrate with/without TiO_2 upon irradiation by 1 lamp; initial pH = 3.0.

The addition of ferric citrate has enormous effect on the efficiency of the combined system, compared to system with TiO_2 alone.

The impact of ferric citrate concentration on Monuron degradation efficiency in the system of ferric citrate with/without TiO_2 is not proportional. The Monuron degradation in combined system was always faster than in the respective binary systems. The highest difference of Monuron degradation efficiency between combined system and ferric citrate alone was observed at the lowest ferric citrate concentration (2.55×10^{-5} mol.L^{-1}), where 94% of Monuron were degraded after 360 minutes of irradiation in the combined system alone, by comparing to only 32% in the ferric citrate system, see **Tab. IV.C.7**.

An important difference in Monuron degradation efficiency was also observed in the systems containing 2.55×10^{-4} mol.L^{-1} ferric citrate. After 360 minutes of irradiation, 90% of Monuron are degraded in the combined system, comparing to the degradation efficiency observed with ferric citrate or TiO_2 alone (both 57%).

At the highest concentration of ferric citrate (8.5×10^{-4} mol.L^{-1}), the kinetics in the first step of degradation was fastest for both systems (with or without TiO_2). On the contrary, the kinetics of degradation in the second step was slightly inhibited for both systems. The difference in Monuron degradation efficieny between the systems was very low: after 360 minutes of irradiation, the combined system of ferric citrate/TiO_2 degraded 9% more Monuron than the ferric citrate alone.

Initial [Fe(III)Cit] [mol.L^{-1}]	Fe(III)Cit		Fe(III)Cit + TiO_2		TiO_2	
	15 min	360 min	15 min	360 min	15 min	360 min
8.5×10^{-4}	29%	68%	44%	77%	–	–
2.55×10^{-4}	19%	57%	22%	90%	–	–
2.55×10^{-5}	9%	**32%**	5%	**94%**	–	–
0	–	–	–	–	8%	57%

Tab. IV.C.7. Impact of ferric citrate concentration on Monuron degradation efficiency (1×10^{-4} mol.L^{-1}) in system of ferric citrate with/without 24 mg.L^{-1} TiO_2 upon irradiation by 1 lamp; initial pH = 3.0.

Large concentration of ferric citrate slowed down the degradation in second phase. As the large amount of Fe(II) is formed in the first phase, it is reoxidized by TiO_2. Fe(II) react with the holes on the surface of the TiO_2 and competes with the principal source of hydroxyl radical formation (via reaction of water species with h^+). A second explanation can be due to

the presence of higher concentration of citrate or degradation products which can react with •OH radicals and as a consequence compete with the reaction of •OH radicals and Monuron.

Impact of ferric citrate concentration on evolution of pH during Monuron degradation in system of ferric citrate with/without TiO_2 system is shown in **Fig. IV.C.15**.

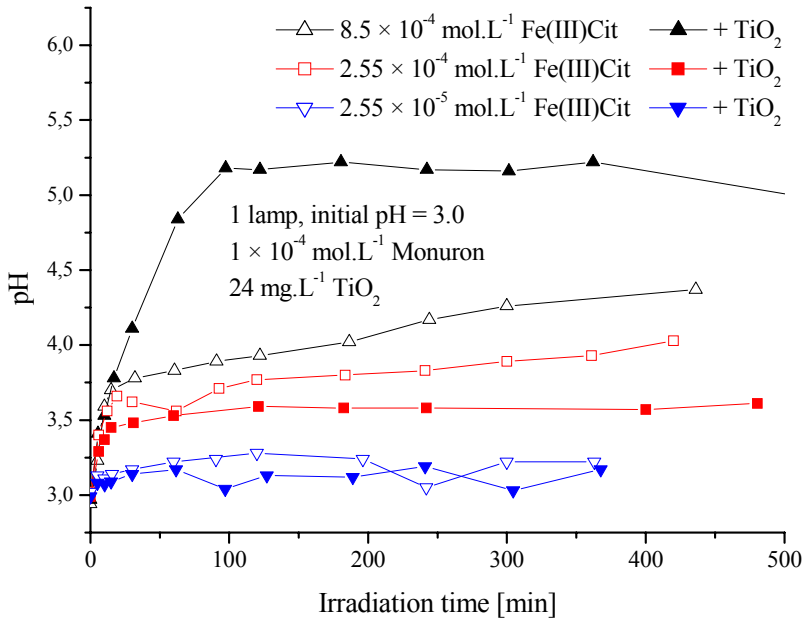

Fig. IV.C.15: Impact of ferric citrate concentration on the evolution of pH during Monuron degradation in system of ferric citrate with/without TiO_2; irradiation by 1 lamp; initial pH = 3.0.

The observed pH during Monuron degradation in the combined system had generally similar evolution: the pH quickly increased in a time from 5 to 60 minutes, afterwards it was slightly increasing up to 120 minutes and then remained at the plateau; the pH values observed during the Monuron degradation process are displayed in **Tab. IV.C.8**.

Initial [Fe(III)Cit] [mol.L^{-1}]	Fe(III)Cit		Fe(III)Cit + TiO_2	
	15 min	360 min	15 min	360 min
8.5×10^{-4}	3.7	4.3	3.7	5.2
2.55×10^{-4}	3.6	3.9	3.45	3.6
2.55×10^{-5}	3.15	3.2	3.1	3.15

Tab. IV.C.8. pH values taken during degradation of 1×10^{-4} mol.L^{-1} Monuron in binary and combined systems (various concentration of ferric citrate, 24 mg.L^{-1} TiO_2); initial pH = 3.0; irradiated by 1 lamp.

In the combined system with ferric citrate concentration equal or lower than 2.55×10^{-4} mol.L^{-1}, lower values of pH were observed than in the system without TiO_2. In the combined system with 2.55×10^{-5} mol.L^{-1} Fe(III)Cit, the pH quickly increased to 3.1 in 5 minutes. With further irradiation, the pH increased to 3.15 in 30 minutes and remained close to this value until the end of irradiation. In the system 2.55×10^{-5} mol.L^{-1} Fe(III)Cit without TiO_2, the pH evolution was similar, but the observed plateau value of pH was 3.2. The systems with 2.55×10^{-4} mol.L^{-1} ferric citrate were already described above; the pH plateau value in combined system was about 3.6; in the system without TiO_2, the pH was, after a steep growth in first 20 minutes, gradually increasing to 4.0 after 420 minutes of irradiation.

At ferric citrate concentration of 8.5×10^{-4} mol.L^{-1}, the effect on pH was inverse; the pH in both combined and binary systems was increasing up to 15 minutes to pH about 3.7. With further irradiation, the pH in system without TiO_2 was continuously slightly increasing up to 4.35 at 435 minutes, opposing to the system with TiO_2, where the pH was still steeply increasing up to 95 minutes, until the plateau value of 5.2 was reached. The higher pH achieved in the combined system could be the reason of notable slowdown of Monuron degradation in the second step (**Fig IV.C.14**).

The pH evolution corresponding to the first step was generally faster with higher ferric citrate concentration. The presence of TiO_2 resulted in lower observed pH evolution at ferric citrate concentration of 2.55×10^{-4} mol.L^{-1} and lower. Inverse effect was observed with 8.5×10^{-4} mol.L^{-1} of ferric citrate.

The effect of TiO_2 presence on evolution of Fe(II) concentration during Monuron degradation in presence of various concentrations of ferric citrate upon irradiation is shown in **Fig. IV.C.16**.

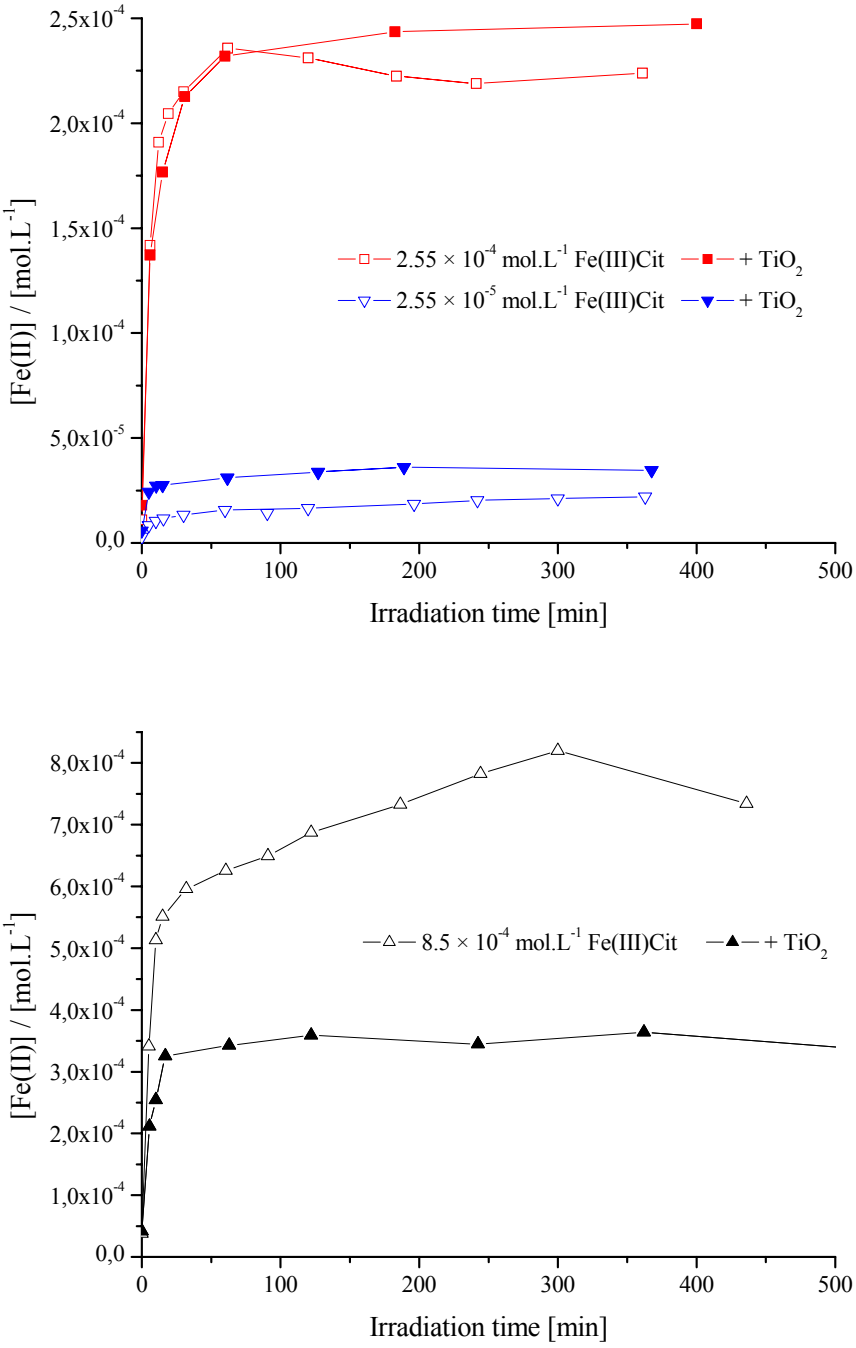

Fig. IV.C.16a+b: Impact of TiO_2 presence on evolution of Fe(II) concentration during Monuron degradation in presence of various concentrations of ferric citrate upon irradiation by 1 lamp; initial pH = 3.0; 24 $mg.L^{-1}$ TiO_2, 1×10^{-4} $mol.L^{-1}$ Monuron.

The impact of TiO_2 presence on evolution of Fe(II) concentration during Monuron degradation was inverse to the evolution of pH. With 2.55×10^{-5} $mol.L^{-1}$ of Fe(III)Cit, the presence of TiO_2 results in higher Fe(II) concentration; on the contrary, a lower Fe(II)

concentration is observed with 8.5×10^{-4} mol.L^{-1} Fe(III)Cit; the values of [Fe(II)] measured during the Monuron degradation process are displayed **Tab. IV.C.9**.

Initial [Fe(III)Cit] [mol.L^{-1}]	Fe(III)Cit		Fe(III)Cit + TiO_2	
	15 min	360 min	15 min	360 min
8.5×10^{-4}	64%	91%	36%	43%
2.55×10^{-4}	78%	88%	69%	97%
2.55×10^{-5}	46%	87%	88%	100%

Tab. IV.C.9. Concentrations of Fe(II) in % of total iron taken during 1×10^{-4} mol.L^{-1} Monuron degradation in binary and combined systems (various concentration of ferric citrate and 24 mg.L^{-1} TiO_2); initial pH = 3.0; irradiated by 1 lamp.

In the systems with 8.5×10^{-4} mol.L^{-1}, the Fe(II) concentration increases steeply for the first 15 minutes, where about one third of total iron was present as Fe(II) in the combined system; without TiO_2, the concentration was almost double. This phenomenon evidences the role of the oxidative species generated in the presence of TiO_2. With further irradiation, the concentration of Fe(II) in the combined system remained practically constant, while it was on a constant increase up to 96% of total iron in system without TiO_2 after 300 minutes of irradiation; after 360 minutes it slightly dropped to 91%. The lower Fe(II) concentration observed in the combined system is in an agreement with the increase of pH. The presence of TiO_2 enhanced the photodegradation of the ferric citrate complex, which resulted in a steeper increase of pH to about 5.2. At this pH, the Fe(II) was partially reoxidized on the TiO_2 surface. This result is also in agreement with the fact that the oxidation of Fe(II), with the oxygen present in water, is higher when he pH is higher.

At the concentration of 2.55×10^{-4} mol.L^{-1}, a crossover of Fe(II) evolution curves was observed: until 20 minutes of irradiation, a steep increase of Fe(II) concentration was observed for both presence and absence of TiO_2, with higher [Fe(II)] in the system without TiO_2. Consequently, the Fe(II) concentrations equalized at about 92% of total iron at 60 minutes. With further irradiation, the [Fe(II)] was slightly increasing up to 97% at 360 minutes in the combined system; at the same irradiation time, 88% were observed in the system without TiO_2. The higher plateau value of Fe(II) concentration in the combined system comparing to the system without TiO_2 corresponds to the observed lower value of pH. This is

in accordance with the generally observed fact, that the Fe(II) concentration decreases with increasing pH.

In the combined system with the lowest ferric citrate concentration, practically all iron was present as Fe(II) after 5 minutes of irradiation and remained at this level until the end of irradiation. After 360 minutes, about 100% of total iron consisted of Fe(II) in the combined system. The Fe(II) concentration in the system without TiO_2 was about 46% of total iron after 15 minutes; with further irradiation, it was gradually increasing to 87% at 360 minutes. At this ferric citrate concentration, the highest impact of TiO_2 presence on Monuron degradation efficiency was observed (**Fig IV.C.14**).

IV.C.6 Conclusion

In this part a combined system (Fe(III)Cit and TiO_2) was studied for the photodegradation of Monuron, the same pollutant than in the previous part. The addition of TiO_2 to the mixture shows no important effect on the photoformation of Fe(II) species. The kinetics of Fe(II) formation are very close with or without TiO_2. The photodegradation of Monuron was previously measured at different TiO_2 concentrations and an optimum concentration was 250 $mg.L^{-1}$.

The degradation of Monuron is much higher in the combined system than in the binary systems (with Fe(III)Cit or TiO_2). After 480 min of irradiation 97% of Monuron is degraded in the combined system and only 58% in the both binary systems. In the combined system, a strong acceleration is observed after 60 minutes of irradiation and the degradation continues with the same efficiency than at the beginning. Addition of TiO_2 has a strong positive effect on the second step of Monuron degradation observed with Fe(III)Cit alone. The second step present in the system with carboxylate ferric complexes, as I mentioned in the previous part, is attributed to the formation of radical species through the photocatalytic cycle based on the couple Fe(III)/Fe(II). Previous studies performed in the laboratory showed that in the presence of Fe(III) aquacomplexes the limiting step was the reoxydation of Fe(II) into Fe(III). Moreover, ***Mestankova et al. (2005, 57)*** showed that the oxidized species photogenerated from TiO_2 increased the oxidation of Fe(II) (reaction 1, 2 and 3) and then the photocatalytic cycle Fe(III)/Fe(II):

$$Fe^{II} + H_2O_2 \longrightarrow Fe^{III} + {}^{\bullet}OH + OH^- \quad (1)$$

$$Fe^{II} + HO_2^{\bullet} + H^+ \longrightarrow Fe^{III} + H_2O_2 \quad (2)$$

$$Fe^{II} + {}^{\bullet}OH \longrightarrow Fe^{III} + OH^- \quad (3)$$

Reaction 1 not only permits the oxidation of Fe(II) but also photogenerates very oxidative species: hydroxyl radicals. Reaction 3 is detrimental in terms of pollutant degradation. But the global balance shows that all these reactions regenerating Fe(III) have a positive influence as evidenced by the degradation curves in the presence and in the absence of TiO_2. Thus, the strong increase of the rate of Monuron degradation observed in our system can be attributed to the same effect of the oxidative species photogenerated by TiO_2 particles.

The combined system was also dependent on pH, like in the system with Fe(III)Cit complex alone. The range of initial pH's, where the combined systems were most active, were similar to those without TiO_2 presence. The most active degradation of Monuron is observed near initial pH = 3.0. At initial pH = 4.0 and higher, a strong decrease of Monuron degradation in the second step was also observed, as the pH rapidly increases. An occurrence of shortcuts of TiO_2 by iron ions was proposed.

The impact of ferric citrate concentration, examined at the most efficient pH (near 3.0), shows that the system is also dependant on this parameter and the results are similar to those obtained with Fe(III)Cit alone. At higher tested concentration (8.4×10^{-4} mol.L^{-1}) the degradation of Monuron after 360 min of irradiation corresponded to 77% and with a concentration of 2.5×10^{-4} mol.L^{-1} the degradation reached 90% for the same irradiation time. Again, the slowdown of Monuron degradation at higher concentration was induced by an increase of pH close to neutral zone. On the contrary, with the lowest concentration used in Fe(III)Cit (2.5×10^{-4} mol.L^{-1}) corresponding to a ratio of Fe/TiO_2 equal to 1/12 the degradation of Monuron was the most efficient (94%). It is little more efficient than the system with approximately equal ratio and also much more efficient than the system with the ratio of 3 (excess of iron).

The most efficient degradation of pollutants with the lowest concentration of ferric complex is a very interesting result for the set up of combined system for the decontamination of water, but also for the advanced oxidation processes using TiO_2, where traces of iron are always present in the waters.

IV.D Competitive photocatalytic degradation: TiO_2 + 4-chlorophenol + organic solvent

IV.D.1 Photodegradation of 4-chlorophenol with TiO_2, comparison of immobilized layers and suspensions

A batch-mode *plate* photoreactor was employed in the study of 4-chlorophenol degradation processes. The purified solution was flowing over an irradiated layer with immobilized TiO_2. The kinetics of 4-chlorophenol degradation at various initial concentration of the pollutant are shown in **Fig. IV.D.1**.

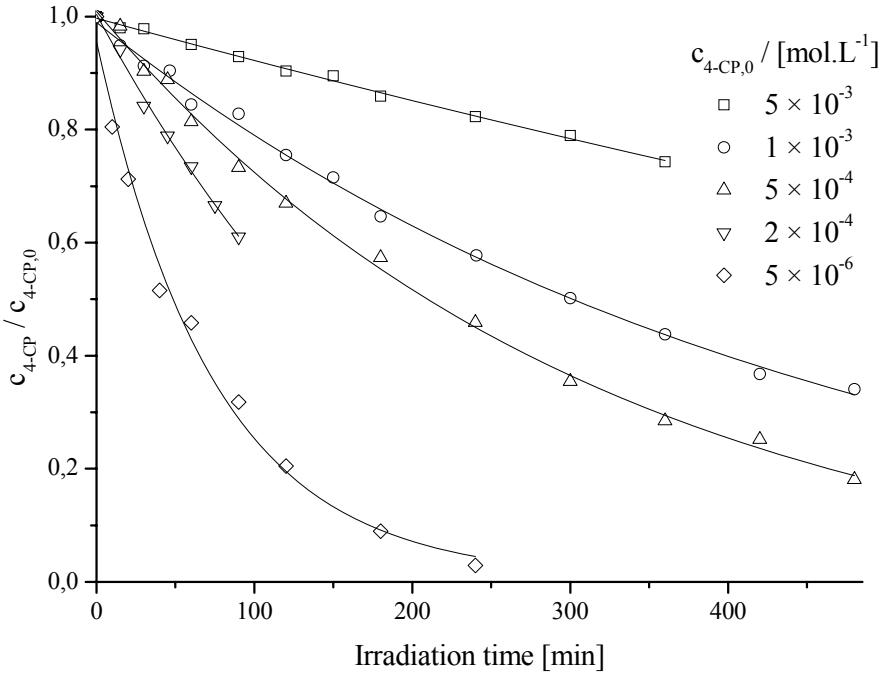

Fig. IV.D.1: Kinetics of 4-chlorophenol degradation at immobilized TiO_2 Degussa P25 layers (0.31 mg $TiO_2.cm^{-2}$) under irradiation at various initial 4-chlorophenol concentrations.

The rate of 4-chlorophenol degradation was decreasing when the initial pollutant concentration increased. The kinetics corresponded to a first order decay; first order rate constants are shown in **Tab. IV.D.1**. The value of rate constant for 2×10^{-4} $mol.L^{-1}$ 4-chlorophenol is not correct due to insufficient experimental data. For this purpose of comparison suspensions (slurries) in quasi-closed systems were also used. The kinetics of

4-chlorophenol photodegradation in a TiO_2 suspension at various initial 4-CP concentrations are shown in **Fig. IV.D.2**.

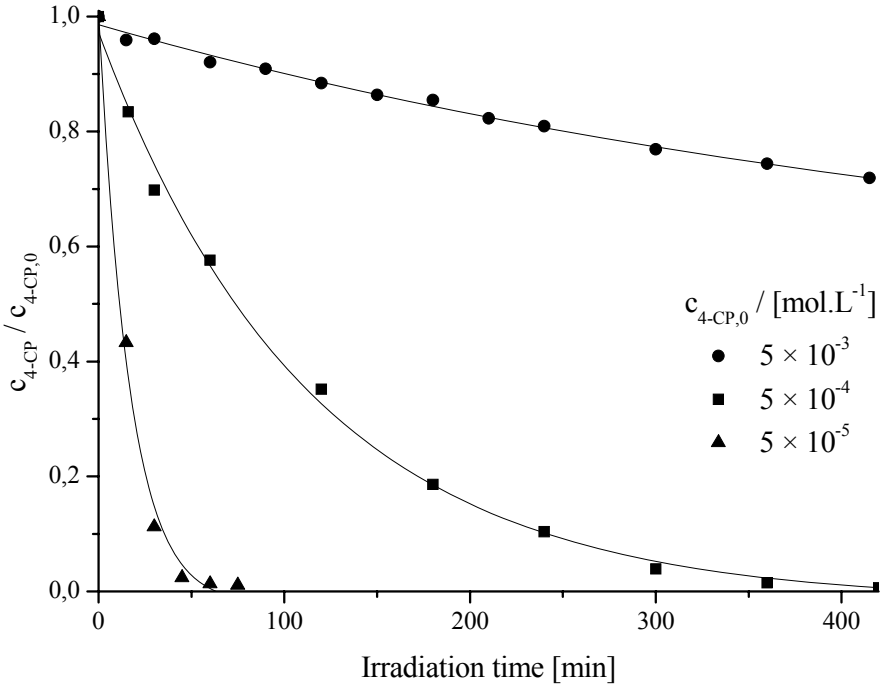

Fig. IV.D.2: Kinetics of 4-chlorophenol degradation in TiO_2 P25 suspension (0.5 g.L^{-1}) under irradiation at various initial 4-chlorophenol concentrations.

The rate of 4-chlorophenol degradation was decreasing with the increase of initial pollutant concentration as well. The degradation kinetics could be described by first order; the values of rate constants are shown in **Tab. IV.D.1**.

A necessity of comparison of these systems logically occurred. Kinetics of 5×10^{-4} mol.L^{-1} 4-chlorophenol degradation at immobilized TiO_2 layers and in the closed system with 0.5 g.L^{-1} TiO_2 P25 suspension are compared in **Fig IV.D.3**.

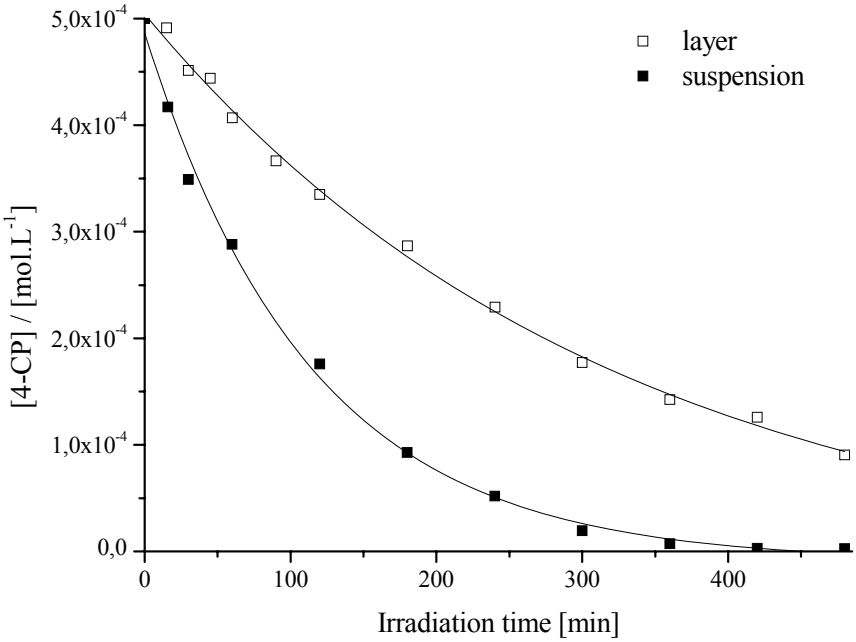

Fig. IV.D.3: Comparison of 4-chlorophenol (5×10^{-4} mol.L^{-1}) degradation kinetics at immobilized TiO_2 P25 layers and TiO_2 P25 suspensions (0.5 g.L^{-1}) under irradiation.

Initial 4-CP concentration [mol.L^{-1}]	Rate constant		$J_{4\text{-}CP,\ 60\ min}$	
	Suspension [s^{-1}]	Layer [s^{-1}]	Suspension [mol.m^{-2}.s^{-1}]	Layer [mol.m^{-2}.s^{-1}]
5.0×10^{-6}	–	2.0×10^{-4}	–	-4.8×10^{-8}
5.0×10^{-5}	1.0×10^{-3}	–	-1.2×10^{-6}	–
1.9×10^{-4}	–	(6.9×10^{-5})	–	-8.2×10^{-7}
5.0×10^{-4}	1.5×10^{-4}	5.2×10^{-5}	-3.6×10^{-6}	-1.3×10^{-6}
1.0×10^{-3}	–	3.7×10^{-5}	–	-2.2×10^{-6}
5.0×10^{-3}	(3.2×10^{-5})	(0.9×10^{-5})	-4.3×10^{-6}	-3.7×10^{-6}

Tab. IV.D.1: Rate constants and 4-CP initial degradation flows (60 minutes) of 4-CP photodegradation with layers or suspensions of P25 (0.5 g.L^{-1}); impact of initial concentration of 4-CP.

As mentioned above, the kinetics of 4-chlorophenol degradation in both systems could be described by first order kinetics. This assumption is reasonable for the 4-chlorophenol concentrations lower or equal to 1.0×10^{-3} mol.L^{-1}. However, the rate constants could not be compared directly, as several parameters of these systems were different (the geometry and

size of irradiated area and total volume of the polluted aquatic solution). Therefore for studied initial concentrations of 4-chlorophenol, the initial degradation flow (or flux density) $J_{4\text{-}CP}$ (60 minutes) was calculated as follows:

$$J_{4-CP} = \frac{V}{A}\left(\frac{dc_{4-CP}}{dt}\right)_{t=0},$$

where V was the total volume, A irradiated area and $(dc_{4\text{-}CP}/dt)_{t=0}$ was the slope of concentration measured during 60 minutes of irradiation (15 minutes for 5×10^{-5} mol.L^{-1} 4-CP degradation in suspension). Percentage of 4-chlorophenol conversion at 60 minutes varied between 15 and 40 %. The results are shown in **Tab. IV.D.1** and **Fig. IV.D.4**.

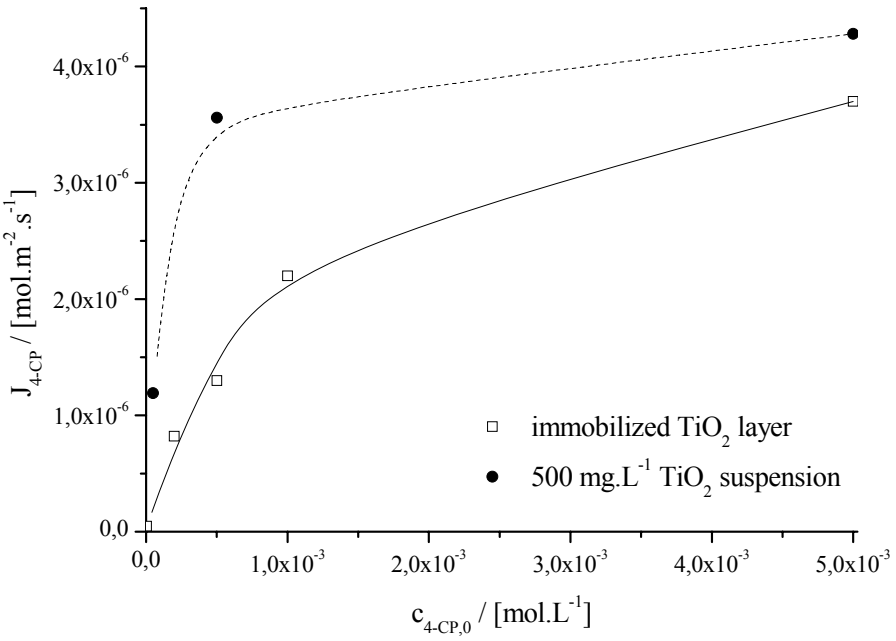

Fig. IV.D.4: Impact of initial concentration of 4-CP on its initial degradation flow (60 minutes) on the layer system (0.31 mg TiO_2.cm^{-2}) and in TiO_2 suspension (0.5 g.L^{-1}).

In both suspension and layer systems, the initial 4-CP degradation flow was increasing with the concentration of 4-chlorophenol. In the suspension system, the 4-CP degradation flow was always higher than in the layer system. For the 4-chlorophenol concentration of 5×10^{-4} mol.L^{-1}, the 4-CP degradation flow was almost triple in the suspension system. At initial pollutant concentrations of 5×10^{-5} mol.L^{-1} or lower, the degradation flow in both systems steeply decreased due to mass transfer limitation.

IV.D.2 Impact of organic solvent presence on 4-CP degradation

As mentioned above, the aim of this study was to connect the process of pollutant sorption on a polymer sorbent, and the process of photocatalytic degradation of the pollutant, which was eluted from the sorbent by an organic solvent. The concentrated solution of pollutant was intended to be repeatedly added into the suspension of TiO_2, where the photodegradation process took place. Thus, an impact of organic solvent addition on 4-chlorophenol degradation was to be examined before studying the effect of repeated addition of pollutant in organic solvent into the system. In the previous study concerning the sorption of the pollutant on the non-ionogenic polymer sorbent (***Jelínek et al., 2004***), two solvents were tested: methanol (MeOH) and acetonitrile (ACN). Methanol showed slightly better elution properties, but acetonitrile was also suitable elution solvent. However, methanol is a powerful $^{\bullet}OH$ radical quencher, and was therefore not much useful. The impact of methanol or acetonitrile presence (0.5 $mol.L^{-1}$) on kinetics of degradation of 5×10^{-4} $mol.L^{-1}$ 4-chlorophenol in P25 suspension is displayed in **Fig. IV.D.5**. Thus, the molar ratio of organic solvent to 4-chlorophenol was 1000:1.

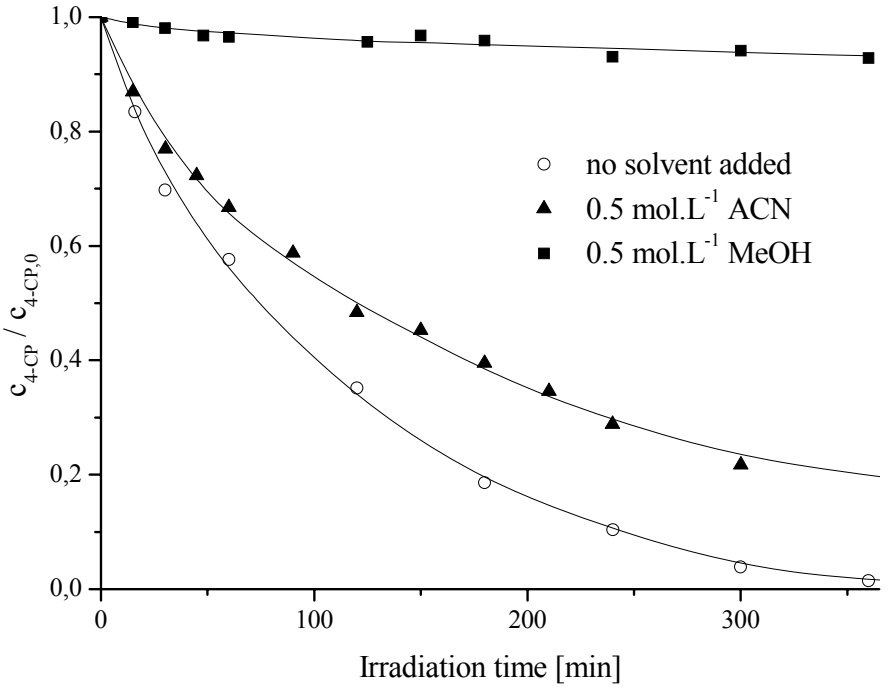

Fig. IV.D.5: Impact of organic solvent presence on degradation of 5×10^{-4} $mol.L^{-1}$ 4-CP in suspension of P25 (0.5 $g.L^{-1}$) upon irradiation.

The degradation of 4-CP alone or in acetonitrile presence could be described by first order kinetics. Rate constants and 4-CP initial degradation flows are shown in **Tab. IV.D.2**.

Solvent	Rate constant k [s^{-1}]	Decrease of k	$J_{4\text{-}CP}$ [$mol.m^{-2}\ s^{-1}$]	Decrease of $J_{4\text{-}CP}$
Without organic solvent	1.5×10^{-4}	100%	-3.6×10^{-6}	100%
Acetonitrile 0.5 $mol.L^{-1}$	1.2×10^{-4}	80%	-2.3×10^{-6}	64%
Methanol 0.5 $mol.L^{-1}$	(8.6×10^{-5})	–	-2.0×10^{-7}	6%

Tab. IV.D.2: Rate constants and initial degradation flows (60 min) for degradation of 4-CP (5×10^{-4} $mol.L^{-1}$) in presence of acetonitrile and methanol (0.5 $mol.L^{-1}$).

According to expectations, the degradation of 4-chlorophenol in methanol presence was strongly inhibited, as the 4-CP initial degradation flow dropped to 6% comparing to the system without any organic solvent. On the contrary, the degradation of 4-chlorophenol in acetonitrile presence was only partially slowed down, while the 4-CP degradation flow decreased to about one third. Methanol, as a powerful radical quencher, showed strong reactivity with $^{\bullet}$OH radicals. Acetonitrile showed to be less reactive with these species. Thus, methanol competed effectively with the pollutant for the $^{\bullet}$OH radicals and was found inappropriate for our purpose.

As mentioned in the bibliographic chapter, the rate constant of •OH radical reaction with 4-chlorophenol (***Stafford et al., 1994***) is about 10 times lower than the corresponding value for methanol (***Buxton et al., 1988***), and about 400 times lower than the corresponding value for acetonitrile (***Neta and Schuler, 1975***). Using these values, a decrease of 4-chlorophenol degradation rate in the presence of an organic solvent can be explained, namely by about two orders of magnitude in the case of methanol and by less than one order of magnitude for acetonitrile. This presumption was correct, however the precision was limited; one of the important factors not taken into account was the impact of degradation intermediates.

IV.D.3 Impact of acetonitrile concentration on 4-CP degradation

The acetonitrile was found more appropriate as a solvent for sorbent regeneration. Influence of acetonitrile concentration on 4-chlorophenol degradation was studied in the system with immobilized TiO_2. The impact of acetonitrile concentration on kinetics of 4-CP degradation is shown in **Fig. IV.D.6**; the 4-CP degradation flows are shown in **Tab. IV.D.3**.

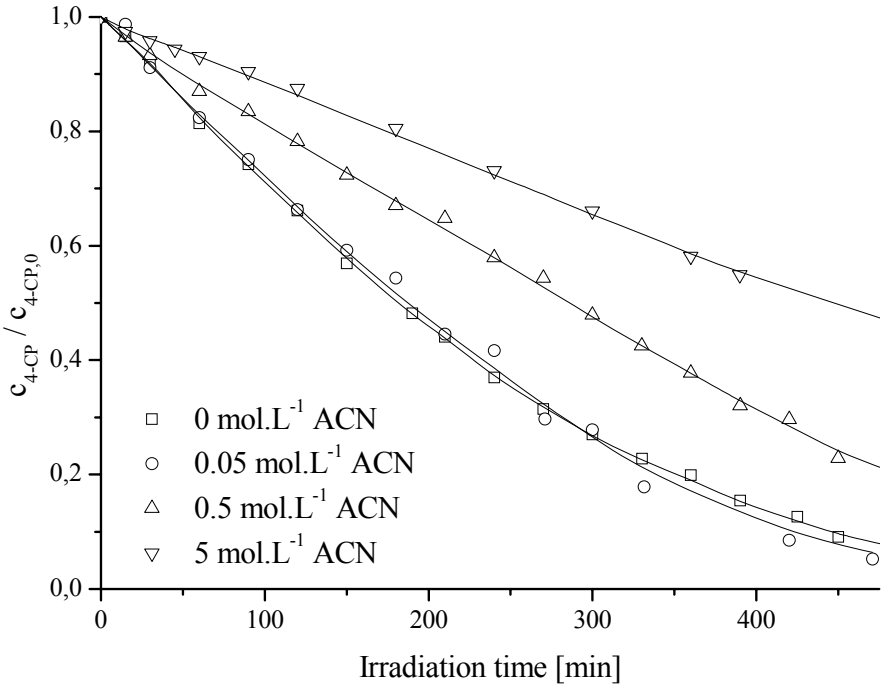

Fig. IV.D.6: Impact of acetonitrile concentration on degradation kinetics of 5×10^{-4} mol.L^{-1} 4-chlorophenol on a P25 layer.

Acetonitrile concentration [mol.L^{-1}]	4-CP degradation flow	
	[mol.m^{-2}.s^{-1}]	Decrease of $J_{4\text{-CP}}$
0	1.2×10^{-6}	100%
0.05	1.1×10^{-6}	96%
0.5	8.7×10^{-7}	7**6**%
5	4.4×10^{-7}	39%

Tab. IV.D.3: Impact of acetonitrile concentration on 4-chlorophenol initial degradation flow ($J_{4\text{-CP},60\ min}$) of 4-chlorophenol (5×10^{-4} mol.L^{-1}).

For acetonitrile concentrations lower than 0.05 mol.L^{-1} the degradation rate of 4-chlorophenol was not practically affected. In presence of 0.5 mol.L^{-1} acetonitrile, the 4-CP degradation flow dropped about by one fourth to 76% of the value corresponding to system without acetonitrile. With the highest acetonitrile concentration of 5 mol.L^{-1} the 4-CP degradation flow comprised 39% comparing to system without acetonitrile.

IV.D.4 Competitive degradation kinetics of 4-CP and acetonitrile

The method of total organic carbon determination (TOC) was employed to follow the mineralization of acetonitrile. TOC evolution in a system of acetonitrile (3.8×10^{-3} mol.L^{-1}) with and without irradiation is shown in **Fig. IV.D.7**.

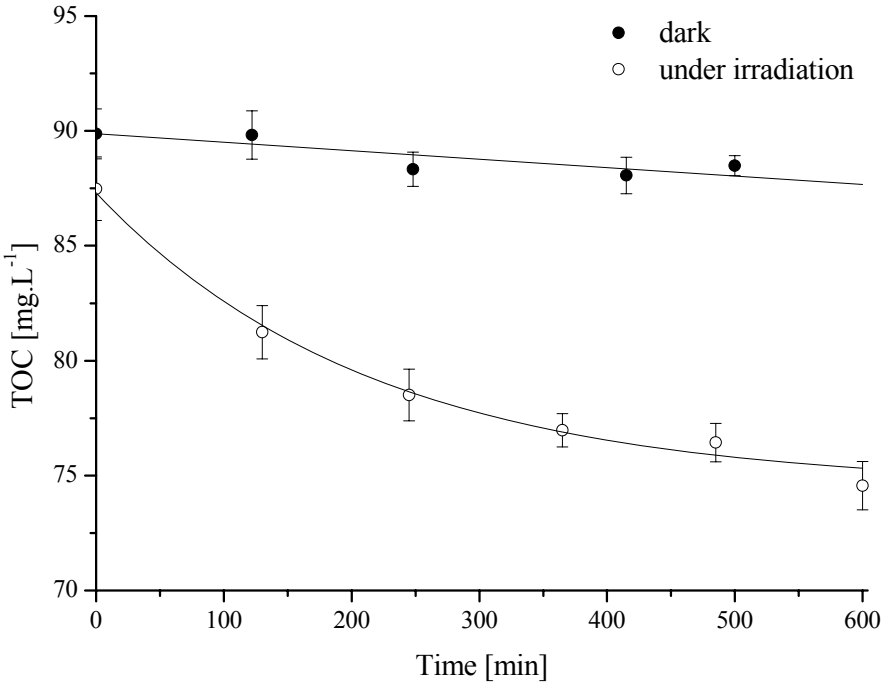

Fig. IV.D.7: Evolution of total organic carbon (TOC) during the mineralisation of 3.8×10^{-3} mol.L^{-1} acetonitrile in suspension of P25 (0.5 g.L^{-1}).

The precision of initial acetonitrile concentration was influenced by multiple dilutions during mixing the initial solution. The TOC of acetonitrile decreased even when the system was not illuminated; this indicated possible slow evaporation of acetonitrile from the system. The rate of decrease of TOC corresponding to acetonitrile lost at dark was corresponding to

9% of TOC decrease during the irradiation. The initial rates of TOC decrease are displayed in **Tab. IV.D.4**.

The comparison of kinetics of TOC decrease during degradation of 5×10^{-4} mol.L^{-1} 4-chlorphenol with/without 3.8×10^{-3} mol.L^{-1} acetonitrile is displayed in **Fig. IV.D.8**.

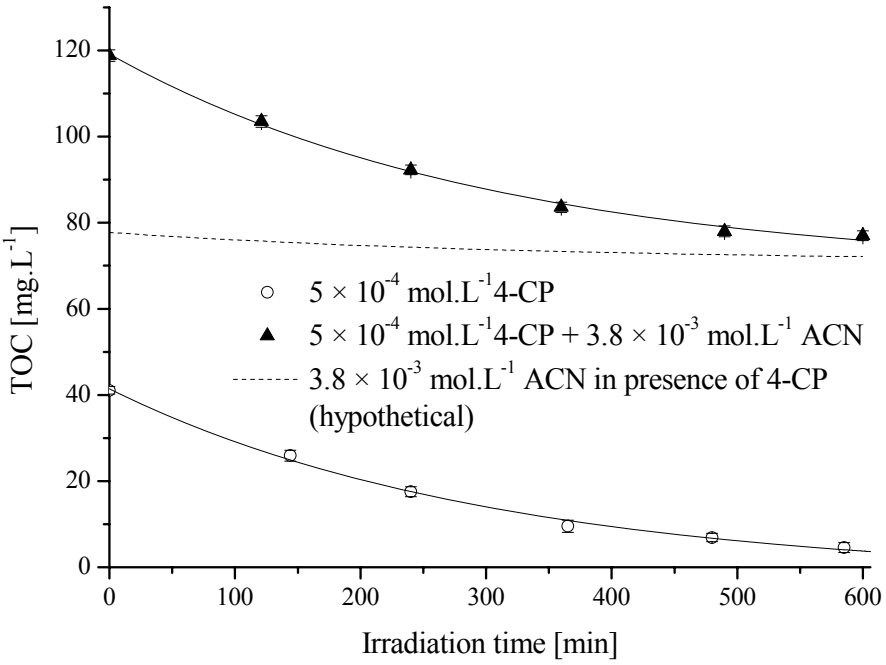

Fig. IV.D.8: Impact of acetonitrile presence on the evolution of total organic carbon (TOC) during the degradation of 5×10^{-4} mol.L^{-1} 4-chlorophenol in suspension of TiO_2 (0.5 g.L^{-1}); [ACN] = 3.8×10^{-3} mol.L^{-1}. Calculated curve of acetonitrile degradation in presence of 4-chlorophenol.

In the system without acetonitrile, the rate of TOC decrease in first 240 min is lower by 12 % than in the system with the solvent; the calculated TOC decrease for both systems is shown in **Tab. IV.D.4**. The contribution of acetonitrile degradation to the total rate of TOC decrease during degradation of both acetonitrile and 4-chlorophenol was calculated using

$$\frac{d\left(TOC'_{ACN}\right)}{dt} = \frac{d\left(TOC_{4-CP+ACN}\right)}{dt} - \frac{d\left(TOC_{4-CP}\right)}{dt},$$

where TOC'_{ACN} was the calculated proportional acetonitrile part of TOC in combined system, $TOC_{4\text{-}CP+ACN}$ was total TOC of combined system and $TOC_{4\text{-}CP}$ was TOC measured at degradation of 4-chlorophenol alone. The hypothetical curve is shown in **Fig. IV.D.8**. The TOC rate, corresponding to acetonitrile degradation in the combined system, corresponds to 37%, comparing to degradation of acetonitrile alone, see **Tab. IV.D.4**.

The concentration of 4-chlorophenol was simultaneously measured. The kinetics of 4-chlorophenol degradation is shown in **Fig. IV.D.9**.

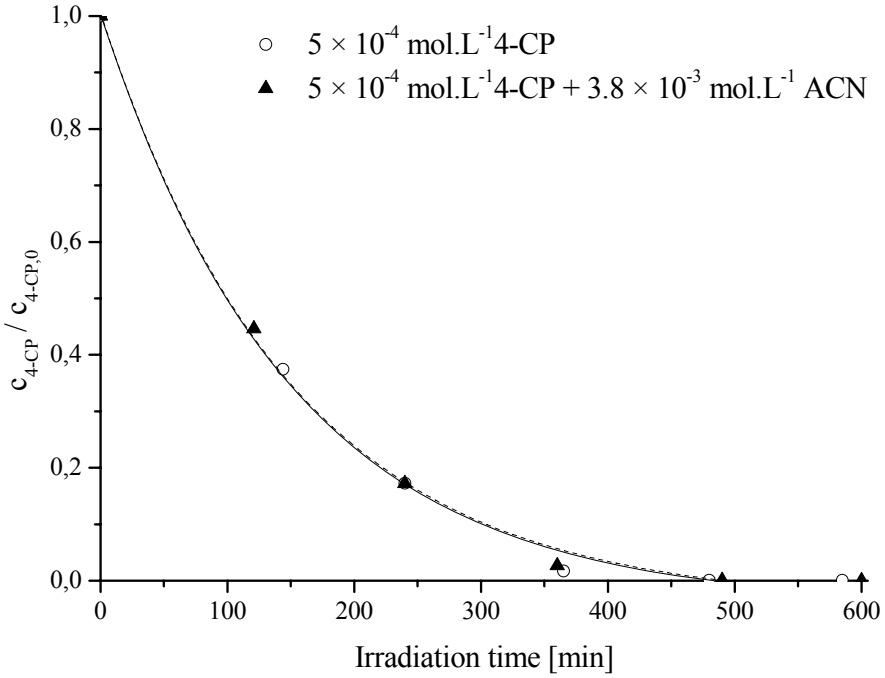

Fig. IV.D.9: Impact of acetonitrile presence (3.8×10^{-3} mol.L^{-1}) on 4-chlorophenol (5×10^{-4} mol.L^{-1}) degradation upon irradiation in TiO_2 suspension (0.5 g.L^{-1}). Lines correspond to first order fit for the absence (solid ——) and the presence (dashed ----) of acetonitrile.

The addition of acetonitrile to total concentration of 3.8×10^{-3} mol.L^{-1} did not change at all the kinetics of 4-chlorophenol degradation; first order rate corresponded to 1.1×10^{-4} s^{-1}. Thus, the rate constant calculated for the system without acetonitrile was also 1.1×10^{-4} s^{-1}.

System composition	dTOC / dt [mg.L^{-1}.s^{-1}]
ACN (dark)	-0.6×10^{-4}
ACN (irradiated)	-6.5×10^{-4}
4-CP	-1.7×10^{-3}
4-CP + ACN	-1.9×10^{-3}
(4-CP + ACN) – 4-CP	-2.4×10^{-4}

Tab. IV.D.4: initial rate of TOC decrease during mineralization of acetonitrile (3.8×10^{-3} mol.L^{-1}), 4-chlorophenol (5×10^{-4} mol.L^{-1}) and the combined system upon irradiation in TiO_2 suspension (0.5 g.L^{-1}).

The presence of acetonitrile during 4-chlorophenol degradation in aqueous solution under studied conditions does not affect the degradation of 4-chlorophenol in the presence of TiO_2. On the contrary, the degradation of the solvent is affected much more significantly than of the pollutant itself; the rate of TOC decrease corresponding to acetonitrile mineralization in the system with 4-chlorophenol dropped to almost one third of the value measured during the mineralization of the acetonitrile alone.

IV.D.5 Degradation of a repeatedly added 4-CP in acetonitrile in aqueous system at TiO_2 – P25

A 0.047 mol.L^{-1} solution 4-chlorophenol in acetonitrile was repeatedly added, one addition per day (irradiation period of 480 minutes); in total, six additions and irradiations were performed. The concentration of pollutant was always set to the initial value (1×10^{-3} mol.L^{-1}). The initial concentration of acetonitrile was 0.5 mol.L^{-1}. The kinetics of 4-chlorophenol degradation on a TiO_2 layer for all additions from "init." to "6th" are plotted at **Fig. IV.D.10**.

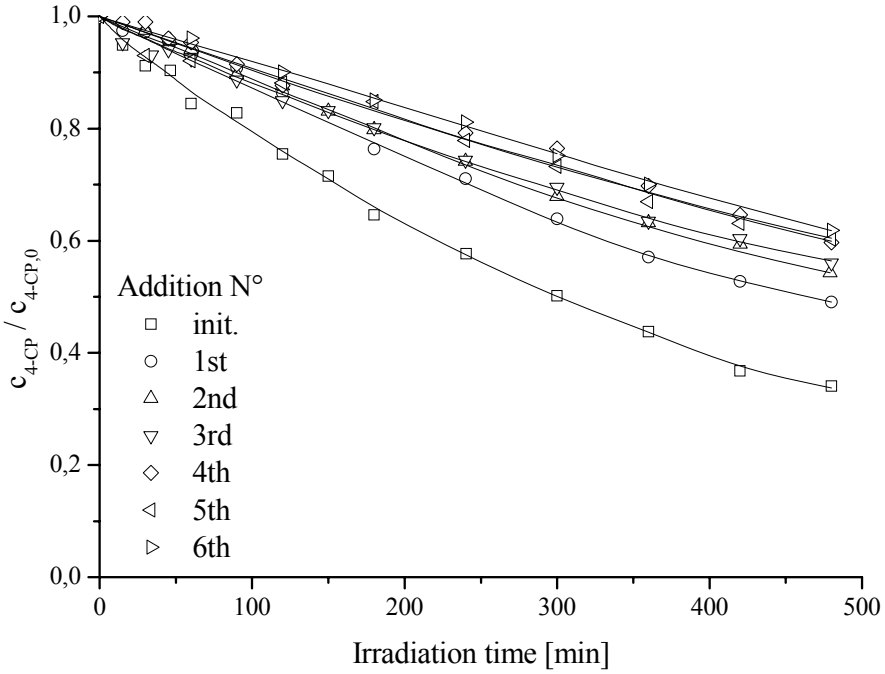

Fig. IV.D.10: Impact of six consecutive additions of 4-chlorophenol (1×10^{-3} mol.L^{-1}) in acetonitrile (0.5 mol.L^{-1}) on degradation of 4-chlorophenol (1×10^{-3} mol.L^{-1}) on an irradiated TiO_2 layer.

The degradation slows down most significantly after first day. During several other days, the rate of degradation was still decreasing, however, the trend seemed to limit to about one third of initial degradation rate. Degradation of 4-chlorophenol became slower because of an increasing concentration of intermediates and because of acetonitrile presence, which competed with 4-chlorophenol for the $^{\bullet}OH$ radicals. The initial rates of 4-chlorophenol degradation (60 minutes) are shown in **Tab. IV.D.5**.

Addition N°	Initial rate [$mol.L^{-1}.s^{-1}$]	Initial 4-CP concentration [$mol.L^{-1}$]	Final 4-CP concentration [$mol.L^{-1}$]	Degraded 4-CP [$mol.L^{-1}$]
Initial	-4.11×10^{-8}	9.86×10^{-4}	3.36×10^{-4}	6.49×10^{-4}
1	-1.58×10^{-8}	8.82×10^{-4}	4.33×10^{-4}	4.49×10^{-4}
2	-1.52×10^{-8}	9.81×10^{-4}	5.29×10^{-4}	4.52×10^{-4}
3	-1.49×10^{-8}	1.03×10^{-3}	5.94×10^{-4}	4.36×10^{-4}
4	-1.43×10^{-8}	1.01×10^{-3}	6.09×10^{-4}	4.01×10^{-4}
5	-1.42×10^{-8}	9.72×10^{-4}	5.86×10^{-4}	3.86×10^{-4}
6	-1.40×10^{-8}	1.04×10^{-3}	6.43×10^{-4}	3.97×10^{-4}

Tab. IV.D.5: Initial rates of 4-chlorophenol degradation, initial and final concentration of 4-chlorophenol and an amount of degraded 4-chlorophenol for several repeated additions of 4-chlorophenol (1×10^{-3} $mol.L^{-1}$) in acetonitrile (0.5 $mol.L^{-1}$).

After six additions, the initial rate of 4-chlorophenol degradation dropped to one third of the value measured for the initial solution. The amount of degraded 4-chlorophenol was also decreasing with each addition; after six additions, an equilibrium seemed to be reached as this value remained practically unchanged for three last additions.

The evolutions of concentration of hydroquinone, a primary intermediate of 4-chlorophenol degradation, are displayed at **Fig. IV.D.11**.

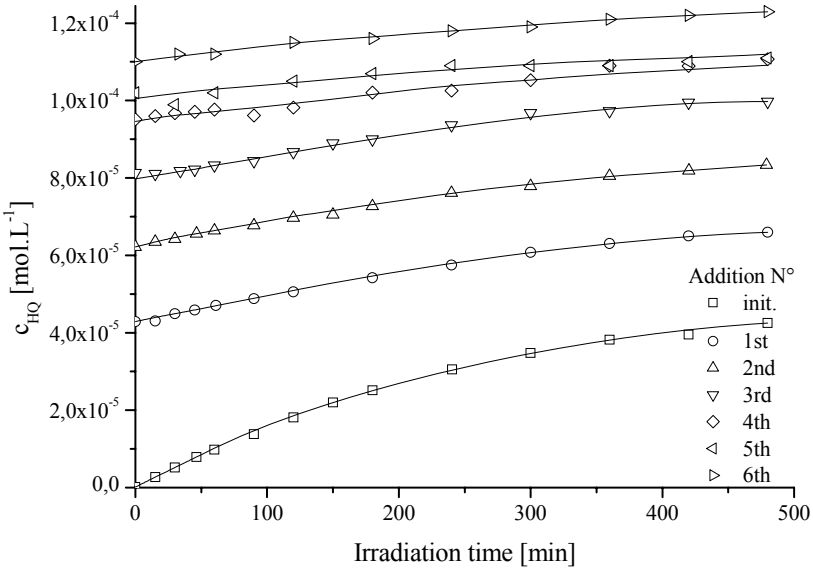

Fig. IV.D.11: Evolution of hydroquinone (HQ) concentration during 4-chlorophenol (1×10^{-3} mol.L^{-1}) photodegradation on a TiO_2 layer within six consecutive additions of 4-chlorophenol (1×10^{-3} mol.L^{-1}) in acetonitrile (0.5 mol.L^{-1}).

The highest increase of hydroquinone concentration was observed during the degradation of initial solution. With subsequent additions, the difference between initial and final hydroquinone concentration is gradually decreasing. In several days, reaching of quasi-equilibrium and limiting of the intermediate concentration to certain plateau value could be expected.

The initial and final concentration of hydroquinone and its ratio to respective concentration of 4-chlorophenol for each addition are shown in **Tab. IV.D.6**.

Addition N°	Initial HQ concentration [mol.L^{-1}]	Final HQ concentration [mol.L^{-1}]	Initial [HQ] / [4-CP]	Final [HQ] / [4-CP]
Initial	1.69×10^{-7}	4.25×10^{-5}	0.0002	0.13
1	4.29×10^{-5}	6.60×10^{-5}	0.049	0.15
2	6.22×10^{-5}	8.34×10^{-5}	0.063	0.16
3	8.13×10^{-5}	9.97×10^{-5}	0.079	0.17
4	9.51×10^{-5}	1.11×10^{-4}	0.094	0.18
5	1.02×10^{-4}	1.11×10^{-4}	0.103	0.19
6	1.10×10^{-4}	1.23×10^{-4}	0.106	0.19

Tab. IV.D.6: Initial and final values of hydroquinone concentration and of hydroquinone to 4-chlorophenol molar ratio during 4-chlorophenol degradation at TiO_2 layer for six repeated additions of 4-chlorophenol (1×10^{-3} mol.L^{-1}) in acetonitrile (0.5 mol.L^{-1}).

For better comprehension, some of the values from **Tab. IV.D.5** and **Tab. IV.D.6** are displayed in **Fig. IV.D.12**, namely initial and final concentrations of 4-chlorophenol and hydroquinone for each addition, as well as amount of degraded 4-chlorophenol.

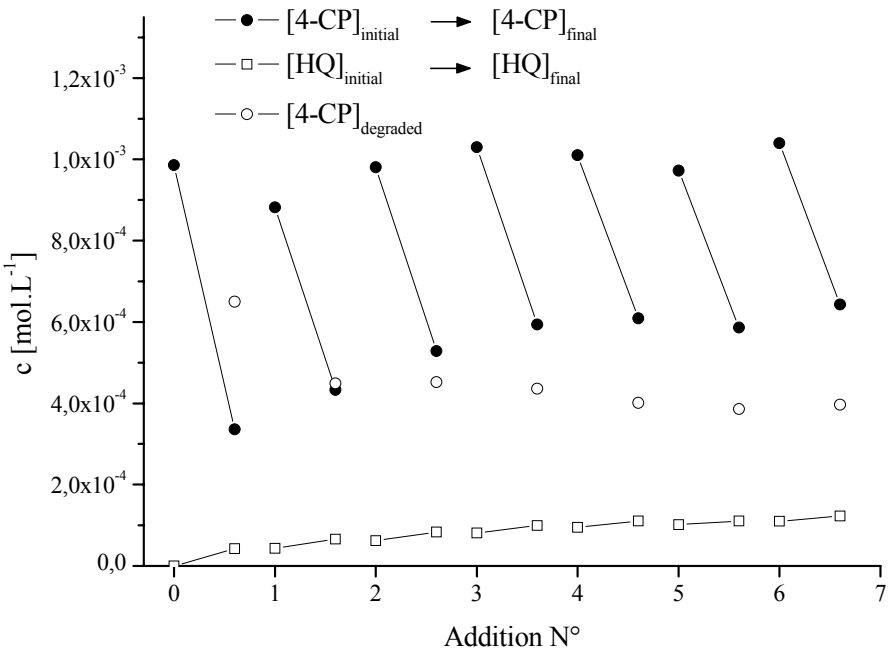

Fig. IV.D.12: Evolution of 4-chlorophenol and hydroquinone concentration during degradation of 4-chlorophenol (1×10^{-3} mol.L^{-1}) on an irradiated TiO_2 layer within six consecutive additions of 4-chlorophenol in acetonitrile (0.5 mol.L^{-1}); comparison with concentration of degraded 4-chlorophenol.

As mentioned above, largest differences between initial and final concentration were observed in the initial solution. After several additions, the amount of degraded 4-chlorophenol and of hydroquinone present finally reaches quasi-equilibrium. This phenomenon could be seen more clearly in the **Fig. IV.D.13**.

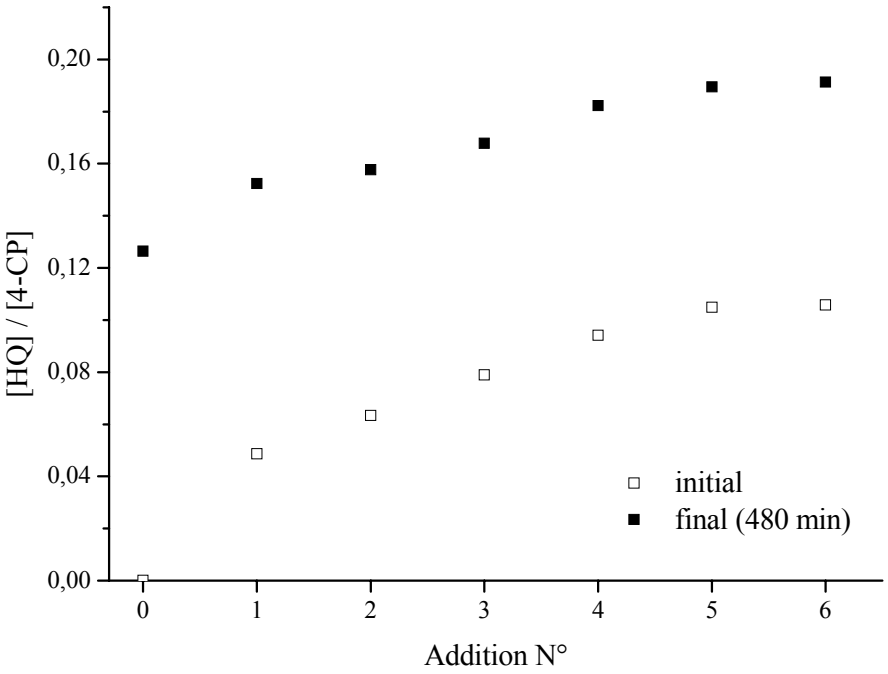

Fig. IV.D.13: Evolution of hydroquinone to 4-chlorophenol molar ratio during degradation of 4-chlorophenol (1×10^{-3} mol.L^{-1}) on irradiated TiO_2 layer within six consecutive additions of 4-chlorophenol in acetonitrile (0.5 mol.L^{-1}); comparison of initial and final molar ratio (after 480 min of irradiation) for all additions.

The ratios of initial and final concentrations of hydroquinone and 4-chlorophenol were continuously increasing since the first addition. After six additions, a plateau was approached. The ratio of hydroquinone to 4-chlorophenol concentration corresponded to 0.2.

IV.D.6 Conclusion

The P25 systems of suspensions and layers were compared, using the values of 4-chlorophenol degradation flow. Various initial concentrations of 4-chlorphenol were used; 4-CP degradation flows were always higher in the system with suspended TiO_2, than in the system with immobilized TiO_2.

The suitability of methanol and acetonitrile as solvents for addition of pollutant to P25 degradation system were tested for the solvent to 4-chlorophenol molar ratio of 1000:1. The presence of methanol led, not surprisingly, to strong inhibition of the 4-chlorophenol degradation, as the 4-CP degradation flow dropped to 6% of the value measured in system

with no solvent. The presence of acetonitrile resulted in a decrease of 4-CP degradation flow to 64%. The organic solvent kinetically competed with the pollutant for •OH radicals.

The impact of acetonitrile concentration on 4-chlorophenol degradation were studied using HPLC and TOC determination. It was found that for acetonitrile concentrations lower than 0.05 $mol.L^{-1}$ the degradation rate of 4-chlorophenol was not practically affected. The competitive degradation of 4-chlorophenol and acetonitrile showed that the degradation rate of ACN is about one order lower than that of 4-CP even the concentration of ACN was about an order higher.

After revealing the optimal parameters, the repeated addition of preconcentrated pollutant in acetonitrile to aquatic solution in photoreactor with P25 immobilized layer was performed. For subsequent repeated additions into degradation system containing 0.5 $mol.L^{-1}$ acetonitrile, the degradation rate of 4-chlorophenol was decreasing. This was probably due to the increasing concentrations of degradation intermediates and acetonitrile, which competed with 4-chlorophenol for •OH radicals. However, the presence of intermediates seems to be more limiting impact for 4-chlorophenol degradation. After six additions, quasi-equilibrium between 4-chlorophenol and the primary degradation intermediate of hydroquinone was reached.

As a conclusion, acetonitrile is very suitable for the combined sorption-degradation process, because it has high solvent power in the first regeneration step and low own reactivity with •OH radical in the second photodegradation step.

References:

Abida O., Doctoral thesis in physical chemistry, *Université Blaise Pascal, Clermont-Ferrand (France)* **2005**, Tab V.6, *176*.

Abrahamson H.B., Rezvani A.B., Brushmiller J.G., *Inorg. Chim. Acta*, **1994**, 226, 117-127.

Buxton G.V., Greenstock C.L., Helman W.P., Ross A.B., *J. Phys. Chem. Ref. Data*, **1988**, 17, 513-886.

Christensen H., Sehested K., *J. Phys. Chem.*, **1988**, 92, 3007.

Field T.B., McCourt J.L., McBryde W.A.E., *Can. J. Chem.*, **1974**, 52, 3119.

Hamm R.E., Schull C.M. Jr., Grant D.M., *J. Amer. Chem. Soc.*, **1954**, 76, 2111.

Herrmann J.M., Tahiri H., Guillard C., Pichat P., *Catalysis Today*, **1999**, 54, 131-141.

Hill G.D., MacGahen J.W., Baker H.M., Finnerty D.W., Bingeman C.W. *Agronom. J.*, **1955**, 47, 93.

Jelínek L., Trpišovský A., Matějka Z., Kolář M., Krýsa J.: Sorption and Desorption of Chlorinated Organic Compounds on Polymeric Sorbents with Respect to their Subsequent Photo-Catalytic Decomposition, Proc. *XIXth International Symposium on Physico-chemical Methods of the Mixtures Separation "Ars Separatoria 2004"*, Zloty Potok n. Czestochowa, Poland, June 10-13, **2004**, p. 190-191.

Měšťánková H., Mailhot G., Pilichowski J.-F., Jirkovský J., Krýsa J., Bolte M., *Chemosphere*, **2004**, 57, 1307.

Měšťánková H., Doctoral thesis in physical chemistry, *Université Blaise Pascal, Clermont-Ferrand (France)* **2004**, Fig. IV-A-4, *65*.

Měšťánková H., Mailhot G., Jirkovský J., Krýsa J., Bolte M., *Appl. Catal. B: Environ.* **2005**, 57, 257.

Neta P., Schuler R.H., *J. Phys. Chem.*, **1975**, 79, 1-6.

Poulain L., Mailhot G., Wong-Wah-Chung P., Bolte M., *J. Photochem. Photobiol. A: Chem.*, **2003**, 159, 81.

Stafford U., Gray K. A., Kamat P. V., *J. Phys. Chem.*, **1994**, 98, 6343-6351.

Theurich J., Lindner M., and Bahnemann D.W, *Langmuir*, **1996**, 12, 6375.

Timberlake C. F., *J. Chem. Soc*, **1964**, 5078-5085.

V. CONCLUSION

In this work, degradation of a pollutant was studied in different homogeneous or heterogeneous photocatalytic systems, where the continuous formation of hydroxyl radicals, highly oxidative species, was particularly employed.

The characterisation of ferric citrate, which was one of the components of photocatalytic systems, showed several important facts. The ferric citrate complex exists in several forms depending on pH. These forms of the complex demonstrate different photoactivity. The highest quantum yields of Fe(II) formation during Fe(III)Cit photodecomposition were found at pH = 3. The released citrate radical provides a source of oxidative radicals (hydroxyl, oxohydroxyl, etc.), that can attack other organic molecules. Besides, the proton is attached to citrate ligand during the photolytic process of the complex, which results in an increase of pH.

The first system used for decomposing the herbicide of Monuron was based on the photocatalytic cycle of Fe(III)/Fe(II), producing hydroxyl radicals. The iron was inserted into system as ferric citrate complex. Two-step kinetics of Monuron degradation was observed. The first fast step corresponded to the steep decrease of pollutant concentration induced by an attack of radicals released during the photolysis of the complex. In the second (slower) step, the source of radicals was the cycle of Fe(III)/Fe(II).

Two crucial factors of Monuron degradation efficiency were identified: pH and O_2 concentration. The pH determined the photoactivity of the ferric citrate complex as well as of the photocatalytic cycle of Fe(III)/Fe(II). The best performance was reported at acid initial pH, particularly between 2.75 and 3.0, for [Fe(III)Cit] = 2.55×10^{-4} mol.L^{-1}. At pH close to neutral, the degradation stopped in the second step. The concentration of O_2 was the other key factor. In the absence of oxygen, the system was practically inhibited; on the contrary, both steps of pollutant degradation were accelerated in an O_2 saturated system. Oxygen was necessary for both steps: it reacted with the ligand radical in the first step, and it participates in the reactions of Fe(II) reoxidation in the second step. The concentration of Fe(III)Cit did not increase the pollutant degradation efficiency proportionally. Since certain value, both steps of degradation kinetics are slowed down. It was caused by a rapid increase of pH in the first step, as the protons are consumed by ligand during the Fe(III)Cit photolysis.

The following photocatalytic system comprised heterogeneous photocatalysis on TiO_2 (P25) inducing the degradation of Monuron, as it was a pre-requisite for the combined system. The pollutant decomposition followed the first-order kinetics; the optimal concentration of TiO_2 was 250 $mg.L^{-1}$.

The third system combined both photocatalytic systems, the Fe(III)Cit and TiO_2 suspension, for Monuron degradation. Two-step kinetics was observed again. The addition of TiO_2 had a positive effect on pollutant degradation at lower initial pH (2.75 – 3.0). At higher initial pH, almost no effect of TiO_2 addition was observed. Moreover, the photocatalytic activity of TiO_2 itself was inhibited, as the deprotonated surface of TiO_2 was shortcutted by iron ions, which made the recombination of the photogenerated electron-hole pair more favourable.

The concentration of Fe(III)Cit was further optimized in a combined system at pH = 3. The system with Fe(III)Cit concentration of 2.55×10^{-5} $mol.L^{-1}$ had higher overall efficiency of Monuron degradation than the system with Fe(III)Cit concentration ten times higher. This result is interesting not only from the point of setting up a combined system for water treatment, but also for AOP (advanced oxidation processes) based on TiO_2 photocatalysis, because the traces of iron are always present in water.

The last photocatalytic system employed TiO_2 fixed layer in a semi-operational photoreactor, for removal of 4-chlorophenol, a product commonly used in industry, and also a frequent degradation intermediate of many compounds. As the pollutant was intended to be repeatedly added in an organic solvent, several solvents were tested. After six additions of pollutant in acetonitrile in six time periods, quasi-equilibrium between the pollutant and the intermediates was reached. Acetonitrile was found as the most suitable solvent for the combined sorption-degradation process because it has high solvent power in the regeneration step, as it had low reactivity with hydroxyl radicals in the photodegradation step.

SUMMARY

The photoinduced degradation of Monuron, an herbicide, was studied in three various systems producing hydroxyl radicals: in the presence of Fe(III)Cit complex, in a TiO_2 suspension and in the combined system of Fe(III)Cit / TiO_2. The main goal of the study was to improve the photocatalytic efficiency. The distribution and photoactivity of the complex species highly depended on pH. The kinetics of Monuron degradation photoinduced by the complex followed two steps with different sources of $^{\bullet}OH$: 1) photolysis of the complex; 2) iron photoredox cycle. The presence of TiO_2 improved the efficiency of the ferric citrate system at acid pH; at neutral pH, the efficiency of the system was totally inhibited. The concentration of oxygen and pH were the most important factors of degradation efficiency in the system containing iron citrate. Moreover, with a semi-operational system employing TiO_2 photocatalysis, the effect of organic solvent on the degradation of 4-chlorophenol in water was examined.

RESUME

La dégradation photoinduite du Monuron (herbicide) a été étudiée dans trois systèmes différents produisant des radicaux hydroxyle: en présence du complexe Fe(III)Cit, dans une suspension de TiO_2 et dans un système combiné Fe(III)Cit / TiO_2. Le but principal était d'améliorer l'efficacité photocatalytique. La spéciation et la photoactivité du complexe ont été déterminées en fonction du pH. La cinétique de dégradation du Monuron photoinduite par le complexe se fait en deux étapes avec deux sources successives de radicaux $^{\bullet}OH$: 1) photolyse du complexe ; 2) cycle photoredox du fer. La présence de TiO_2 améliore l'efficacité du système Fe(III)Cit à pH acide alors qu'à pH neutre l'efficacité du système est complètement inhibée. La concentration en oxygène et le pH sont les facteurs clés en présence du complexe Fe(III)Cit. De plus, dans un système pilote utilisant du TiO_2, l'influence d'un solvant organique lors de la dégradation du 4-chlorophénol en milieu aquatique a été examinée.